AFRL-AFOSR-UK-TR-2011-0035

Assessment of Air Vehicle Design Evolution over Mach Number and Altitude Operating Envelope With and Without S&C Considerations as Part of the Design Synthesis

Raj K Nangia

Nangia Aero Research Associates
West Point, 78-Queens Road
Bristol, United Kingdom BS8 1QX

EOARD GRANT 10-3067

August 2011

Final Report for 27 April 2010 to 27 April 2011

Distribution Statement A: Approved for public release distribution is unlimited.

Air Force Research Laboratory
Air Force Office of Scientific Research
European Office of Aerospace Research and Development
Unit 4515 Box 14, APO AE 09421

REPORT DOCUMENTATION PAGE

Form Approved OMB No. 0704-0188

Public reporting burden for this collection of information is estimated to average 1 hour per response, including the time for reviewing instructions, searching existing data sources, gathering and maintaining the data needed, and completing and reviewing the collection of information. Send comments regarding this burden estimate or any other aspect of this collection of information, including suggestions for reducing the burden, to Department of Defense, Washington Headquarters Services, Directorate for Information Operations and Reports (0704-0188), 1215 Jefferson Davis Highway, Suite 1204, Arlington, VA 22202-4302. Respondents should be aware that notwithstanding any other provision of law, no person shall be subject to any penalty for failing to comply with a collection of information if it does not display a currently valid OMB control number.
PLEASE DO NOT RETURN YOUR FORM TO THE ABOVE ADDRESS.

1. REPORT DATE *(DD-MM-YYYY)*	2. REPORT TYPE	3. DATES COVERED *(From – To)*
30-08-2011	Final Report	27 April 2010 - 27-Apr-11

4. TITLE AND SUBTITLE

Assessment of Air Vehicle Design Evolution over Mach Number and Altitude Operating Envelope With and Without S&C Considerations as Part of the Design Synthesis

5a. CONTRACT NUMBER

FA8655-10-1-3067

5b. GRANT NUMBER

Grant 10-3067

5c. PROGRAM ELEMENT NUMBER

6. AUTHOR(S)

Dr. Raj K. Nangia

5d. PROJECT NUMBER

5d. TASK NUMBER

5e. WORK UNIT NUMBER

7. PERFORMING ORGANIZATION NAME(S) AND ADDRESS(ES)

Nangia Aero Research Associates
West Point, 78-Queens Road
Bristol, United Kingdom BS8 1QX

8. PERFORMING ORGANIZATION REPORT NUMBER

N/A

9. SPONSORING/MONITORING AGENCY NAME(S) AND ADDRESS(ES)

EOARD
Unit 4515 BOX 14
APO AE 09421

10. SPONSOR/MONITOR'S ACRONYM(S)

AFRL/AFOSR/RSW (EOARD)

11. SPONSOR/MONITOR'S REPORT NUMBER(S)

AFRL-AFOSR-UK-TR-2011-0035

12. DISTRIBUTION/AVAILABILITY STATEMENT

Approved for public release; distribution is unlimited. (approval given by local Public Affairs Office)

13. SUPPLEMENTARY NOTES

14. ABSTRACT

Currently there is interest in developing aircraft with long-range capability at very high speeds. Typical anticipated roles could be reconnaissance and bombing missions. A concern is that, often for the sake of expedience, the conceptual design phases focus more on performance and much less on the more complex S&C aspects (about all axes). Consequently, S&C aspects considered later in the design cycle can severely compromise the original design objectives (L/D, strike capability range, weight growth). A better approach will be to include the major aspects of S&C in the conceptual design phases. Supersonic aircraft require a compromise between low-speed and high-speed capabilities and S&C issues remain very central throughout the operational envelope. The safety considerations may shift the balance more toward low-speed capabilities. The payloads in supersonic aircraft are generally smaller than those of subsonic aircraft.

The main objective has been to assess vehicle design evaluation over Mach number and altitude operating envelope with S&C considerations as part of the design synthesis. It is implied that design tools have needed to be "anchored", so as to focus on the importance of S&C. In this Phase 1 report, we have addressed a series of issues. It is worth mentioning that the analyses tended to expand as we went more deeply into the various aspects, often beyond the initial expectations.

15. SUBJECT TERMS

EOARD, Aerodyanamics, Aircraft Design, Supersonic and Hypersonic Flows

16. SECURITY CLASSIFICATION OF:			17. LIMITATION OF ABSTRACT	18, NUMBER OF PAGES	19a. NAME OF RESPONSIBLE PERSON
a. REPORT	b. ABSTRACT	c. THIS PAGE			Gregg Abate
UNCLAS	UNCLAS	UNCLAS	SAR	105	19b. TELEPHONE NUMBER *(Include area code)* +44 (0)1895 616021

RKN / AERO / REPORT / 2010-10
Issue 1, 29 August 2011

Study for Air Vehicles at High Speeds

Assessment of Air Vehicle Design Evolution over Mach Number & Altitude Operating Envelope With and Without S&C Considerations as Part of the Design Synthesis

Dr. R. K. Nangia

SUMMARY

Currently there is interest in developing aircraft with long-range capability at very high speeds. Typical anticipated roles could be reconnaissance and bombing missions.

A concern is that, often for the sake of expedience, the conceptual design phases focus more on performance and much less on more complex Stability and Control (S&C) aspects (about all axes). Consequently, S&C aspects considered later in the design cycle can severely compromise the original design objectives (L/D, strike capability range, weight growth). A better approach will therefore be to include the major aspects of S&C in the conceptual design phases. Supersonic aircraft require a compromise between low-speed and high-speed capabilities and S&C issues can remain very central throughout the operational envelope. The payloads in supersonic aircraft are generally smaller than those of subsonic aircraft.

It is therefore of great interest to know, quantitatively, the significance of such issues.

This report covers work in Phase 1. S&C issues covering Longitudinal and Lateral/ Directional aspects have been included. Several avenues for future work have been indicated including conceptual designs.

The work performed in this report was requested by the Air Force Research, Laboratory, Air Vehicles Directorate, High Speed Aerodynamics Configuration Branch with the technical monitor identified as Charles F. Suchomel

EOARD Grant No.10-3067

Consulting Engineers
Nangia Aero Research Associates
WestPoint, 78 Queens Road, Clifton
Bristol BS8 1QU, UK

The work performed in this report was requested by the Air Force Research, Laboratory, Air Vehicles Directorate, High Speed Aerodynamics Configuration Branch with the technical monitor identified as Charles F. Suchomel. It was facilitated via the USAF - EOARD, 86 Blenheim Crescent, Ruislip, London HA4 7HB, UK and was carried out under the terms of Grant No 10 – 3067

INITIAL DISTRIBUTION LIST

1	Dr. Gregg Abate	USAF-EOARD, 86 Blenheim Crescent, Ruislip London HA4 7HB, UK
1	Charles F. Suchomel	AFRL/RBAA, Bldg 45, Rm 256, 2130 8th Street, WPAFB, OH 45433 -7542
1.	Dr. James Miller	AFRL/RBAA, Bldg 45, Rm 256, 2130 8th Street, WPAFB, OH 45433 -7542
1	Mr. Dieter Multhopp	AFRL/RBAA Bldg 45, 2130 8th Street, WPAFB, Ohio, USA 5433-7542
1	Dr. Carl P. Tilmann	AFRL/RBAA Bldg 45, 2130 8th Street, WPAFB, Ohio, USA 5433-7542
1	Mr. William Blake	AFRL/RBCA Bldg 146, 2130 8th Street, WPAFB, Ohio, USA 45433-7542
1	Mr. Cale Zeune	AFRL/RBAA Bldg 45 8th St, Bldg 45, Rm 262, WPAFB, Ohio, USA 45433- 7542
1	Mr. Ryan Plumley	AFRL/RBAA Bldg 45 8th St, Bldg 45, Rm 262, WPAFB, Ohio, USA 45433- 7542
2	Dr. R.K. Nangia	Nangia Aero Research Associates, WestPoint, 78-Queens Road, Clifton, BRISTOL BS8 1QU, UK.

CONTRACTUAL DECLARATIONS

"The Contractor, Dr. R. K. Nangia**,** hereby delcares that, to the best of its knowledge and belief, the technical data delivered herewith under Grant No10-3067 is complete, accurate, and complies with all requirements of the grant."

DATE: 29 August 2011 Name and Title of Authorized Official: Dr R K Nangia

"I certify that there were no subject inventions to declare as defined in FAR 52.227-13, during the performance of this contract."

DATE: 29 August 2011 Name and Title of Authorized Official: Dr R K Nangia

CONTENTS

1. INTRODUCTION

1.1. Air Vehicles at High Speeds

Currently there is interest in developing aircraft with long-range capability at very high speeds, developing further the supersonic concepts illustrated in **Fig.1.1.1**. Typical anticipated roles could be reconnaissance and bombing missions.

A concern is that, often for the sake of expedience, the conceptual design phases focus more on performance and much less on more complex Stability and Control (S&C) aspects (about all axes). Consequently, S&C aspects considered later in the design cycle can severely compromise the original design objectives (L/D, strike capability range, weight growth). A better approach will therefore be to include the major aspects of S&C in the conceptual design phases. Supersonic aircraft require a compromise between low-speed and high-speed capabilities and S&C issues can remain very central throughout the operational envelope. The payloads in supersonic aircraft are generally smaller than those of subsonic aircraft.

It is therefore of great interest to know, quantitatively, the significance of such issues.

The **OBJECTIVE** is to assess air vehicle design evaluation over Mach number and altitude operating envelope with and without S&C considerations as part of the design synthesis. It is implied that there is a need to anchor the tools available, so as to focus on the importance of S&C.

1.2. Content and Layout of this Report

The remainder of this report is contained in **Sections 2 to 13**.

Section 2 outlines the design requirements and questions to be addressed and
Section 3 refers to the scope of the work, showing the wide range of possibilities. The phased programme of work is outlined.
Section 4 reviews the main drivers associated with the design of supersonic aircraft and discusses examples (XB-70 and Concorde). The importance of assessing vortex lift contributions is then discussed in **Section 5.**
Section 6 reviews the effects of planform geometry on S&C aspects.
Section 7 examines Ground Effects on Longitudinal and Sideslip control.
Section 8 looks briefly at variable geometry possibilities, e.g. Folded Tips.
A brief assessment of various control aspects on typical planforms over a wide M range is given in **Section 9**.
Section 10 looks at Inertial Coupling aspects and the importance of configuration and control surface geometry.
Section 11 presents an initial performance evaluation for Strike Aircraft with comparisons for Concorde and XB-70. The effects of S&C and L/D on Range are discussed.
In **Section 12** areas for further work are outlined.
Section 13 presents Conclusions.

2. DESIGN REQUIREMENTS and QUESTIONS TO BE ADDRESSED

There are several options and design requirements feasible. Currently the ideas are towards the following:

2.1. Typical Design Requirements:

- Tailless (horizontal) configuration Bomber in the size/weight class of Concorde and the XB-70 - that implies MTOW around 400,000 – 600,000 lbs.

- Questions arise about certain aspects e.g. low observability, variable geometry, presence of vertical fins etc.!! Folding wing tips may be required for very high speed designs to avoid excess Lift.

- Low observability and stealth considerations may influence the presence of additional surfaces (tail, canard and fin).

- Thrust vectoring could be a possibility especially for low speed.

- Cruise Mach number: 1.0+ to 2.0 to 3.0 or more – using turbo-jets. At the higher speed end, Space shuttle type concepts appear.

- Range circa 4000 nm and payload about 3-6% MTOW – to be confirmed.

- Field Performance near Mach 0.2 – 0.3, highlighting the S&C compromises between low speeds and high speeds. Adequate control powers needed throughout flight envelope. This may imply cg movements, controlled through fuel transfer.

- This implies adequate α (AOA) range capability: from about 2 deg to 20 deg. (maximum and minimum estimates at his stage)

- Similarly, β (Side-Slip angle), α etc. capability is required for maneuvering, landing and possible engine-out situations. In the longer term transients analysis is also required (if do-able)

- In the long run, Longitudinal S&C aero elastic modes need to be included. Early studies may use simplified estimations of deflections and corrections

- Static and Dynamic S&C factors are to be considered in design synthesis

A classic example was the design of Concorde with respect to cg position and effects on L/D, see Section 5. AOA limits also resulted because of vortical flow breakdown as well as keeping the undercarriage weight low (The weight is of the same order as the payload).

2.2. Typical Aspects and Questions to be addressed

There is wide scope for interesting but challenging configuration work in the light of the bias towards different levels of S&C requirements. Typical aspects at present, based on early discussions with AFRL, are as follows. However, these ideas will develop as further discussions take place:

1. How [qualitative and quantitatively] do S&C requirements influence vehicle shape, performance, fuel efficiency etc., throughout the flight envelope? First order cost estimates can be given.
2. To gain an understanding at the onset of the programme, attention will be devoted to an analysis of typical existing designs and knowledge base available.
3. What S&C requirements have greatest / smallest impact on the vehicle shape, performance, cost, etc.?
4. Are there configuration solutions where static and dynamic S&C factors have minimal impact on vehicle shape, performance, cost, etc., but still satisfy S&C requirements? What level of variable geometry is appropriate?
5. At the end of the study, what can be said about the process? How effective was it? How can it be improved? What S&C factors brought about the greatest changes [vehicle shaping, other]? What were the overwhelming S&C considerations/factors that dominated/drove the configuration shape/mold lines [e.g., were they static or dynamic factors, which ones, etc.?

3. SETTING THE SCOPE OF THE PRESENT PROGRAMME

3.1. Wide Range of Possibilities

From the viewpoint of setting up the scope of the Programme, the first step is towards using some of the existing knowledge on larger supersonic aircraft from an S&C perspective. Refs.1-9 give an idea of our previous work on supersonic configurations, including work carried out for AFRL scientists.

The subsequent stages are to exploit the knowledge within the context of the present programme in a more integrated sense. This then initiates the main body of work.

Final stages will lead to firming up on the inferences and recommendations for future work. Including comments on methodology and improvements.

This subject is considered very timely in view of the time-frames for the high-speed project.

Obviously, the scope of the work is broad. The Work Programme is to be phased, in line with availability of funds and time estimates. Following recent discussions with AFRL Technical Monitor (Mr. Charles Suchomel), the proposals are to work through initially in 2-3 phases, addressing the aspects and questions raised in **Sections 1 & 2**.

3.2. Phase 1 Work Programme

The following aspects will be addressed in this phase:

1. Use two or three existing / historical configurations to derive guide-lines for S&C, including Payload – range diagrams, Mach capability, cg variation, fuel transfer, control sizing (for all 3 axes flight), etc. Some guide-lines for longitudinal S&C follow from Concorde experience.

For supersonic aircraft, attaining an adequate low-speed performance is the key to success and this leads to the next point.

2. Select / derive generic configuration. Assume Flight envelope (Mach, altitude), payload – range capability. No horizontal tail but Vertical tail (Fin) may be an option. Concorde provides a useful starting point for laying out longitudinal S&C aspects.

(a). Design without and with S&C aspects for all 3-axes

(b). Assess at important points on flight envelope at all speeds (low, transonic and high)

(c). Assess Impact on L/D, weight growth, Thrust / Weight ratio.

(d). Engine out, about 4^{o} β requirement. The presence of vertical surfaces remains an important issue during preliminary design process. So it needs to be included.

Phase 1 makes the outline case. The results from this phase will then be exploited in more detail in second and subsequent phases.

3.3. Phase 2 Work Programme Envisaged

Extend the work of Phase 1 in more detail.

Use a few representative generic configurations in co-operation with technical monitors. Variable wing sweep configurations may be a possibility. Assume Flight envelope (Mach, altitude), payload – range capability.

The work programme is aimed towards answering the typical questions in Section 1.

3.4. Subsequent Phases of work

Assess the effect of possible morphing aircraft. One such design would be a configuration with an expandable wing tip that holds fuel and retracts as fuel is burned. Although open ended, this is an important item as other types of morphing are possible and more effort can be directed as needed.

Assess the effect of alternate fuels, and possible alternate reserve fuels (liquid hydrogen as reserve fuel).

Assess potential effect on efficiency if an unconventional aerial refueling infra-structure were constructed.

4. THE MAIN "DRIVERS" ASSOCIATED WITH SUPERSONIC AIRCRAFT DESIGN

4.1. General Supersonic Configurations

Figs. 4.1.1 – 2 show several supersonic aircraft and planform developments. It is interesting to note the diversity. Notable designs that were developed are the XB-70 with folding outer wing panels, the B-1 with variable wing geometry and Concorde with complex ogival wing planform and camber distribution. Possible advanced technologies that may be included in future designs are outlined in **Fig.4.1.3**. These have particular relevance to S&C aspects at low and high speed. They include variable LE geometry for both separation control and drag reduction. "Virtual" control surfaces at TE arise from morphing wing technology. This may be considered in conjunction with powerplant thrust vectoring.

We consider the anticipated flight envelope for Civil and Military applications. We then look in detail at a civil application, Concorde, and typical military applications, XB-70.

4.2. Flight Envelope Considerations and Properties of Supersonic Aircraft

Figs. 4.2.1 – 2 refer to Altitude – C_L considerations for different Mach numbers (M 0.3, 0.6, 0.9, 2.0, 3.0 and 4.0) and wing-loading (W/S). In particular, **Fig.4.2.2** refers to the relationships near sea-level (speed of sound 661.9 kts) for take-off and landing estimates. We have shown relationships for M 0.2, 0.25 and 0.3 (132.4, 165.5 and 198.6 kt respectively).

Considering that α achievable near ground is about 14 deg, the slender supersonic configurations enable C_L of about 0.5-0.6. At typical ground speeds (M 0.25 to 0.3), we imply W/S near 60.

For high speeds, higher altitudes are required to obtain reasonable levels of C_L and hence good L/D. This can be beset by limitations associated with air-breathing propulsion technology.

Fig.4.2.3 gives an idea of weight fractions, aerodynamic efficiency and power-plant efficiency variations with M and weight, based on DARPA estimates and challenges set for the QSP programme, Ref.15. We note that designs taken through to test flight and, in some cases, beyond into service (Concorde, XB-70 and SR-71) lie on fairly consistent trends, L/D – M, M.L/D – M, WP/MTOW – M, etc. Advanced projects, such as the HSCT, Douglas SCR and Lockheed SCR have generated their own trend with typical increased efficiency levels. The long-term goal of the QSP project was a magnitude more efficient and extremely challenging.

Typical altitude versus time or range plots, for Concorde, are shown in **Fig.4.2.4**. In **Fig.4.2.4(a)** aircraft weight and fuel used fraction are shown at various significant points during the flight. We note that 23% of the block fuel (WFB) has been consumed by the time the aircraft reaches M 1.7 at 47,000 ft. Aircraft weight (%MTOW) is shown at significant points during the flight in **Fig.4.2.4(b)**. At M 1.7, 47,000 ft, the aircraft weight has reduced by almost 10%, representing 23% WFB. On landing, WFB (total consumed) is equivalent to 42% MTOW.

Typical flight profiles (altitude versus M and C_L) from M^{c}Donnell studies are shown in **Fig.4.2.5**. In this case, 26% WFB is consumed during climb to M 2.0 cruise at 55,000 ft and 10% WFB is used during descent.

We consider typical weight breakdown of Concorde and projected cruise vehicles as shown in **Fig.4.2.6**. Using current technology (fly-by-wire, improved materials and structures, more efficient engines etc.), the overall weight of a "derived Concorde" could be reduced and the range increased. The payload fraction would increase from 5 or 6% to 7.6%. Further, a scaling to a 250-seater, 760,000 lb aircraft is shown. Aircraft structure weight (OEW) ratio remains fairly constant at 42% to 43% MTOW. Typically supersonic aircraft are 50% fuel which includes reserves equivalent to 9% to 10% MTOW. The reserves amount to 50 - 60% more than the payload. Aircraft weight varies during supersonic cruise from about 75% to 55% MTOW. This implies corresponding reductions in W/S, noting that C_L is near 0.1 at supersonic cruise. Typical landing weights may be up to 60% MTOW.

An example of fuel usage and weight breakdown for a SST over a range of 5,500nm is shown in **Fig.4.2.7** (Ref.10). It is interesting to note that a quarter of the fuel (26%) is burnt in climb-out / acceleration in reaching a M 2 cruise speed at 55,000 ft. Approximately 10% MTOW fuel is carried for contingency and reserves.

Fig.4.2.8 (based on Ref.10) emphasizes the drag breakdown for a SST. Extreme care needs to be exercised in the interpretation of C_{D0}. The correction required from model tests to flight is large and its impact on aircraft fuel burnt is of the same order as the payload. Further detail is in Ref.10. Reduction of C_{D0} is literally the challenge for supersonic flight. Wing skin friction drag contributes 35% of C_{D0} , while the fuselage skin friction contributes 15% of C_{D0}. For the future, this continues to emphasise the need for laminar flow control, passive or active.

Fig.4.2.9 shows a possible military mission. We would obviously like to quantify the configuration related parameters e.g. C_L, best altitude etc. within practicality and feasibility limits considering current (state of the art) and future technology. The military mission shows in-flight delivery/release of the "payload" but we have to cater for the fail-safe or aborted mission when the payload may not be dropped.

Fig.4.2.10 shows the sfc trends against cruise specific thrust. M and engine bypass ratio are also varied, Ref.11. Thrust requirements, drag levels, at cruise M of up to 4.0 will impose sfc limitations on conventionally designed turbojet engines and intakes.

From this brief overview of supersonic aircraft design, future ambitions and current capabilities, we compile the following list of areas of interest and concern.

Areas of Interest and Concern

As cruise design target rises, the aircraft design will become more slender, M 3 desired
Slender aircraft have limited low speed capability (Take-Off and Landing)
- Low speed problems can dominate
- With or without vortex lift – substantial difference to be noted at design stage
- Runway length limitations (up to 10,000 ft)
- Take-Off and Landing speeds
- AR, 14^o rotation limit, undercarriage weight / strength limits

S&C complications associated with slender aircraft – with or without vertical fin
Need to quantify impact of S&C at all stages of design
Two surfaces, Canard or Tail-plane
Re-Design Concorde without S&C constraint

Specific Problem Areas

Asymmetric case (4^o – 5^o β), Engine-out, Cross-wind 30 kt (low or high speed)
Wing drop – Transonic speeds in yaw (4^o).
- "Springing" vortices – one wing supersonic, the other not.
- TE sweep low – mixed flow – could diverge. Outer elevons locked

Vertical Fin on Super Sabre F-100 had to be enlarged
High Speed Yaw on Blackbird SR71 due to mixed compression engine unstarts, move spike to equalize.
Controls – often over-sized. Increases OEW and hinge-moment penalties
Inertia implications. Full aileron deflection required first to give impetus, then ease off.
$C_{l\beta}$ and Wallowing, Dutch Roll
Propulsion issues sfc, Payload Range
Fuel Transfer to shift cg to compensate for CoP shift with M
Controllability at high α,
HP 115 boundaries beyond usual but pilots could handle it – low roll inertia

General Comments Relating to Supersonic Aircraft Design

High speed design beset by low speed issues
Propulsion sfc and M variation
Current estimates (low by-pass) – 1.2 at M 2.0, 1.4 at M 3.0, etc
Weights and intended Range – note trade-off with sfc
Number of engines and layout
T/W near 0.4
High speed yaw, XB-70, vertical fin(s), $C_{l\beta}$
Take-Off speed about 200 kt (M 0.3) α 14^o
Vortex lift implications
Descent, operating at back of drag curve, consider thrust reversal
Landing with parachutes
Fuel Transfer

4.3. XB-70

The North American XB-70, Valkyrie, was the prototype for the proposed B-70 deep penetration bomber. It was designed in the late 1950s with M 3.0 capablity at 70,000 ft. It was powered by six GE YJ93-GE-3 turbo-jet engines (with re-heat). The engines were rated at 30,000 lb static thrust. The intended design range was “Intercontinental” but flight test analysis suggested that this had been over estimated by 25%. This was attributed to a combination of L/D over-estimation and transonic drag and inlet performance under-estimation. The S&C aspects with two surface layout played a great role in bestowing adequate low-speed handling.

Two prototypes were built and flown from 1964 to 1969 but the development project had been cancelled in 1961. Several publications, including Refs.16 to 21, are specifically related to XB-70 design, development and flight test. The experience gained during the XB-70 flight test and evaluation progranmme will be invaluable in the design of future supersonic aircraft.

Analysis of early flight data, Ref.18, highlighted key areas of interest relating to handling, performance and noise (observability). The general handling qualities and performance were found to be satisfactory. However, excessive elevon trim requirements led to adverse aileron yaw characteristics. Landing and approach speeds were 40 to 50 kt higher, with similar sink rates, than jet transports of that era. An appreciable Lift increase in Ground effect was noted. Temperature increases due to skin friction heating effects at high speed were measured and compared well with predictions. It was noted that “dense” structures such as the folding tip actuators experienced thermal gradient lag. This would be of interest and perhaps concern to structural engineers. Cockpit noise levels at supersonic speeds were comparable to jet transports in cruise flight. It was found that sonic boom effects, measured on the ground, might occur with the aircraft operating at higher altitudes than anticipated. S&C discrepancies between flight test data and those predicted from wind tunnel tests are partially attributed to aero-elastic effects.

The general assembly and leading particulars for the XB-70 are shown in **Fig.4.3.1**, noting in particular folding tips hinge-line and control surface range and axis of movements (Fin/Rudder, Trailing Edge Flap (TEF) and Canard). **Fig.4.3.2** shows the flight envelope and restricted areas for particular tip deflection angles. Flight test and predicted data are compared in **Fig.4.3.3** at typical cruise conditions, M 3.0, α 4^{o}.

XB-70 weight variation during a M 3.0 test flight is shown in **Fig.4.3.4** together with corresponding cg shift, Ref.17. Take-Off (TOW) and Landing weights are 534,700 lb and 280,300 lb. Typical OEW is about 210,000 lb (39 % MTOW). Total fuel consumed at end of M 3.0 cruise is about 230,000 lb and after landing is 254,700 lb WFB 47% MTOW).

Typical climb-out profiles (Altitude v M) for proposed supersonic transports and a hypothetical XB-70 profile are compared in **Fig.4.3.5**. In general, the less extensive transport profile lies within the XB-70 profile. Also shown are the climb-out profile for an XB-70 M 3.0 test flight and test data-points, Ref.17. Further climb-out and descent profiles and test data-points are shown in **Fig.4.3.6** together with tip deflection requirements. The latter envelope compares with **Fig.4.3.2**. The variation of moments and products of inertia with aircraft weight are shown in **Fig.4.3.7** during M 3.0 flight.

XB-70 S&C characteristics were evaluated from early phases of the flight test programme. It was noted that S&C flight test data, for the three wing tip deflection cases, compared well with predictions based on wind-tunnel tests and theoretical estimates of structural flexibility effects (aero-elasticity). During the early phases of the test flight programme, Take-Off and Landings, the “augmentation” system (effectively dampers within the flight control system) was disabled.

The following summarises some of the key points noted from the flight test analysis:-

- Short-period and Dutch roll modes of the unaugmented Aircraft were positively damped.
- Longitudinal damping characteristics tended to correspond with predictions for the flexible aircraft.
- Fairly heavy damping ratio of about 0.5 evident at low speeds.
- Light damping ratio of about 0.1 at high supersonic speeds
- Dutch roll damping of about 0.2 or less throughout M range had been underestimated at supersonic conditions due to underestimation of yaw damping due to yaw rate.
- Neutral point was at approximately 30% c_{aero} for 25^{o} and 65^{o} wing tip deflection cases at supersonic speeds and at 27% to 29% c_{aero} at subsonic speeds with wing tips undeflected. Predicted values had been slightly higher.
- The XB-70 exhibited adverse (negative) aileron-yaw coupling at M > 0.9. Favourable coupling characteristics had been predicted. Positive values of aileron-yaw coupling were obtained at subsonic speeds but of lower magnitude than predicted.
- Flight evaluated effective dihedral was negative for 65^{o} deflected tips and higher than predicted. This, combined with the adverse aileron-yaw characteristics, could lead to pilot induced oscillations.
- Flight tests showed a marked reduction in directional stability beyond β 2^{o}. Wind-tunnel data showed this non-linearity to be a canard interference effect.
- Rigid wind-tunnel model compared with flight test data showed the effects of aero-elasticity to be significant for static pitch stability, pitch control effectiveness, roll-control effectiveness, static directional stability and effective dihedral derivatives.

4.4. Concorde

The following are selected key observations relevant to low speed handling S&C issues for supersonic aircraft design, Ref.22.

Ground handling

The entire Concorde structure was designed to tolerate heat and thermal expansion. To ensure that the expansions did not induce structural loads in their own right, pin jointed arrangements were incorporated, allowing deflections without extra loads. This led to a very floppy structure. As a result the flight-deck ride was "quite violent" during the take-off run, reaching +/-2g. This was sufficient to dislodge pilots' headsets and flight instrumentation became unreadable as rotation speed was approached. Modifications resulted which included replacement of the original single-stroke oleos with a two-stroke system. This produced a 25% reduction in loads but was still not fully satisfactory.

Take-off

Re-heat is on at take-off. This gives very impressive acceleration at lighter weights. The engines were certified with a contingency rating allowing them to be "over-rated" in the event of an engine failure during take-off. The reheat system was found to be unstable in high ambient temperatures when operated at the contingency rating. There were many occurrences during early flight test phases and this led to a redesign of the reheat fuel spray system. Fortunately, concerns over the engine life limitations due to frequent over-rating were unfounded.

The main parameter for accurate performance is a requirement to rotate to a very precise attitude depending on T/W. This was established after considerable trial and error.

High Incidence

The vortical flow over the wings arises at α 7^o, virtually irrespective of speed, and this led to high frequency buffet of the wing-tips. The wing-tips appeared blurred when viewed from the cabin. The induced buffet was stronger at higher weights.

As α increases, C_m becomes unstable (pitch up). At around α 20^o, there is a marked breakdown in directional stability due to the fin being effectively blanked. One way of delaying this was by using nose strakes on the forward fuselage to re-energise the flow. Douglas pioneered such strakes on DC-9 and MD-80/90 series.

At higher α, beyond the breakdown of directional stability, more marked C_m occurred but flight is impractical at such high α.

Each of these aspects need to be considered during the design phase of any supersonic aircraft.

5. SUPERSONIC PLANFORMS (Vortex Lift, Drag and S&C)

A preliminary assessment of planform variations was made in Section 4. **Fig.4.1.1** shows the kernel of the idea on deriving a combat configuration from the Concorde planform. We note that intake positions are likely to be different from that on Concorde. A driver for this is stealth.

5.1. Vortex Lift Significance

Vortex development and possible breakdown trends are sketched and outlined in **Fig.5.1.1** for various planforms. Highly swept, straight LE Deltas encourage vortices to form close to the LE. At some spanwise location, the vortex strength will be sufficient for it to detach from the LE and align streamwise. A LE crank created when the outer wing panel is unswept will encourage the vortex on the highly swept inner panel to align streamwise. The outer panel does not create a LE vortex. Concorde relied upon a carefully designed curved LE to generate a stable vortex system for high lift at low speed.

Typical $C_L - \alpha$ and $C_{Di} - C_L$ relationships are sketched in **Fig.5.1.2** for a planar wing without and with LE devices. This figure illustrates the additional vortex lift and its effect on drag. LE devices utilize the suction forces in reducing drag.

Fig.5.1.3 gives an idea of other planforms that can be envisaged. For the current discussion we use planform ES01 (AR 2.09). **Fig.5.1.4** shows the high-speed characteristics assuming neutral longitudinal stability, at low speed. **Fig.5.1.5** shows the evaluation of the same wing at low speeds. **Fig.5.1.6** refers to L/D and low speed performance available without (**Fig.5.1.6(a)**) and with (**Fig.5.1.6(b)**) assumption of vortex lift. The plots show L/D – M with W/S and C_L varying. Such figures help in deciding the take-off and landing characteristics of the viable design. Incidences of more than 14^o are not feasible. L/D reduces with vortex lift.

Fig.5.1.7 shows take-off characteristics with respect to range, without and with vortex lift assumptions. In these figures, M – Range, carpets of constant W and W/S are layered for varying α. Such fundamental graphs and cross-plots begin to indicate the viability of the unique application within the weight constraints envisaged. The concept looks encouraging and further work is needed to focus on appropriate detail.

A similar arrow wing planform but with increased sweep on the outer wing panel is shown in **Fig.5.1.8**. The effects of deploying LEF at various angles have been assessed. Without the LEF deployed, the C_L – α relationship indicates that vortical flow is present above α 4^o. As α increases, C_m becomes more positive (unstable). LEF deployment "kills off" the vortical flow. The configuration becomes more stable at higher α and drag is reduced. Typical vortex patterns, at α of interest, are also sketched in **Fig.5.1.8**. The variation of L/D with C_L, at low speed, with LEF deployments is shown in **Fig.5.1.9**. Also shown are the attained suction levels and the effect of LEF angle.

This type of analysis highlights the various technologies that need to be studied and possibly "pushed".

5.2. Drag Breakdown, Typical Example

The development of ATSF planforms with increasing AR are shown in **Fig.5.2.1** and compared with the Concorde planform. We note the increasing L/D as AR increases. The effects of wing planform and engine location are significant.

Typical supersonic transport drag breakdown is shown in **Fig.5.2.2**. This figure was previously discussed in Section 4.2 and has been revisited to emphasise the importance of, and difficulty in assessing, overall drag. Corrections required from model tests to flight are large and their impact on aircraft fuel burn is of the same order as the payload in this civil transport example. At cruise, maximum L/D requires that C_{Di} and C_{D0} are similar. In this example C_{Di} and C_{D0} are 61 "counts". Reduction of C_{D0} is literally the challenge for supersonic flight. Wing skin friction drag contributes 35% of C_{D0} , while fuselage skin friction contributes 15% of C_{D0}. This emphasises the need for laminar flow control, either passive or active in future aircraft designs.

5.3. S&C Implications

A series of flight tests were carried out on Concorde test aircraft (towards the end of the flight test programme) to simulate the advantages of relaxed longitudinal stability in terms of increased L/D at low speed. **Fig.5.3.1**, Ref.23, shows L/D variation at constant trimmed C_L values (0.45, 0.55 and 0.65) as xcg is varied (53%c_o, 56% c_o and 59%c_o). As M increases from 0.20 to 0.75, the aerodynamic centre shifts from about 53%c_o to 56%c_o. The results in **Fig.5.3.1** indicate up to 15% increase in L/D at C_L 0.55 for about 5% c_o relaxed stability. However, this potential could not be introduced for the aircraft in airline service. The aircraft featured fuel transfer tanks for trim and most probably, there was insufficient capacity for the instability range required. Elevon angles required to trim are also noted in the figure.

Using Linear Theory and a First Order Panel method we have been able to simulate the relaxed longitudinal stability cases, estimate Elevon angle required to trim and predict increases in L/D

arising from reduced C_{Di}. Results in key areas have been confirmed using Euler methods. **Fig.5.3.2** shows the simplified Concorde planform, c_o location and typical 50% to 60%c_o range. The variation of cg position with M is shown in **Fig.5.3.2(b)** from published data, e.g. **Fig.5.3.1**. Areas where the envelope is restricted due to controls travel limitations, stability and hinge moments are noted. The predicted aerodynamic centre movement with M from Linear Theory and Euler agree well with the aircraft data at high speed ($1.2 < M < 2.0$). There is a minor, consistent difference at low speed (<1.0%c_o) using the Panel method. This is very encouraging from "anchoring" the technique available.

Considering the low speed, M 0.3, neutrally stable case (cg at aerodynamic centre, zero static margin) **Fig.5.3.3** shows $C_{L\alpha}$ variation with M. There is good agreement between the various theoretical methods. **Fig.5.3.4** shows $C_L - \alpha$ variation at M 0.3 from Linear theory. We note the 0% and 100% suction trends. The attained suction values for flight Re based on c_o assuming representative t/c distribution gives an indication of the vortex lift contribution.

The variation of C_{Di} with C_L, Linear Theory, is shown in **Fig.5.3.5**. Curves for 0% and 100% suction levels show the typical C_{Di} range. Assuming C_{D0} of 0.0070, we obtain L/D variation with C_L, **Fig.5.3.6**, for 0%, 100% and attained suction levels. The fuselage has not been modelled for these preliminary cases. Neutrally stable L/D values from experiment are shown in **Fig.5.3.6**. As C_L increases, L/D values from experiment tend towards the 0% suction values. Further published low speed L/D trends with C_L are shown in **Fig.5.3.7**. These data have been used to confirm the theoretical methods and analysis.

Theoretical $C_m - C_L$ trends were established at low speed for the datum case as static stability margin varied. The TEF deflection required to trim was evaluated. The resulting theoretical L/D at constant C_L (0.45, 0.55 and 0.65) and constant TEF values (0^o, 5^o and 10^o) are compared with experiment (**Fig.5.3.1**) in **Fig.5.3.8**. The data from **Fig.5.3.8** is replotted in **Fig.5.3.9** as L/D versus %c_o instability margin. **Fig.5.3.10** shows the variation of %L/D gains (based on L/D value at 0% stability margin) achieved with increased instability margins. There is good agreement between theory and experiment and the advantages in terms of aerodynamic efficiency for relaxed stability are evident.

At low speed, theory predicts that relaxing stability by 7%c_o provides an increase of 25% L/D at C_L 0.55. In experiment, an increase of over 21% was achieved.

6. PLANFORM VARIATIONS

Aircraft with a wide M range capability will experience significant changes in centre of pressure (CoP) location. For trimmed flight the cg coincides with the CoP. Variable geometry (swing wing) moves CoP appropriately, allowing the cg to remain fixed with only small control surface deflections to trim. Fuel transfer systems move the cg appropriately to match CoP. Relying totally on control surface deflections to trim will results in unacceptable drag penalties.

We seek the near optimum planform having minimal CoP movement over the desired M range. However, we anticipate that the optimum planform may not have the M range capability or be suitable in other respects for the design requirement. A desirable compromise may require variable geometry, e.g. sweeping or folding wings, etc. We review various planform options, taking into account M range, S&C aspects (CoP shift with M) and Efficiency (L/D achieved).

6.1. Series of Planforms with Mach Effects

A series of planforms was evaluated, Ref.12, to determine CoP characteristics over a wide M range. Results are shown in **Fig.6.1.1**. The basic delta type (WA-T) has a large CoP variation with M. As AR increases (reduced sweep outer wing panels introduced – WA-1, WA-2, WB-1

and WC-1) the CoP shift decreases. Planform WB-1 exhibits the least CoP shift with M varying but low supersonic $C_{L\alpha}$ is quite poor.

We consider a simplified XB-70 planform, Leading Edge and Trailing Edge sweeps, Λ_{LE} 65^o and Λ_{TE} 0^o with finite tip chord and use Linear Theory to predict CoP movement through the M range (0.2 to 3.0). Retaining the inner planform (0.0 < y/s < 0.6), the outer Λ_{LE} is reduced by increasing the span by factors of 1.20 and 1.35. The AR increases from 1.713 to 2.263 and 2.697 respectively. The process is repeated for a Λ_{LE} 70^o planform, AR 1.337. In this case the span is increased by factors of 1.30 and 1.60, giving AR of 1.991 and 2.695 respectively. The resulting planforms are compared in **Fig.6.1.2**. The $C_{L\alpha}$ variation and CoP location (%c_o) are plotted against M in **Fig.6.1.2**. In terms of CoP shift from low speed location to M 3.0 cruise location, the 70/48 planform has the least change. However, this planform exhibits the widest CoP variation within the 1.0 < M < 3.0 range.

Considering an XB-70 planform (Λ_{LE} 65^o) with TE cut-outs (see Section 8), uncambered sections, at supersonic conditions the CoP location could be controlled by folding the wing about 65% semi-span. At a fold angle of 90^o, M 2.0, the CoP is co-incident (streamwise) with the subsonic location (0^o fold).

Further planform shapes of interest are shown in **Figs.6.1.3** & **4**.

7. GROUND EFFECTS

We consider Ground Effect on S&C characteristics as a possible requirement early in the design sequence. Conventional Ground Effect and S&C wisdom is based on aircraft test flights rather than considerations during design. Control sizing may therefore be compromised.

In general, early theory work has been carried out with Vortex / doublet lattice methods and simple trailing wakes parallel to the ground with results presented in several papers. Also a considerable number of papers have used panel methods without and with relaxed wakes.

For delta planforms, TE flow dominates. Based on intuitive arguments, starting from slender-wing theory, the lift on a delta type planform is simply dependent on AR and the slope at TE (or effective upwash at TE). Thus

$$C_L = AR*0.5*\pi*(w/V)_{TE}$$

Under ground-effect, using an image of the wing as a reflection plane, the w/V term becomes larger and C_L increases. However, we need to be more accurate in this analysis and take into account many other geometry and flow characteristics.

For slender delta wing planforms, in particular, further complexities may arise due to LE Vortex flow. If present, its inclusion will affect the results since at a given α, the total lift is higher.

We consider a simplified XB-70 planform (Λ_{LE} 65^o, finite tip chord and Λ_{TE} 0^o) and look at the effects of ground proximity (h/b) on longitudinal and lateral control at low speed. Trailing Edge (TE) control surfaces are modelled and deflected symmetrically or differentially to provide pitch and roll control. The effects of modelling the trailing wake parallel to the stream flow or fully relaxed are assessed. Various theoretical methods are compared.

7.1. Longitudinal Effects

The rigid trailing wake geometry in free air (out of Ground Effect) at M 0.3, α 16^o (Panel method) is shown in **Fig.7.1.1**. Resulting C_L and C_m values are 0.597 and –0.00358 (0% static stability margin). Relaxing the wake reduces C_L and C_m slightly (0.595 and –0.00206). The effects of wake relaxation in Ground Effect are more significant.

The relaxed trailing wake geometries at M 0.3, α 12^o, free air and h/b 0.2 (PMARC method) are shown in **Fig.7.1.2**. Resulting C_L and C_m (wing apex) values are 0.5161 and –0.4968 for free air and 0.5843 and -0.5653 at h/b 0.2.

For the corresponding case, Panel method gave C_L and C_m (0% static stability margin) 0.452 and –0.00024, free air and 0.559 and –0.01728 h/b 0.2.

The increase in C_L and nose pitch down experienced by this class of wing on landing is immediately evident. However, the PMARC method did not appear to give a reasonable representation of the wake geometry roll-up. Wake relaxation analysis continued using Panel methods.

The Panel method was used to extend the Ground Effect database at M 0.3. A nominal C_L range was targeted (0.4 to 0.6) requiring an incidence range of $10^o < \alpha < 16^o$ for the free air and h/b 0.5 and 0.2 cases. The effects of TE flap (TEF) angle, 0^o and -5^o (TE up), were included. The resulting $C_m - C_L$ carpet, for 0% static margin, is shown in **Fig.7.1.3**. We note the non-linear trends arising from the effects of ground proximity, TEF deflection and wake relaxation. Increasing the static stability margin (5% c_o) implies a further non-linearity, **Fig.7.1.4**. TEF deflections required to trim at various C_L, h/b and static stability margins, M 0.3, are shown in **Figs.7.1.7-9**.

Relaxed wake geometries are shown for M 0.3, C_L 0.6, trimmed (C_m 0.0, 0% stable static margin) in **Fig.7.1.5**. The "free air" case, **Fig.7.1.5(a)**, shows typically rolled-up tip vortices lying nearly parallel to the freestream. An incidence of 16.4^o with -0.5^o TEF deflection is required to provide C_L 0.6 with C_m 0.0 (trimmed). As the aircraft sinks and enters ground proximity, h/b 0.2, C_L tends to increase with an accompanying nose down pitch tendency. The TEF deflection is increased to -5.0^o to trim and α reduced to 14.0^o to maintain C_L 0.6. A rolled-up vortex pattern can be seen forming at the inboard end of the TEF, **Fig.7.1.5(b)**. At the outboard end of the TEF, the trailing vortices roll-up and into the tip vortices which splay outwards due to ground proximity.

In "free air", the 5% stable case requires more TEF deflection (TE up) to trim. The subsequent loss of lift requires increased α to maintain C_L 0.6. Relaxed Wake geometries are shown for M 0.3, C_L 0.6, trimmed (C_m 0.0, 5% stable static margin) in **Fig.7.1.6**. The "free air" case is shown in **Fig.7.1.6(a)**. Again, as the aircraft enters ground proximity, h/b 0.2, it experiences an increase in C_L and a nose down pitch tendency. The TEF deflection is further increased to compensate (-12.9^o) but α reduced to 15.7^o to maintain C_L 0.6. Both the tip vortices and the TEF inboard vortices are more noticeably splayed outwards due to ground proximity, **Fig.7.1.6(b)**.

The TEF deflection requirements are summarized in **Fig.7.1.7** for two stability margins (0% and 5%c_{ave} stable) and effects of ground proximity. The effect of wake relaxation is clearly evident when **Figs.7.1.7(a)** and **(b)** are compared.

The variation of TEF required to trim as static stability margin varies is shown in **Fig.7.1.8**. Results for rigid trailing wake are shown in **Fig.7.1.8(a)** and for relaxed wakes in **Fig.7.1.8(b).** The additional TEF deflections required using relaxed wake analysis are shown in **Fig.7.1.8(c)** and are shown as percentage increments in **Fig.7.1.9**. We note, in certain cases, e.g. "free air" or out-of-ground-effect case at 0% stability, that we are looking at small angular increments due to wake relaxation as a percentage of small TEF angles predicted using rigid wakes. Results for the 5% c_{ave} stability case are more suitable, where, across the C_L range considered, rigid wake analysis predict TEF of about 10^o at h/b 0.2. Using relaxed wake analysis 10% more TEF is required at C_L 0.45 rising to 18% more TEF at C_L 0.6.

This brief analysis of Ground Effects on trim and control surface requirements has clearly shown that these S&C effects must be considered early in the design sequence to ensure that adequate

control power is available (control area and angular deflection). We have considered two stability margins, a third would confirm any non-linearity effects that may need to be considered.

7.2 Sideslip Effects

On landing and take-off, cross-winds may be present. Even though supersonic aircraft have somewhat higher ground speeds, effectively reducing cross-wind effects, 4^o β still needs to be allowed for. Also, yaw arising from engine flame-outs may be considerably greater and needs to be considered.

The Panel method was used to determine sideslip effects in Ground Effect at M 0.3, 0% static margin. A nominal incidence was selected (α 12^o). Free air, h/b 0.5 and 0.2 cases were considered. The effects of Aileron deflection are included.

TE devices "neutral" (Undeflected)

Rolling moment (positive right wing up) and pitching moment variations ($C_\iota - C_m$), arising due to sideslip and ground effects are shown in **Fig.7.2.1** (M 0.3, α 12^o, TEF 0^o). Results from rigid and relaxed wake analysis are compared, dashed and solid lines respectively. Relaxing the wakes tends to give lower C_ι results. In "free air", the small $-C_m$ (nose down) result, arising from errors introduced by rigid wake representation at incidence, is eliminated when the wakes are relaxed. As h/b is reduced, C_m becomes more negative. The effect of wake relaxation is significant, increasing the magnitude of the negative C_m as h/b is reduced. At β 10^o, rigid wake results over predict C_ι (equivalent to $2^o\beta$) and under predict C_m by up to 30% at h/b 0.2.

TE devices, Differential Deflection (Ailerons)

Aileron roll power and variation of C_ι due to sideslip are shown in **Fig.7.2.2** (rigid trailing wakes). Positive aileron angle, of 10^o say, implies right TEF deflected 10^o TE down and left TEF deflected 10^o TE up. This induces positive C_ι. Rolling moment increases linearly with aileron angle. As height above ground (h/b) is reduced aileron roll power reduces slightly. As β increases, C_ι becomes proportionally more negative. Wake relaxation will have a significant effect.

The combined effects of aileron, β and h/b on C_ι - C_m variation and the effects of wake relaxation are shown in **Fig.7.2.3**. Incidence remains constant at 12^o and, as a result, C_L varies slightly over the h/b – β carpet. This would require trimming to constant C_L for a full analysis. Rigid wake results are shown in **Fig.7.2.3(a)** and those for relaxed wake analysis in **Fig.7.2.3(b)**. We note immediately, the non-linear trends arising from the effects of h/b, aileron deflection and wake relaxation. At β 5^o, h/b 0.2, rigid wake analysis predicts that 14^o aileron is required to trim C_ι. A further -1.3^o TEF (TE up) is required to trim C_m giving TEF deflection of -15.3^o / $+12.7^o$ to trim with rigid wake analysis. Using relaxed wake analysis, TEF deflection required is -14.5^o / $+10.5^o$.

Relaxed Wake geometries are shown in **Fig.7.2.4** for two cases at M 0.3, α 12^o, β 10^o, 0% stable static margin, free air **Fig.7.2.4(a)** and h/b 0.2 **Fig.7.2.4(b)**. We note the 23% increase in C_L as h/b reduces to 0.2, the nose down pitch tendency (C_m -0.06731) and the increase in C_ι. Relaxed wake geometry for M 0.3, α 12^o, β 10^o, 0% stable, h/b 0.2, but with 20^o aileron, is shown in **Fig.7.2.5**. Comparing this wake with that in **Fig.7.2.4(b)** shows the effect of aileron and h/b. At M 0.3, β 0^o, 20^o aileron gives almost constant C_ι +0.055 as h/b reduces to 0.2. Out of ground effect, "free air", as β is increased to 10^o, C_ι reduces almost to zero. At this condition, reducing altitude to h/b 0.2, induces negative C_ι equal to 5^o aileron. These effects are somewhat different to those obtained with rigid trailing wakes (wakes parallel to freestream).

Further theoretical predictions with TEF deflected to trim C_L to a constant value, are required to complete the trim analysis. However, a further estimate of 30^o aileron to trim at β 10^o, h/b 0.2

(possible engine-out case) can be made. When pitch trim is also taken into account it is possible that control saturation may become significant.

It should also be noted that aero-elasticity is likely to have significant effects on the prediction of control surface requirements.

8. FOLDED TIPS

The XB-70 research aircraft was discussed in detail in Section 4.3. The Flight Envelope and Performance enhancement aspects of variable geometry (folding tips) are now considered.

8.1. XB-70

Typical XB-70, Concorde and a folding wing type SST flight envelopes (Altitude – M) are shown in **Fig.8.1.1**. **Fig.8.1.1(a)** shows the XB-70 envelope from Refs.24-25. In **Fig.8.1.1(b)** the Concorde flight envelope is superimposed on that of the XB-70. For a configuration without folding tips or variable geometry for supersonic flight, the restricted envelope is evident. **Fig.8.1.1(c)** considers expanding the flight envelope of a next generation SST using folding tip geometry. Typical fold angle (ϕ) requirements are noted.

8.2. XB-70 derived planform

A derived XB-70 planform is shown in **Fig.8.2.1**. Using Linear Theory and Euler methods, $C_{L\alpha}$ (based on unfolded wing area) has been evaluated for various ϕ across the supersonic M range, **Fig.8.2.1(a)**. Flight test data for the XB-70 is also shown, assuming ϕ of 25^o and 65^o at M 1.2 and 2.0 respectively. Linear theory and flight test data compare well at M 2.4 – 2.5, ϕ 65^o and are reasonably close at 25^o at M 1.2, the discrepancies may be attributed to modeling methods and AR effects.

Normalised $C_{L\alpha}$ data ($C_{L\alpha}$ / $C_{L\alpha\,\phi=0}$) are shown in **Fig.8.2.1(b)**. This emphasises the fact that the non-linear Euler predictions indicate lower Lift loss due to fold angle than Linear Theory.

8.3. ES Series derived planform

For this series of planforms, the wing flies supersonically with the tip folded down by specific angles (40^o, 60^o, 70^o, 75^o). When folded, all the wings have the same projected planform. Two spanwise locations for the hinge-line were considered (y/s 0.667 and 0.800). The effect of tip fold location and angle on lift performance at M 2.0 is shown in **Fig.8.3.1**. Assuming requisite fold angles at supersonic conditions, the CoP shift is relatively limited.

We have noted that the potential CoP rearward shift, as M increases, on this class of wings can be reasonably controlled by use of folding tips. During flight test of the XB-70, longitudinal stability was adequately controlled and no significant problems were encountered. Performance penalties attributable to the folding tip technology (weight, stress, etc.) need to be quantified.

9. CONTROLS

In this section we look, briefly, at various aspects of stability and control on typical planforms over a wide M range. The wing planforms considered are representative of Concorde, XB-70, Space Shuttle and a typical Hypersonic vehicle.

9.1. Fin Effects – Concorde (Single Fin)

High Order Panel and Euler Methods, M range, Incidence and Sideslip effects

Surface flow patterns (Euler method) on various combinations of Concorde wing, fuselage and fin are shown in **Figs.9.1.1** to **4**. Asymmetry in the wing (only) upper surface flow field, M 2.0, α

4^o, β 4^o, can be seen in **Fig.9.1.2**. Introducing fuselage geometry does not significantly alter the asymmetry, **Fig.9.1.3**. Further addition of fin geometry only slightly affects the wing upper surface flow field but there are significant effects on the fin itself. Typical force and moment variations with sideslip, Euler and High Order Panel methods, at M 2.0, α 4^o are in **Fig.9.1.5**. Wing, fuselage and fin contributions are shown. These variations are shown at M 0.3, High Order Panel method, in **Fig.9.1.6**. Typical lateral derivatives are presented in **Fig.9.1.7** to show the effects of Fin modelling.

The effects of fin on the lateral derivatives are shown in **Fig.9.1.7**. Results from High Order Panel and Euler methods are compared. The main contribution to $C_{Y\beta}$ arises from the fin and this varies with M. There is very good agreement between the methods at M 2.0. Fin loading has its own input to roll and yaw and also, with the fin present, there are Mach line interference effects on the wing, which vary with sideslip. This results in noticeable fin effects on $C_{n\beta}$ and $C_{\iota\beta}$. There is good agreement in $C_{n\beta}$, fin on, between the methods at M 2.0. The panel method, fin off results, indicate unstable $C_{n\beta}$. There is an apparent disagreement in overall $C_{\iota\beta}$. We note that the fuselage is modelled in the Euler calculations but not in the High Order method. Both methods indicate stable, negative $C_{\iota\beta}$. There is very good agreement in the magnitude of $C_{\iota\beta}$ increment due to the fin at M 2.0. There is a slight variation in $C_{\iota\beta}$ subsonic to supersonic with a peak near M 1.0.

The variation with α at M 2.0 of the various component contributions to $C_{\iota\beta}$ are shown in **Fig.9.1.8**. At α 4^o, the addition of the fuselage to the wing model halves $C_{\iota\beta}$. The addition of the fin quadruples the wing-fuselage $C_{\iota\beta}$.

9.2. Aileron Effects - Concorde, Fin effects

Strong interactions between fin and elevons were noted during the design and testing stages of Concorde. As a result, fin design and control surface scheduling modifications were necessary.

Inner Elevons only deflected, full M range

The Concorde geometry, shown in **Fig.9.1.1**, with inboard elevons deflected +/- 1^o was used to determine the variation of rolling moment coefficient (C_ι) at α 4^o throughout the M range. The results, with and without fin present, are shown in **Fig.9.2.1** for both first and high order panel methods. There is a marked non-linearity effect as M varies. In the subsonic range applicable, there is very good agreement between the two methods. At M 0.3 to 0.8, the presence of the fin reduces elevon roll power by about 14%. Elevon roll power reduces dramatically in the range M 1.2 to 2.0. The presence of the fin reduces roll power by 36% at M 1.2 and by 47% at M 2.0. Although unrealistic in terms of C_L requirements over the M range, the constant α results give an insight to the non-linearity effects.

Inner and Outer Elevons deflected, M 0.3, C_L and sideslip effects

The effects of fin, sideslip, C_L and wake modelling on differential elevon roll power at low speed were assessed using a first order panel method. The inner and outer elevons were deflected +/- 0^o, +/- 5^o and +/- 10^o and sideslip varied 0^o, 5^o and 10^o at M 0.3. Incidence was varied to cover the C_L range 0.0 to 0.6. The variation of C_ι with C_L, rigid wake modeling, is shown in **Fig.9.2.2(a)**. In general, the variation is linear and C_ι is proportional to elevon angle for the wing only cases. Positive sideslip (nose to right) results in negative C_ι (right wing down). The fin increases the negative C_ι. The fin effects are proportional to elevon angle but the interference effects decrease slightly with C_L.

The effect of wake relaxation and sideslip angle on the fin present, +/- 10^o elevon case at C_L approximately 0.6 is shown in **Fig.9.2.2(b)**. The wake relaxation increments are significant and proportional to sideslip angle.

It has been noted that the Concorde planform relies heavily on vortex lift at low speed. Using a combination of linear theory and panel method results we are able to assess the effects of vortex lift modeling. The variation of C_ι with β at M 0.3, C_L 0.6 is shown in **Fig.9.2.3** without and with vortex lift contribution to C_L. The effects of fin and differential elevon are shown. The variation with β of differential elevon angle required to trim at M 0.3, C_L 0.6 is shown in **Fig.9.2.4**. Including vortex lift contributions in the analysis reduces the elevon angle required to trim by about 16% for the wing and fin case and by 19% for the wing only case.

9.3. Fin Effects - XB-70 (Twin Fins)

Euler Method M 2.0 and 3.0 Incidence and Sideslip (α 0^o & 4^o, β 0^o & 4^o)

Surface flow patterns (Euler method) on a representative XB-70 wing planform with fuselage, canard and fins (on / off) are shown in **Figs.9.3.1 to 6**. Typical lateral derivatives are shown in **Fig.9.3.7** to show the effects of Fin modeling.

For the complete configuration, surface flow patterns at M 2, α 4^o (β 0^o & 4^o) are shown in **Fig.9.3.1**. Asymmetry in the wing upper surface flow field is clearly evident in **Fig.9.3.1(b)**. Surface flow patterns at M 3, α 4^o (β 0^o & 4^o) are in **Fig.9.3.2**.

Surface flow patterns without the fins present at M 2, α 0^o (β 0^o & 4^o) are shown in **Fig.9.3.3** and at α 4^o (β 0^o & 4^o) in **Fig.9.3.4**. Patterns without the fins present at M 3, for the same α and β angles are shown in **Fig.9.3.5** and **Fig.9.3.6**. The XB-70 fins are integral with the wing and clearly have a significant effect on the wing flow field in sideslip. This is in contrast to the fin effects on the Concorde configuration.

The effects of fin on the lateral derivatives are shown in **Fig.9.3.7**. Naturally there is a significant effect on Side Force derivative ($C_{Y\beta}$) due to fin. This effect appears to decrease slightly as M increases (2 to 3). The loads on the fins have their own input to roll and yaw and also, with the fins present, there are Mach line interference effects on the wing which vary with sideslip. This results in noticeable fin effects on $C_{n\beta}$ and $C_{\iota\beta}$. Without the fins present, $C_{n\beta}$ is negative (unstable). The addition of fins provides positive increment $C_{n\beta}$ which results in positive $C_{n\beta}$ at M 2.0 but near zero $C_{n\beta}$ at M 3.0. At M 2.0, $C_{\iota\beta}$ is negative (stable) but the magnitude reduces as M increases to 3.0. The presence of fins has little effect on $C_{\iota\beta}$. There appears to be no effect of fin on $C_{m\beta}$ and only a small variation with M.

9.4. Space Shuttle (Single Fin)

The Space Shuttle is shown in **Fig.9.4.1**. The (outer) wing planform is 45^o delta with swept TE and extensive fuselage strakes. A Body Flap, spanning the width of the fuselage, is attached beneath nozzles, aft of the effective wing TE. The Shuttle operates over a wide M range, up to M 24. The fuselage has a low fineness ratio. High α are experienced under various conditions and consequently the aircraft has a relatively tall fin. The variations with M of several lateral derivatives are shown in **Fig.9.4.2**. **Fig.9.4.3** shows CoP variation with M and also the variation with M of C_m due to α, elevators and Body Flap. **Fig.9.4.4** shows the variation of $C_{n\beta}$ with α at various M and $C_{n\beta}$ and $C_{n\beta}$* with M. For positive stability, the Dutch Roll stability ($C_{n\beta}$*) must be greater than zero. At this stage we limit our interest to $C_{n\beta}$. Variation of $C_{n\beta}$ with M is summarized, for several configurations considered, in Section 9.6.

In general, there is significant variation of each of these parameters in the subsonic regime and up to about M 2.0. Beyond M 4.0 there is little variation. Current analysis has therefore concentrated on the subsonic and supersonic regimes up to M 3.0.

9.5. Typical Hypersonic Vehicle (Single and Twin Fin)

A possible hypersonic vehicle layout is shown in **Fig.9.5.1**. The wing planform (A0) is similar to the space shuttle. The fuselage is more slender. The analysis has focused briefly on lateral stability aspects of a single, centerline, vertical fin mounted on the fuselage (A1) or twin fins located at the wing tips (A2). The total side projected area of the twin fins is approximately equal to that of the single fin.

The variations of C_L at α 4^o and lift curve slope ($C_{L\alpha}$) with M are shown in **Fig.9.5.2**. At subsonic speeds, the twin fins act as winglets and increase Lift. There is little effect under supersonic conditions. The variation of CoP with M is shown in **Fig.9.5.3**. The addition of fins dramatically reduces the CoP shift experienced by the wing only case (A0). Low speed (M 0.4) Force and Moment results are shown in **Figs.9.5.4** to **6**. We note the Lift increment afforded by the twin fins up to α 15^o. Beyond this incidence there is a detrimental effect on Lift. The $C_A - C_L$ curves indicate a slightly earlier and more significant break for the twin fin case compared to the wing only. **Fig.9.5.5** shows CoP variation with α and C_L at M 0.4. CoP for the wing only remains fairly constant with α and C_L. As α increases, 4^o to 20^o, CoP shifts rearwards by about 4% c_o on the twin fin case. Pitch and Drag variations with α and C_L, for wing only and twin fin cases are shown in **Fig.9.5.6** at M 0.4. The fins introduce a drag rise at about C_L 0.55. This is confirmed in the $C_D - C_L^2$ plot **Fig.9.5.6(b)**. At M 0.4, pitch up on the wing only occurs at about α 18^o, C_L 0.65, **Fig.9.5.6(c** & **d)**. Addition of the fins results in early pitch up, α 8^o, C_L 0.30.

A comparison between single and twin fin effects on the lateral derivatives is shown in **Fig.9.5.7**. Results for M 2.0, α 4^o are currently available. Despite the twin fins having total area equal to the single fin, the twin fin $C_{Y\beta}$ value is approximately half that of the single fin. At α and β, the "leeward" fin is masked by the wing and fuselage. The effect is more marked in $C_{n\beta}$. Most significantly, the single fin provides positive (stable) $C_{n\beta}$ whereas the twin fins are unstable. Similarly in Roll, the single fin provides negative (stable) $C_{\iota\beta}$ but twin fins are again unstable. The single fin does not appear to have a significant contribution to $C_{m\beta}$. However, the twin, tip mounted fins affect the wing flow, resulting in a noticeable contribution to $C_{m\beta}$.

All these aspects will need to be carefully considered at the initial design and planform layout stage. Further consideration will be required throughout the S&C design and performance estimation stages.

9.6. Lateral Derivative Comparisons

One of many very important S&C parameters to be considered early in the design process is the lateral stability derivative $C_{n\beta}$. Configuration layout, e.g. the choice of single or multiple fins (vertical tails), canted tail surfaces (V-tail), wing tip mounted fins or other directional control devices, will have fundamental influence on the overall stability and hence efficiency and performance of the aircraft.

The variation of $C_{n\beta}$ with M for a variety of subsonic, transonic and supersonic aircraft is shown in **Fig.9.6.1**, Ref.14. The M range has been extended to M 3.0 and current analysis data added. Flight test data for the XB-70, Ref.18, and the Space Shuttle, Ref.13, continue the general trends implied as M increases. It is noted that, for the Space Shuttle, $C_{n\beta}$ at nominal entry α $+/-5^o$ is negative above M 1.4. However, $C_{\iota\beta}$ is always negative and of relatively high value. The combined effects provide stability in Dutch Roll.

Euler results for Concorde (Wing + Fuselage + Fin) lie within the expected range and those for the XB-70 (Wing + Fuselage + Fin) follow the trends with M but at lower values than those derived from flight test. A full analysis is required using consistent parameters in the derivation of $C_{n\beta}$ before direct comparisons are truly valid. Using a high order panel method to predict subsonic $C_{n\beta}$ for Concorde Wing and Fin geometry gives values in the range 0.18 to 0.20 / Rad,

Fig.9.6.1. The fuselage contribution will be negative and reduce these values considerably. The most significant conclusion is drawn from the initial design analysis of the typical hypersonic vehicle, Section 9.5. At M 2.0, the single fin configuration, A1, gives reasonable positive $C_{n\beta}$, the twin fin configuration, A2, gives negative $C_{n\beta}$ of greater magnitude.

All these aspects will need to be carefully considered at the initial design and planform layout stage. Further consideration will be required throughout the S&C design and performance estimation stages.

10. INERTIAL COUPLING

As aircraft design speeds increased from subsonic, through transonic to supersonic during the 1950s various dynamic instabilities, violent motions about all three axes, were experienced. Prevention and control of these instabilities would require a new field of aircraft design encompassing aerodynamics, structures and controls under the broad heading of "Coupling Dynamics".

10.1. Coupling Dynamics

Coupling Dynamics problems associated with "Slender" supersonic aircraft, **Fig. 10.1.1**, are discussed in Refs.13 & 26. Of these, two are delta-wing based (Space shuttle and the YF-102). The coupling dynamics problems are very much dependent on aerodynamic control derivatives and the inertia parameters. An approximate correlation has been proposed in terms of a Primary Coupling Inertia ratio (Ixx-Iyy)/Izz. Coupling tendencies increase as the values approach –1.0.

X-15	–0.94
X-3	–0.88
Space Shuttle	–0.84
YF-102	-0.81
F-100A	-0.71
X-2	-0.70

The YF-102 had a greater tendency towards Inertial Roll coupling than either the F-100A or the X-2.

10.2. Fin Sizing – Geometry Review

The Vertical Tail (Fin) geometry of many aircraft had to be modified after initial design as a result of interference effects noted during wind tunnel or flight testing. Typical examples are F-100 and Panavia Tornado. Several geometric fin variables may be considered at the design stage, e.g. fin area, fin height and hence roll moment arm, longitudinal position and hence yaw moment arm, single or twin fins, etc. The effects of single centerline fin or twin wing tip fins are noted in Section 9.5.

We take an initial look at the variation of two fin height parameters with wing AR. The two parameters are Height of fin tip above wing mean plane and Height of exposed fin centroid above wing mean plane. Results for a range of delta wing aircraft and the F-100 are shown in **Fig.10.2.1**. During the development of the F-100, these parameters had to be increased by 20% to overcome stability issues.

Fin sizing is also driven by the "engine out" condition. The variation of fin/rudder effectiveness with a function of engine out induced yaw at zero payload for a range of subsonic transport aircraft is shown in **Fig.10.2.2**, Ref.27. A smooth trend has been established for fairly complex variables. **Fig.10.2.3** shows the variation of the product of fin area coefficient (S_v/S) and tail arm coefficient (ι_v) with S_v/S derived from data in **Fig.10.2.2**. The gradient of the mean line is simply a measure of ι_v (ι_v = 0.4 shown). Data from Fig.10.2.2 has been annotated with consistent

identifiers. Values for Concorde, XB-70, F-100A, F-100C and YF-102 have been added. All data lie close to the $\iota_v = 0.4$ line.

10.3. Inertial Roll Coupling - Importance of Fin Size

The F-100A was a single engined, low swept-wing (relatively high AR) plus tailplane configuration. Both the X-3 and the F-100A had a highly loaded, high fineness ratio fuselage, **Fig.10.3.1**. The F-100A vertical fin is in relatively good flow-field (low wing + body + tail) yet there were serious problems associated with it. During flight testing of both aircraft in 1954, dynamic instabilities were encountered. **Fig.10.3.1(a)** shows a time history of S&C parameters following an abrupt aileron input. Immediately, α and β began to diverge, negatively. After about 3 seconds the rates of divergence increased. At about 6 seconds, the vertical tail load was at 50% of its design load, **Fig.10.3.1(b)**. Divergence subsided when the controls were returned to neutral. The instabilities were attributed to inertial roll coupling via low directional stability.

Two vertical tail modifications were proposed. Tail B was 11.3% larger and tail C 27.5% larger than the original tail A, **Fig.10.3.4**. Also shown in **Fig.10.3.4** is the effect on $C_{n\beta}/^o$ through the M range due to the enlarged tail. Tail C doubled the directional stability. The effect of vertical tail size on maximum change in α and β ($\Delta\alpha$, $\Delta\beta$) at the first peak is shown in **Fig.10.3.5** as a function of roll rate. The circular symbol denotes the test flight case with tail A. The five degrees of freedom (5-D-of-F) simulator predictions for tails B and C show marked improvements.

The aircraft α at which roll initiates has a significant effect on the magnitude of subsequent instabilities. **Fig.10.3.2** shows simulator results for the F-100A with vertical tail A. Flight results for the aircraft fitted with tail C are shown in **Fig.10.3.6**. The beneficial effects of the enlarged tail are evident.

The simulated effects of engine gyroscopics during left and right rolls on the F-100A on $\Delta\alpha$ and $\Delta\beta$ as roll rate varied are shown in **Fig.10.3.3**. Flight tests with tail C fitted confirmed the trends. Naturally, the roll rate at which the peak motions occurred and the magnitude of the peaks depended upon the interaction between the engine rotor angular velocity and the roll angular velocity.

The F-100 was returned to service with the modified tail without further significant inertia roll coupling incidents.

It is noted that on a delta wing + body arrangement, there would be more blanking of the fin and the possibility of greater inertia roll coupling effects.

10.4. YF-102 (Delta Wing)

The YF-102 delta winged aircraft was delivered for flight testing in 1954 at about the time of the roll coupling test programme on X-3 and F-100A. The YF-102 design did not have the benefit of the experience being gained from those tests. It was apparent that the YF-102 would have coupling problems. **Fig.10.4.1**, Ref 13, shows a time history of an aileron roll at M 0.75 at 39,500 ft. A large increase in the rate of sideslip build-up at about 4 seconds. The pilot then reversed aileron. However, the roll-rate and sideslip continued to build-up at ever-increasing rates until side-slip reached -30^o and recorded α went off scale at -12^o. The analogue match (5-D-of-F simulator) showed α more negative than -20^o. The motions subsided after the pilot neutralized the controls. These divergences were larger than those of YF-100 and X-3. However, because the dynamic pressure was quite low (158 lb/ft^2), excessive loads on the structure were not imposed.

10.5. Supersonic Cruise Aircraft

Inertia ratios in Roll/Pitch/Yaw for Concorde are 1:7:8, approximately. This gives the coupling inertia ratio of -0.67. This is better than that of YF-102 delta (-0.81). The differences are due to the comparative fuselage length and volume with respect to the wing area.

The corresponding figure for XB-70 is about -0.84 at landing with the tips unfolded. This is not as good as either the YF-102 or Concorde, possibly due to the longer front fuselage and canard arrangement.

This brief review of Inertial Coupling problems of early swept winged aircraft has highlighted the problems that might be experienced. The importance of fin sizing is apparent. It was noted that the sizing and location of the fins needs careful assessment. Oversizing the fin or fins will result in excess OEW and reduced range performance.

11. PERFORMANCE and STRIKE AIRCRAFT

Useful performance data is available from Concorde and XB-70 flights. From these, with matching studies, we can establish the Range parameter (X), specific fuel consumption (SFC) and L/D data. This in turn will lead to parametric studies for supersonic Strike Aircraft.

An aircraft component weight breakdown establishes weight ratios with respect to Maximum Take-Off Weight (MTOW). The primary components are Empty Weight (OEW), Fuel capacity (WFT) and Payload (WP). The fuel component is broken down further into Block Fuel (WFB) and Reserve Fuel (WFRes). For a given aircraft, WP can be reduced for increased range and vice versa.

There are simplifications implicit in using and matching such data but this offers a good starting point.

11.1. Matching Studies on Concorde

Concorde has a MTOW of 408,000 lb. OEW is 173,000 lb and the fuel capacity (WFT) is 210,800 lb. The design range was 3550 nm for 100 passengers (WP = 21,000 lb).

Data for an actual scheduled service between London, Heathrow (LHR) and New York (JFK) is shown in **Fig.11.1.1** as an Altitude – Time - Distance plot. Take-Off weight (TOW) was 405,440 lb, WFB 172,180 and WP approximately 21,000 lb. The range completed was 3142 nm.

We obtain the following data for the M 2.0 segment: X value of 7100 with SFC = 1.2 and L/D about 7.4. We can easily derive the improvements due to any parametric changes.

The flight profile can be matched for various, typical flight constraints. Allowing C_L to increase (0.1004 to 0.147) in cruise climb (40,000 ft to 60,000 ft) results in the profile in **Fig.11.1.2(a)** whereas constraining C_L to 0.100 gives the profile in **Fig.11.1.2(b)**.

11.2. Matching Studies on XB-70

This aspect will be completed in Phase 2. Confidence in the predictive methods has been gained using extensive flight data (test and “in-service”) available on Concorde. Flight data for the XB-70, in its design mode, is not readily available. The aircraft were basically used to explore the flight envelope of supersonic planforms with folding tips.

11.3. Possible Strike Aircraft Performance Predictions

We take a preliminary look at the design of a Strike aircraft, SR301 based on previous work, Ref.6. The planform is shown in **Fig.11.3.1**. Forces and moments and spanwise loadings at M 2 for the neutrally stable, CL 0.1, M 2 design are also shown in **Fig.11.3.1**, from original data. The variations of $C_{L\alpha}$, k and L/D with M for this design are shown in **Fig.11.3.2**. Typical L/D achieved at M 0.3 and M 2.0 is about 7.5.

We now look at the effect of varying stability margin on the M 2.0 design. Results for 0% stable, 5% stable and 5% unstable are shown in **Figs.11.3.3**, **4** and **5** respectively. At C_L 0.1, L/D increases slightly (7.1, 7.2, 7.3) as stability margin increases (5% unstable to 5% stable). The M 2.0, 0% design is "re-designed" for C_L 0.4 at M 0.3 with varying degrees of low speed stability (-5% to +5%). The M 2.0, 0% stability design is frozen and the TEF region deflected for the low speed design cases. The results for 0%, 5% stable and 5% unstable designs at low speed are shown in **Figs.11.3.6** to **8**. At C_L 0.4, M 0.3, a rise of 11% L/D is implied as stability is relaxed from +5% to –5%.

11.4. Predicting Performance, Varying Parameters L/D and sfc.

Considering a possible L/D range (7.5, 8.0, 8.5, 9.0) and sfc of 1.20 or 1.25 aircraft component weight breakdown as Range varies is shown in **Fig.11.4.1** for the SR301 configuration. Original data from Ref.6 has been used for this example. A nominal MTOW of 392,000 lb was chosen. At this weight and sfc of 1.2, predicted range increases from 4630 nm to 5590 nm as L/D increases from 7.5 to 9.0. To a first order, Range is proportional to L/D and both show 20% increase approximately. For L/D of 7.5, WFB is 46% of MTOW but if L/D is improved to 9.0, WFB falls to 34% of MTOW.

These results are presented in a different fashion in **Figs.11.4.2** and **3**. We consider L/D of 9.0 and look at the effect of doubling the design MTOW. For sfc of 1.20, doubling the MTOW from 200, 000 lb to 400,000 lb increases the range form 3315 to 5750 nm (73% increase). Doubling MTOW of 250,000 lb increases range by only 59%.

These estimates are for a fixed payload of 50,000 lb. In the above examples, WP/MTOW varies significantly. However, the non-linearity of the prediction process (aerodynamic and engine efficiencies) is very evident.

Trade-offs that can be done in Phase 2.

12. CONCLUDING REMARKS

Currently there is interest in developing aircraft with long-range capability at very high speeds. Typical anticipated roles could be reconnaissance and bombing missions.

A concern is that, often for the sake of expedience, the conceptual design phases focus more on performance and much less on the more complex S&C aspects (about all axes). Consequently, S&C aspects considered later in the design cycle can severely compromise the original design objectives (L/D, strike capability range, weight growth). A better approach will be to include the major aspects of S&C in the conceptual design phases. Supersonic aircraft require a compromise between low-speed and high-speed capabilities and S&C issues remain very central throughout the operational envelope. The safety considerations may shift the balance more toward low-speed capabilities. The payloads in supersonic aircraft are generally smaller than those of subsonic aircraft.

The main objective has been to assess vehicle design evaluation over Mach number and altitude operating envelope with S&C considerations as part of the design synthesis. It is implied that design tools have needed to be "anchored", so as to focus on the importance of S&C.

In this Phase 1 report, we have addressed a series of issues. It is worth mentioning that the analyses tended to expand as we went more deeply into the various aspects, often beyond the initial expectations.

Configuration & Layout

Overall, an early definition of design cruise speed, flight envelope, payload, range is desirable. This in turn leads to planform and configuration limitations.

Definition of planform will define the aerodynamic aspects that take priority, e.g. vortex Lift at low speed.

"Off-Design" requirements need to be established at an early stage, e.g. sideslip, engine-out, cruise climb or constant altitude limitations, etc.

Efficiency priorities needs to be established and balanced e.g.

Design for long range cruise and then deploy high lift devices for low speed

OR Design for efficient low speed and climb and then "morph" for high speed cruise (XB70)

OR Compromise both regimes (Concorde)

Supersonic cruise design will be compromised to a certain extent by Subsonics: Take–Off and Landing requirements.

Longitudinal Aspects

The CoP variation with Mach number in relation to possible CG location has been considered for a series of wings.

Such aspects are strongly affected by fuselage location and size. Presence of fuselage tends to ameliorate CoP shift with M variation.

Folded Wing Tips concept as on the XB-70 enables the CoP variations with Mach number to be favourably controlled.

Design without and with Vortical flow has extremely strong effects. Without vortical flow, better L/D is obtained but the AoA required for landing and take-off (ground clearance) becomes large and this in turn leads to heavier undercarriage. Now the undercarriage weight is about 5% of the MTOW and the payload is of the same order. AoA increase by 2-3 deg. leads to increase in undercarriage by 10-15% as a first guess. So this has an equivalent penalty on payload.

With vortical flow, lower L/D is obtained but the AoA is lower and undercarriage weight will be generally lower. Which philosophy to utilize remains a strong S&C driver. We have considered brief implications of the aspect at this stage. Inclusion of vortical flow completely changes S&C aspects e.g. in trim, Cm behaviour at high AoA (vortical breakdown).

Ground Effect has been shown to play a very important role from S&C viewpoint. The trailing wake deforms and spreads outwards near the ground. With cross-winds, the effectiveness of ailerons / elevons can be strongly compromised – possibly lead to saturation. We may need to include TE sweep.

Relaxing longitudinal stability requirements uing positive static margin has a very beneficial 20% effect upon L/D. On the Concorde this has been demonstrated in flight. We have been able to predict this with our theoretical approach. This is a very useful "anchor" for future work.

Lateral & Directional Aspects

For "Slender delta" type layouts, the S&C, Inertial Coupling derivatives vary significantly with M up to M 2.5. Beyond M 2.5 the derivatives tend to "level-out". Choice of single or twin vertical fins, or alternative lateral / directional control devices, will be driven initially by the most demanding phase in the flight envelope. A few selected comparisons on sideslip effects have been shown. The S&C implications are very dominant.

Many avenues for further work, analysis and investigation have arisen. Similarly, deeper analysis of topics already covered will be required. These will be addressed in Phase 2 and subsequent phases.

13. FURTHER WORK

The work in this report on Phase 1 has shown that the role of S & C is very important in conceptual design for high speeds vehicles. We highlight continuation aspects for subsequent work phases as follows. The scope remains large.

1. Flight Envelope considerations through M, Altitude, Wing loading requirements with emphasis for supersonic Cruise aircraft up to 70,000 ft. These aspects are much broader than those for conventional transonic aircraft. Further work is needed with advanced engines to achieve 85,000 ft altitude. This implies flying through a wider C_L range. For supersonic aircraft, balancing of high speed cruise against adequate low speed field performance (10,000 ft runway at 160-180 kts) remains challenging.
2. Initial typical weight breakdowns emphasise the S&C connections via L/D, fuel etc.
3. Useful results available on Supersonic cruise aircraft e.g. Concorde and the XB-70. (It is realized that a military aircraft will not have a long tail fuselage as on Concorde). Some of the S&C aspects were discovered too late (i.e. during special test flights and could not be exploited in later designs). These results allow a verification / calibration of the approaches being used. In turn, these allow more confident predictions for the main part of the work in more detail.
4. More “Modern” Supersonic Cruise Planforms with least movement of Neutral point as a function of M, hence reducing the need for fuel management and cg relationships. Some planforms may produce better balance between low-speed and high-speed trim and S&C. Further continued work on derivation of planforms.
5. Inclusion of Vortical Flow meant a great difference in S&C derivatives and control power required at high AoA. Undercarriage height and weight parameters are intimately related to Vortical flow presence. Undercarriage weight is of the same order as payload. Vortical flow implies lower L/D but smaller AoA. Conversely, attached flow with LE devices, implies higher L/D but a longer undercarriage height and so on. Further work is needed for Strike Configurations.
6. Longitudinal Stability levels at low speeds. Using our methods, including vortical flow effects, we can confirm the trimmed (elevon down) flight test results on Concorde at low speeds. Relaxed stability, (c.g. moved rearwards, unstable) allowed up to 15-20% improvement in L/D at low speeds. This aspect could not be however exploited in production models – too late! This aspect has a large bearing on elevon size or indication of the need for another trim surface, Fuel transfer and cg management etc. Further continued work.
7. Preliminary Ground Effect studies. We show that wake shape distorts (expands) near the ground and this produces a strong effect on control power needed. Further, the control power depends on the static margin available. Additional complexities arise as sideslip variation is introduced. For example 30 kts cross-wind can lead to 10 deg. sideslip. Need to continue work on Strike type planforms.
8. Control interactions. We show preliminary work on Aileron / Elevon / Rudder interactions in roll and yaw due to sideslip. At certain supersonic M, Elevon deflections produced adverse effects on rudder control power. Such aspects have a strong bearing on

Control sizing. There is a large amount of work to do in geometry variations, studying single, twin and canted fins.

9. Folded Wing Tips. Preliminary studies initiated show that the concept, first exploited by the XB-70 remains attractive for attainment of higher supersonic speed. This concept allows an appropriate balance between “high” aspect ratio (about 2.4) for low speeds and lower aspect ratio for supersonic speeds. The movement of neutral point between low and high speeds can be controlled. The importance of S&C during design phase becomes extremely important. Need to continue with work in more detail
10. The emergency case of 2-engine failure (2 on same side out of 4) and side-slip effects are being assessed. Fin geometry and size is very dependent on S&C considerations.
11. Inertial coupling aspects have been introduced. We need to do further work in relation to possible strike planforms.
12. Performance of Strike Aircraft. We initiated the work by matching the performance of selected previous cruise aircraft. This has enabled a degree of confidence in beginning to predict performance for strike aircraft. There are several parametrics to study and we anticipate further work.
13. Speed Stability – Operating on back of L/D curve etc. More to be done.
14. M 1.6 aircraft can be anticipated that may provide a simpler design challenge. This could be attractive and we could demonstrate this with some further work.

We are open to any other suggestions that you may have.

The work focus remains on showing that S&C considerations should be included in design synthesis. In most cases we need to present the results on the various aspects with and without adequate and appropriate S&C. The performance then is intimately related to the S&C effects.

ACKNOWLEDGEMENTS

The author has pleasure in acknowledging helpful technical comments and discussions with Dr Surya Surampudi and recently Dr Gregg Abate (both from USAF-EOARD), Mr. Charles Suchomel, Dr James Miller, Mr. Dieter Multhopp, Dr. Carl Tilmann and Mr. William Blake and Mr. Cale Zeune (US-AFRL). The technical help of Dr. M. E. Palmer is appreciated.

This material is based upon work supported by the European Office of Aerospace Research and Development, Air Force Office of Scientific Research, Air Force Research Laboratory, under Grant No. 10-3067.

Any opinions, findings and conclusions or recommendations expressed in this material are those of the author(s) and do not necessarily reflect the views of the European Office of Aerospace Research and Development, Air Force Office of Scientific Research, Air Force Research Laboratory.

REFERENCES

1. NANGIA, R.K. & PURSHOUSE, M., "Applications of Linearized Supersonic Wing Theory to Calculation of Some Aircraft Interference Flows, "Computational Methods & Problems in Aeronautical Fluid Dynamics", Academic Press 1976.
2. NANGIA, R. K., "Low Speed Performance Optimisation of Advanced Supersonic Civil Transport with Different LE & TE Devices", EAC'94, Toulouse, France, October 1994.

3. NANGIA, R.K. & MILLER, A.S., "Vortex Flow Dilemma S & Control on Wing Planforms for High Speeds", Paper Presented at RTO - AVT Symposium, Loen, Norway, May 2001.

4. NANGIA, R.K., PALMER, M.E., & DOE, R.H., "A Study of Supersonic Aircraft With Thin Wings of Low Sweep", Paper AIAA-2002-0709, AIAA Aerospace Sciences Meeting & Exhibit, Reno, USA.

5. NANGIA, R.K., PALMER, M.E. "Unconventional Joined-Wing Concept for Supersonic Aircraft", Paper 24, RTO-AVT-99 Conference, Brussels, April 2003.

6. NANGIA, R.K., PALMER, M.E. & IWANSKI, K.P. (AFRL), “Towards Design of Long-range Supersonic Military Aircraft”, AIAA Paper, 2004-5071, Providence Rhode Island, USA, 2004.

7. NANGIA, R.K., PALMER, M.E. & DOE, R.H., “Towards Design of Mach 1.6+ Cruise Aircraft”, AIAA Paper, 2004-5070, Providence, RI, USA, 2004

8. NANGIA, R.K., PALMER, M.E. & IWANSKI, K.P. (AFRL), “Towards Design of Long-range Supersonic "Large" Military Aircraft”, RAeS Paper 16, Sept. 2004, London, UK.

9. NANGIA, R.K. & PALMER, M.E., BLAKE, W. (AFRL) & TILMANN, C.P (AFRL), “Supersonic Aircraft Formation Flying to Increase Flight Efficiency”, ICAS 2008-1.10.2, Sept. 2008.

10. THIBERT, J.J, “The Aerodynamics of Future Supersonic Transport Aircraft; Research Activities at ONERA”, RTO-EN-4, May 1998.

11. LOWRIE, B.W, “Future Supersonic Transport Propulsion Optimisation”, Paper III,2.1, Proceedings of the European Symposium on Future Supersonic Hypersonic Transportation Systems, November 1989.

12. ELKAYAM, S. & SIGAL, A., “Wing Planforms Having Minimum Centre-of Pressure Shift from Subsonic to Supersonic Mach Numbers”, AIAA 93-3501.

13. DAY, R.E., “Coupling Dynamics in Aircraft: Historical Perspective”, NASA SP 532, 2000.

14. RAYMER, D.P., “Aircraft Design: A Conceptual Approach”, AIAA Education Series, 1992.

15. WLEIZEN, R. & VEITCH, L., “Quiet Supersonic Platform Program”, AIAA-2002-0143, 2002.

16. RAZGONYAEV, V. & MASON, W.H., “An Evaluation of Aerodynamic Prediction Methods Applied to the XB-70, for Use in High Speed Aircraft Stability and Control System Design”, AIAA-95-0759, 1995.

17. WOLOWICZ, C.H., STRUTZ, L.W., GILYARD, G.B. & MATHENY, N.W., “Preliminary flight Evaluation of the Stability and Control Derivatives and Dynamic Characteristics of the Unaugmented XB-70-1 Airplane Including Comparisons with Predictions,” NASA TN-D-4578, 1966.

18. ANDREWS, W.H., “Summary of Preliminary Data Derived from the XB-70 Airplanes”, NASA TM X 1240, June 1966.

19. KORDES, E.E. & LOVE, B.J., “Preliminary Evaluation of XB-70 Airplane Encounters with High-Altitude Turbulence”, NASA TN D-4209, October 1967.

20. FITZHUGH, L. & FULTON, Jr., “Lessons from the XB-70 as Applied to the Supersonic Transport”, NASA TM X 56014. 1968.

21. LARSON, T.J. & SCHWEIKHARD, W.G., “Verification of Take-off Performance Predictions for the XB-70 Airplane”, NASA TM X 2215, March 1971.

22. P, K.M., “Concorde Flight Test Certification. The Low Speed Envelope”, RAeS Gatwick Branch Lecture, February 1994.

23. CORMERY, G. & NEGRE, Y., “Electric Flying Control Experiments on Concorde Associated with a Sidestick”, Paper I,3.2.A2, Proceedings of the European Symposium on Future Supersonic Hypersonic Transportation Systems, November 1989.

24. HEFFLEY, R.K. & JEWELL, W.F., “Aircraft Handling Qualities Data”, NASA CR-2144, December 1972.

25. McCORMICK, B.W., “Aerodynamics, Aeronautics & Flight Mechanics”, Wiley, December 1979.

26. ILLIF, Kenneth W. SHAFER, Mary.F., “Space Shuttle Hypersonic Aerodynamic and Aerothermodynamic Flight Research and the Comparison to Ground test Results”, NASA TM-44991, June 1993

27. TORENBEEK, E., “Synthesis of subsonic airplane design”, Delft University Press, 1976

LIST OF SYMBOLS AND ABBREVIATIONS

Only the general symbols are defined here. Other symbols are of local significance within the Section they arise in.

Performance Related

DOC	Direct Operating Costs
EXP	Exponential
HBPR	High By-Pass Ratio Engines
OEW	Operating Empty Weight
PRE	= WP *R/WFB, Payload Range Efficiency
Pt	Point
R	Range (nm or km)
Radius	Radius of Operation (Tankers, Surveillance and Bombers)
SFC	Specific Fuel Consumption
T	Thrust
VEM	= PRE/MTOW, Value efficiency per MTOW unit
VEO	= PRE/OEW, Value efficiency per OEW unit
VEMPX	= VEM*WP/X, Non-Dimensional Value Efficiency, Section 6
VEOPX	= VEO*WP/X, Non-Dimensional Value Efficiency, Section 6
WFB	Block Fuel Load
WFB / WP	Fuel Payload Fraction (FPF)
WFRes	or WFR, Reserve Fuel Load
WFT	Total Fuel Load
WP	Payload
WP/WFB	Payload Efficiency
X	= V * (L/D) / SFC
Z	= R/X
Z_T	= Radius/X
ZFW	Zero Fuel Weight (MZFW, Maximum)

General

AoA	Angle of Attack (α), usually referred to the body axis
AR	Aspect Ratio
A	Axial Force along wing-plane x-axis (for definition of C_A)
b	= 2 s, Wing span
BL	Boundary Layer
c	Local Wing Chord
c_{aero}	= c, Mean Aerodynamic Wing Chord
c_{ave}	= c = c_{ref}, Average Wing Chord
C_A	= A/(q S), Axial Force Coefficient, measured in Wing plane
C_{AL}	= Local Axial Force Coefficient
C_D	= Drag Force /(q S), Drag Coefficient
C_{D0}	Drag Coefficient at zero lift (see text)
C_{Di}	Lift Induced Drag
cg	Centre of Gravity
C_l	= l/(q S b), Rolling Moment Coefficient (Body Axis), positive right tip up
C_L	= CL = L/(q S), Lift Coefficient
C_{LL}	= Local Lift Coefficient
C_{Lmax}	Maximum Lift Coefficient
C_m	= m/(q S c), Pitching Moment Coefficient (Body Axis), positive nose up

C_{mo}	Cm at zero Lift
C_n	= n/(q S b), Yawing Moment Coefficient (Body Axis), positive nose to left
C_N	= N/(q S), Normal Force Coefficient
CoP	Centre of Pressure
C_P	Coefficient of Pressure
$c_{r,}$ c_t	Wing Root chord, Wing Tip chord
C_Y	= Y/(q S), Side Force Coefficient, positive to right
D	Drag Force
DOF	Degrees Of Freedom
k	= π A C_{Di}/C_L^2, Lift Induced Drag Factor
l	Rolling moment (Body Axis), positive right tip up
l	Length
L	Lift Force
LE	Leading Edge
m	Pitching moment (Body Axis), positive nose up
L/D	Aircraft Lift / Drag Ratio
M	Mach Number
MRC	Moment Reference Centre
n	Yawing moment (Body Axis)
N	Normal Force
Non-D	non-dimensional
q	= 0.5 ρ V^2, Dynamic Pressure
r	Aerofoil radius
rn	Aerofoil radius normal to c
R	Reynolds Number, based on c_{ave} (unless otherwise stated)
s	Wing semi-span
S	Wing Area, taken here as (front-wing + tip-wing) area
t	Aerofoil thickness
TE	Trailing Edge
V	Airstream Velocity
x,y,z	Orthogonal Wing Co-ordinates, x along body axis
x_{ac}	Location of Aerodynamic Centre along x-axis
x_{cp}	Location of Centre of pressure along x-axis
Y	Side Force, positive to right
α	Angle of Attack (AoA), usually referred to the body ax
β	Sideslip angle, positive nose to right
λ	Wing Taper Ratio
Λ	LE Sweep Angle
ρ	Air Density
η	= y/s, Non-dimensional spanwise Distance

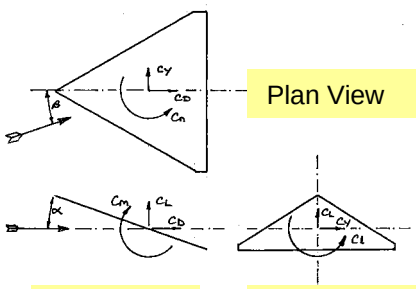

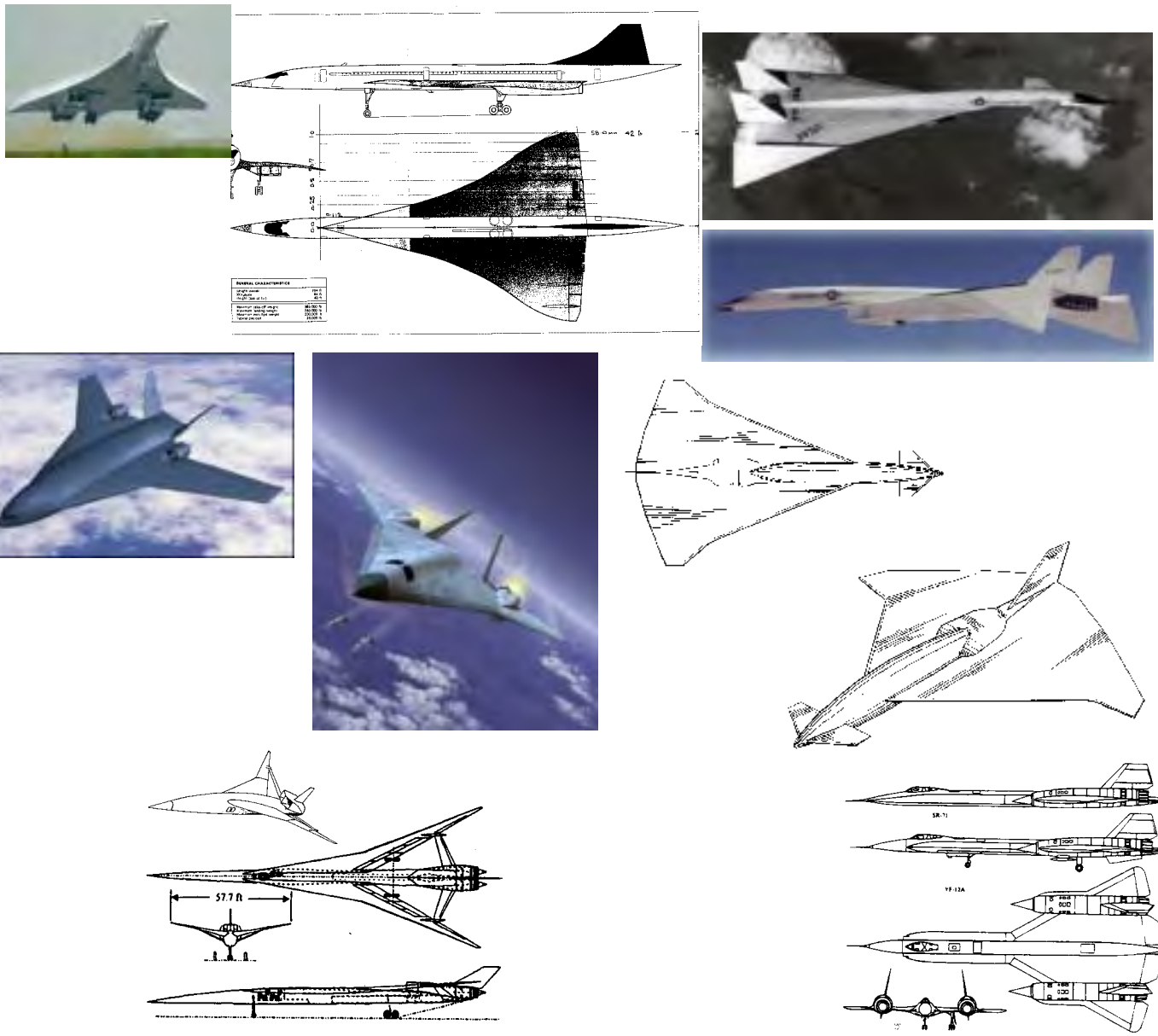

POSSIBLE LOW SONIC-BOOM JOINED-WING LAYOUT

Fig. 1.1.1. SOME HIGH SPEED CONFIGURATIONS (Miscellany, Real & Possible)

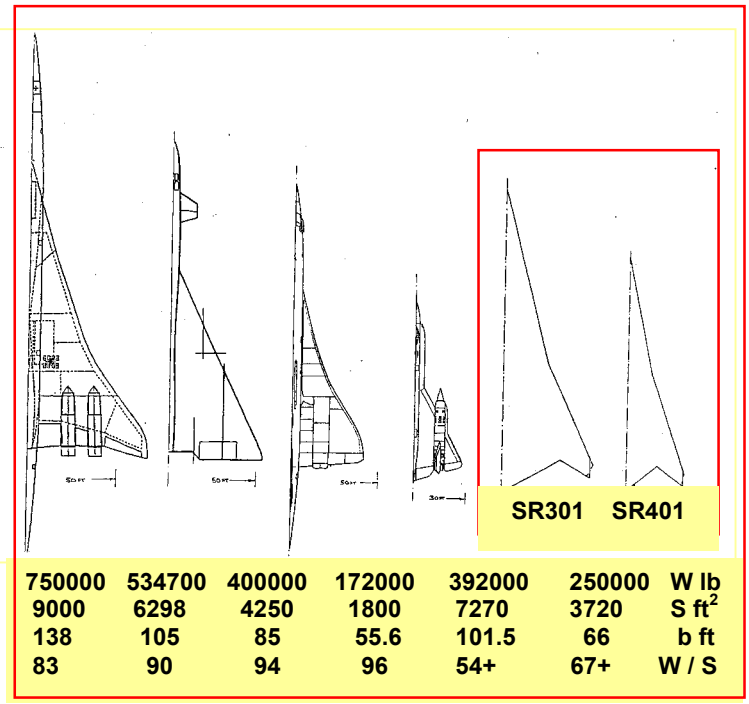

Fig. 4.1.1. SUPERSONIC AIRCRAFT PLANFORMS

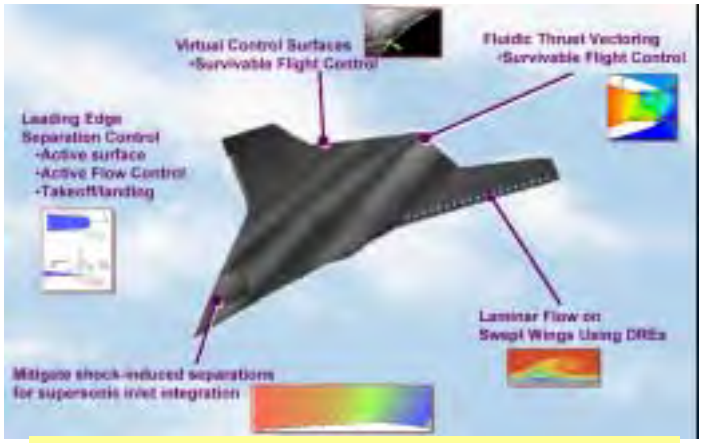

Fig. 4.1.3. POSSIBLE TECHNOLOGY APPLICABLE

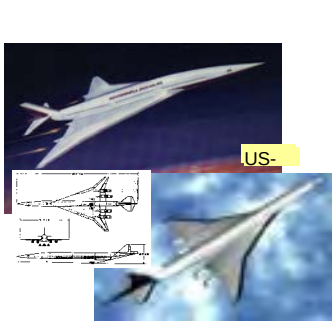

Fig. 4.1.2. SUPERSONIC CONFIGURATIONS, CIVIL & MILITARY

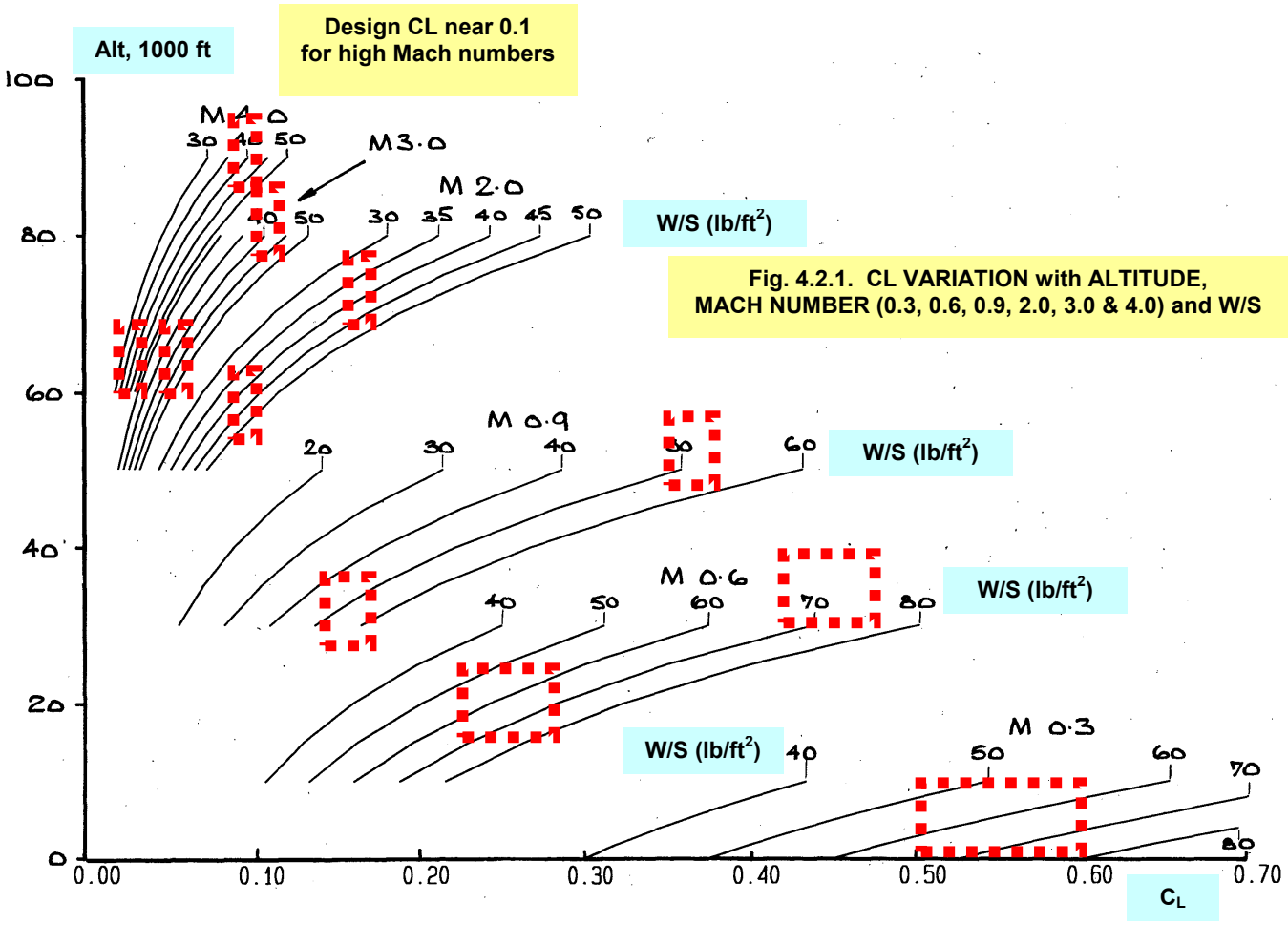

Fig. 4.2.1. CL VARIATION with ALTITUDE, MACH NUMBER (0.3, 0.6, 0.9, 2.0, 3.0 & 4.0) and W/S

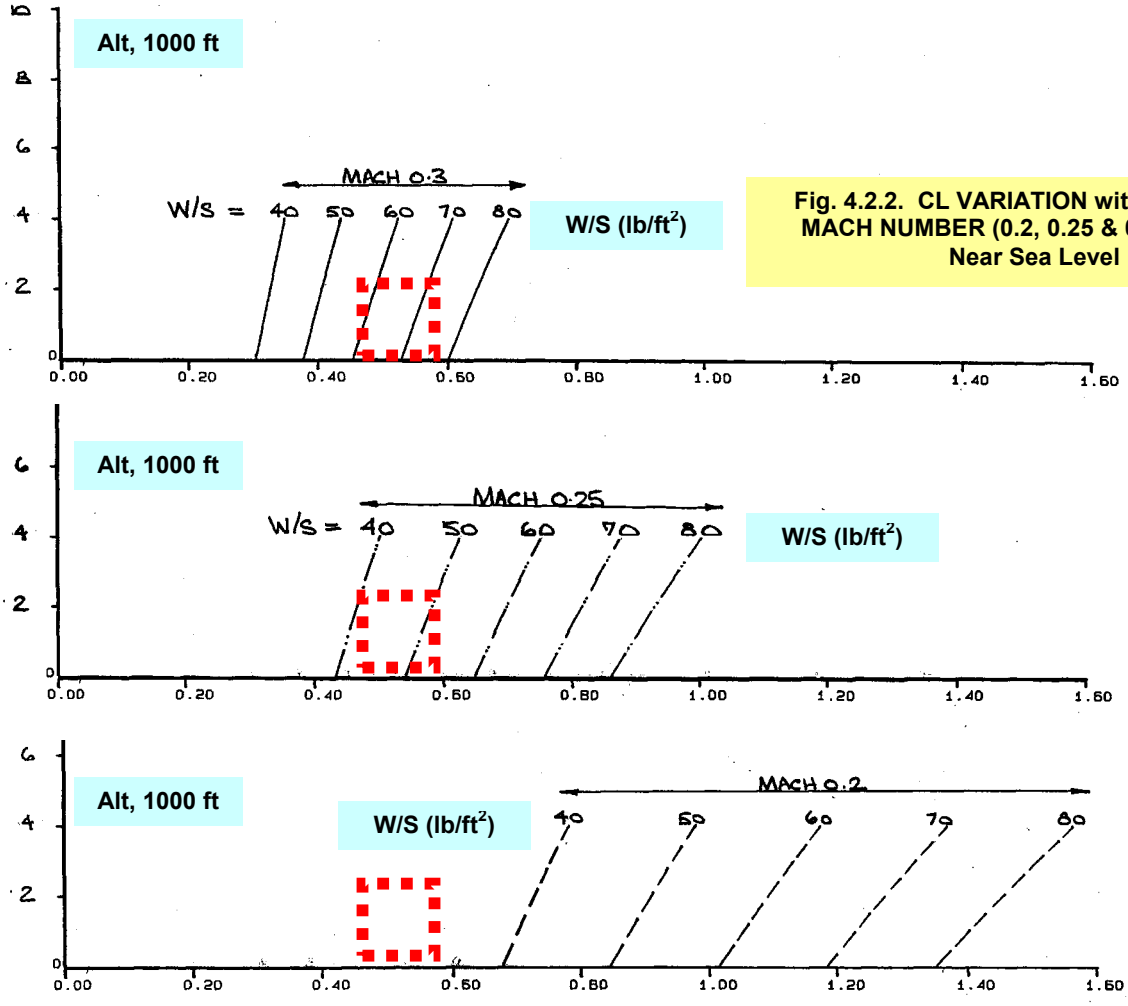

Fig. 4.2.2. CL VARIATION with ALTITUDE, MACH NUMBER (0.2, 0.25 & 0.3) and W/S Near Sea Level

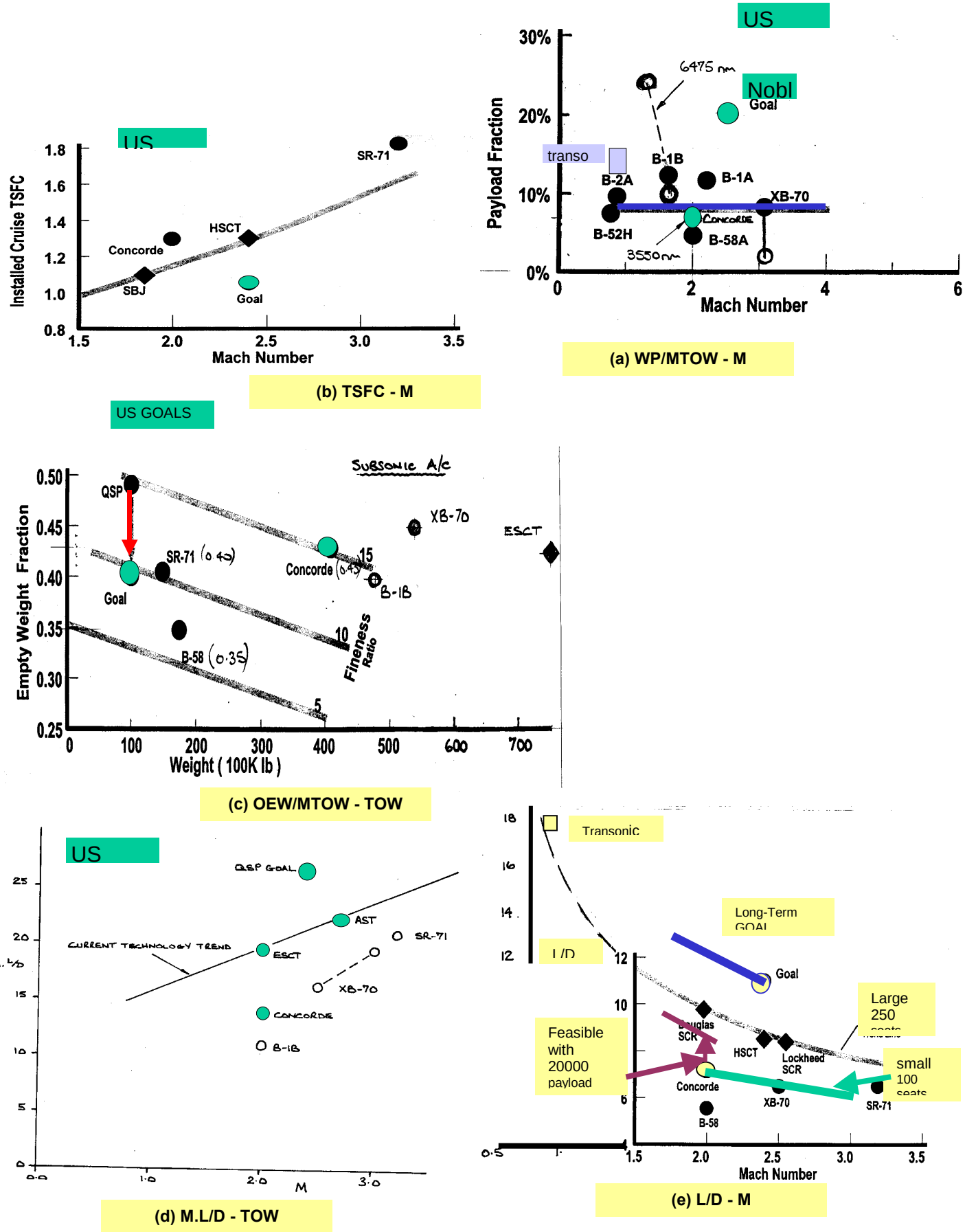

Fig. 4.2.3. DARPA GRAPHS (2000) & FURTHER INTERPRETATION & UPDATING

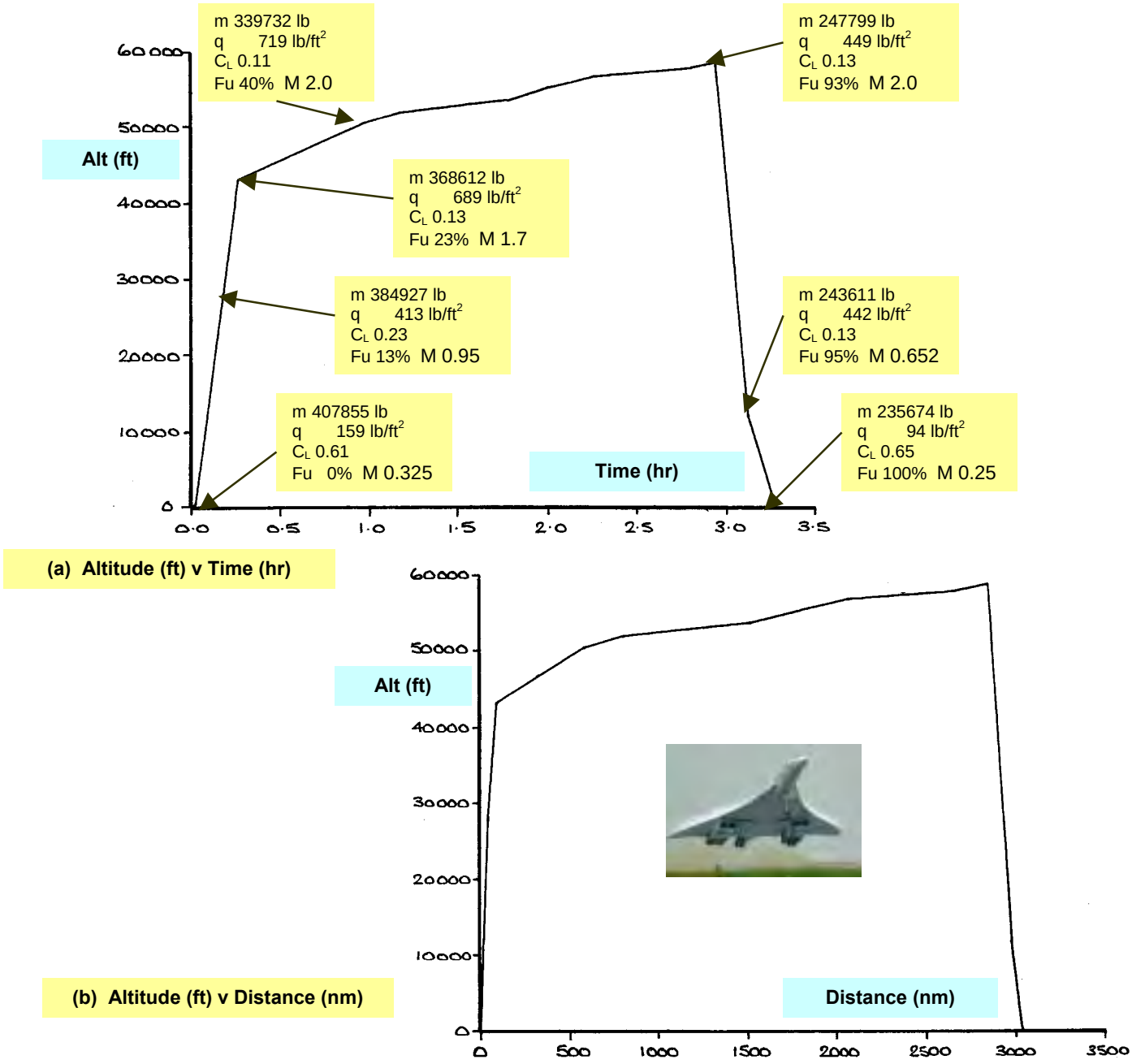

Fig. 4.2.4. ACTUAL CONCORDE FLIGHT HISTORY, LHR - JFK
Altitude v Time and Distance, Weight Variation

Altitude (1000 ft) v Time (Hr)

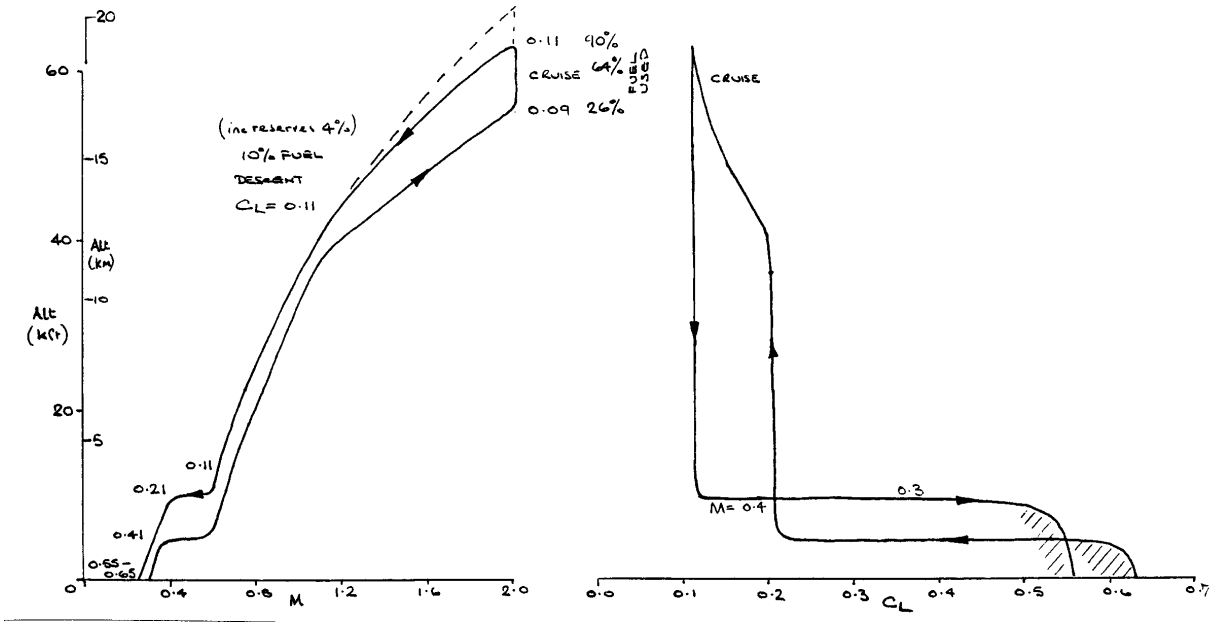

Fig.4.2.5. TYPICAL FLIGHT PROFILE SHOWING CL VARIATION (McD Studies)

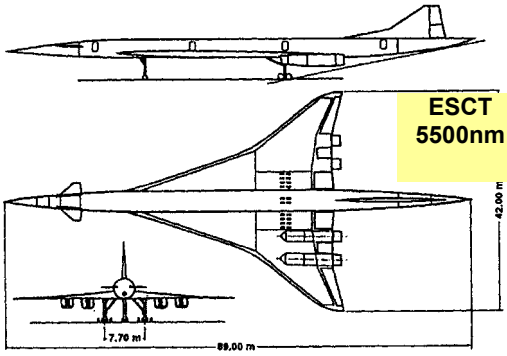

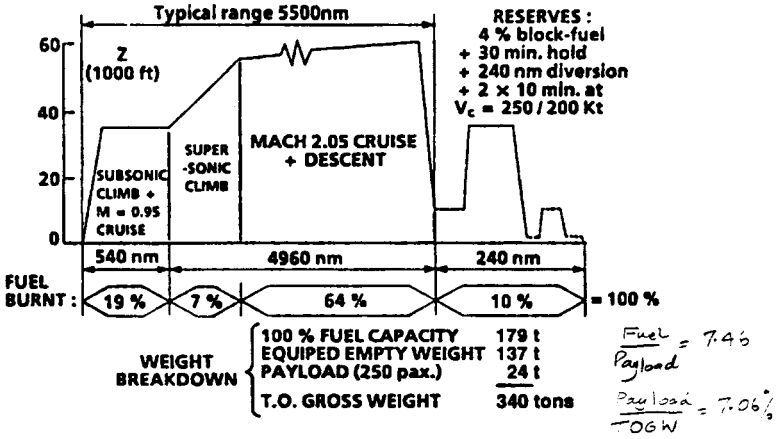

Fig. 4.2.7. FUEL WEIGHT BREAKDOWN FOR 5500 NM FLIGHT
Ref. Thibert

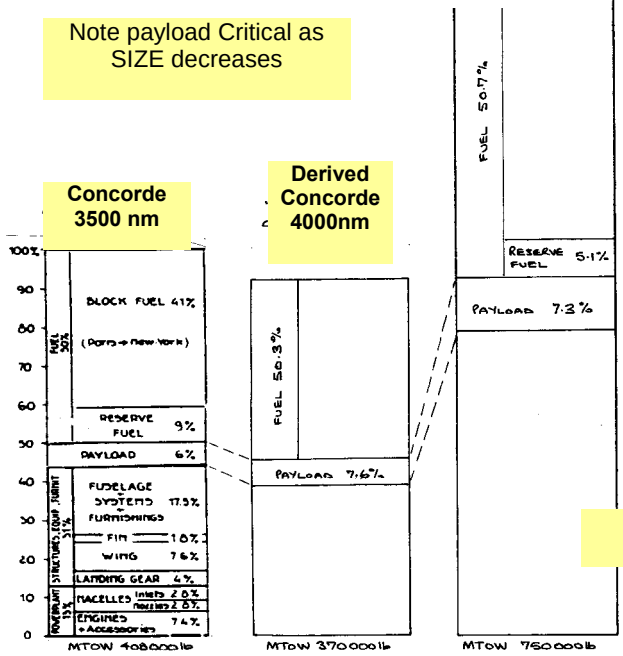

Fig. 4.2.6. SST WEIGHT BREAKDOWN

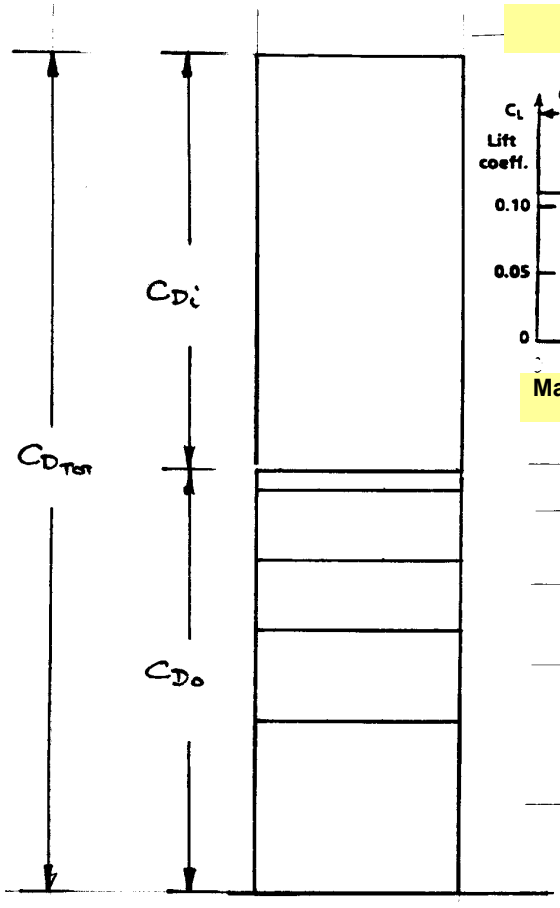

CD Extrapolation, Model to Full-scale

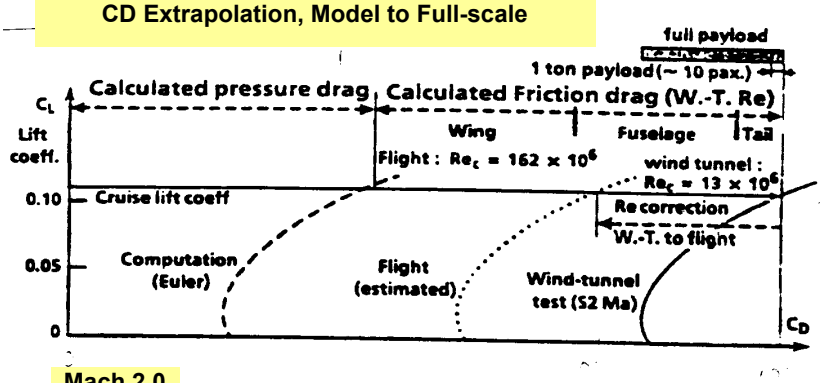

Mach 2.0

CD Build-up

Remainder (Nacelles, Fin, etc.)	C_{D0Rem}
Fuselage Wave Drag	C_{D0WF}
Wing Wave Drag	C_{D0WW}
Fuselage Skin Friction	C_{D0SFF}
Wing Skin Friction	C_{D0SFW}

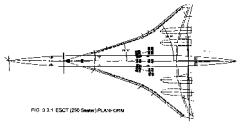

Fig. 4.2.8. SUPERSONIC DRAG, DESIGN
ISSUES & SPECIAL CHARACTERISTICS

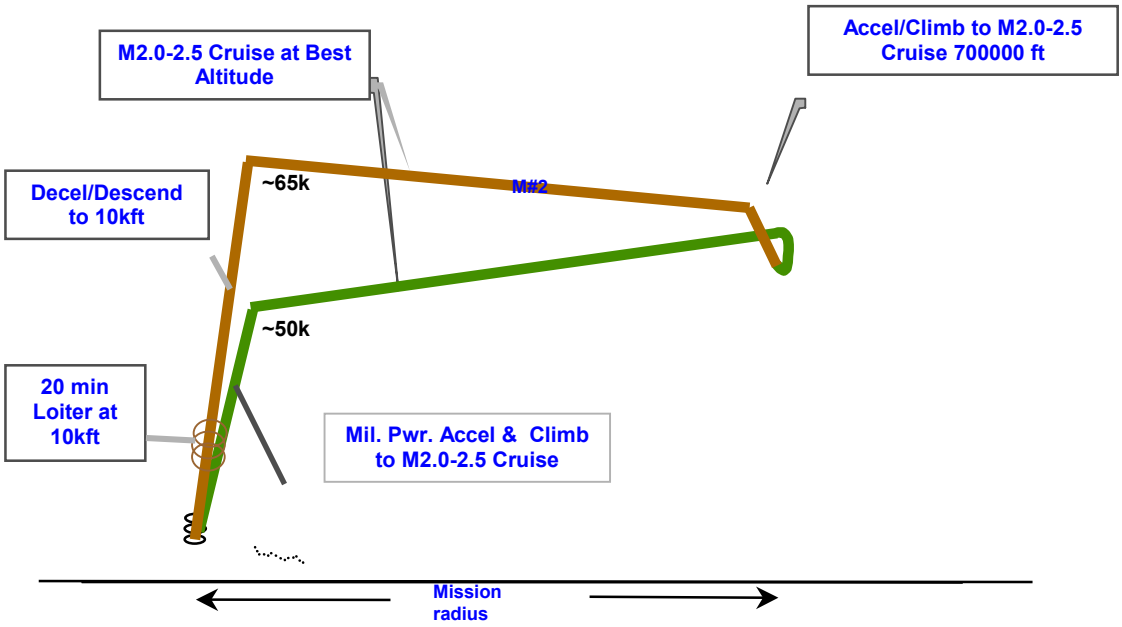

Warm-up, Taxi, Takeoff Allowance: 20 Minutes Idle + Max Pwr Take-off to 0.3M
Landing Reserves: Optional 20 Minutes Loiter at 10,000 ft + 5% Internal Fuel

Fig.4.2.9. POSSIBLE OPERATIONAL FLIGHT PROFILE, Mach 2

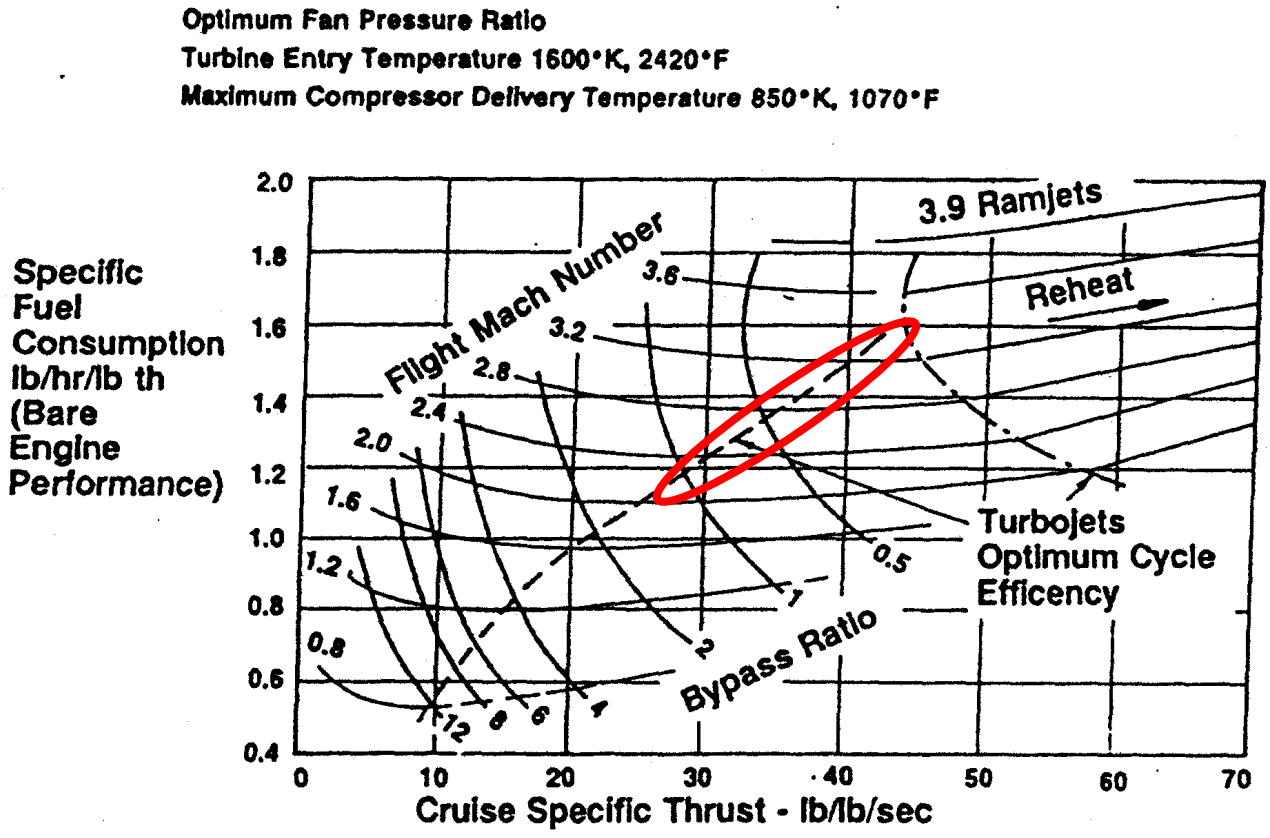

Fig. 4.2.10. TRENDS OF SFC WITH MACH No. (LOWRIE)

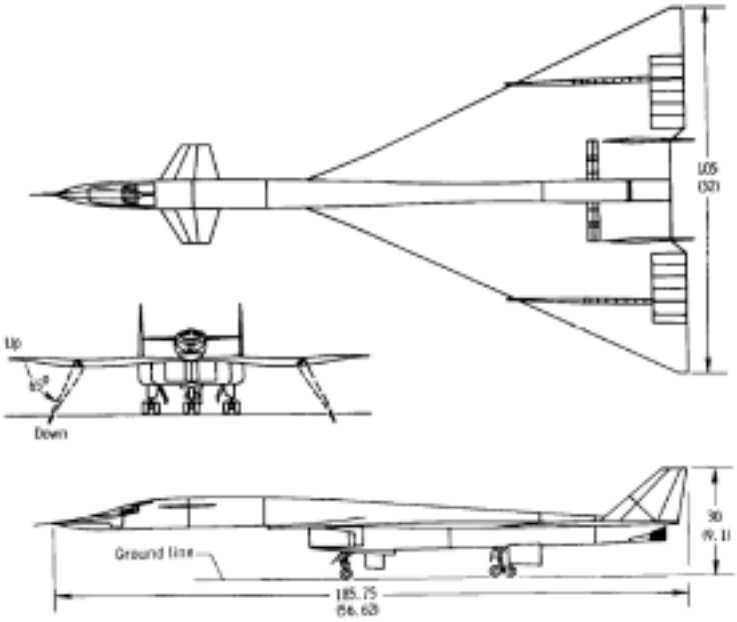

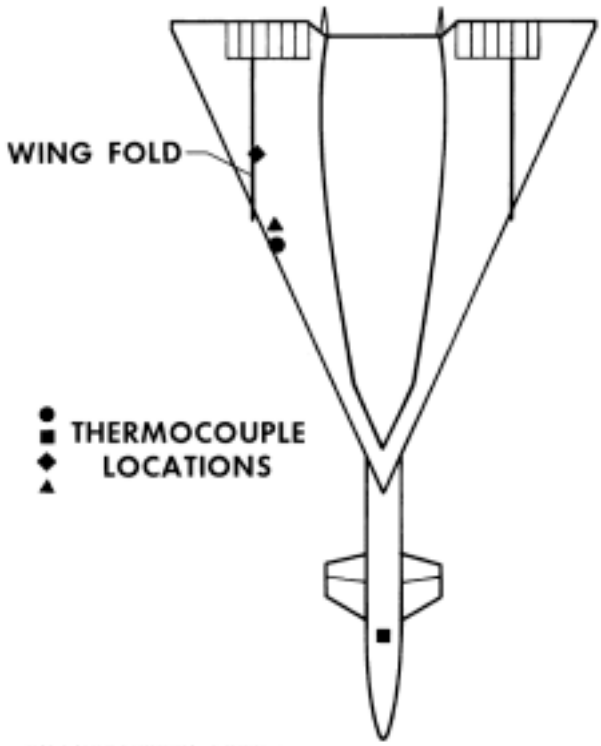

XB-70-1, 3-view Drawing (feet and inches)

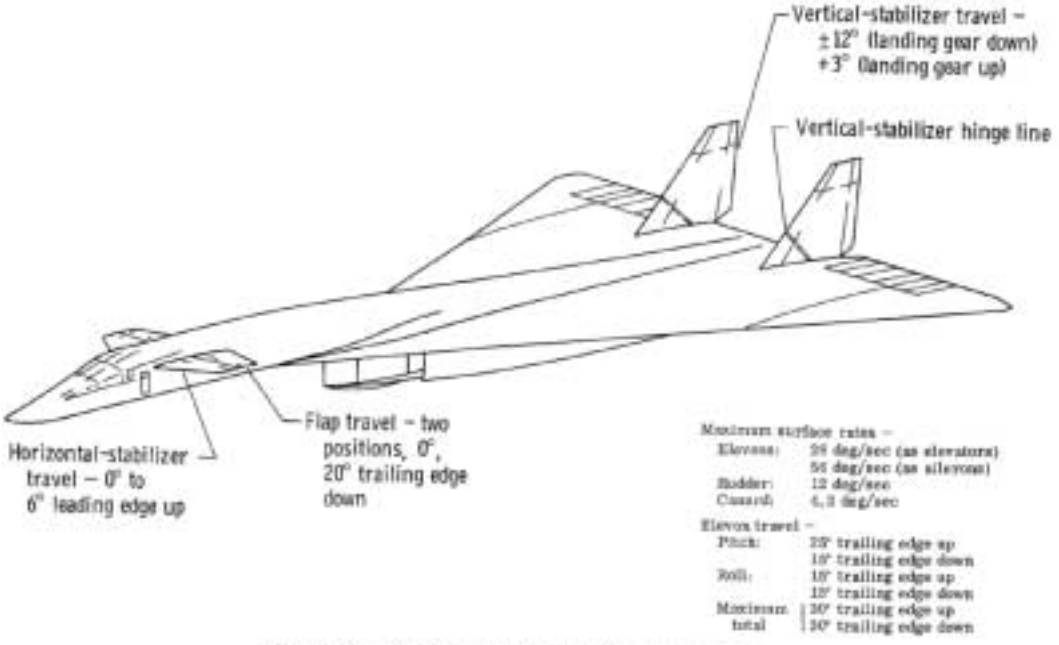

XB-70-1 Control Surface Movements

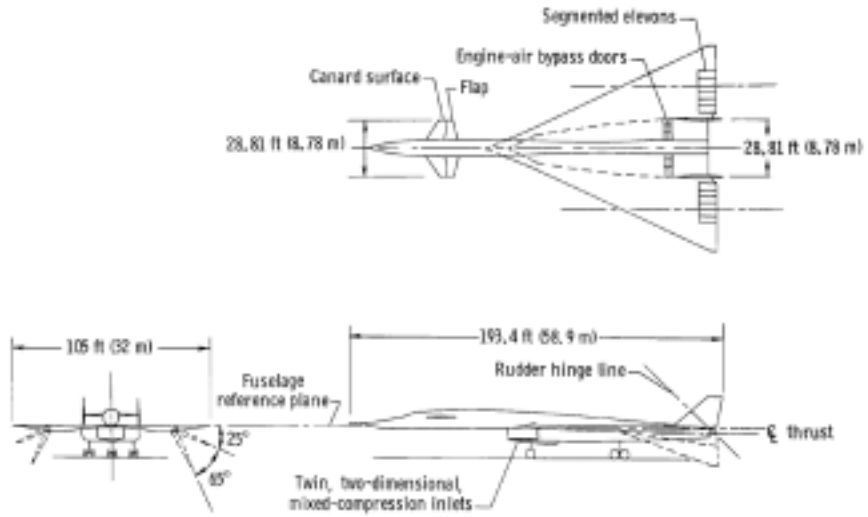

Fig. 4.3.1. XB-70 GENERAL ASSEMBLY, DIMENSIONS, CONTROL SURFACE MOVEMENTS

Nominal Configuration

Tips folded according to flight condition
50% internal fuel
$W = 384{,}524$ lb
cg at $0.218\bar{c}$. W.L. -7.2

$I_x = 1.8 \times 10^6$ slug-ft^2
$I_y = 19.9 \times 10^6$ slug-ft^2
$I_z = 22.1 \times 10^6$ slug-ft^2
$I_{xz} = -0.88 \times 10^6$ slug-ft^2
} body axis

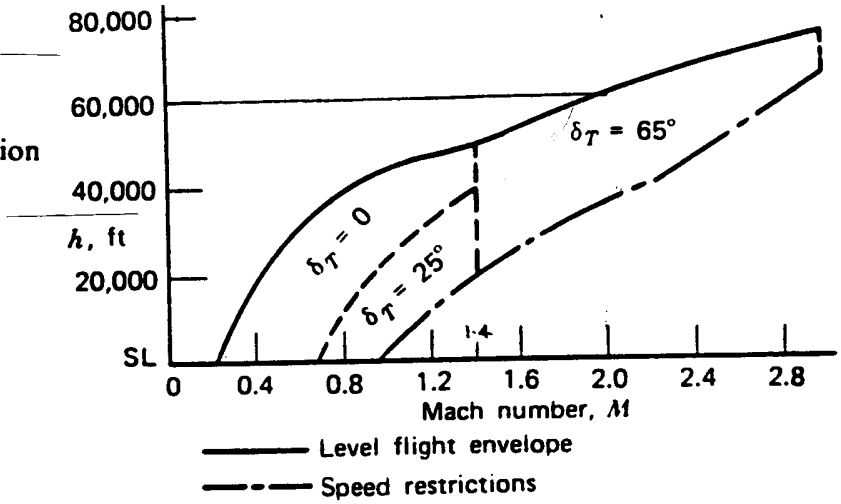

Power Approach Configuration

Tips extended
19% internal fuel
Canard flaps down
Gear down
$W = 300{,}000$ lb
cg at $0.235\bar{c}$

$I_x = 1.45 \times 10^6$ slug-ft^2
$I_y = 16 \times 10^6$ slug-ft^2
$I_z = 17.2 \times 10^6$ slug-ft^2
$I_{xz} = -0.6 \times 10^6$ slug-ft^2
} body axis

Canard Flaps Down

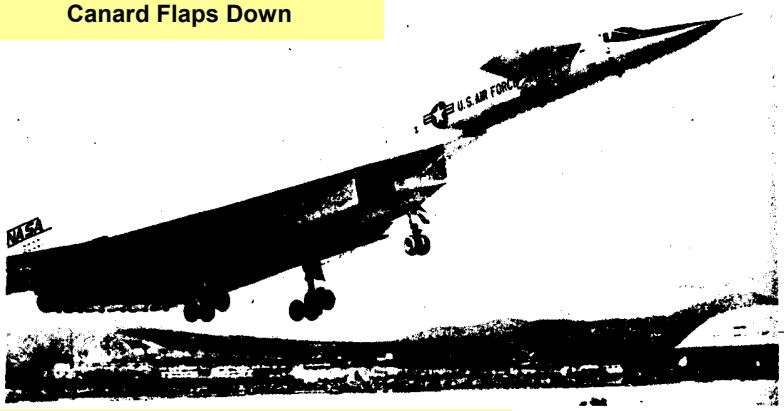

Fig. 4.3.2. XB-70, FLIGHT ENVELOPE WITH TIP FOLD REQUIREMENTS

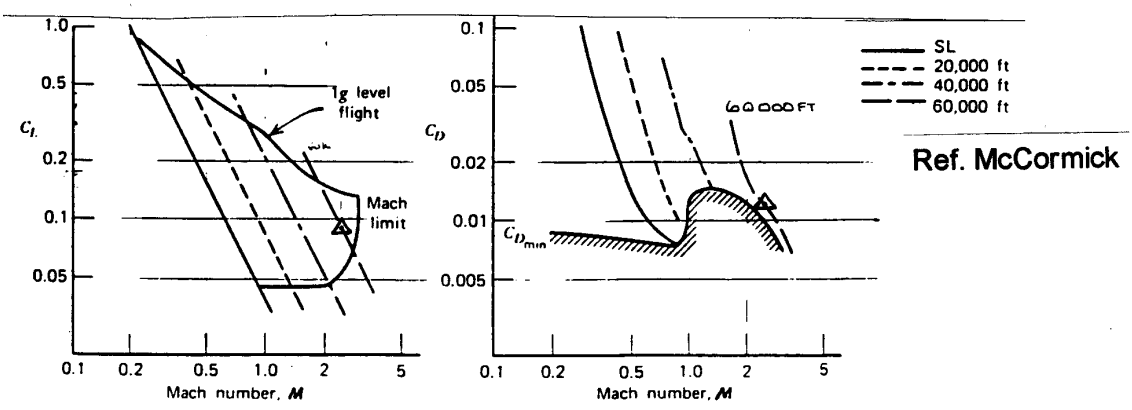

Ref. McCormick

△ typical cruise condition

Ref. Ayers

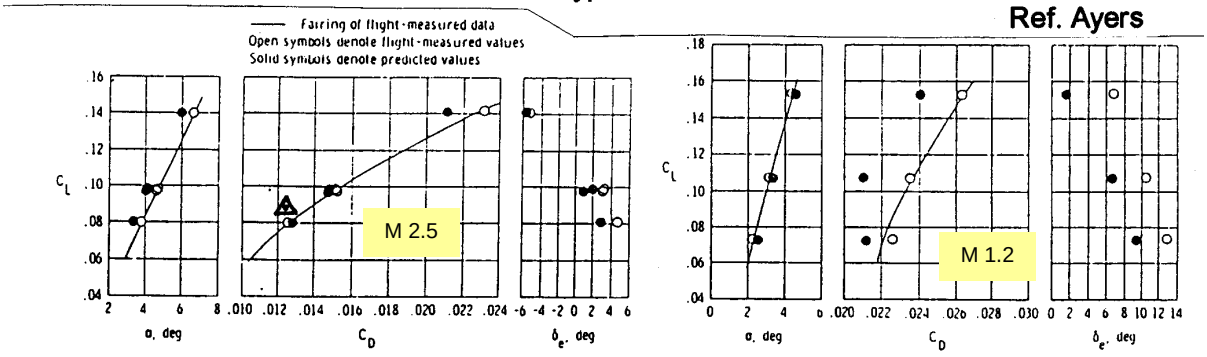

Fig. 4.3.3. XB-70 FLIGHT TEST DATA (Ref. Ayers & McCormick)

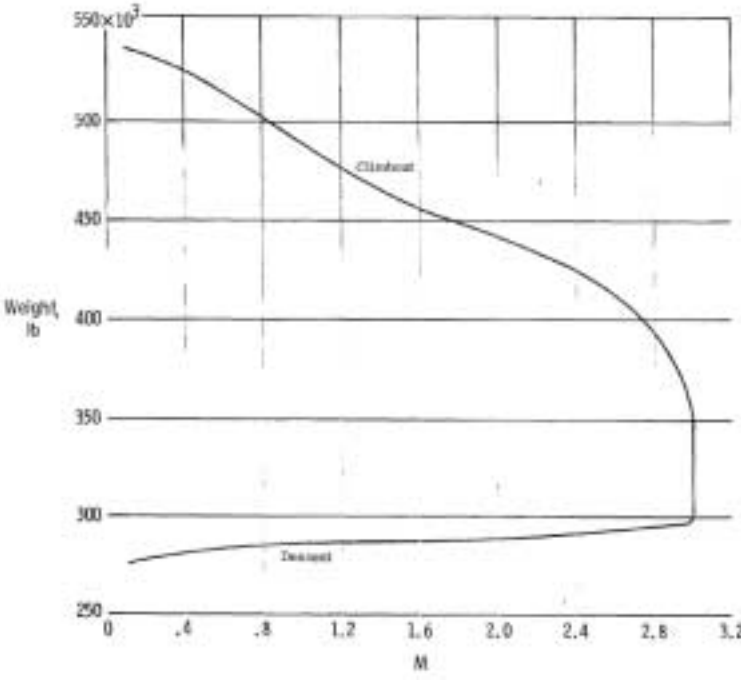

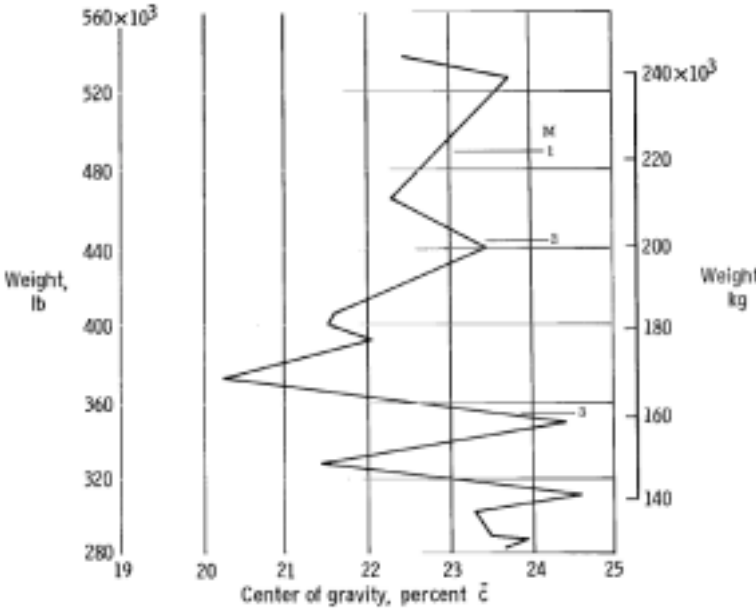

Figure 8. – Variation of center of gravity of XB-70-2 with weight during Mach 3.0 flight.

Fig. 4.3.4. VARIATION of XB-70-2 WEIGHT with MACH No. DURING MACH 3.0 FLIGHT, Ref.14

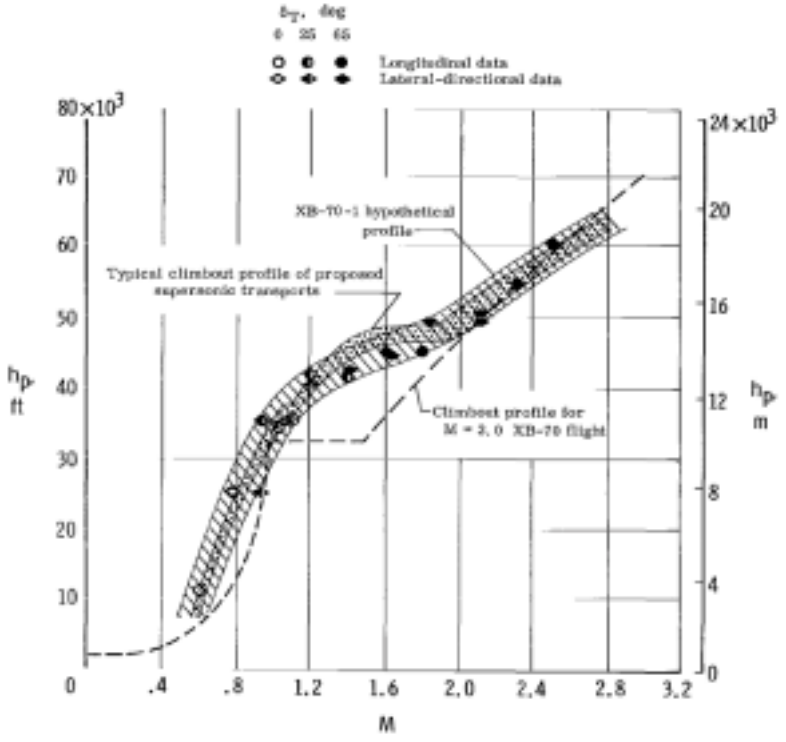

Figure 6. – Comparison of typical climbout profile of proposed supersonic transports with hypothetical climbout profile and flight data of the XB-70-1.

Fig. 4.3.5. TYPICAL CLIMB-OUT PROFILE OF PROPOSED SUPERSONIC TRANSPORTS, XB-70-1 HYPOTHETICAL PROFILE and CLIMB-OUT PROFILE FOR M 3.0 XB-70 FLIGHT, Ref.14

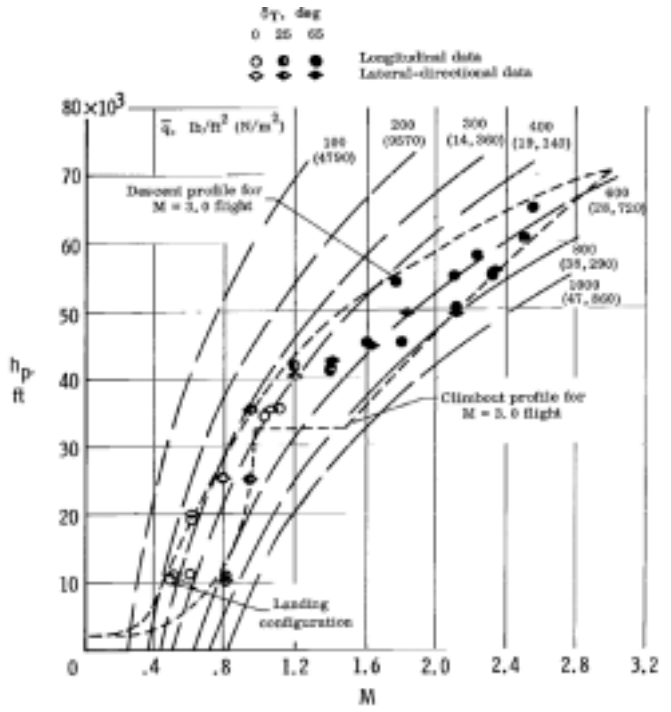

Figure 5. – XB-70-1 stability and control data points. (See table and IV for flight conditions.)

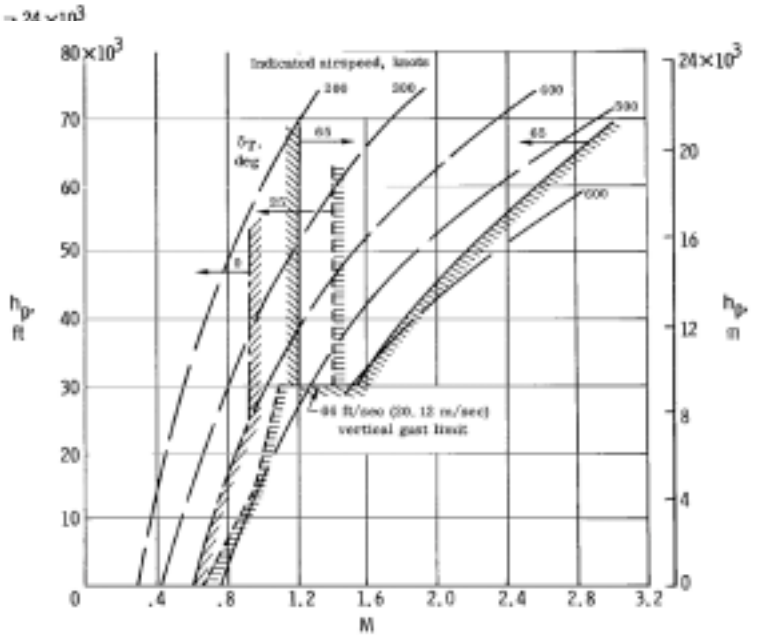

Figure 2. – Operational limits of the three wing-tip configurations of the XB-70-1

Fig. 4.3.6. XB-70 FLIGHT ENVELOPE, TIP DEFLECTION REQUIREMENTS, Ref.14

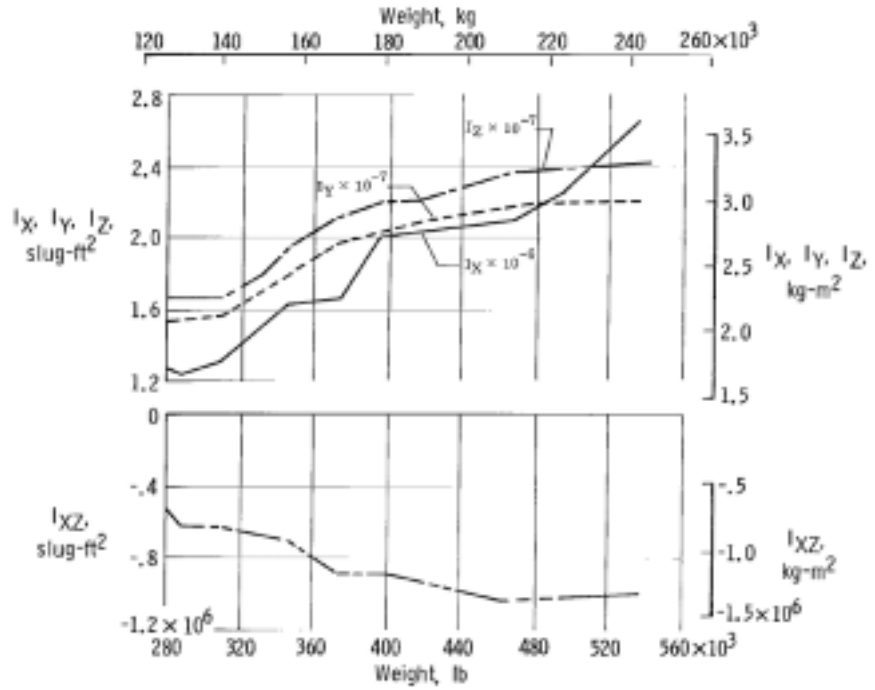

Figure 9. – Variation of moments and product of inertia of XB-70-2 with gross weight during Mach 3.0 flight.

Fig. 4.3.7. VARIATION OF MOMENTS and PRODUCT OF INERTIA with WEIGHT XB-70-2, M 3.0 FLIGHT, Ref.14

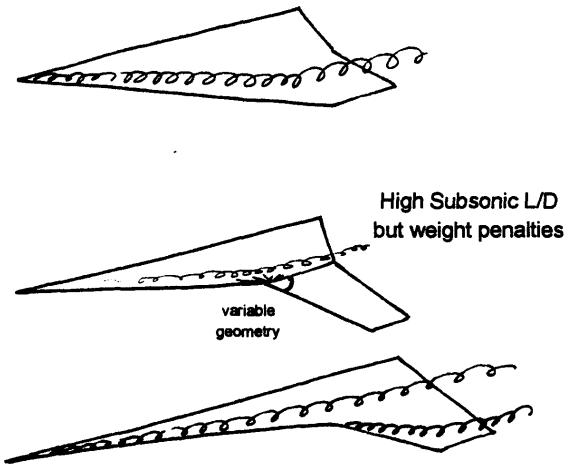

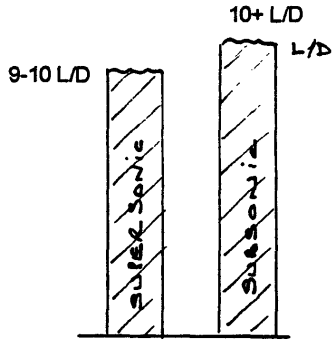

Typical Vortex Patterns Arising on Delta, Variable Geometry Delta, Cranked Delta

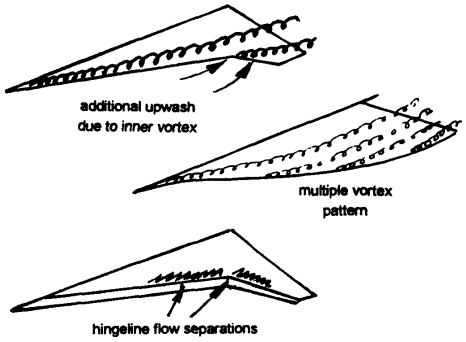

Typical Vortex Patterns Arising on Cranked Delta, Curved LE

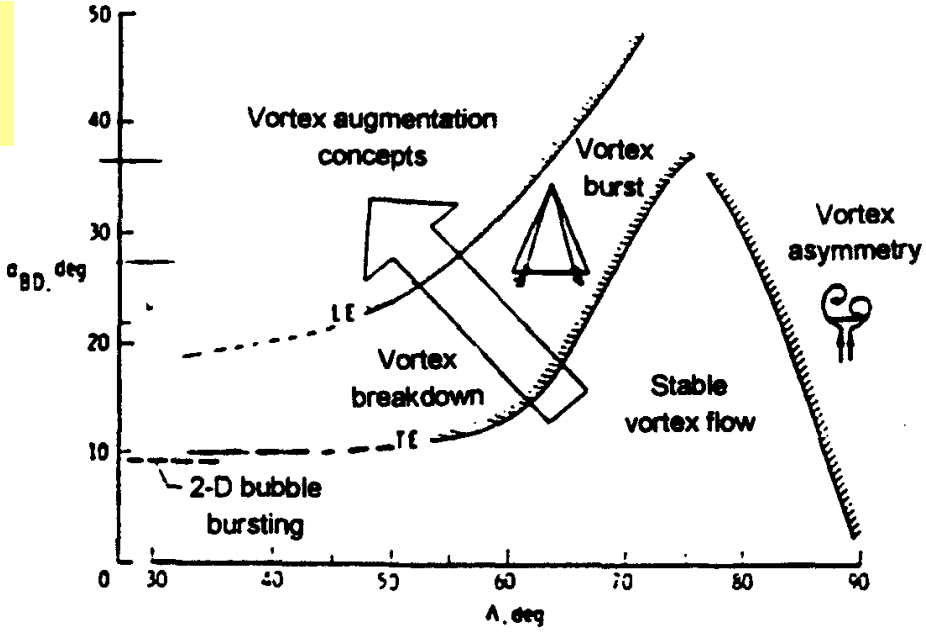

LE VORTEX BREAKDOWN TRENDS, LOW SPEED (Lamar)

Fig. 5.1.1. LE VORTEX DEVELOPMENT and BREAKDOWN TRENDS, PLANFORM and VARIABLE GEOMETRY EFFECTS

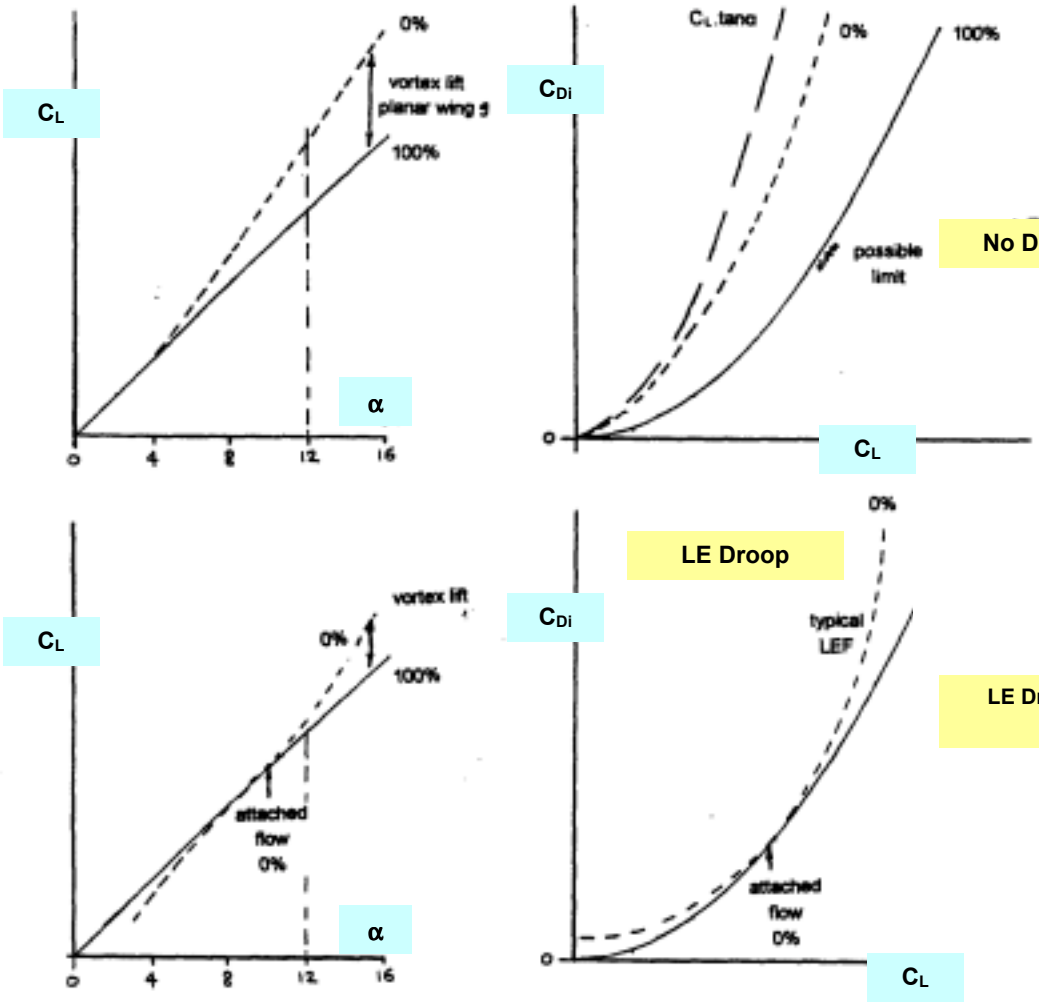

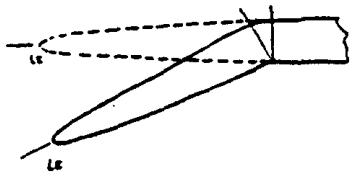

LE Droop, Hinge-line at lower surface, rounded "knuckle"

Fig. 5.1.2. LIFT, DRAG with / without LE /TE Devices

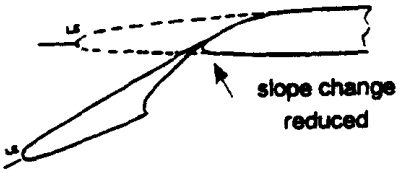

LE Slats (Sealed & Unsealed)

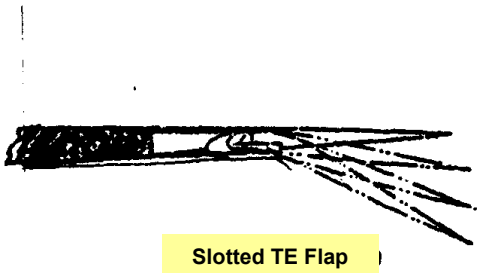

Slotted TE Flap

CONCORDE TYPE

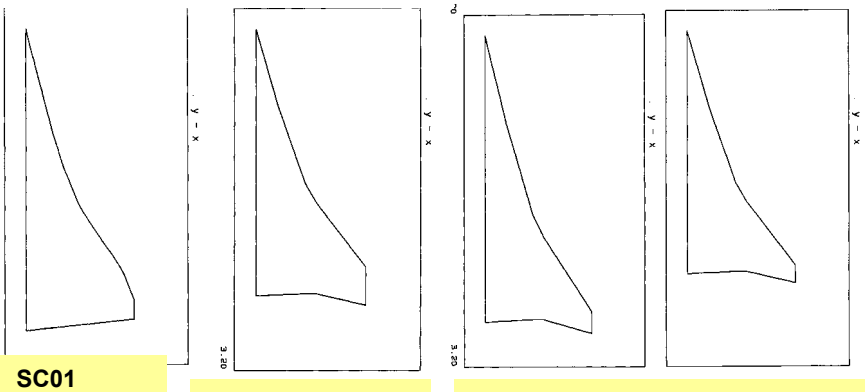

ES Series

SC01
AR = 1.54

ES01 + TE Ext
AR = 1.75

STRETCHED ES01
AR = 1.75

ES01
AR = 2.09

Fig. 5.1.3. PLANFORM DEVELOPMENT INCREASING AR

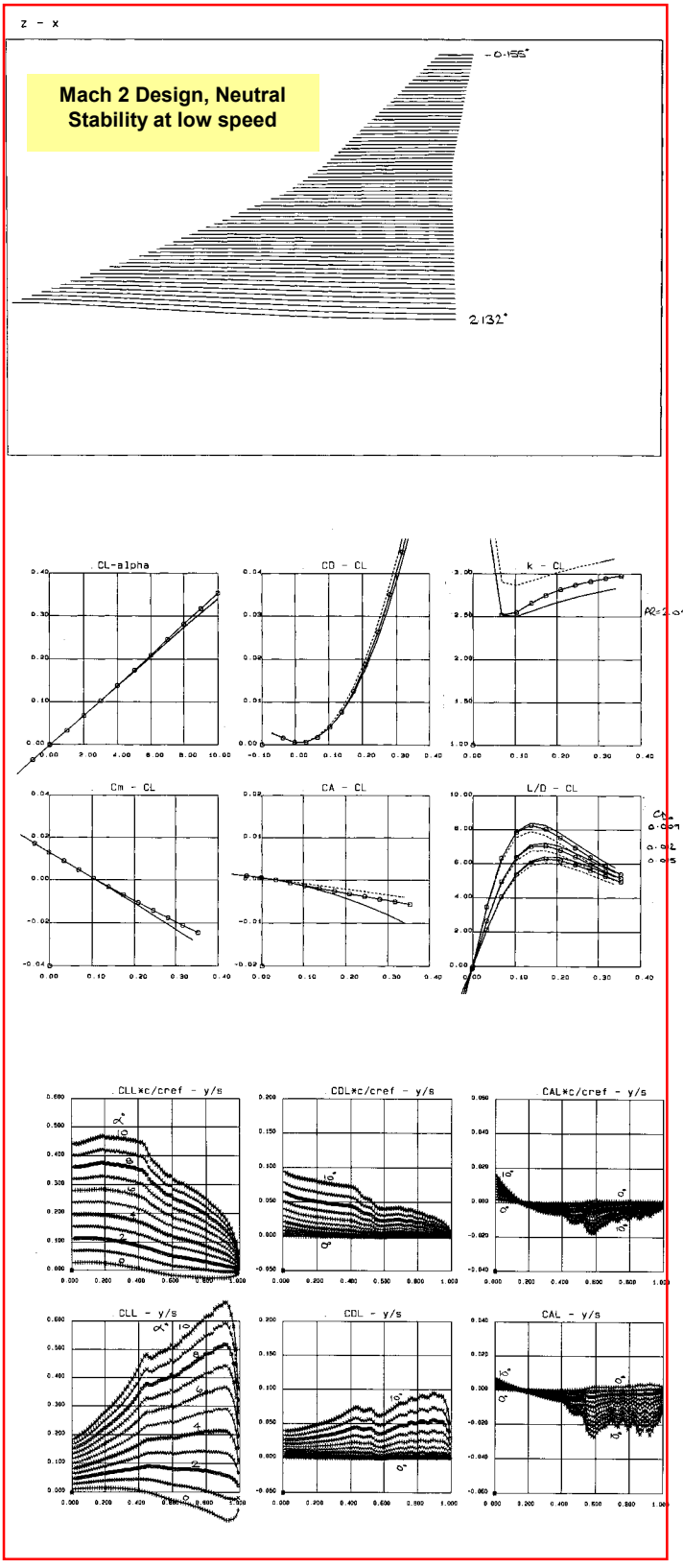

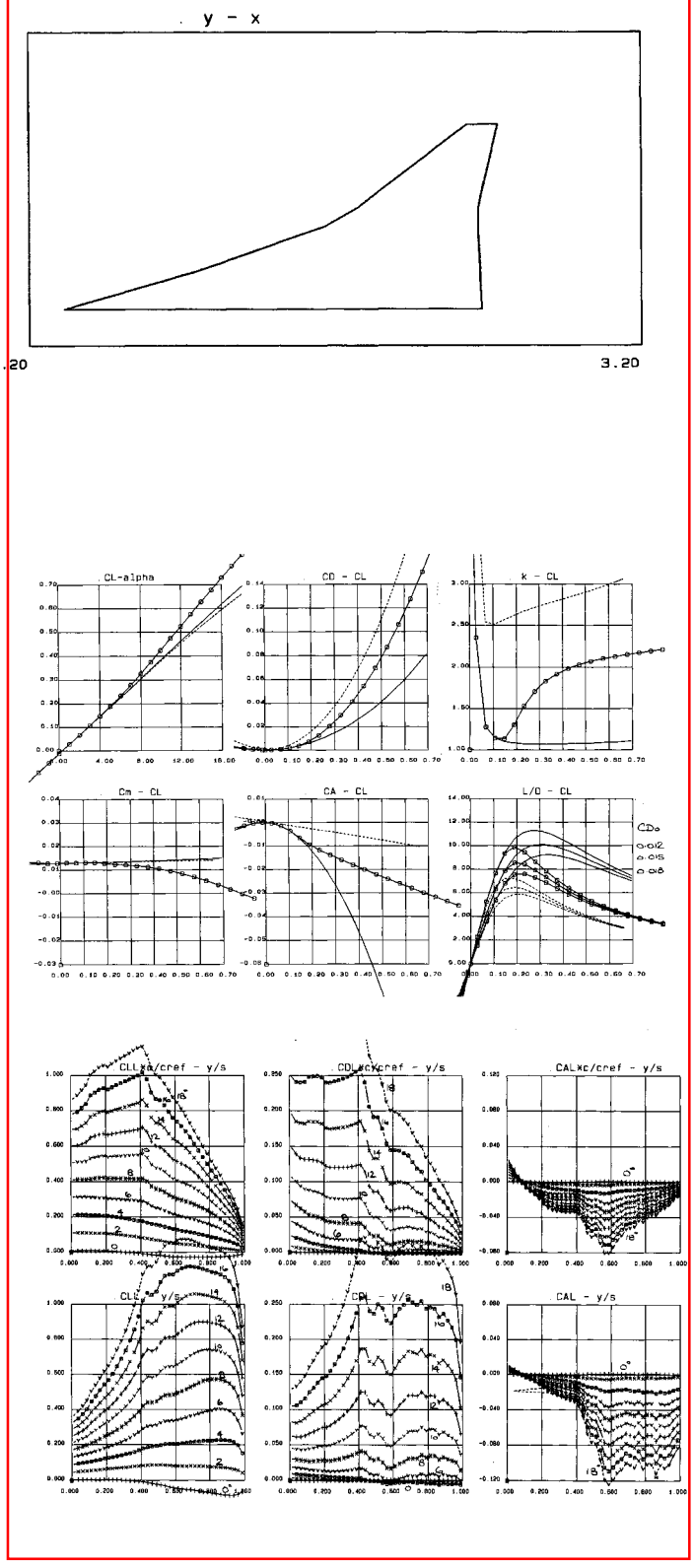

Fig. 5.1.4. ES01 DESIGNED FOR M 2, CL = 0.1 PREDICTED AERODYNAMIC CHARACTERISTICS, M 2

Fig. 5.1.5. ES01 M 2, CL=0.1 DESIGN EVALUATED AT M 0.3

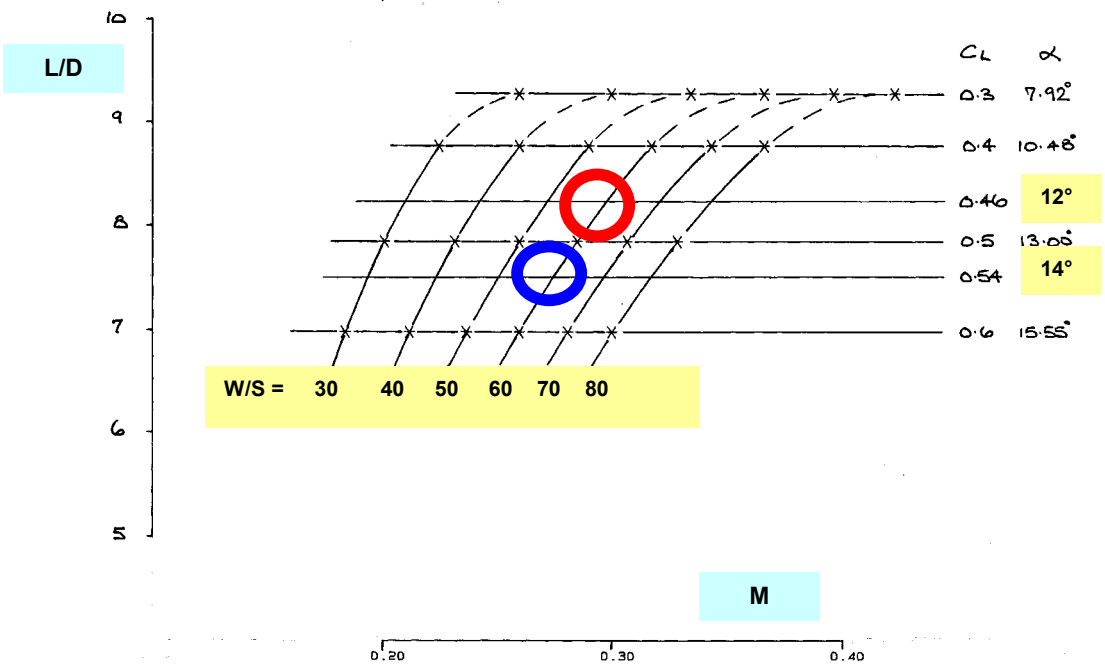

(a) No Vortex Lift

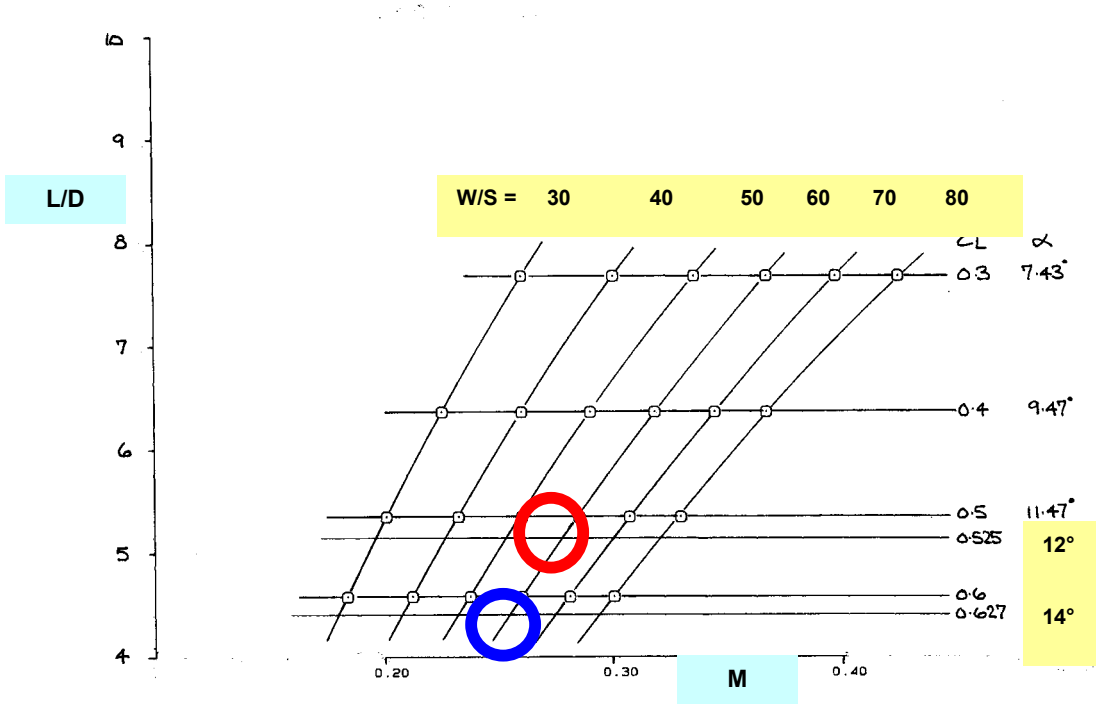

(a) Assuming Vortex Lift

Fig. 5.1.6. ES01 LOW-SPEED PERFORMANCE OF CL=0.1 DESIGN, EFFECT OF VORTEX LIFT

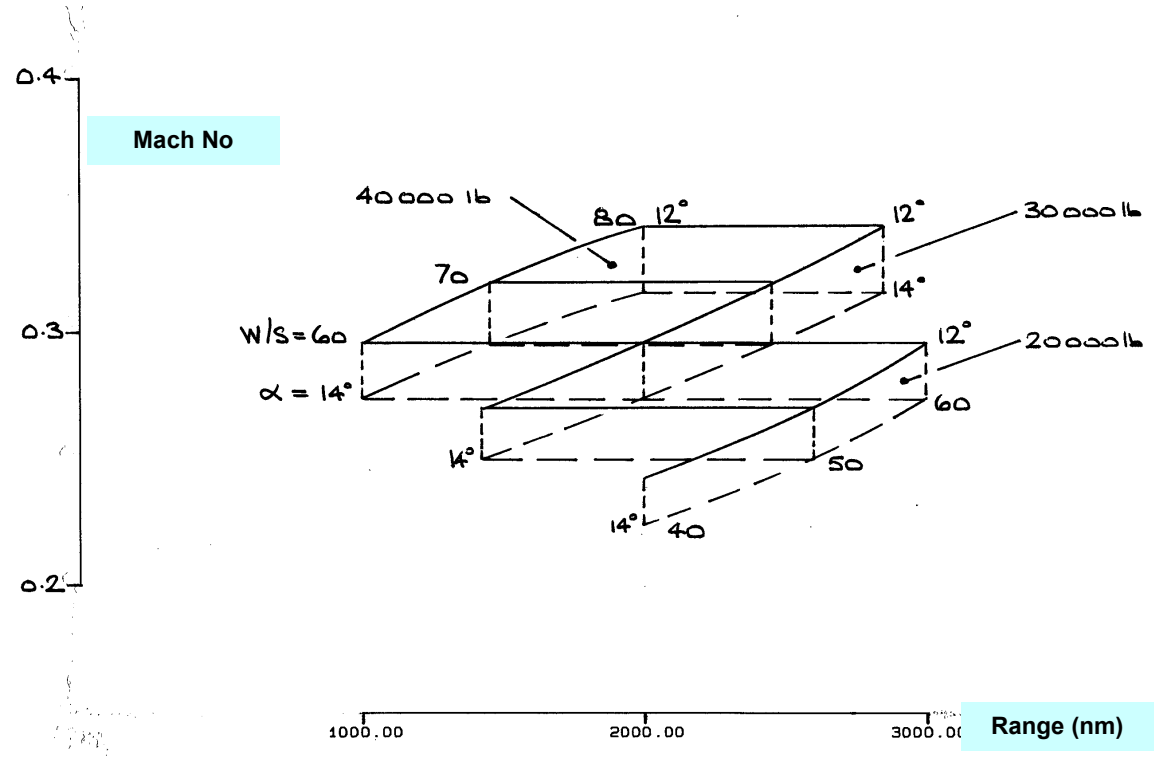

(a) Low-Speed (Take-off or Landing), Without Vortex Lift

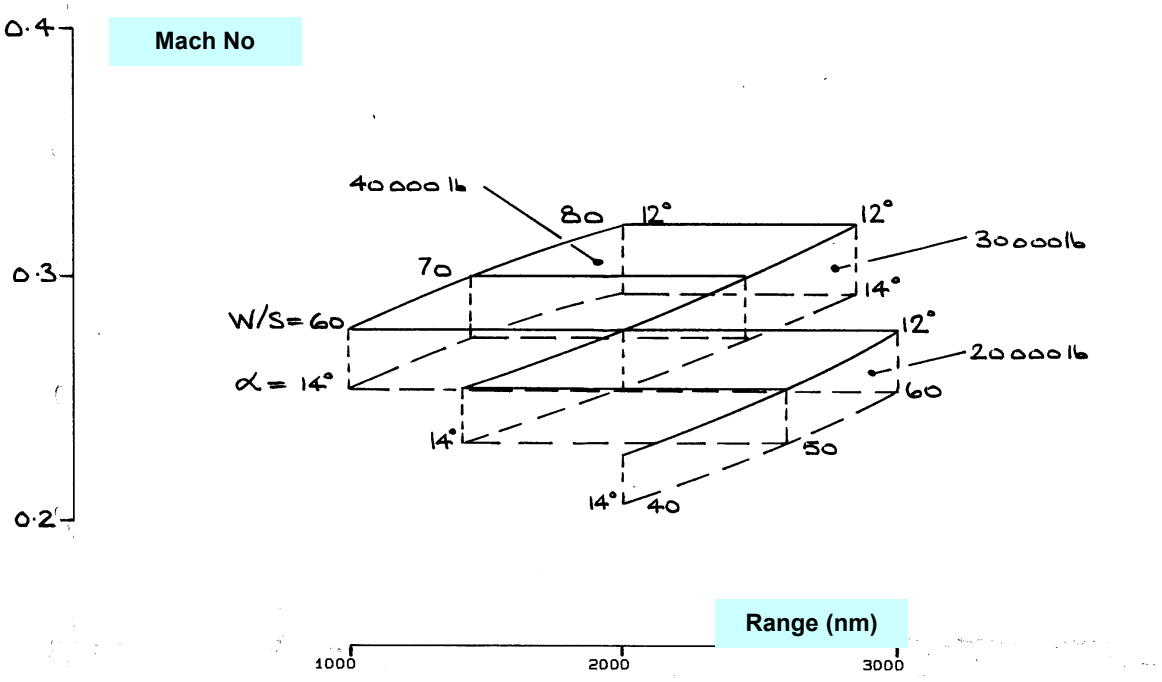

(b) Low-Speed (Take-off or Landing), Assuming Vortex Lift

Fig. 5.1.7. TAKE-OFF MACH NUMBER PLOTTED AGAINST RANGE ACHIEVED FOR DIFFERENT WING LOADINGS AND AIRCRAFT WEIGHT VARIATIONS, PLANFORM ES01.

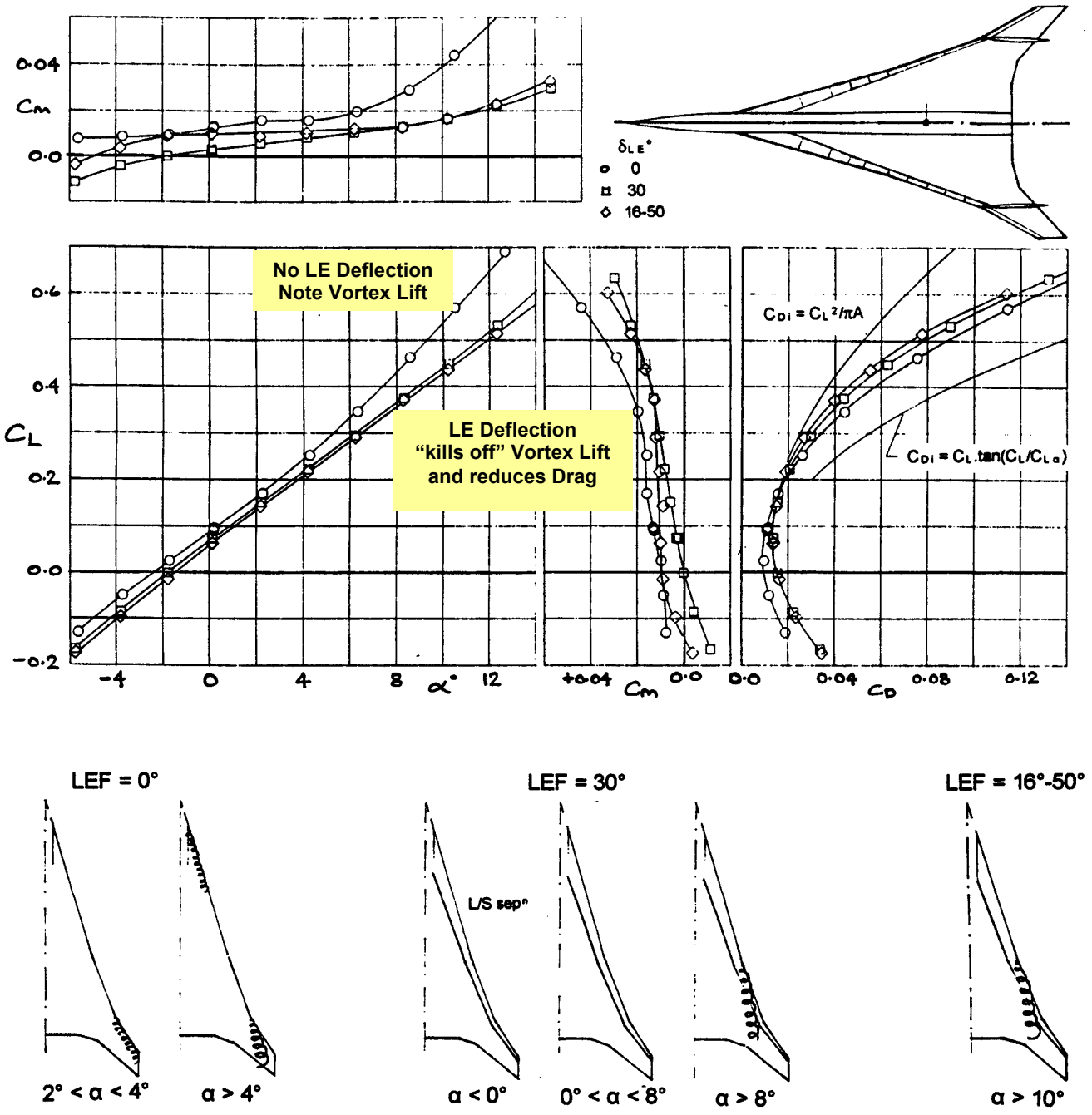

Fig. 5.1.8. LIFT, DRAG & PITCHING MOMENT, EFFECT OF LE DEFLECTION, ARROW WING CONFIGURATION

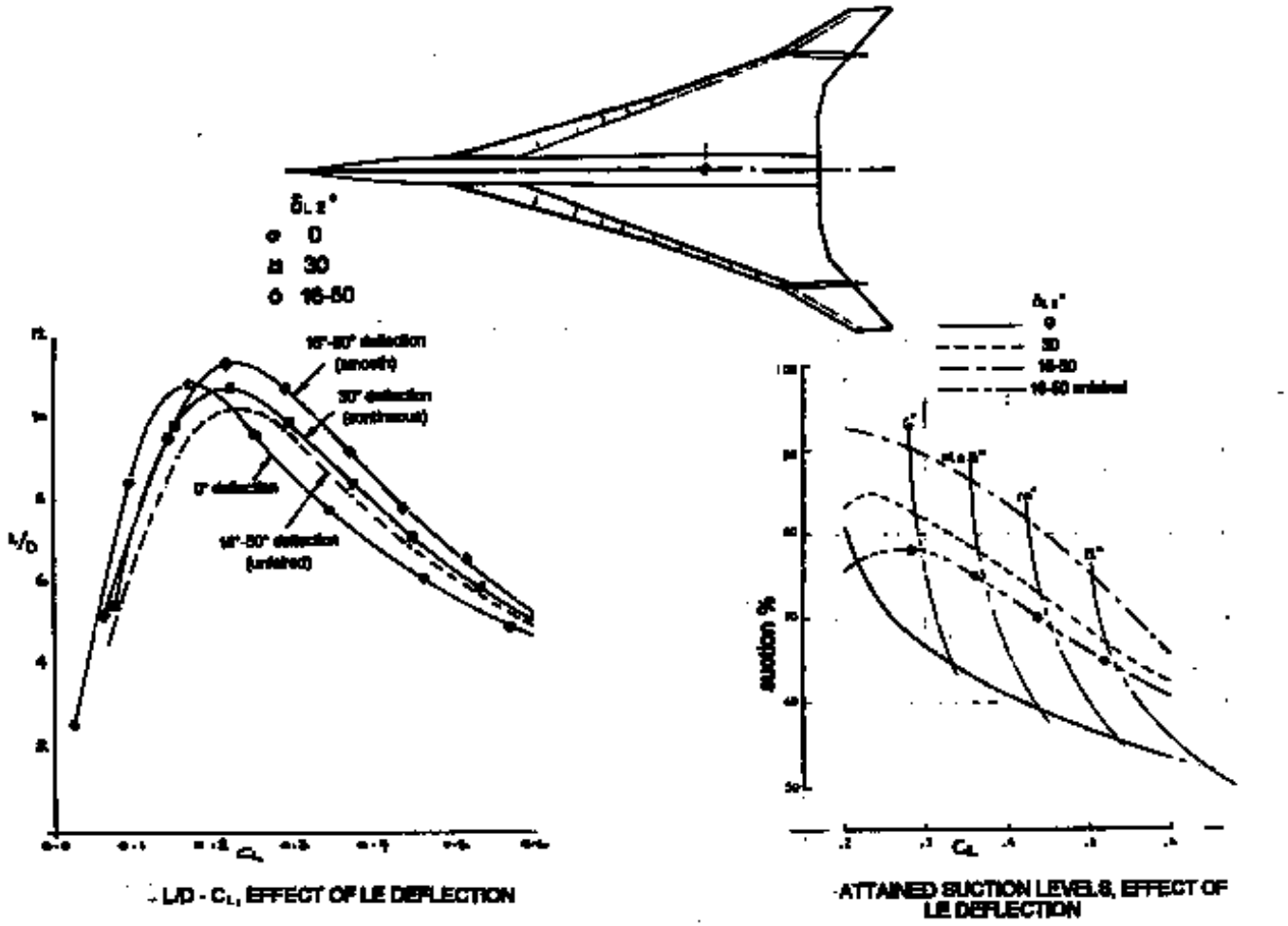

Fig. 5.1.9. LOW SPEED LE DEFLECTION OPTIMISATION ON A HIGHLY SWEPT ARROW WING CONFIGURATION (AR = 1.9). Ref.xx

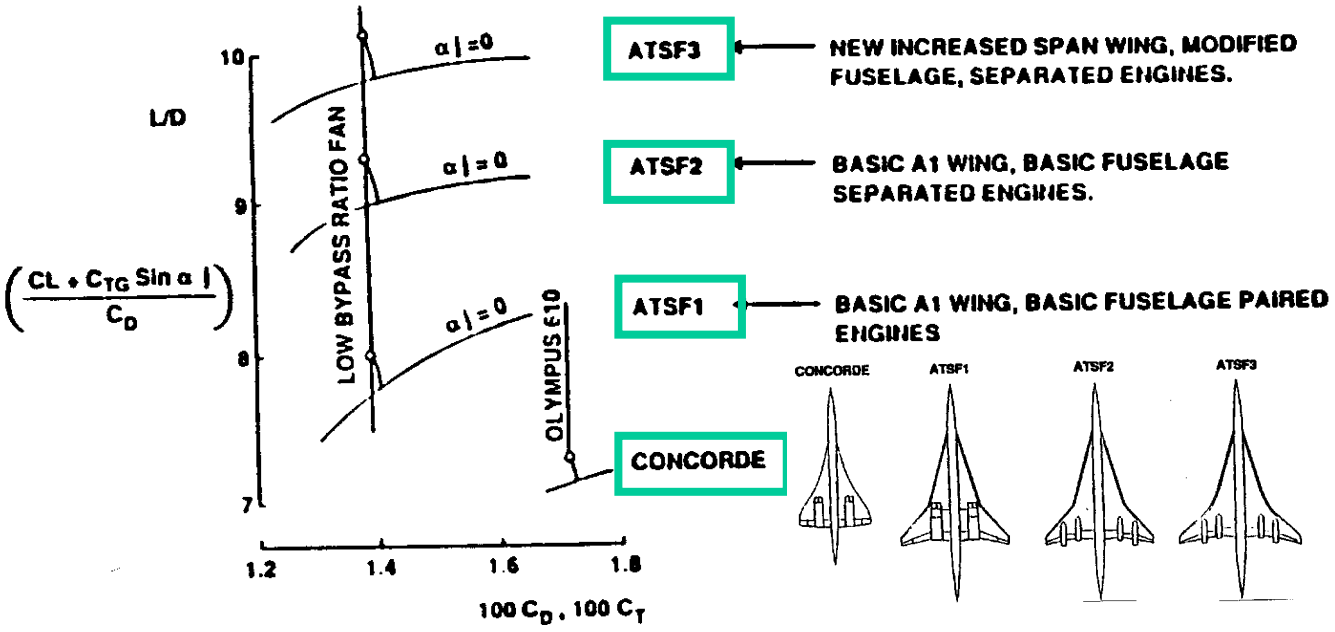

CL Lift Coefficient

$C_{T\,G} \sin \alpha_j$ Coefficient of Gross Thrust Lift Contribution

(a) Cruise L/D Improvements Relative to First Generation SST

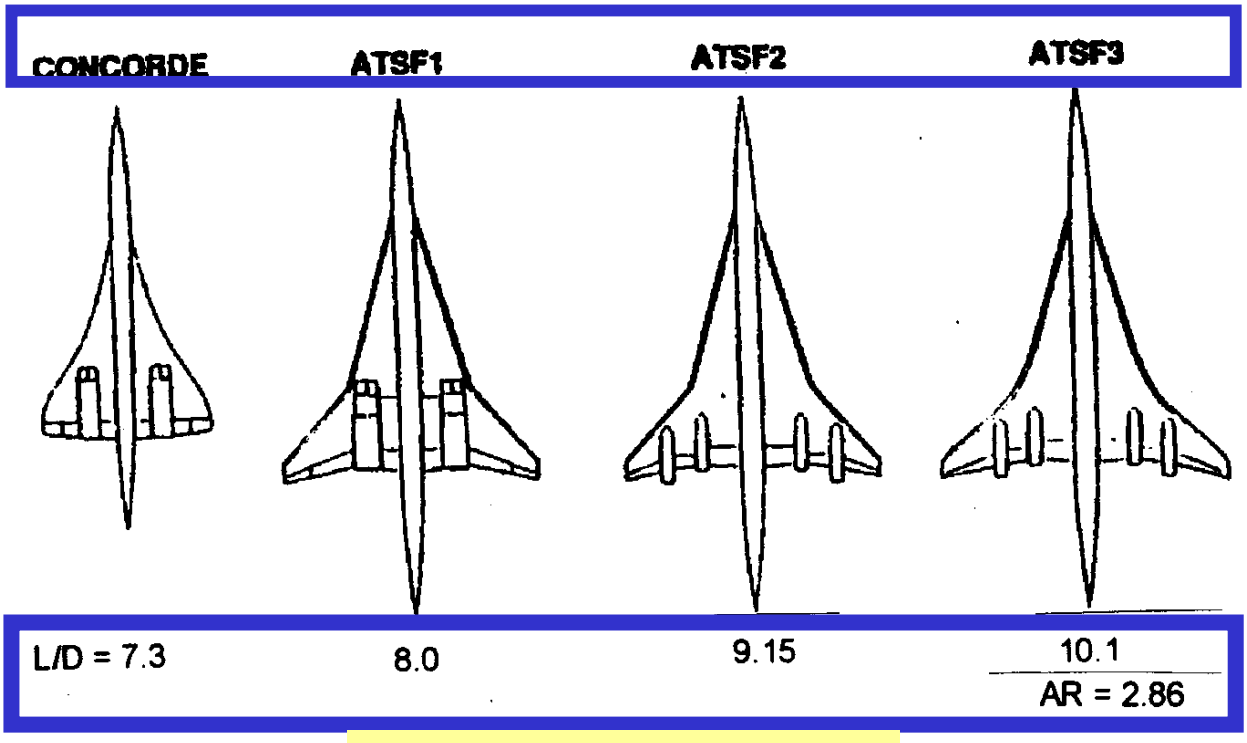

(b) Cruise Efficiency, M 2.0

Fig. 5.2.1. ATSF CONFIGURATION EVOLUTION

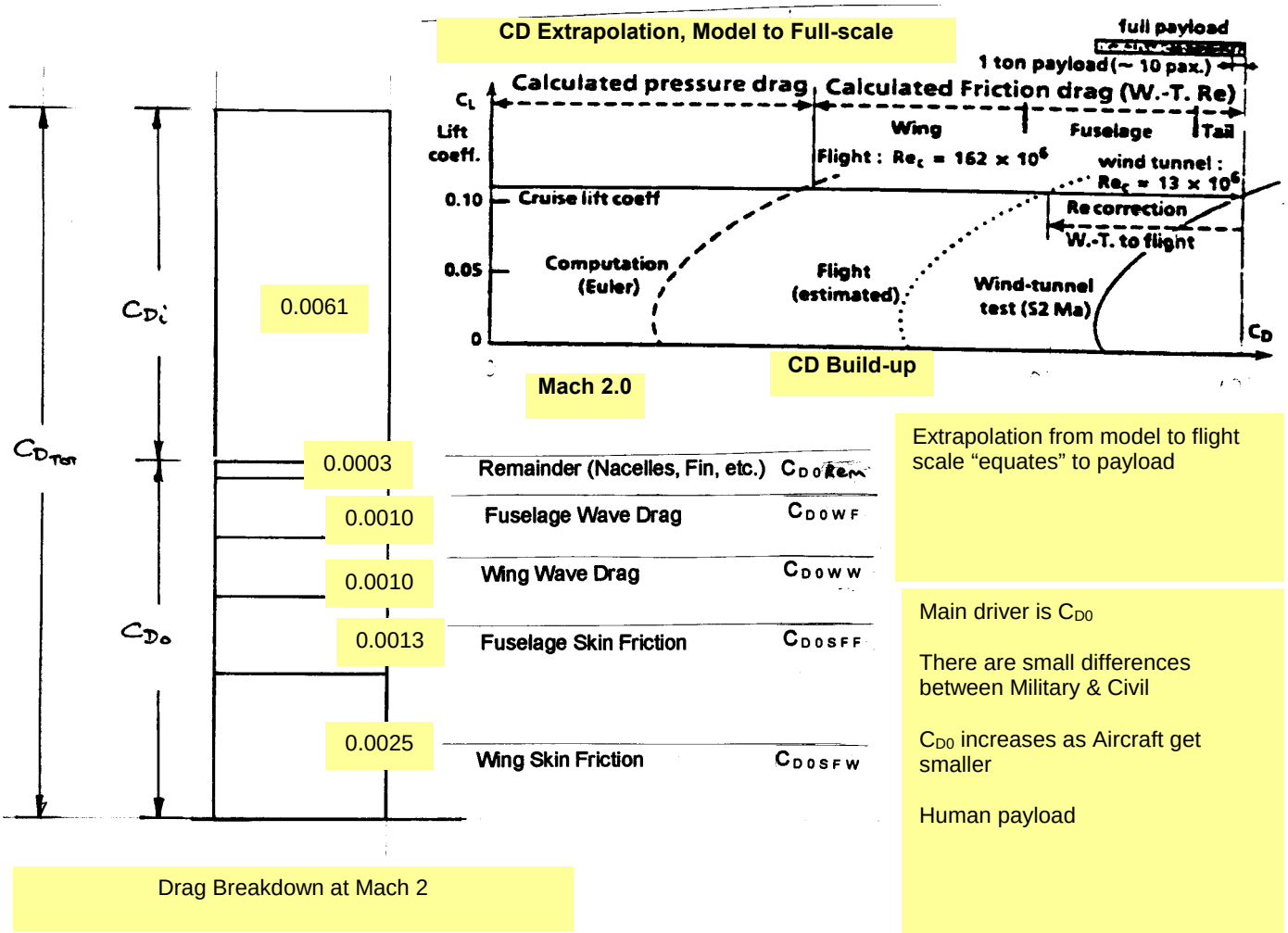

Fig. 5.2.2. TYPICAL DRAG BREAKDOWN (Derived From Fig.4.2.8)

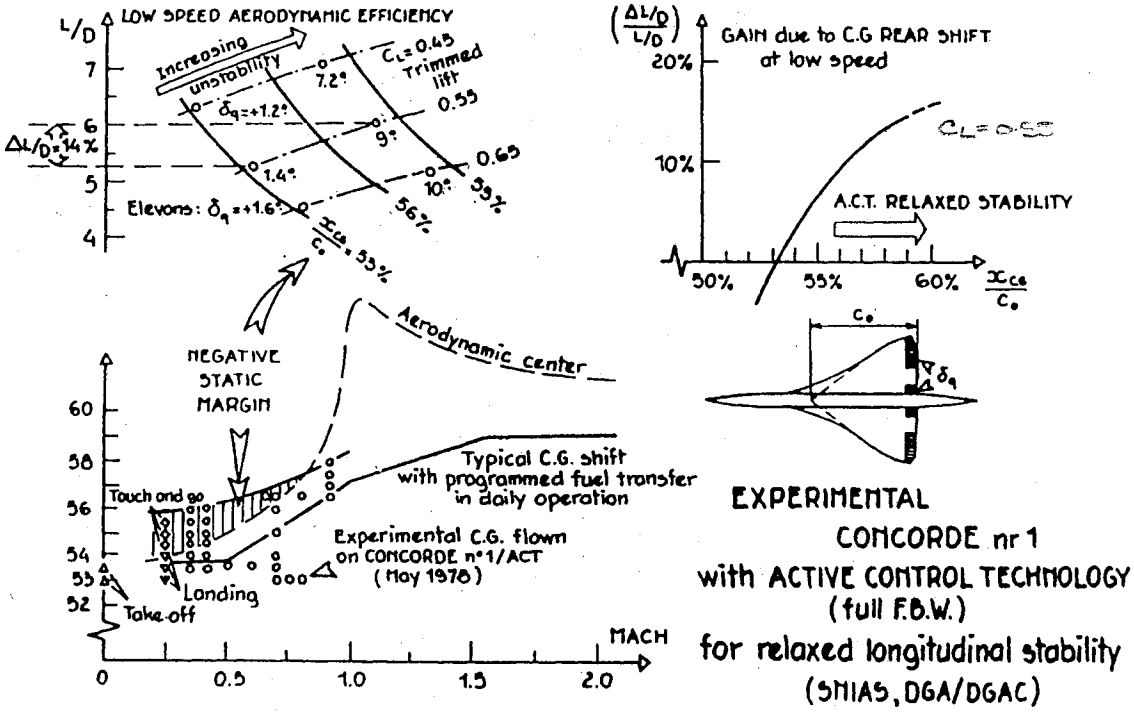

Fig. 5.3.1. CONCORDE LOW SPEED AERODYNAMIC EFFICIENCY IMPROVEMENTS ARISING FROM RELAXED STABILITY, Ref.23

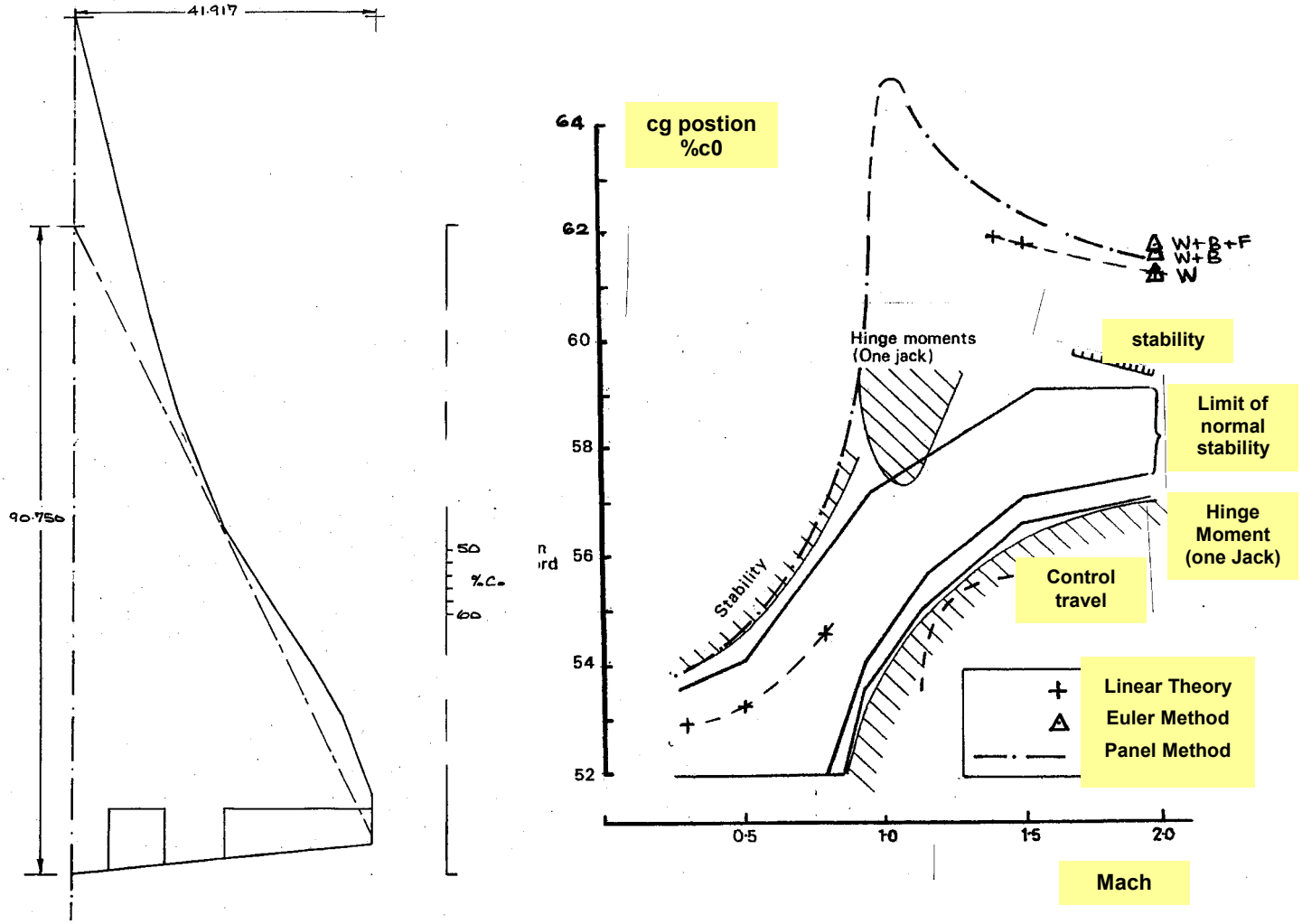

(a) Simplified Concorde Planform Reference c_o Location

(b) Centre of Gravity Location (%c_o) and Centre of Pressure Variation with M

Fig. 5.3.2. CONCORDE CENTRE OF PRESSURE and CENTRE OF GRAVITY LOCATION AS M VARIES

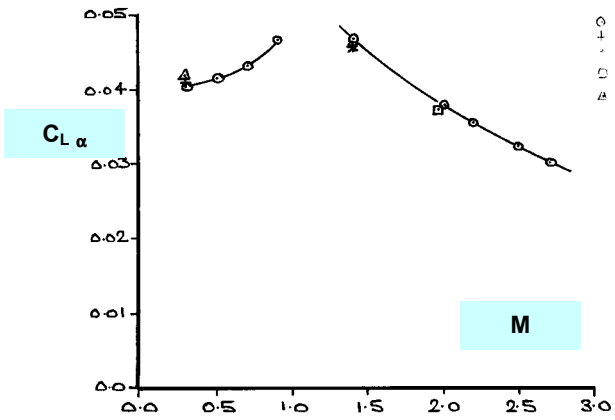

Fig. 5.3.3. $C_{L\alpha}$ VARIATION with MACH NUMBER

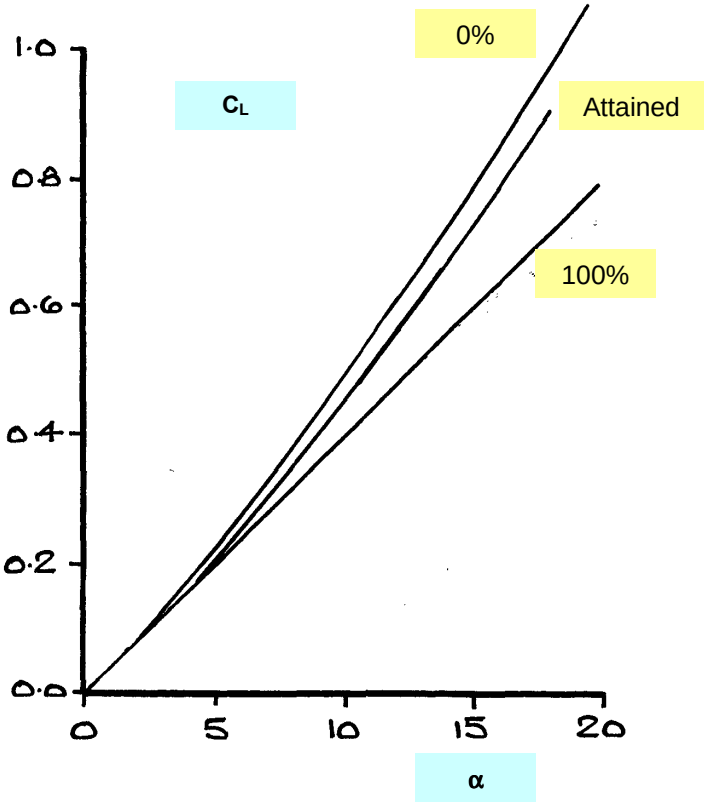

Fig. 5.3.4. C_L – α, M 0.3

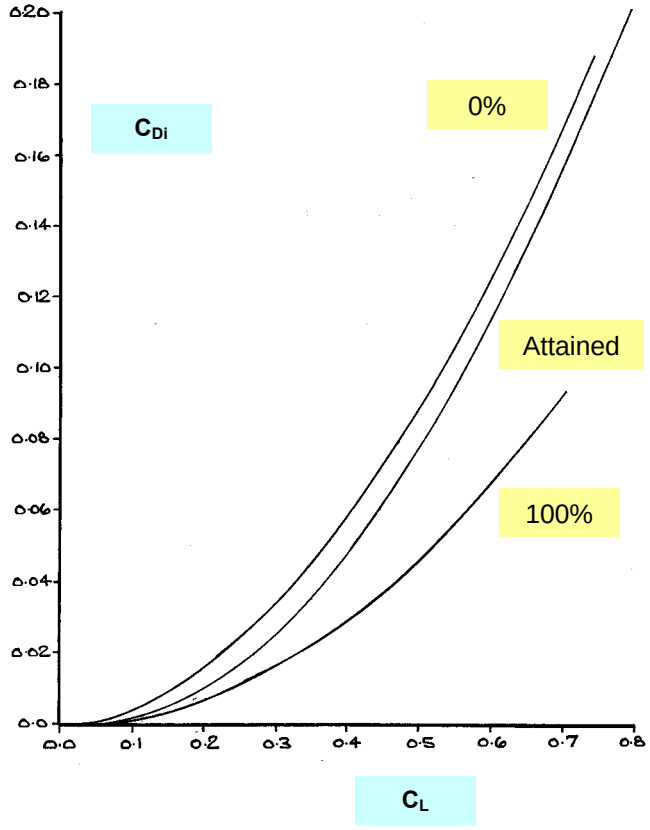

Fig. 5.3.5. CONCORDE PREDICTED C_{Di} - C_L, M 0.3

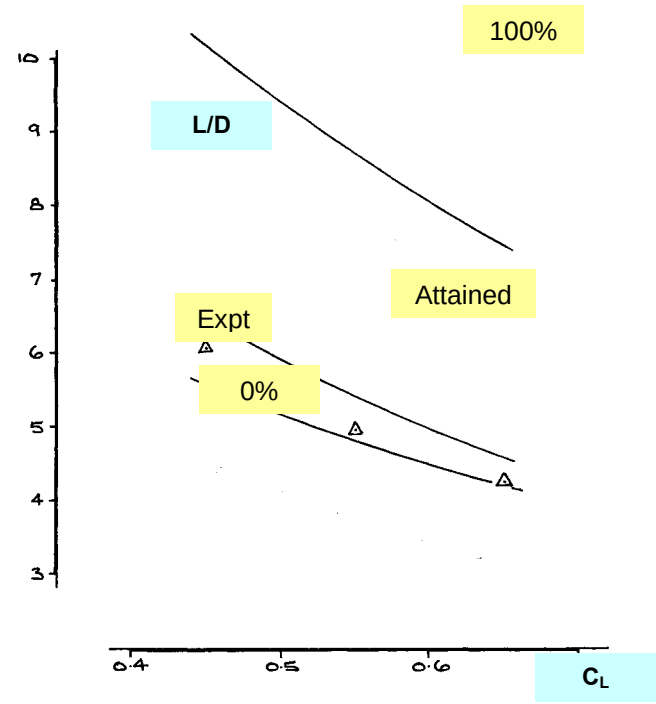

Fig. 5.3.6. CONCORDE L/D - C_L, M 0.3, THEORY (C_{Do} 0.0070) and EXPERIMENT

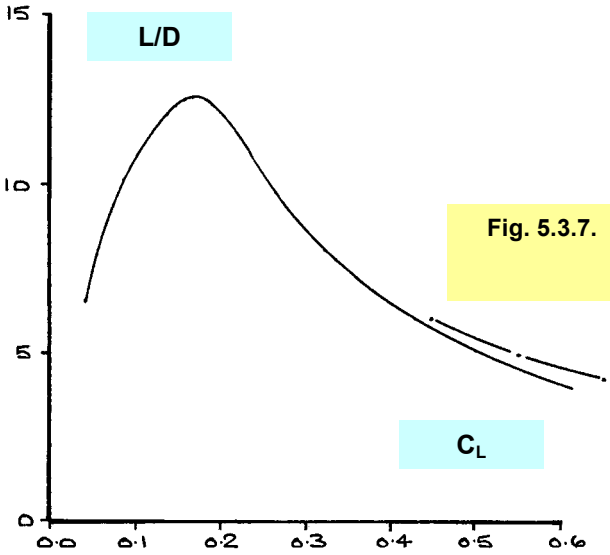

Fig. 5.3.7. L/D - C_L, LOW SPEED, EXPERIMENT, Refs. 10 & 11

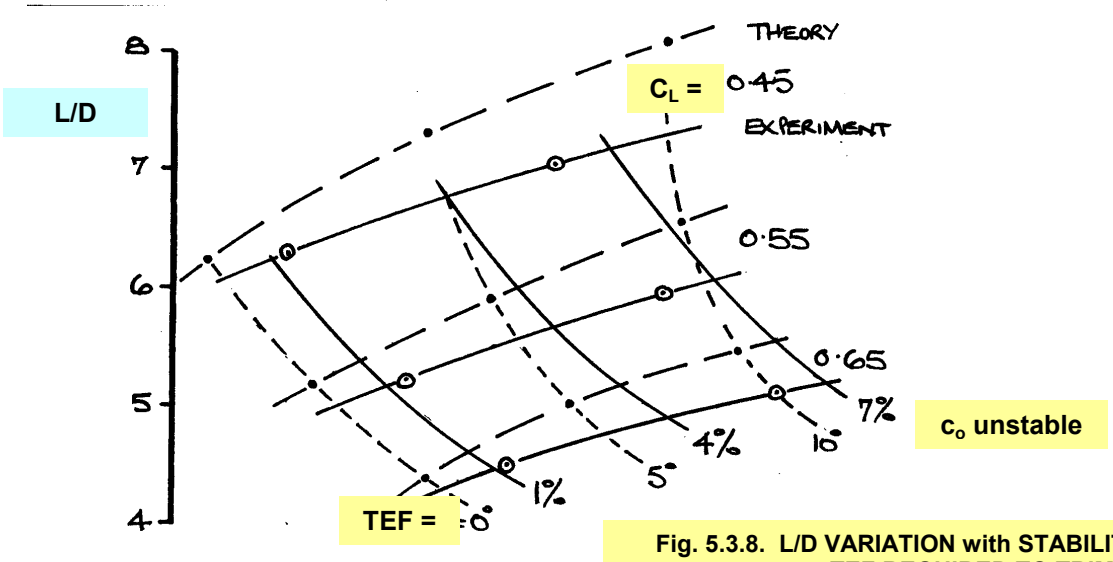

Fig. 5.3.8. L/D VARIATION with STABILITY MARGIN and TEF REQUIRED TO TRIM, THEORY (M 0.3) and EXPERIMENT (Low speed) C_L = 0.45, 0.55 & 0.65

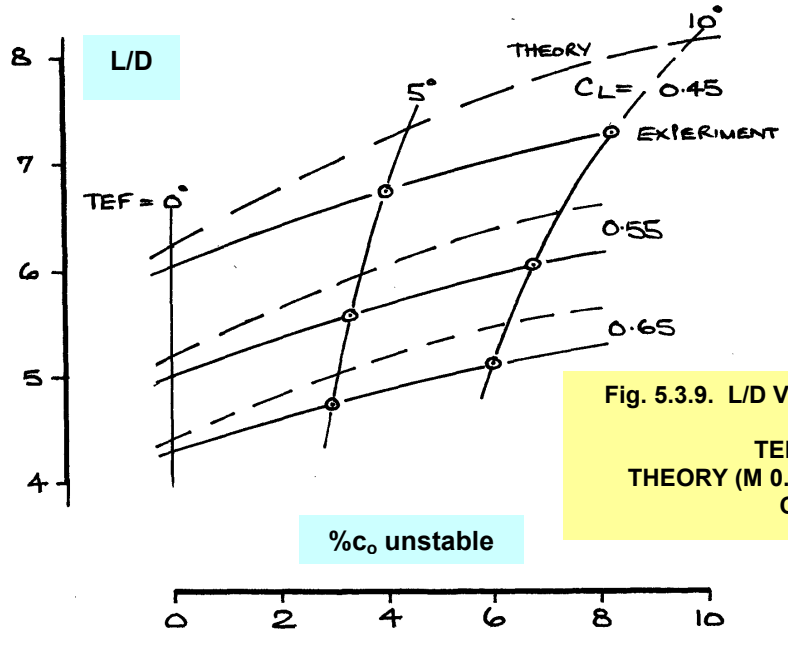

Fig. 5.3.9. L/D VARIATION with STABILITY MARGIN and TEF REQUIRED TO TRIM, THEORY (M 0.3) and EXPERIMENT (Low speed) C_L = 0.45, 0.55 & 0.65

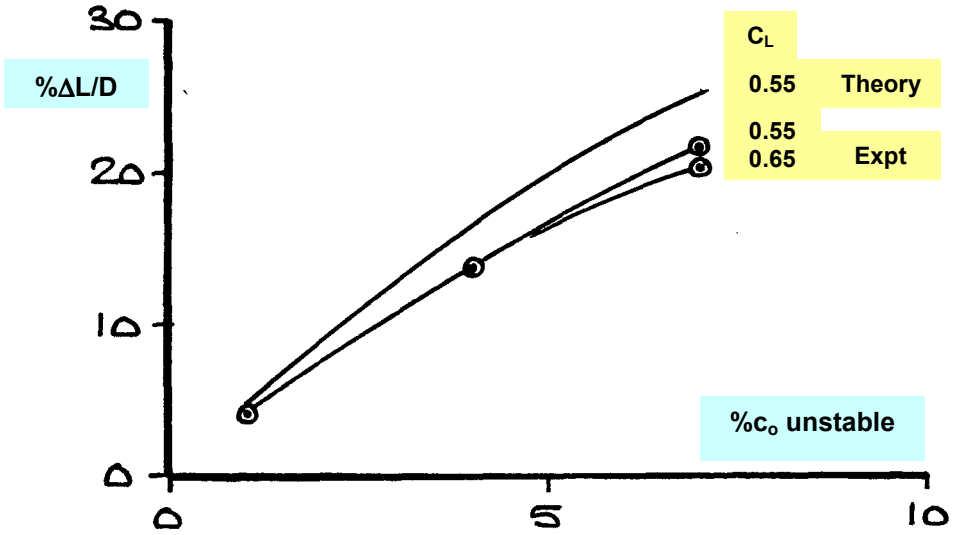

Fig. 5.3.10. ΔL/D% (based on L/D at 0%) VARIATION WITH INSTABILITY MARGIN THEORY (M 0.3) and EXPERIMENT (Low speed)

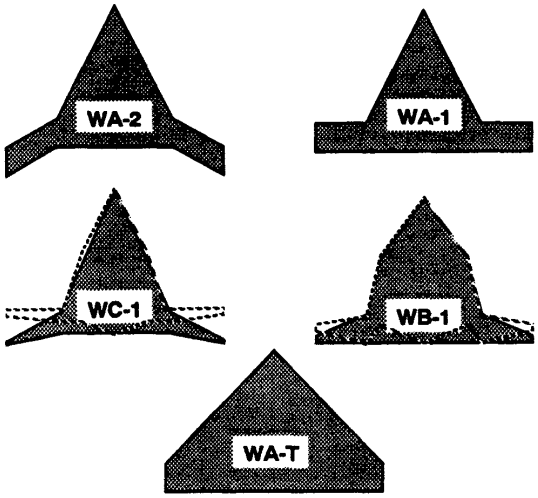

Fig. 17: **Planform of the wings tested at the validation phase**

Wings WA-1, WA-2, and WA-T have a root of 16

Schlieren photographs of transonic and supersonic Mach number tests are shown in Fig. 22

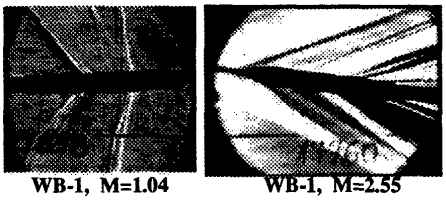

Fig. 22: **Schlieren photograph of the wing attachment**

The CoP shift obtained from the six angle of attack sweep tests are compared with the analytical predictions for wings WA-T, WB-1 and WC-1 (8DOF wings) in Fig. 23, and the lift curve slope for the same wings is compared in Fig. 24.

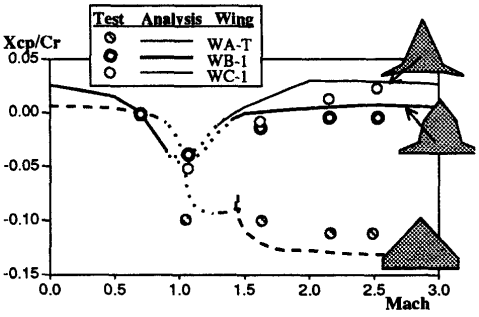

Fig. 23: **Xcp vs. Mach for three test wings**

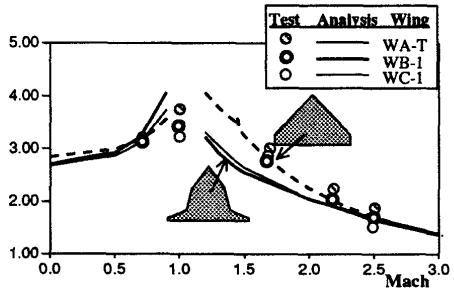

Fig. 24: $C_{L\alpha}$ **vs. Mach for three test wings**

The CoP shift of the reference wing in the supersonic regime (11% of the root chord) was clearly reduced in the optimized wings, to about 1% for wing WB-1, and less than 2% for wing WC-1 (90% and 80% improvement respectively). Even in the transonic regime, for which no optimization was done, the maximum CoP shift was reduced to 4% and 5% respectively.

The same results for the 2DOF wings, WA-1, WA-2 and the reference wings WA-T are shown in Fig. 25 and 26.

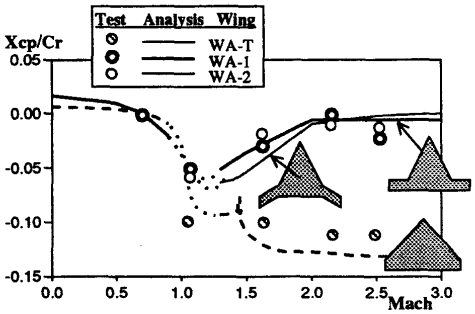

Fig. 25: **Xcp vs. Mach for three test wings**

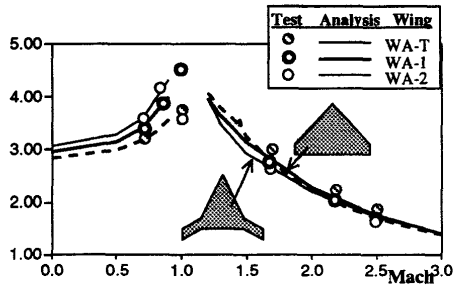

Fig. 26: $C_{L\alpha}$ **vs. Mach for three test wings**

CONCLUSIONS

The results of the wind tunnel investigation validated the results of the numerical calculation of the analytical study. The accuracy of the calculation was found to be very good for the center of pressure (3% of the wing root chord) and quite good for the lift curve slope (12%).

The test results validated the numerical optimization of the three wings and showed up to 90% reduction in CoP shift, relative to a matching trapezoidal wing.

Fig. 6.1.1. PLANFORM VARIATIONS, EFFECT ON $C_{L\alpha}$ and CoP versus M (Excerpt from Ref. 12)

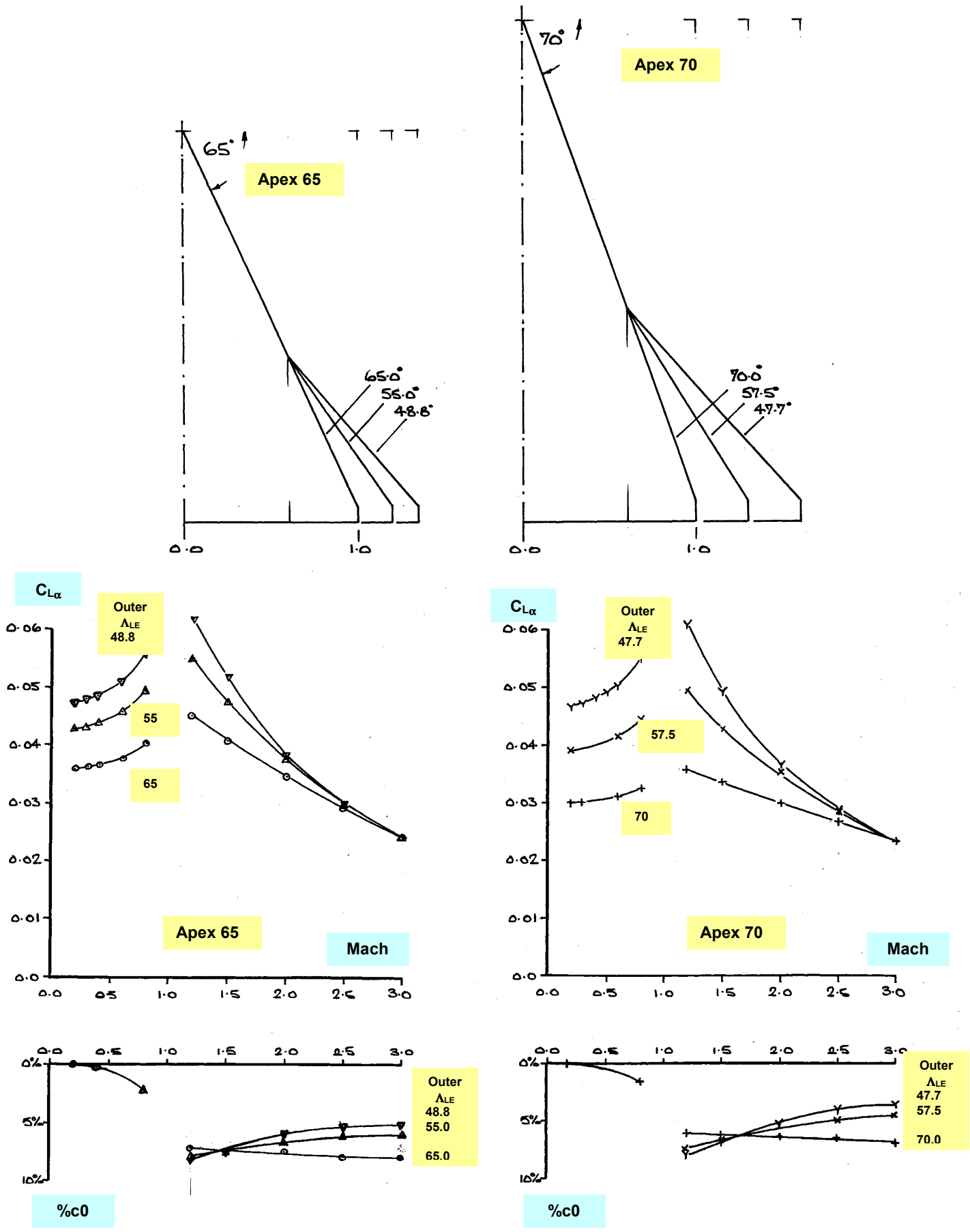

Fig.6.1.2. CRANKED PLANFORM SERIES, APEX LE SWEEP 65° & 70°, OUTER LE SWEEP VARIES LINEAR THEORY, EFFECT OF M on $C_{L\alpha}$ and %c_o MOVEMENT FROM LOW SPEED LOCATION

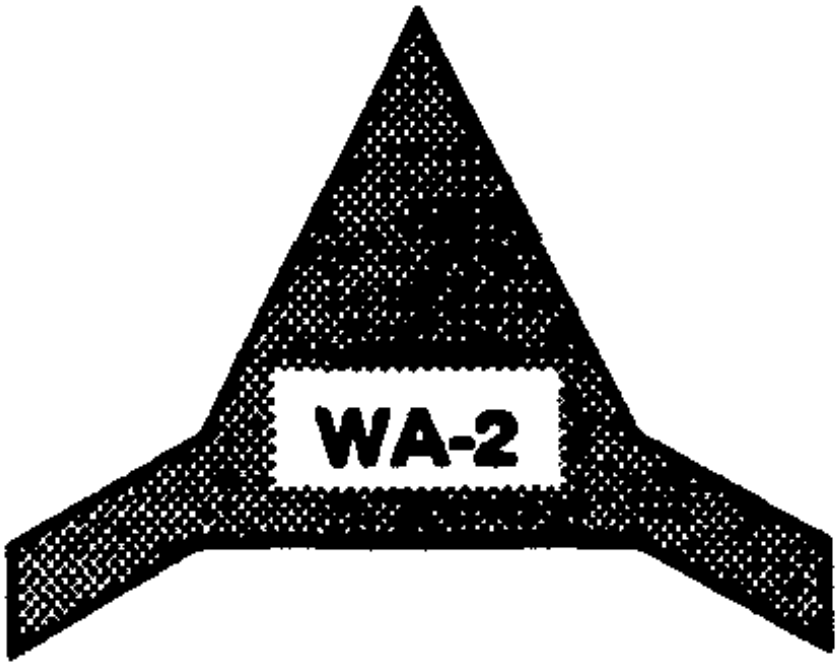

Fig.6.1.3. DELTA PLANFORM WITH TRAPEZOIDAL (CONSTANT CHORD) TIPS

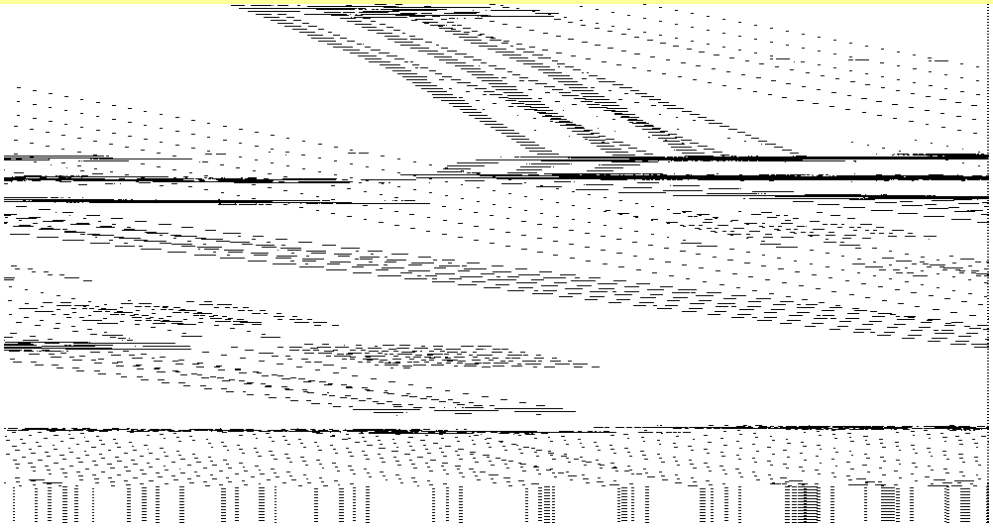

Fig.6.1.4. CRANKED PLANFORM WITH HIGHLY SWEPT TIP

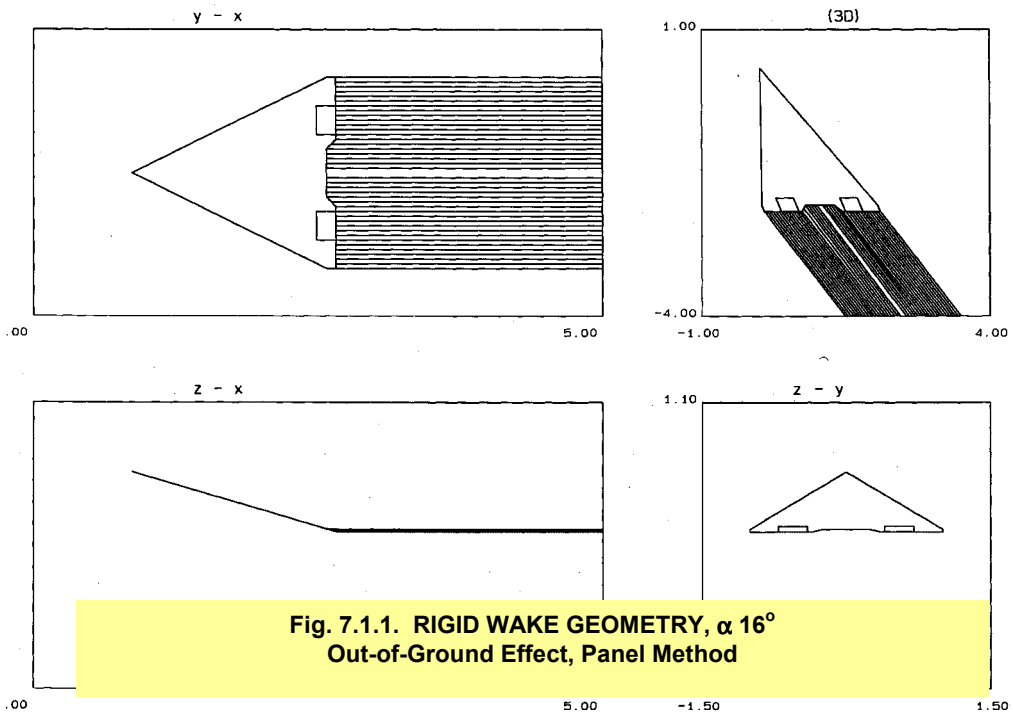

Fig. 7.1.1. RIGID WAKE GEOMETRY, α 16°
Out-of-Ground Effect, Panel Method

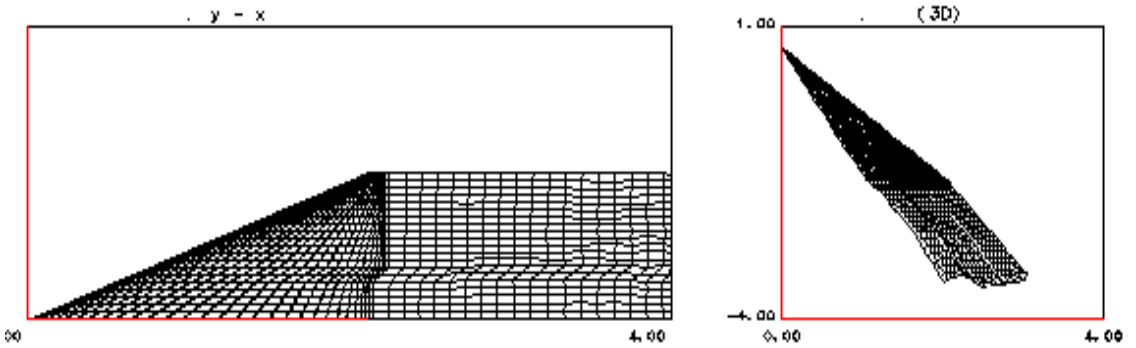

Free Air, α 12°

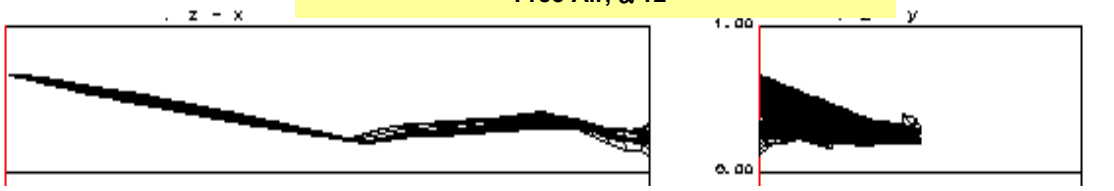

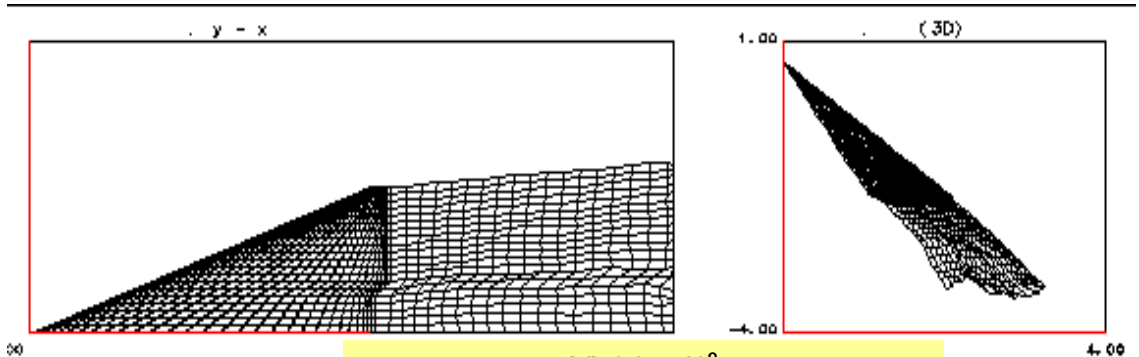

h/b 0.2, α 12°

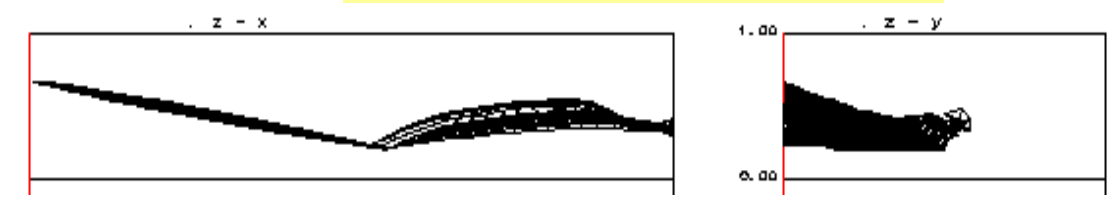

Fig. 7.1.2. RELAXED WAKE GEOMETRY, EFFECT OF GROUND PROXIMITY, M 0.3, α 12°, Using PMARC

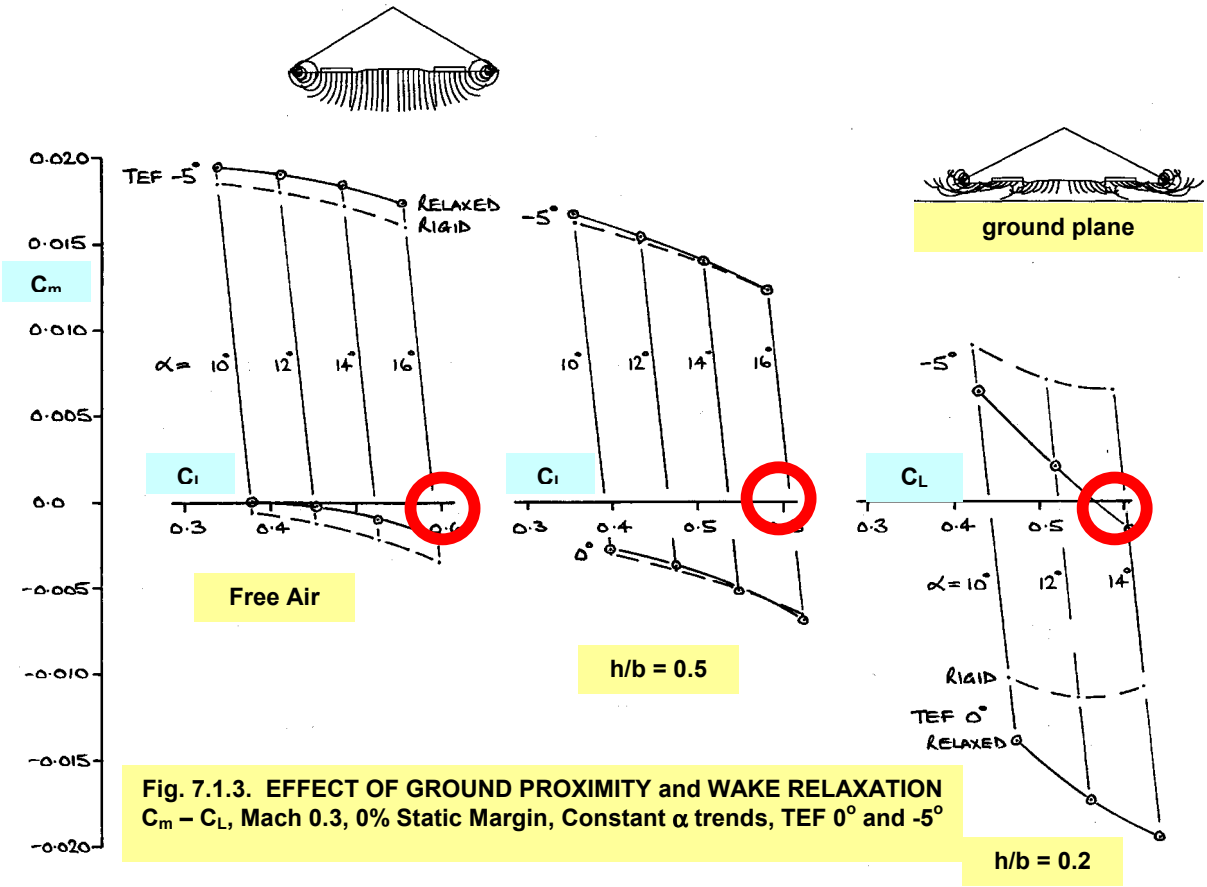

Fig. 7.1.3. EFFECT OF GROUND PROXIMITY and WAKE RELAXATION
C_m – C_L, Mach 0.3, 0% Static Margin, Constant α trends, TEF 0° and -5°

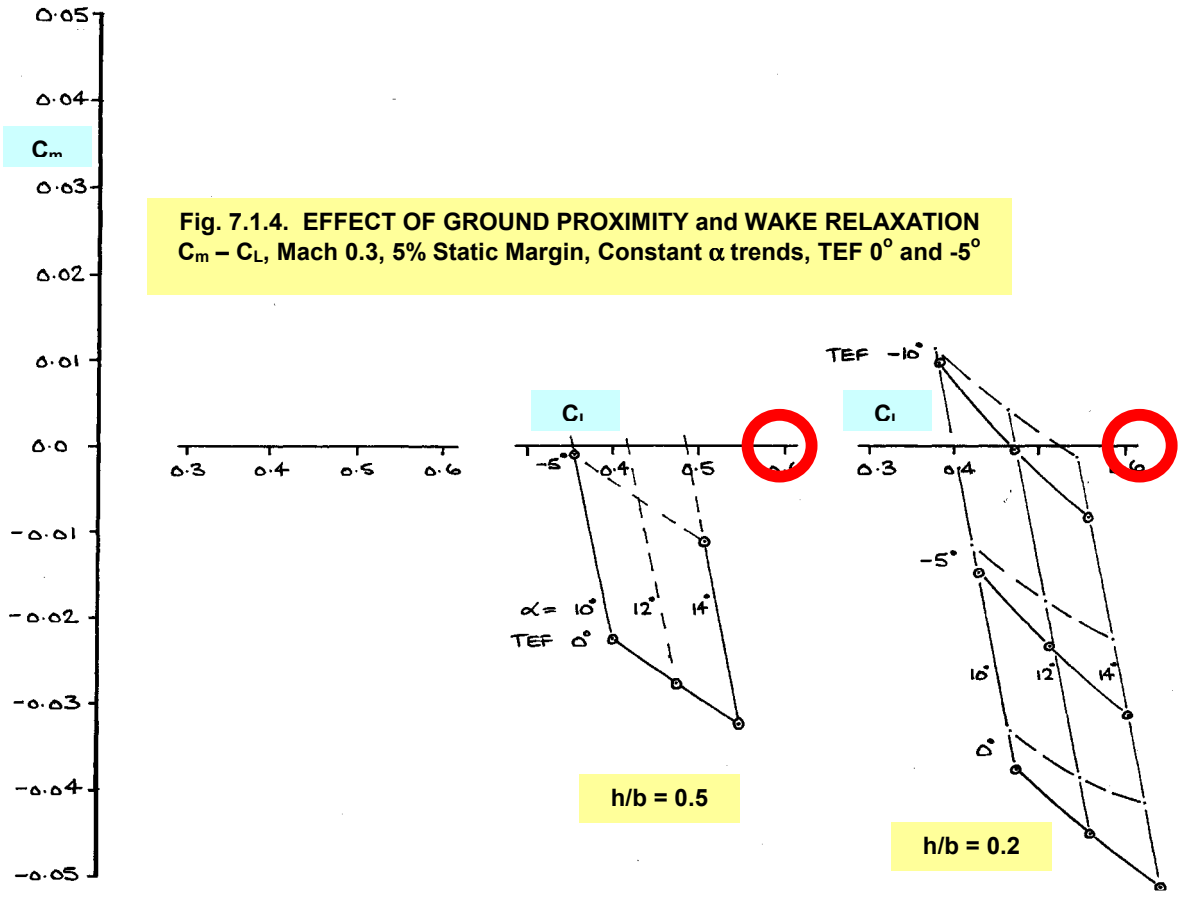

Fig. 7.1.4. EFFECT OF GROUND PROXIMITY and WAKE RELAXATION
C_m – C_L, Mach 0.3, 5% Static Margin, Constant α trends, TEF 0° and -5°

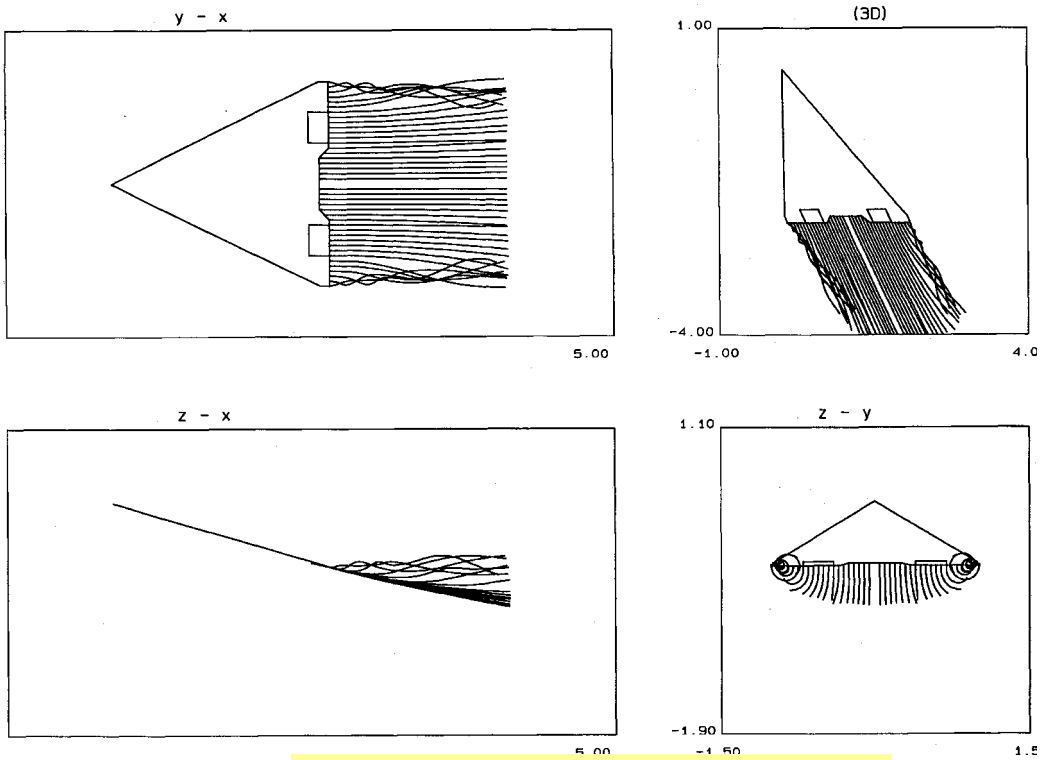

(a) Free Air, α 16.4°, TEF -0.5°

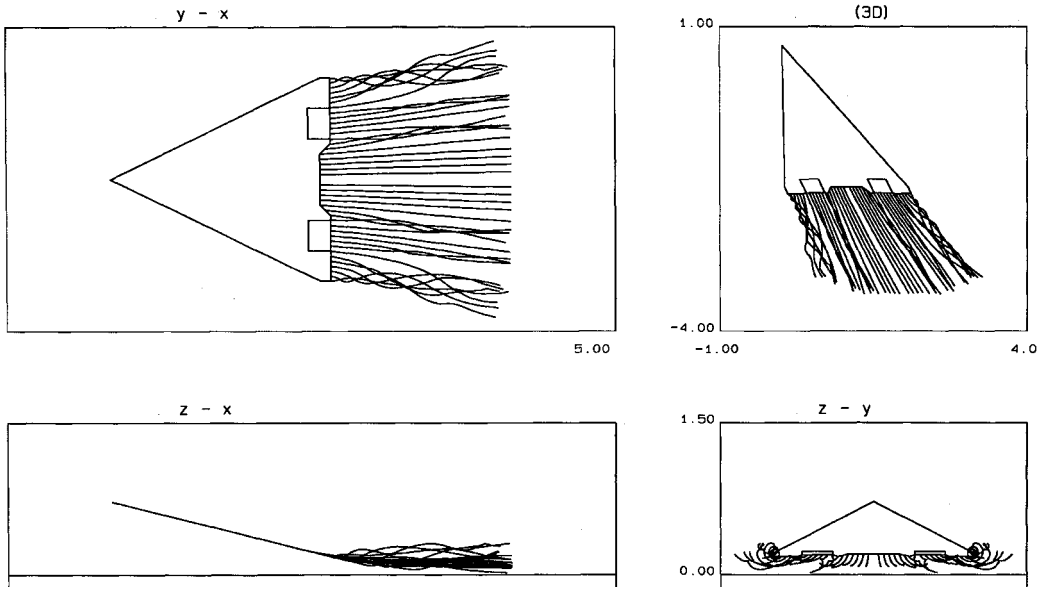

(b) h/b 0.2, α 14.0°, TEF -5.0°

Fig. 7.1.5. RELAXED WAKE GEOMETRY, EFFECT OF GROUND PROXIMITY, Mach 0.3, 0% Stable Static Margin, C_L 0.6, C_m 0.0 (trimmed)

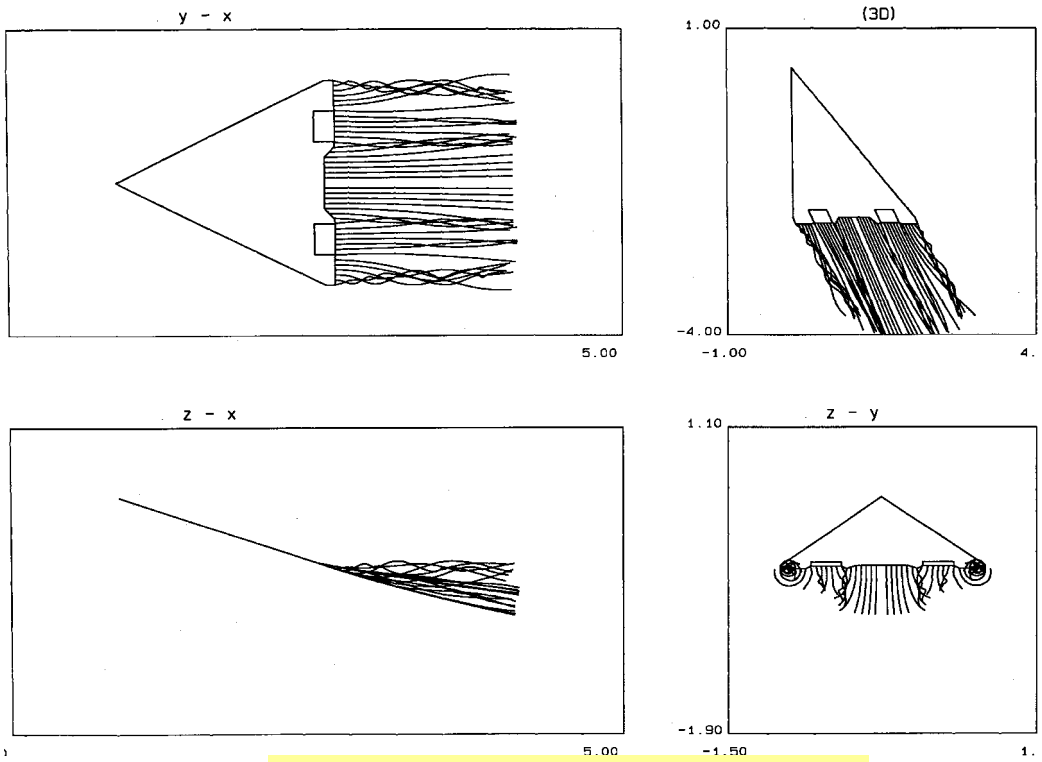

Free Air, α 18.3°, TEF -8.3°

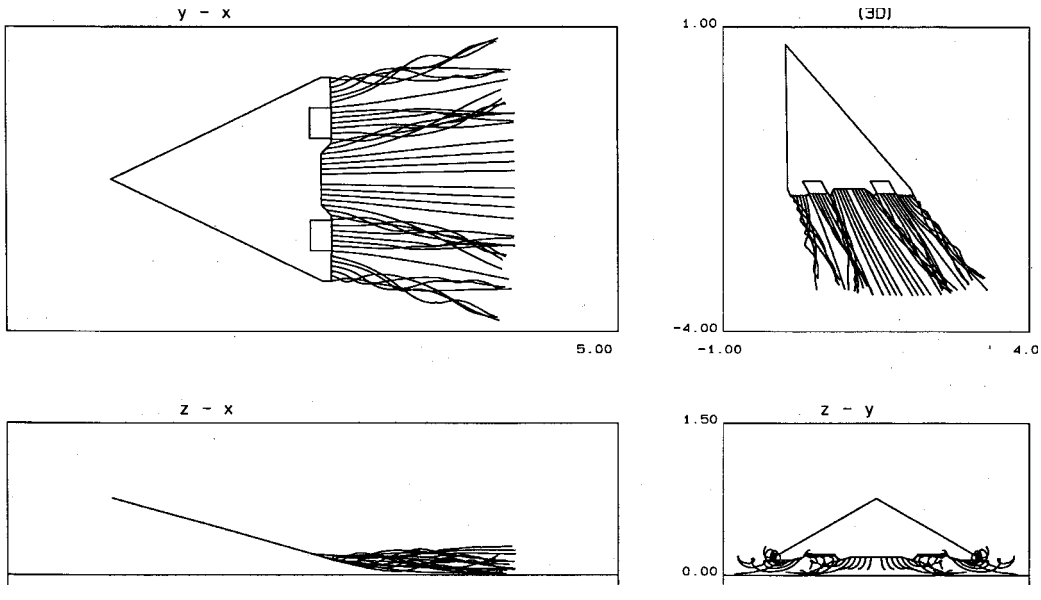

h/b 0.2, α 15.7°, TEF -12.9°

Fig. 7.1.6. RELAXED WAKE GEOMETRY, EFFECT OF GROUND PROXIMITY, Mach 0.3, 5% Stable Static Margin, C_L 0.6, C_m 0.0 (trimmed)

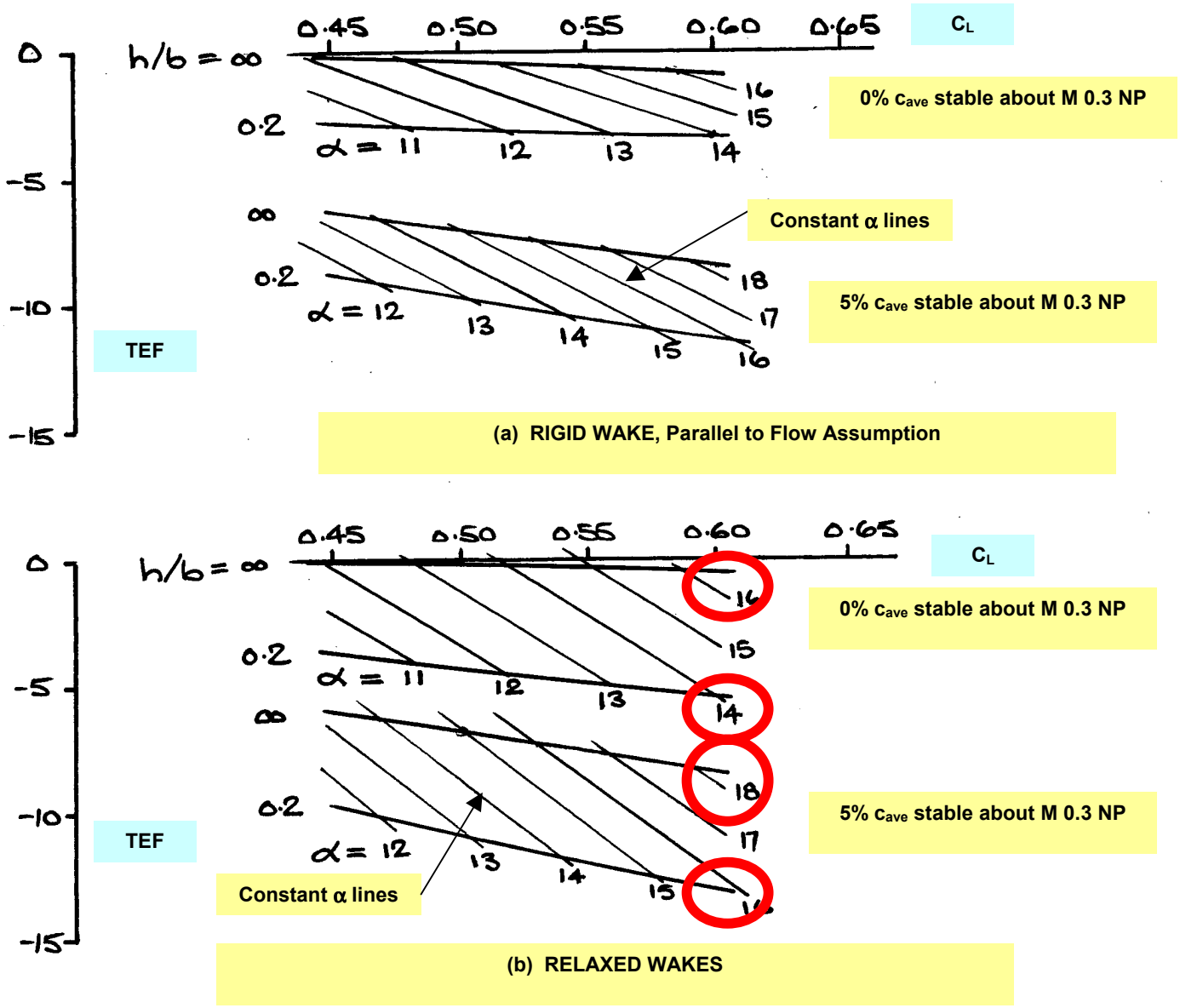

Fig. 7.1.7. TEF REQUIRED TO TRIM VARIATION WITH C_L, M 0.3
EFFECT OF GROUND PROXIMITY, RELAXED WAKES and STATIC MARGIN

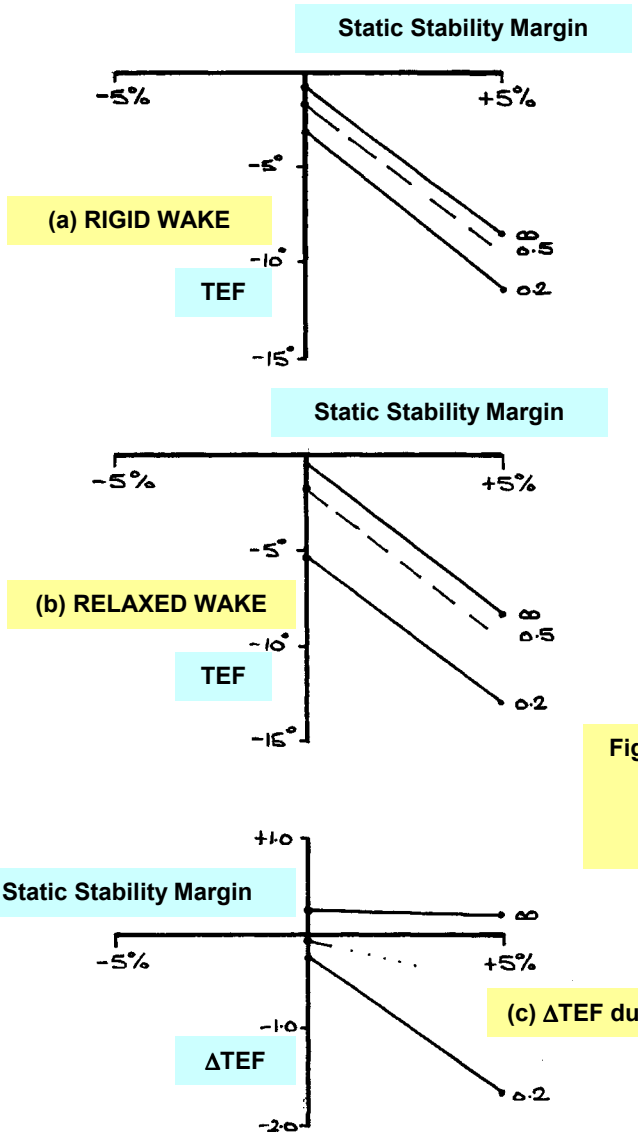

Fig. 7.1.8. TEF REQUIRED TO TRIM, VARIATION WITH STATIC MARGIN
C_L 0.6, M 0.3, EFFECT OF GROUND PROXIMITY, EFFECT OF WAKE MODELLING

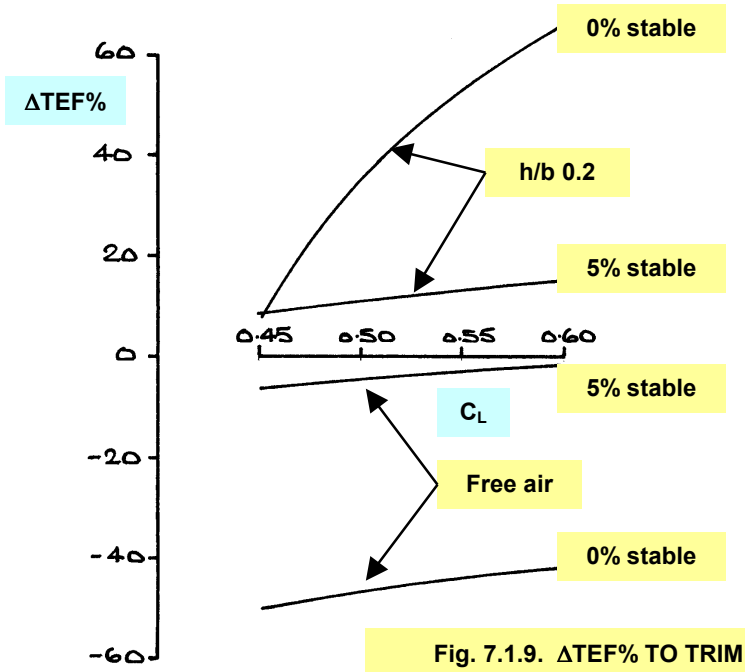

Fig. 7.1.9. ΔTEF% TO TRIM DUE TO WAKE RELAXATION, VARIATION WITH C_L
M 0.3, EFFECT OF GROUND PROXIMITY and STATIC MARGIN

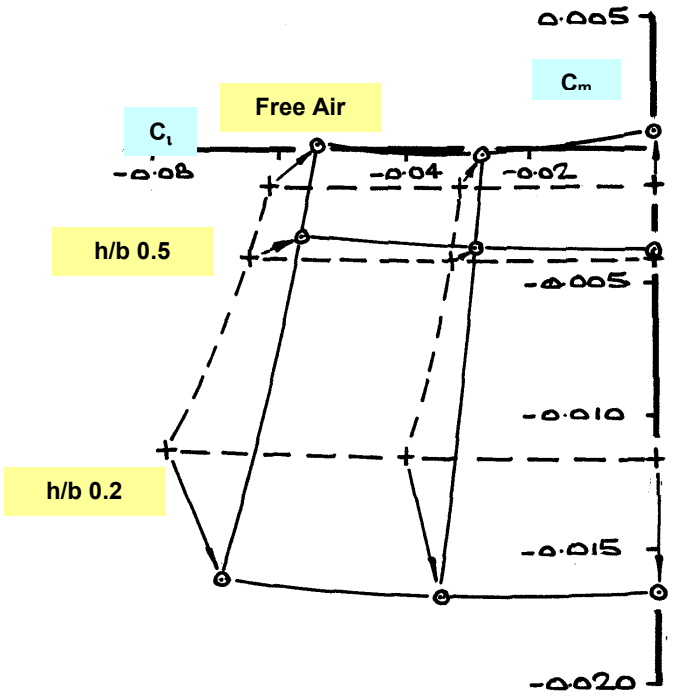

Fig. 7.2.1. EFFECT OF GROUND PROXIMITY & SIDESLIP EFFECT OF WAKE RELAXATION
Mach 0.3, α 12°, 0% Static Margin, C_t - C_m, TEF 0° and AIL 0°

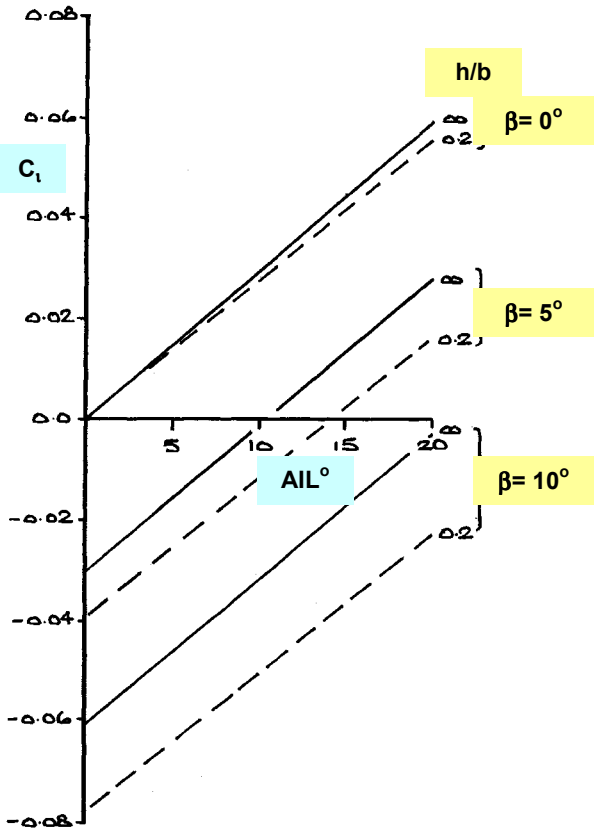

Fig. 7.2.2. AILERON CONTROL POWER, EFFECT OF GROUND PROXIMITY & SIDESLIP
Mach 0.3, α 12°, 0% Static Margin, C_t - AIL°

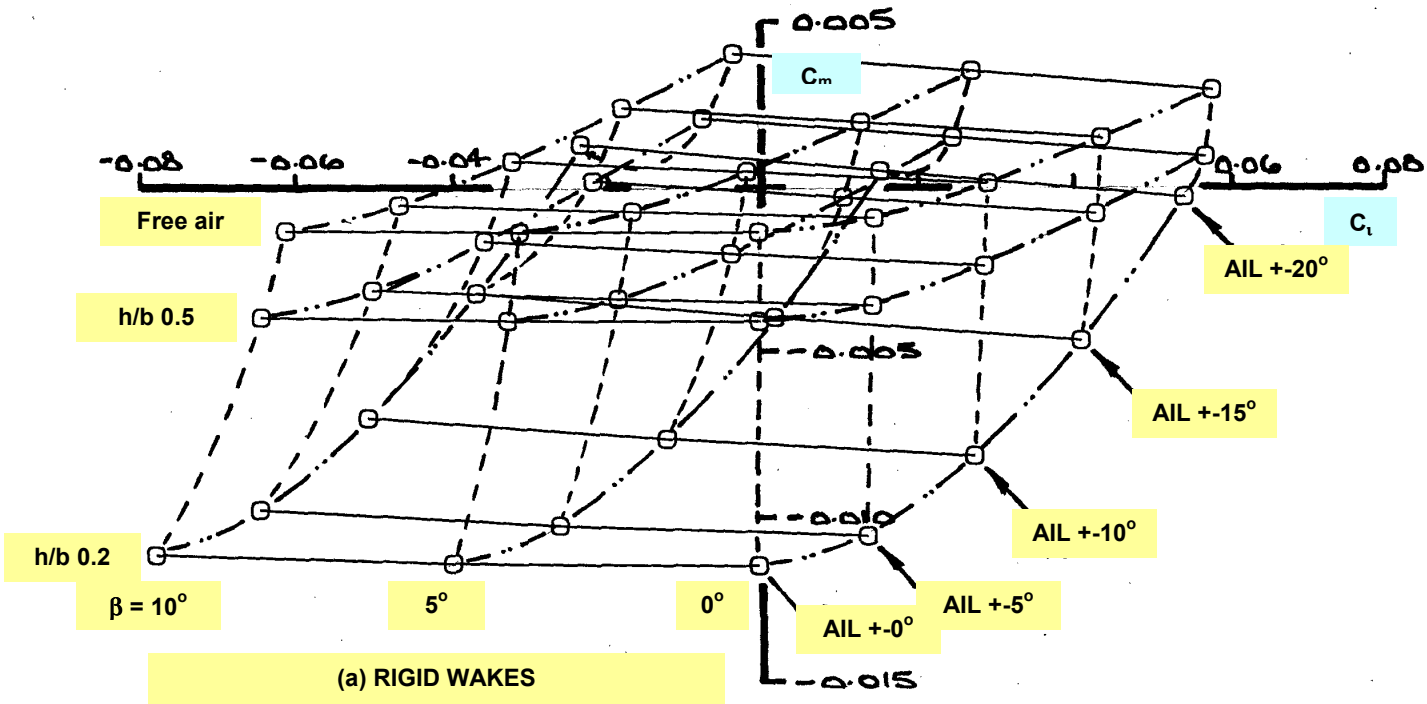

(a) RIGID WAKES

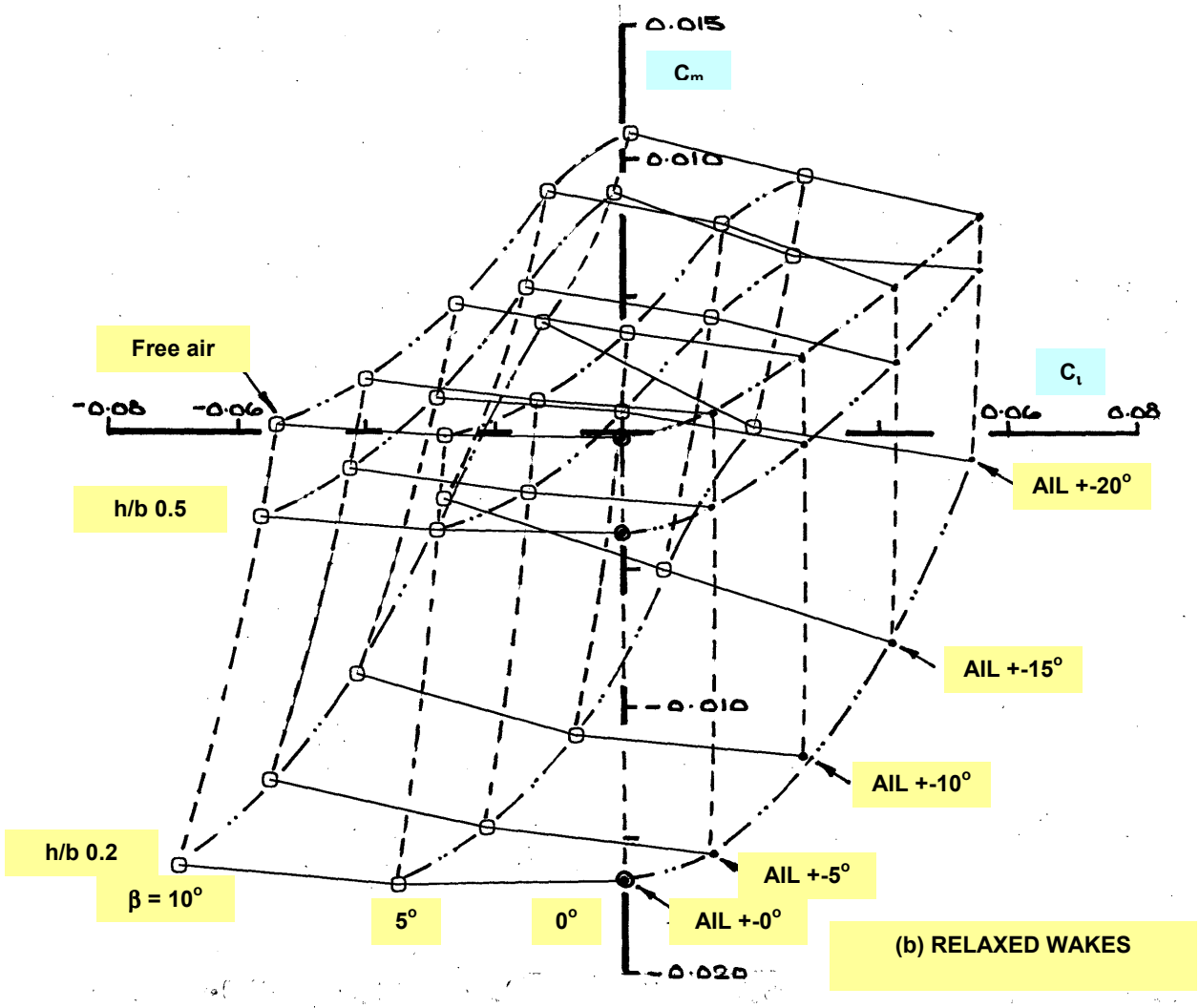

Fig. 7.2.3. EFFECT OF GROUND PROXIMITY, SIDESLIP, AILERON & WAKE RELAXATION
Mach 0.3, α 12°, 0% Static Margin, C_t - C_m,
β, AILo, h/b Matrix, TEF 0°

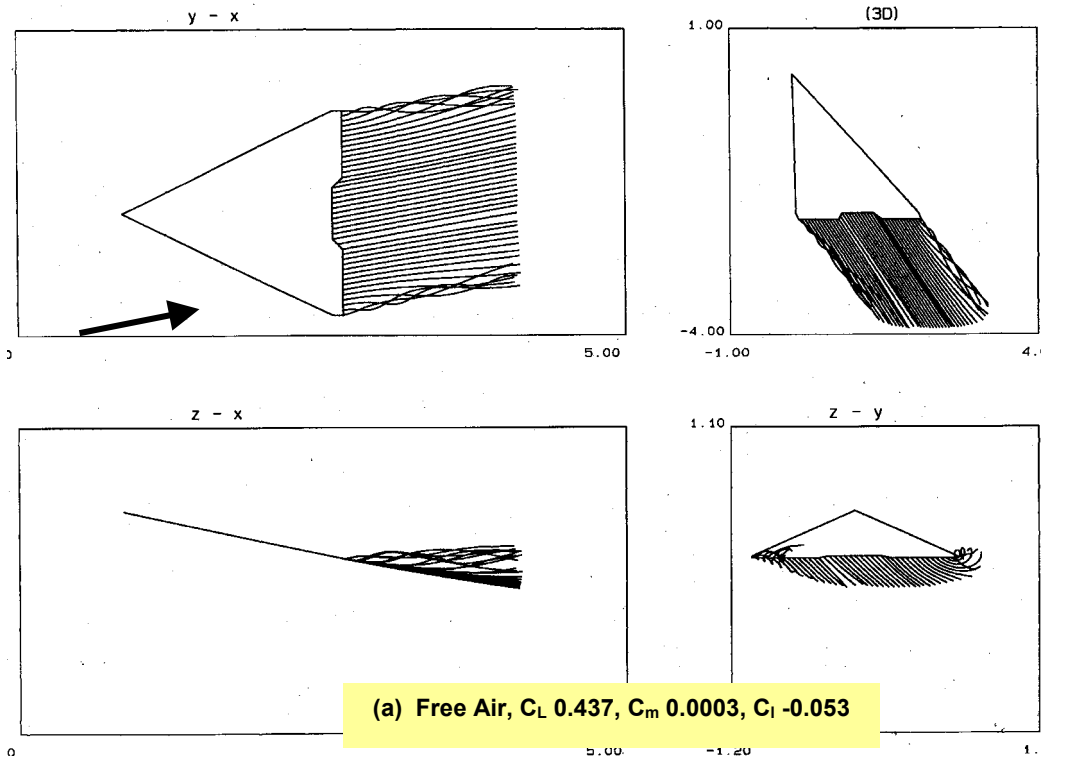

(a) Free Air, C_L 0.437, C_m 0.0003, C_l -0.053

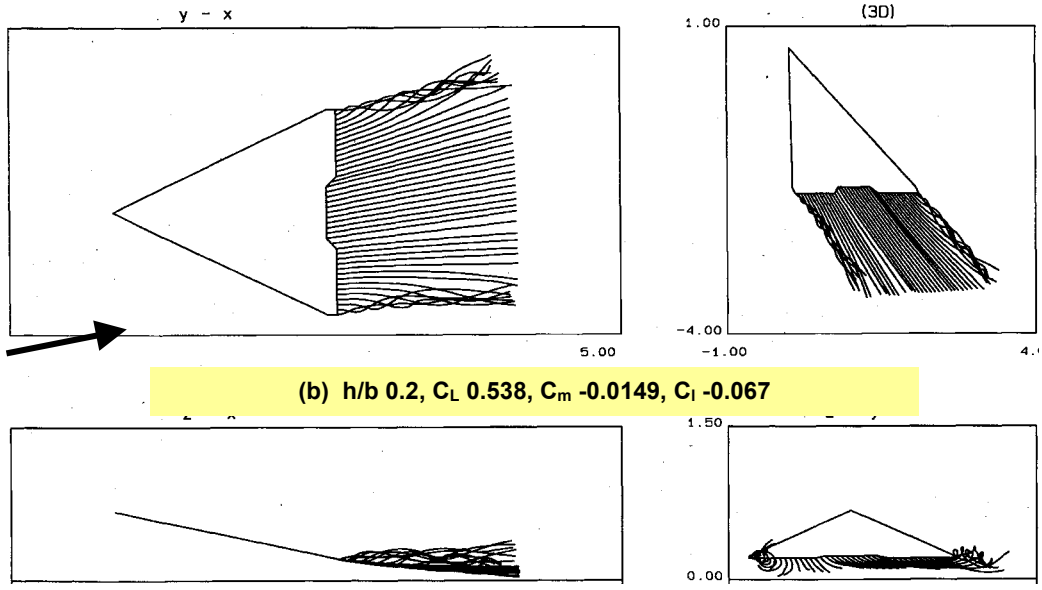

(b) h/b 0.2, C_L 0.538, C_m -0.0149, C_l -0.067

Fig. 7.2.4. RELAXED WAKE GEOMETRY, EFFECT OF GROUND PROXIMITY, AIL 0°
Mach 0.3, α 12°, β 10°, 0% Stable Static Margin

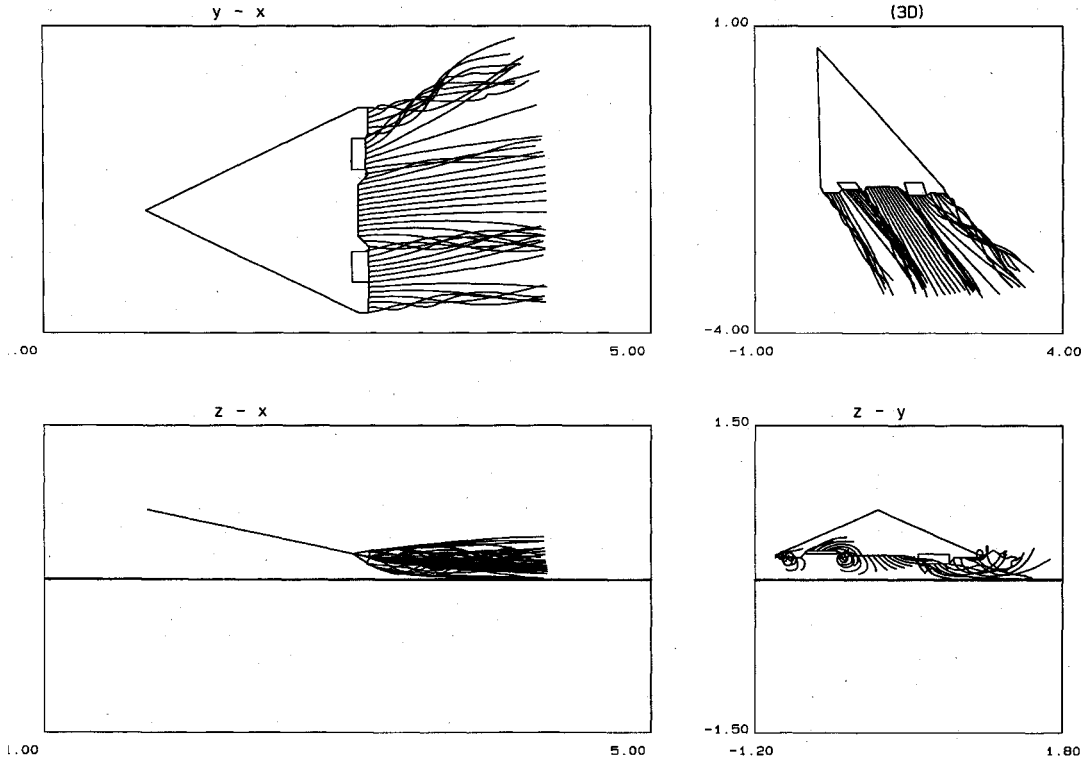

Fig. 7.2.5. RELAXED WAKE GEOMETRY, EFFECT OF GROUND PROXIMITY, AIL -+20° Mach 0.3, α 12°, β 10°, 0% Stable Static Margin

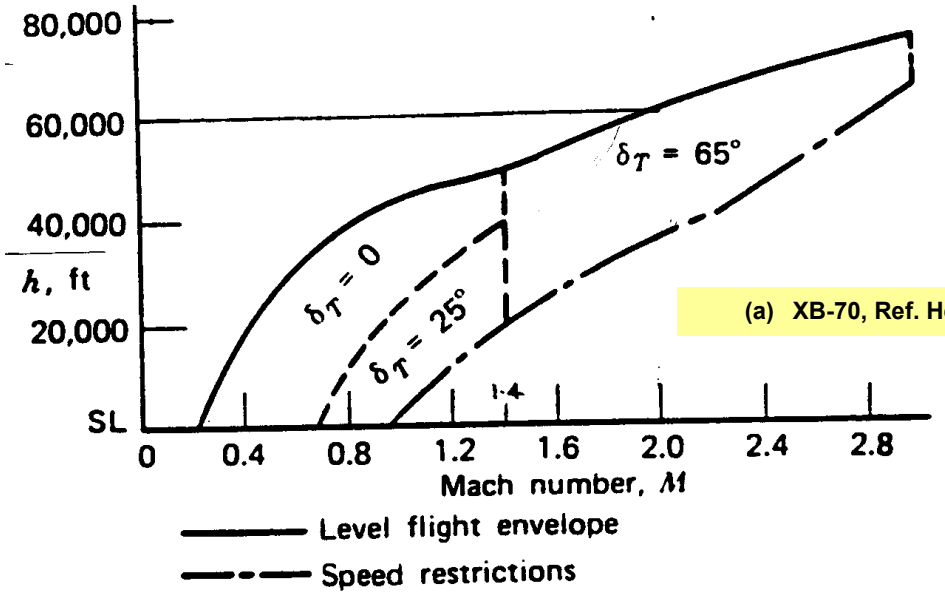

(a) XB-70, Ref. Heffley & Jewell

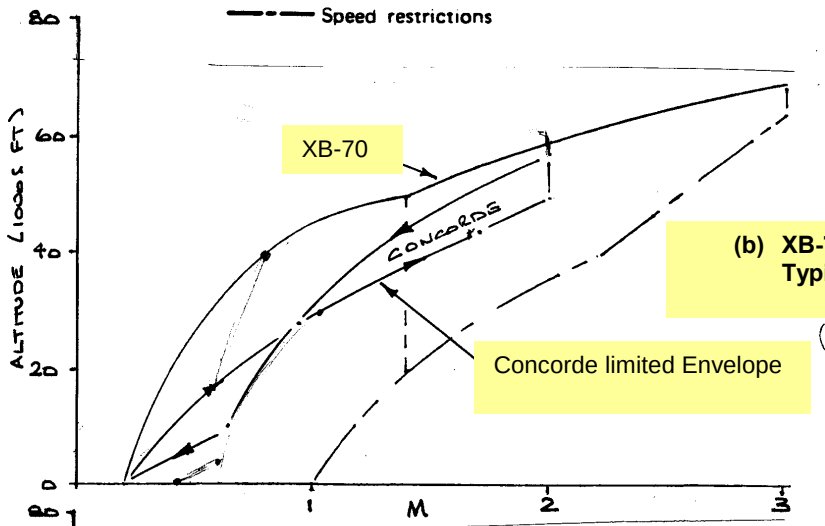

(b) XB-70 & Concorde
Typical Flight Envelope

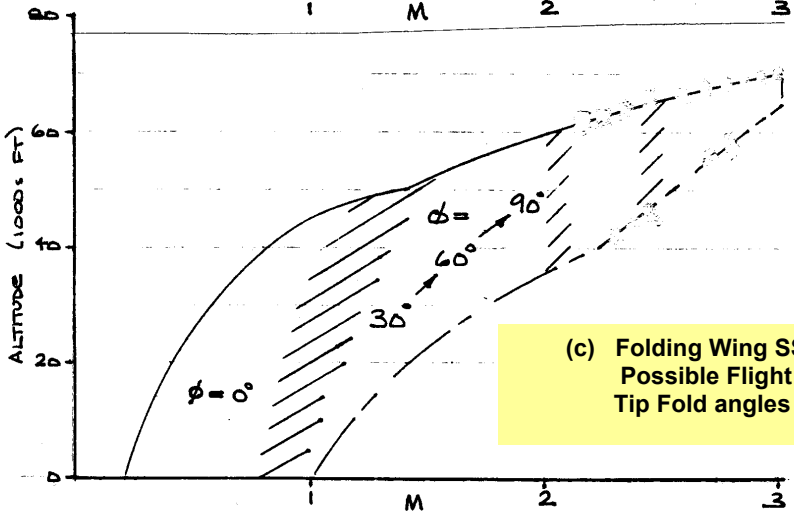

(c) Folding Wing SST
Possible Flight Envelope
Tip Fold angles

Fig. 8.1.1. FLIGHT ENVELOPES, XB-70 & CONCORDE COMPARED, FUTURE SST WITH FOLDING TIP GEOMETRY PROJECTED

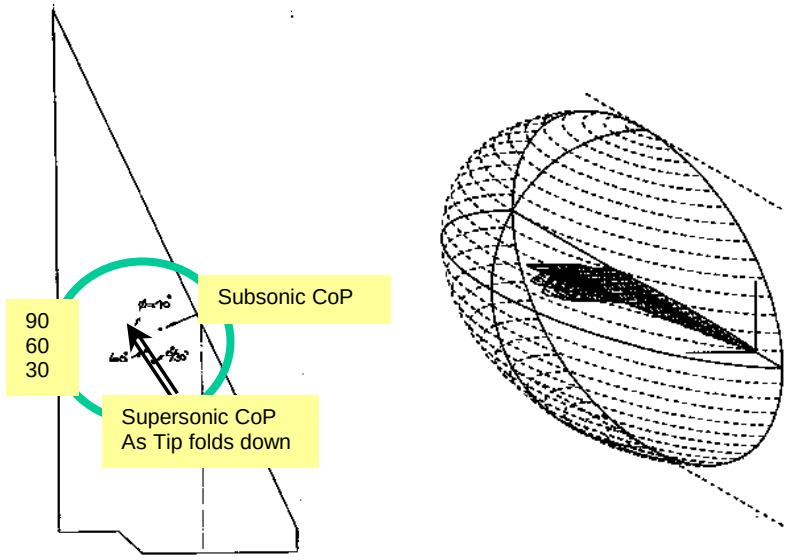

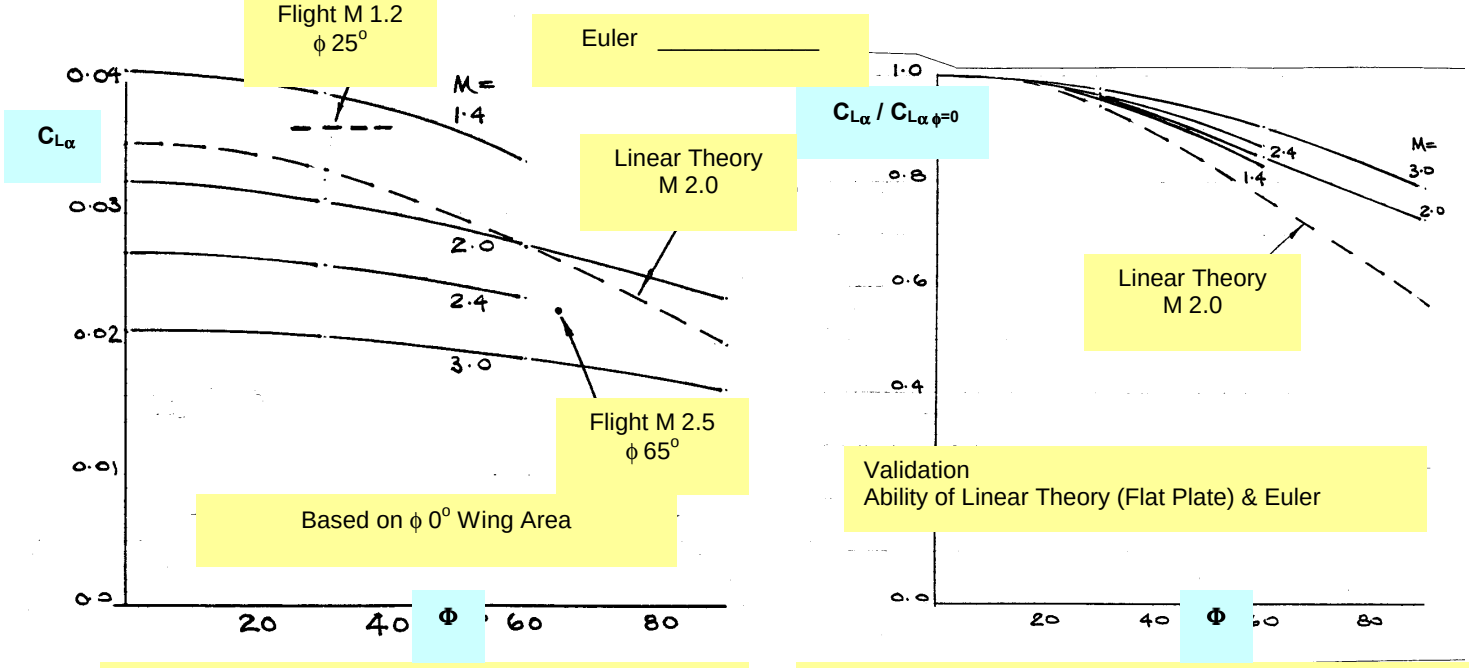

(a) Variation of $C_{L\alpha}$ with ϕ
M varies

(b) Variation of Normalised $C_{L\alpha}$ ($C_{L\alpha}$ / $C_{L\alpha\,\phi=0}$) with ϕ
M varies

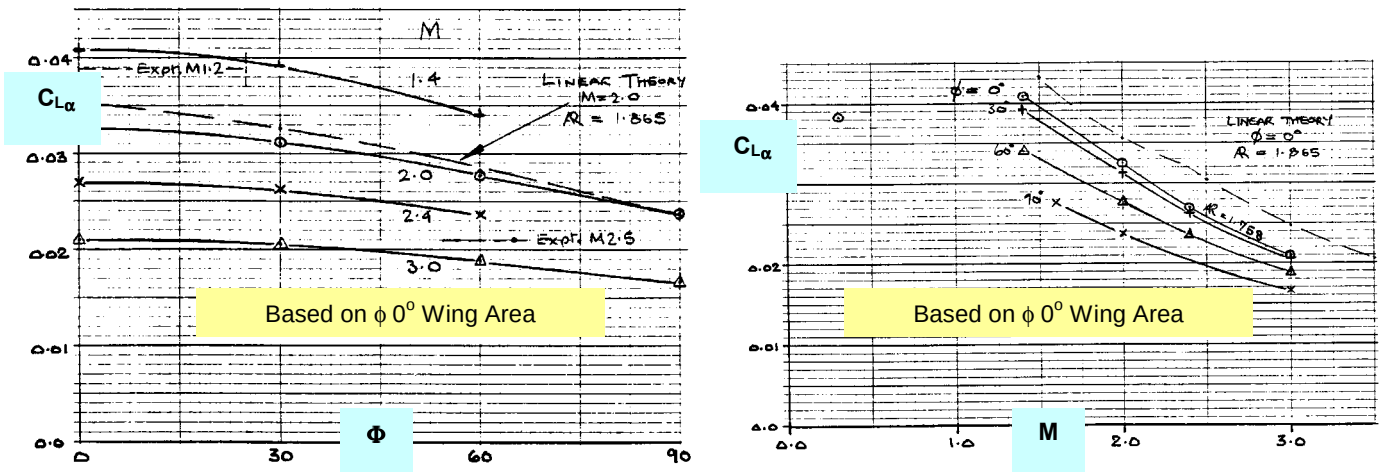

(c) XB-70 Wing, Variation of $C_{L\alpha}$ with Tip Fold Angle
M varies

(d) XB-70 Wing, Variation of $C_{L\alpha}$ with M
Tip Fold Angle varies

Fig. 8.2.1. XB-70, EFFECT OF TIP FOLD ANGLE ON LIFT
(Linear Theory & Euler Compared)

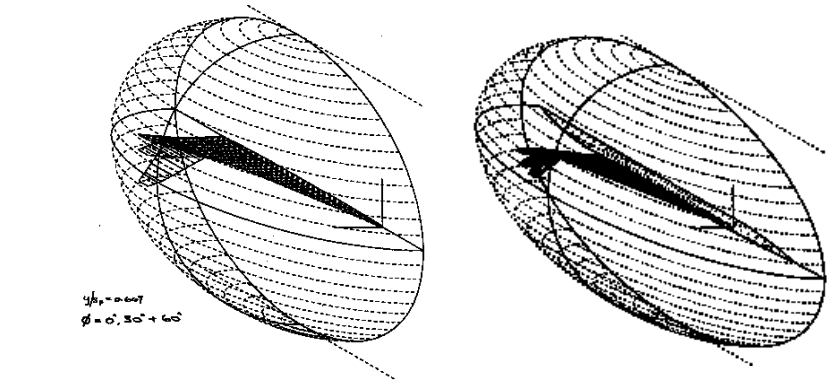

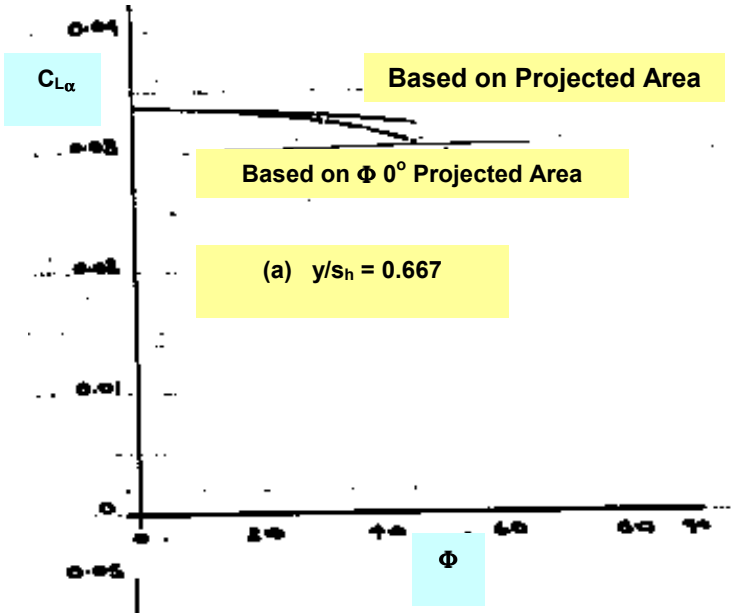

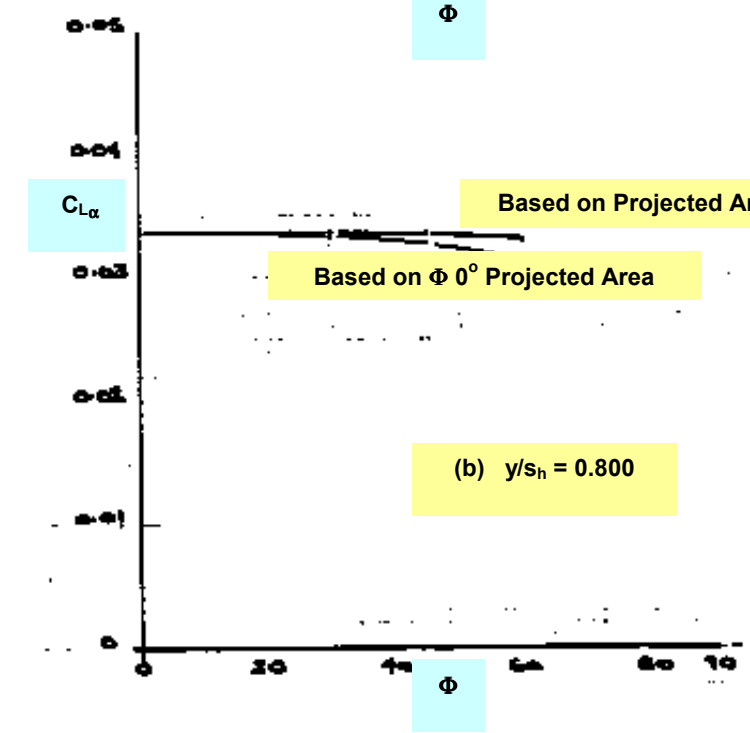

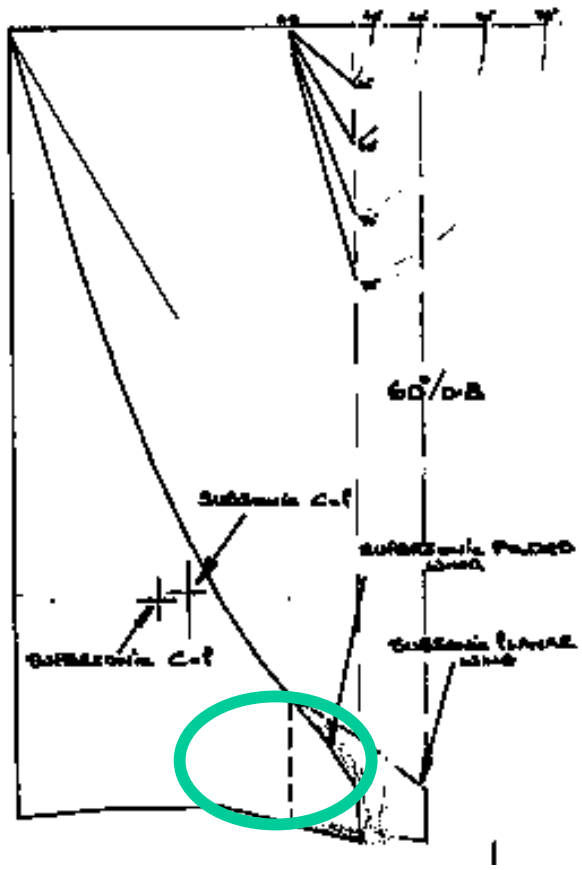

Folded Wing Geometries having ES Projected Planform

Fig. 8.3.1. ES PLANFORM, VARIATION OF $C_{L\alpha}$ WITH TIP FOLD ANGLE (Φ) and HINGE LOCATION (y/s_h)
M 2.0 (Euler Method)

(a) Concorde

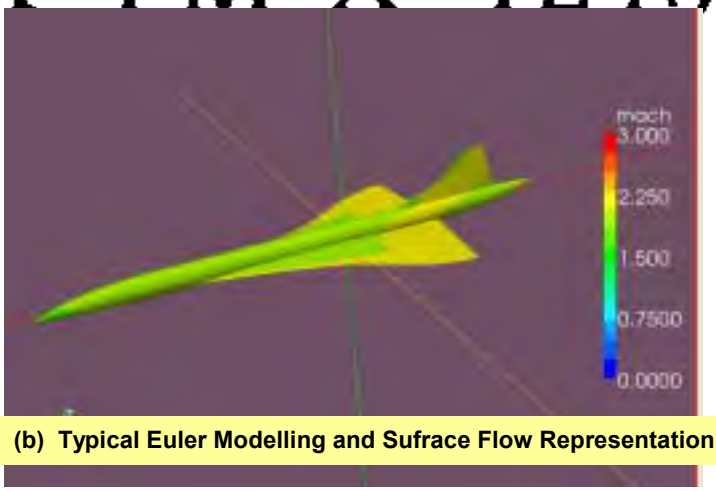

(b) Typical Euler Modelling and Sufrace Flow Representation

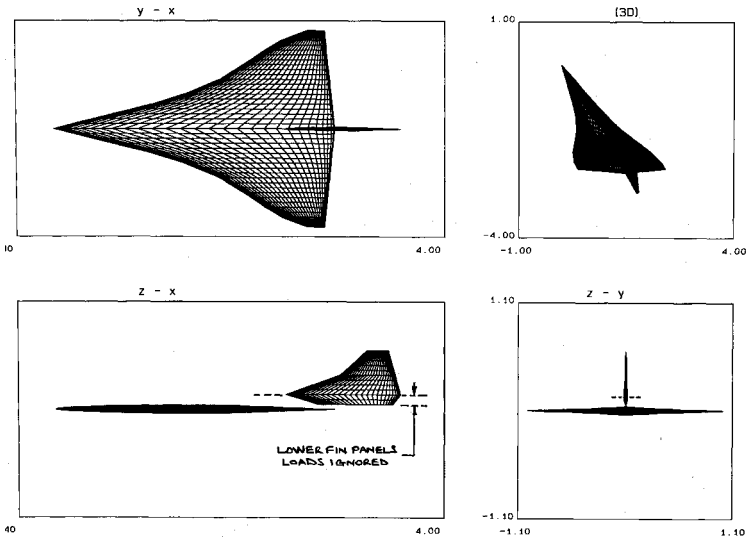

(c) Typical Panelling, Wing and Fin Modelling

Fig. 9.1.1. CONCORDE GEOMETRY and THEORETICAL MODELLING (Panel Methods and Euler Method)

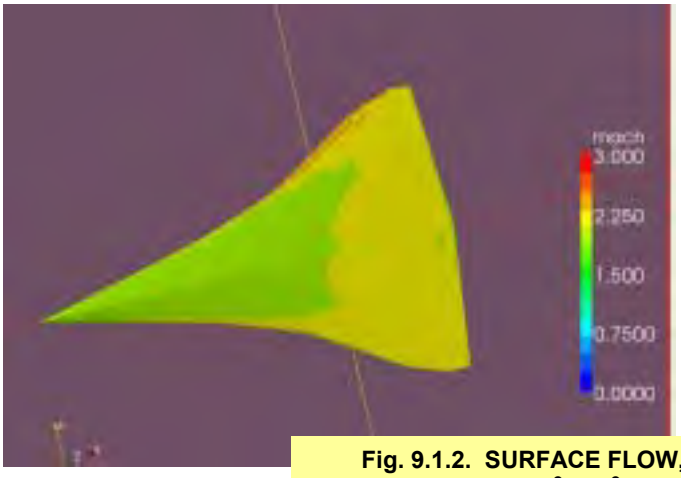

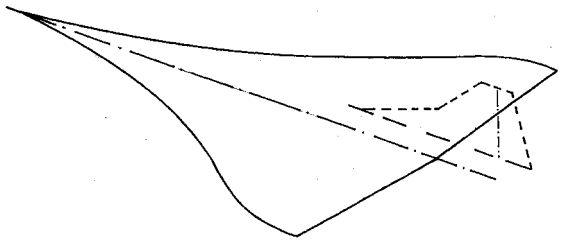

Fig. 9.1.2. SURFACE FLOW, Concorde Wing M 2.0, α 4°, β 4°, Euler Method

Fig. 9.1.3. SURFACE FLOW, Concorde Wing and Body
M 2.0, α 4°, β 4°, Euler Method

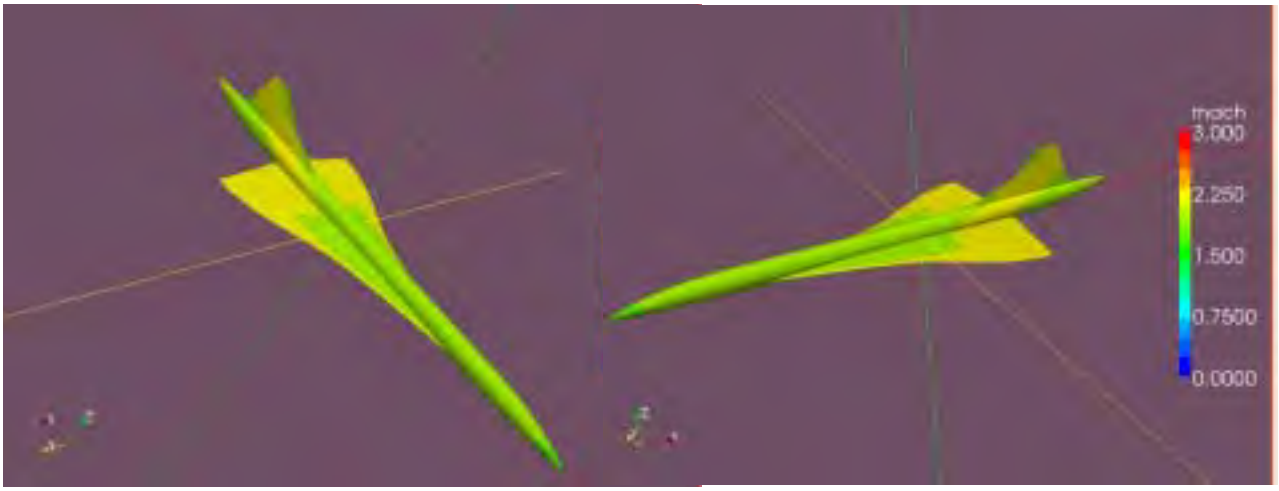

(a) α 4°, β 0°

(b) α 4°, β 4°

Fig. 9.1.4. SURFACE FLOW, Concorde Wing, Body and Fin
M 2.0, Euler Method

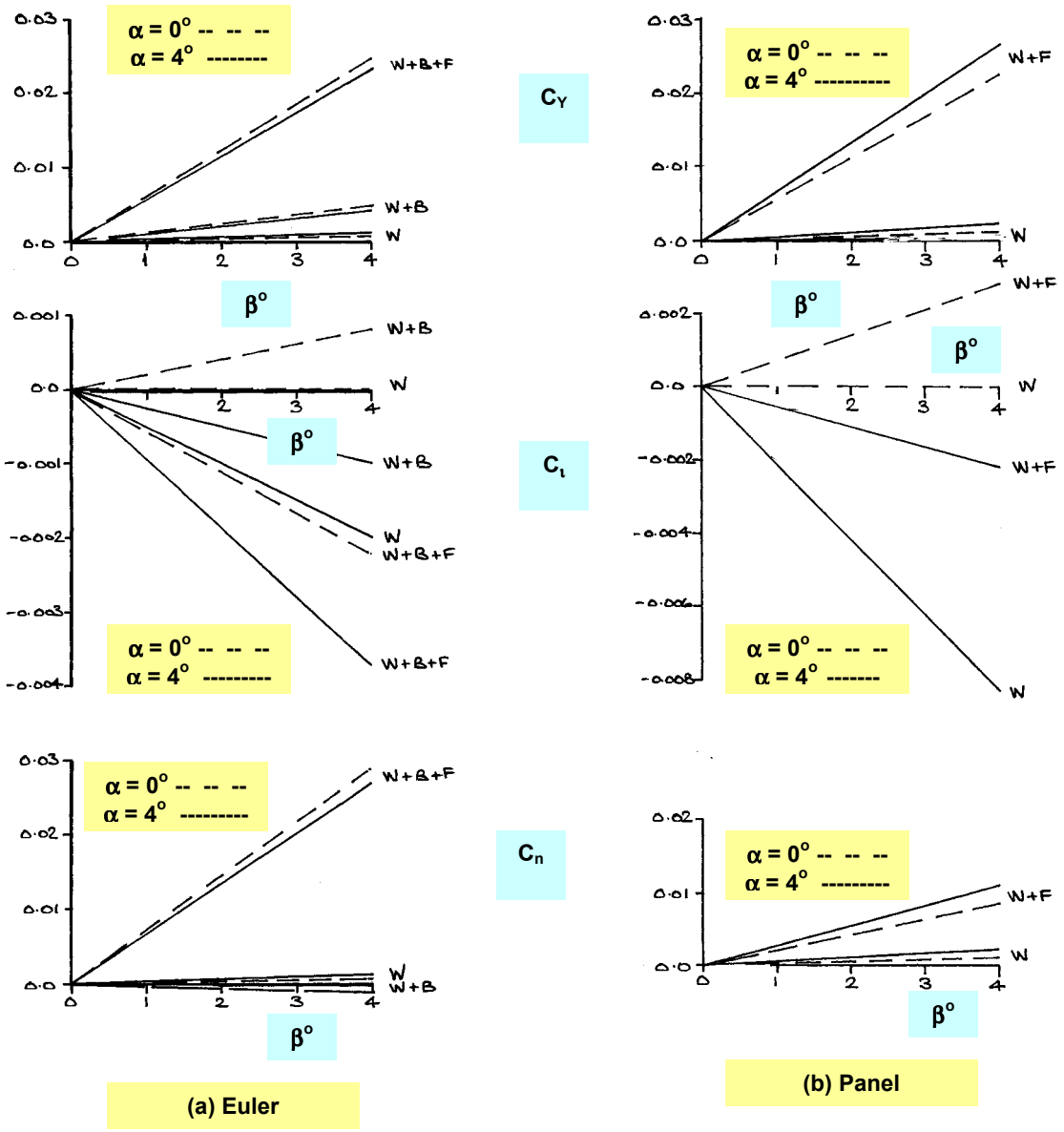

Fig. 9.1.5. CONCORDE LATERAL FORCE and MOMENT (C_Y, C_l, C_n) VARIATION WITH β COMPONENT CONTRIBUTION
M 2.0, α 4°, Euler Method & Higher Order Panel Method

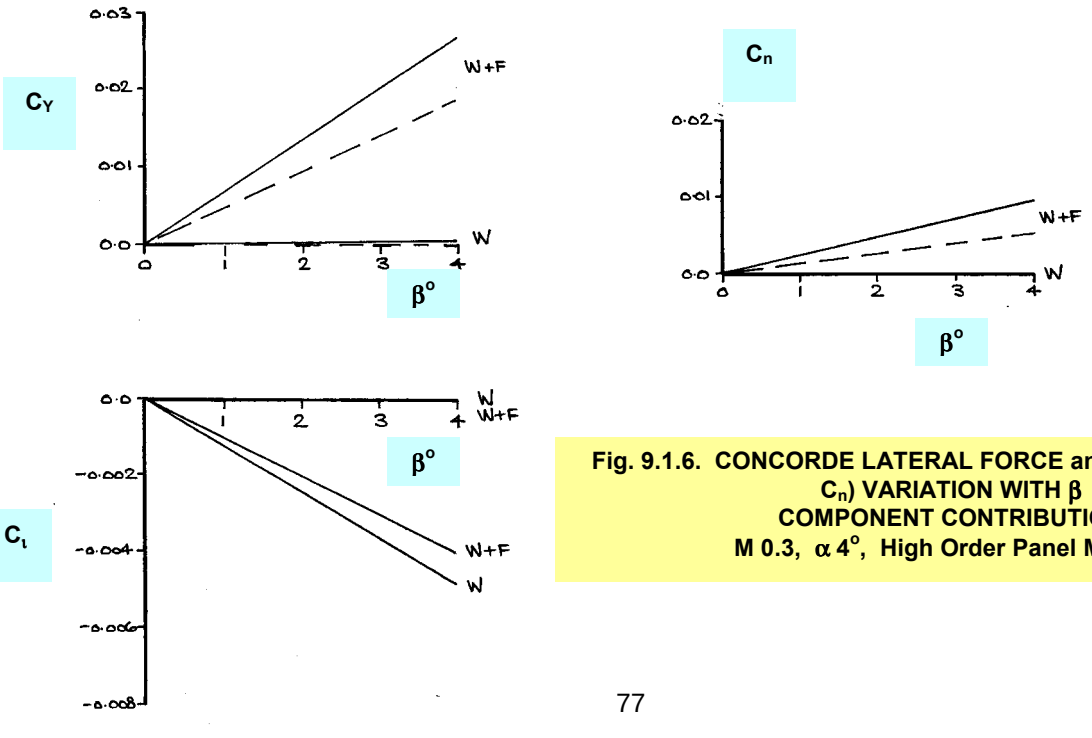

Fig. 9.1.6. CONCORDE LATERAL FORCE and MOMENT (C_Y, C_l, C_n) VARIATION WITH β COMPONENT CONTRIBUTION
M 0.3, α 4°, High Order Panel Method

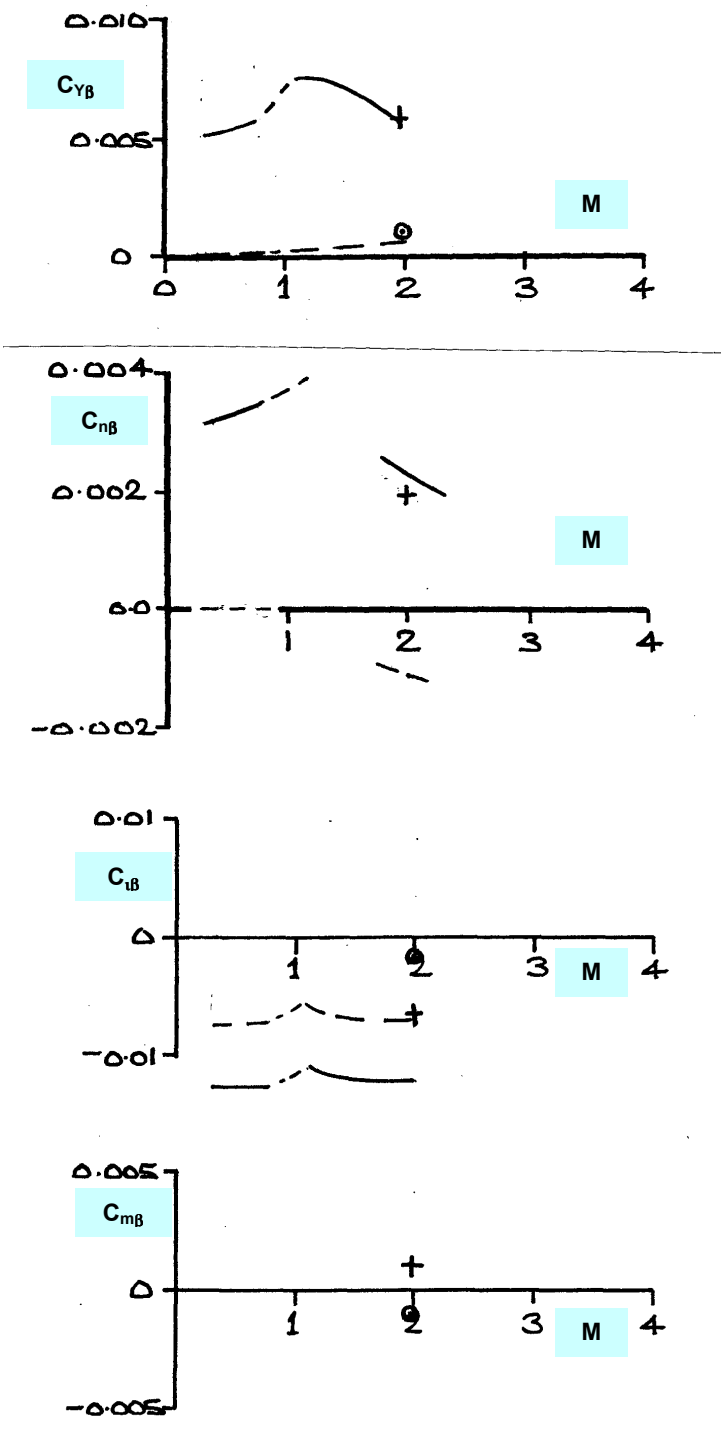

Fig. 9.1.7. LATERAL DERIVATIVES v M
CONCORDE

COMPONENT CONTRIBUTION
Panel Methods and Euler Method

$C_{Y\beta} = dC_Y/d\beta$
$C_{n\beta} = dC_n/d\beta$
$C_{\iota\beta} = dC_\iota/d\beta/C_L$
$C_{m\beta} = dC_m/d\beta/C_L$

+ Wing/Body/Fin } Euler
O Wing/Body }

-------- Wing/Fin } Panel Method
-- -- - Wing }

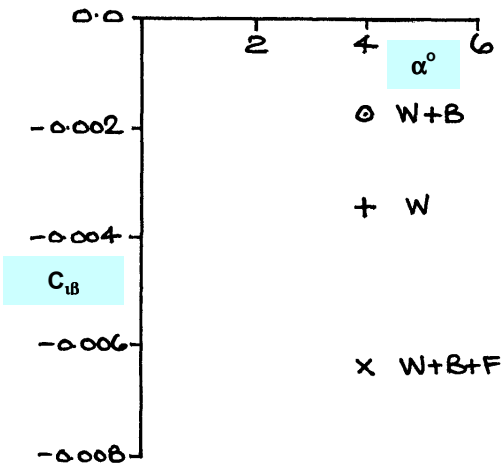

Fig. 9.1.8. CONCORDE $C_{\iota\beta}$ v α
COMPONENT CONTRIBUTION
M 2.0, Euler Method

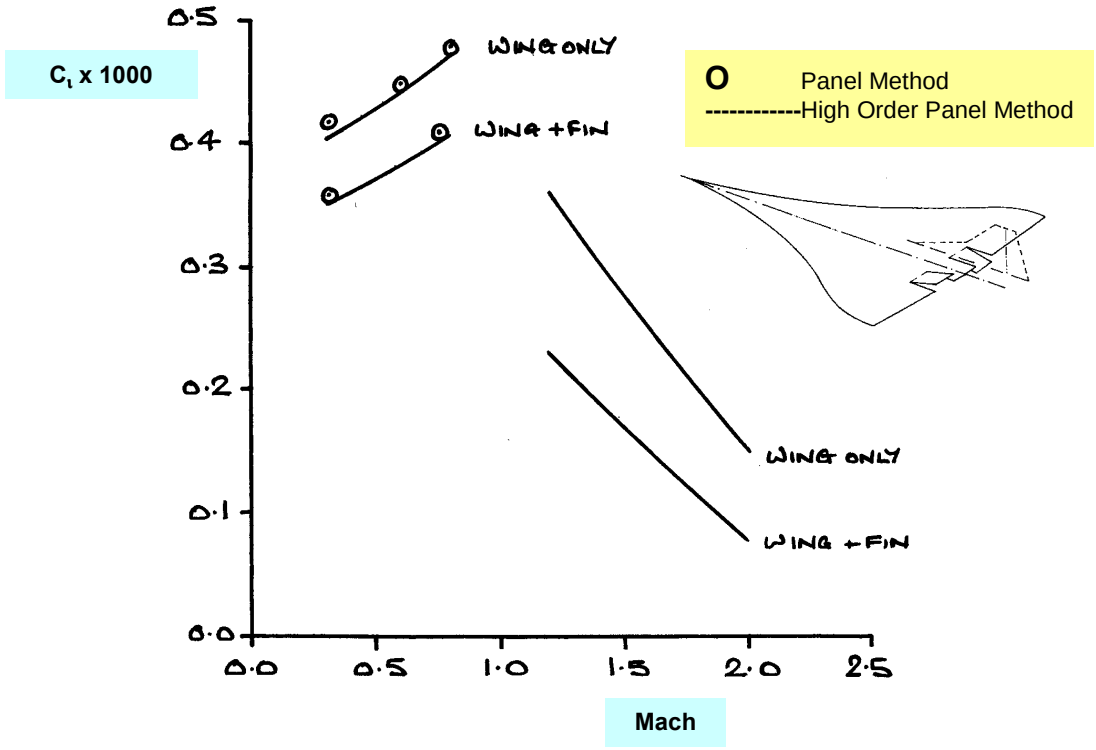

Fig. 9.2.1. CONCORDE, EFFECT OF FIN ON ROLL POWER OF INNER ELEVONS (DIFFERENTIAL, +/-1°) α 4. M varies. Panel Methods

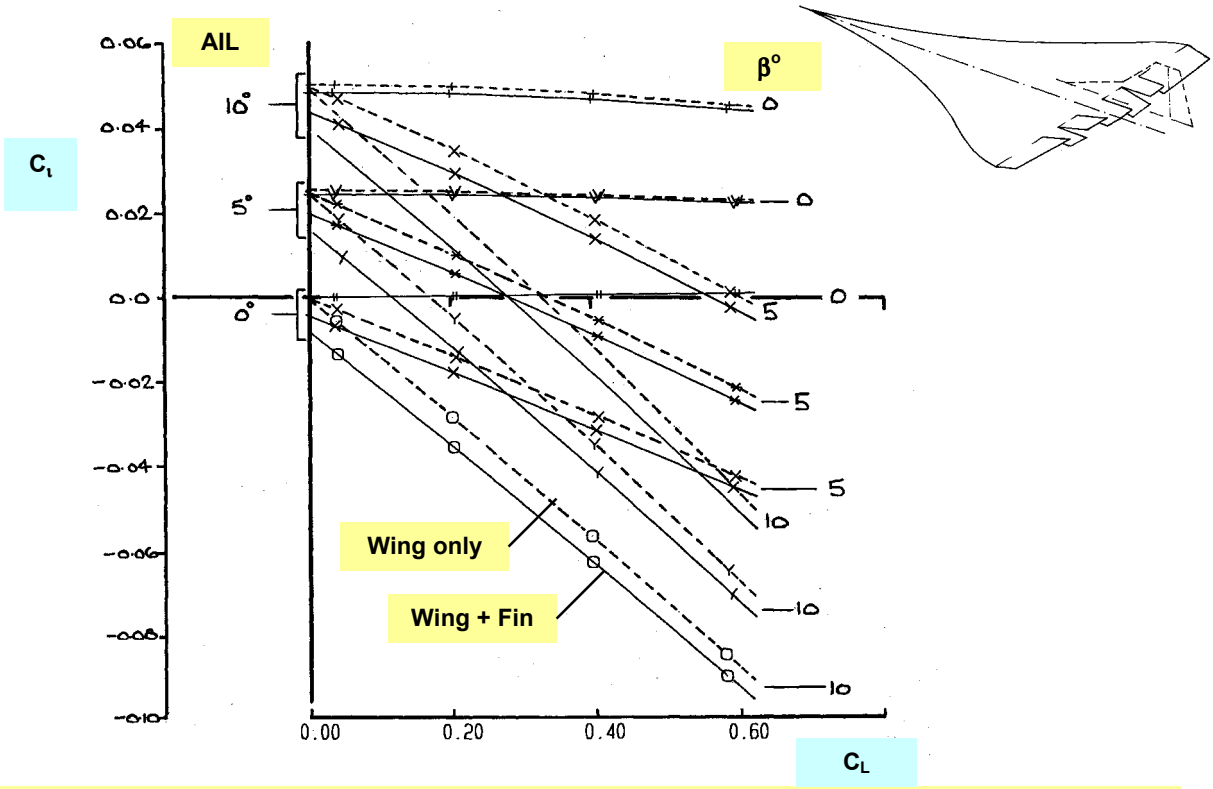

(a) Differential Elevon (+/-0° , +/-5° , +/-10°) , Fin and Sideslip Effects, Rigid Wake Modelling

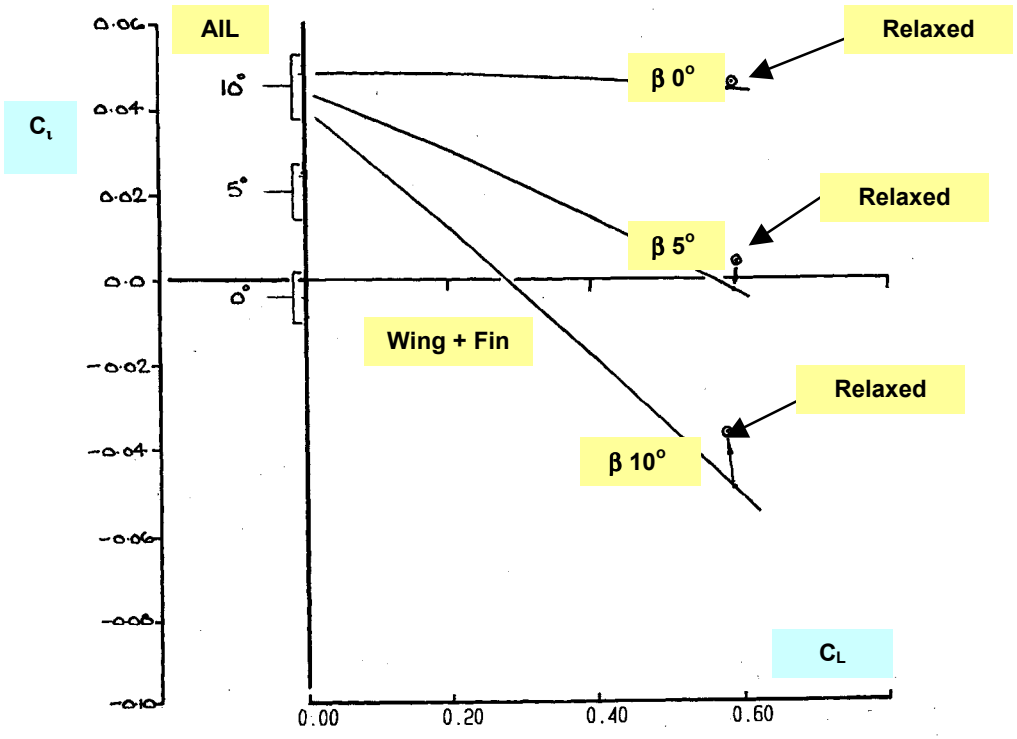

(b) Effect of Wake Relaxation, Differential Elevon +/-10° , C_L, ~0.6

Fig. 9.2.2. CONCORDE, ELEVON ROLL POWER (DIFFERENTIAL, +/-0° , +/-5° , +/-10°) VARIATION WITH C_L, M 0.3 FIN and SIDESLIP EFFECTS, Panel Method, EFFECT OF WAKE MODELLING

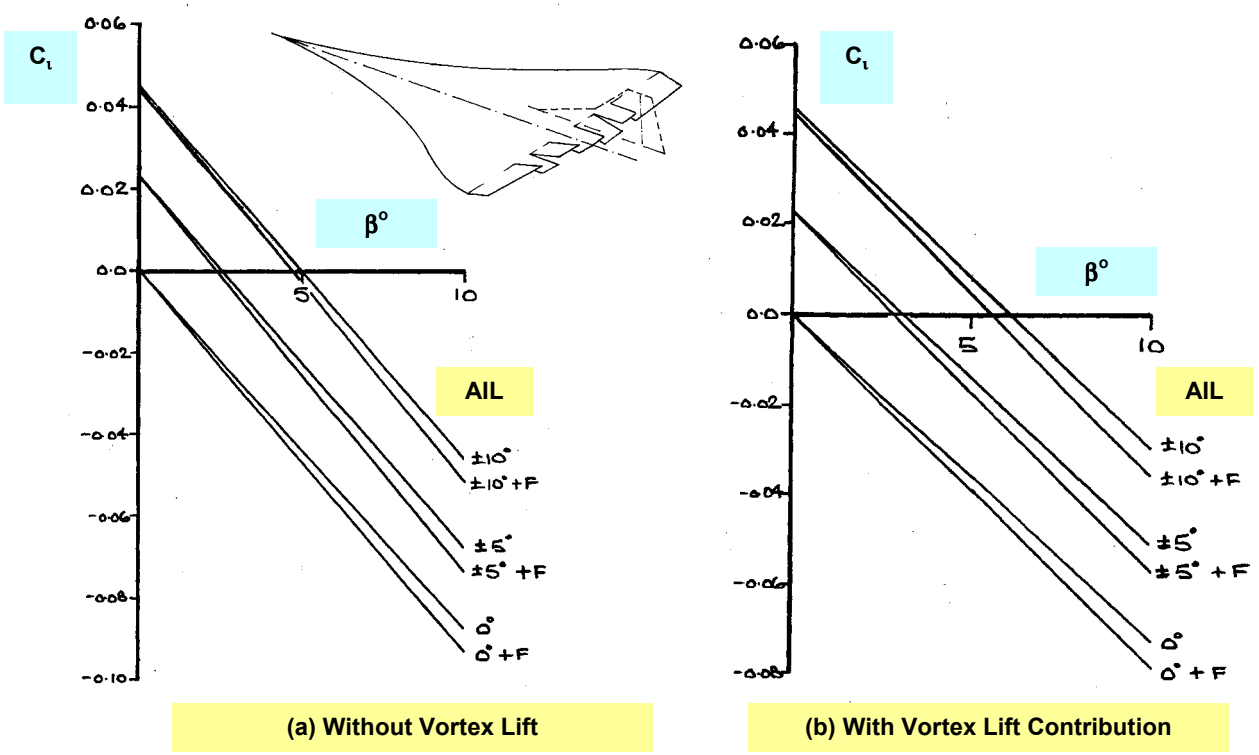

(a) Without Vortex Lift

(b) With Vortex Lift Contribution

Fig. 9.2.3. CONCORDE, ROLLING MOMENT (C_l) VARIATION WITH β
EFFECT OF AILERON DEFLECTION, FIN EFFECT, M 0.3, CL 0.6, Panel Method

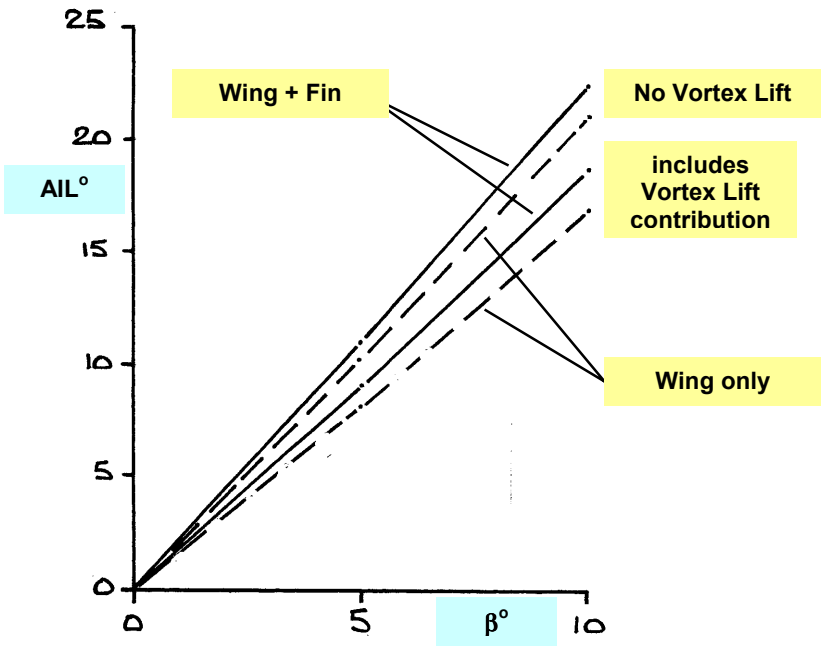

Fig. 9.2.4. CONCORDE, DIFFERENTIAL AILERON REQUIRED TO TRIM (C_l = 0.0) VARIATION WITH β
EFFECT OF FIN
M 0.3, C_L 0.6, Panel Method

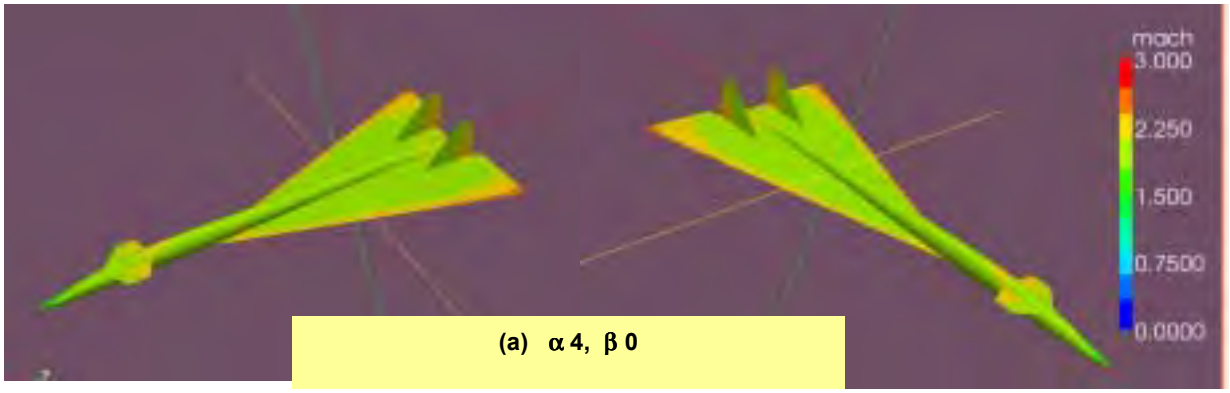

(a) α 4, β 0

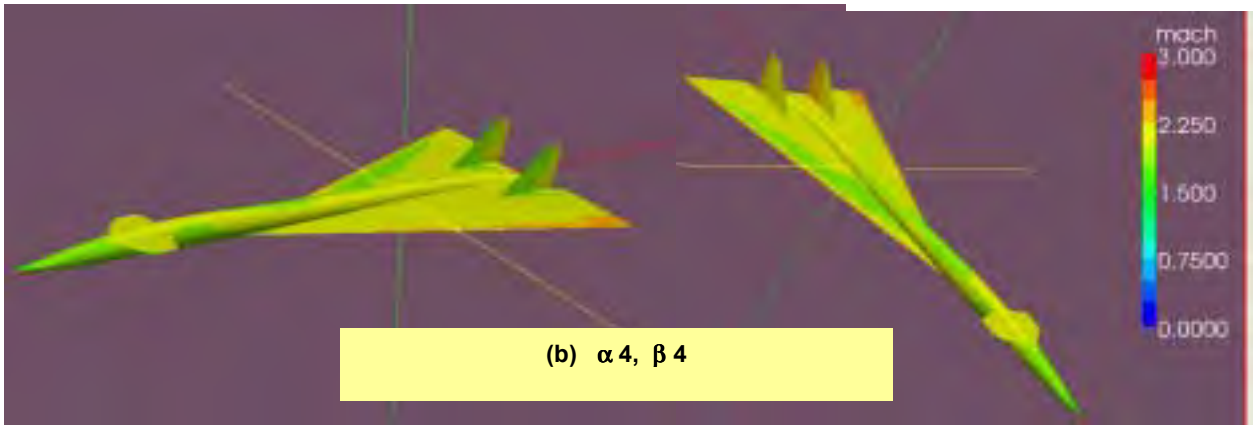

(b) α 4, β 4

FIG. 9.3.1. XB-70, WING + FUSELAGE + FINS, M 2.0

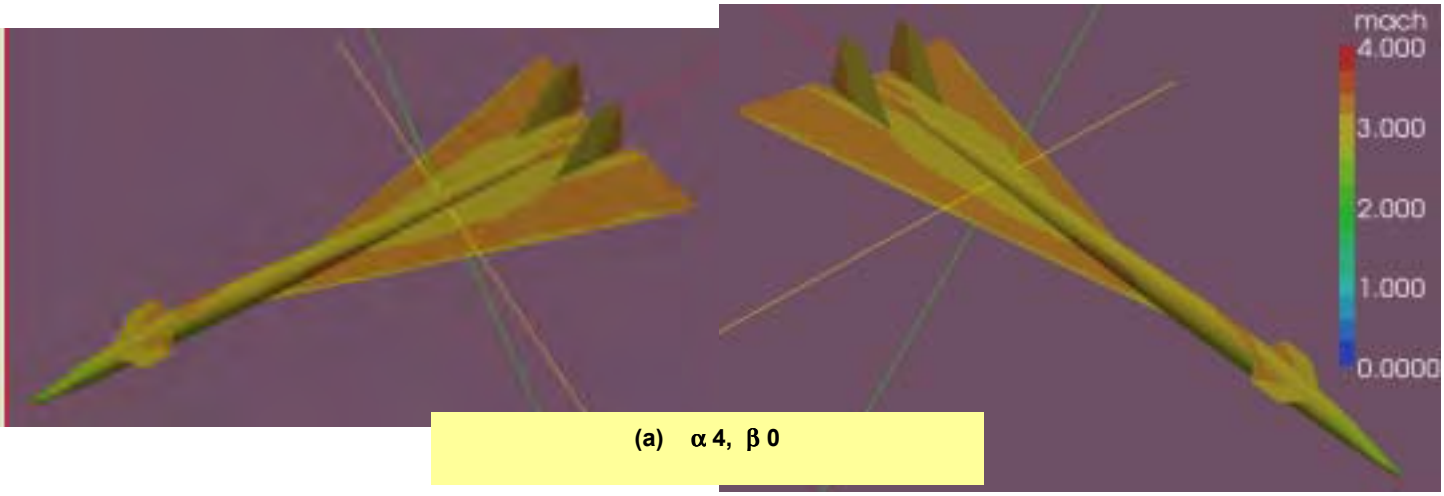

(a) α 4, β 0

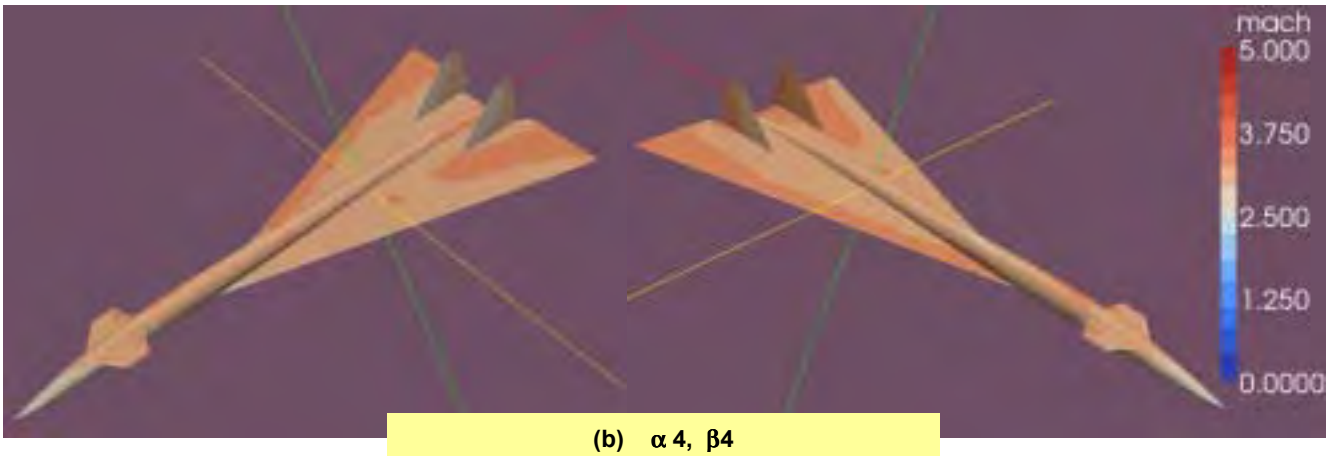

(b) α 4, β4

FIG. 9.3.2. XB-70, WING + FUSELAGE + FINS, M 3.0

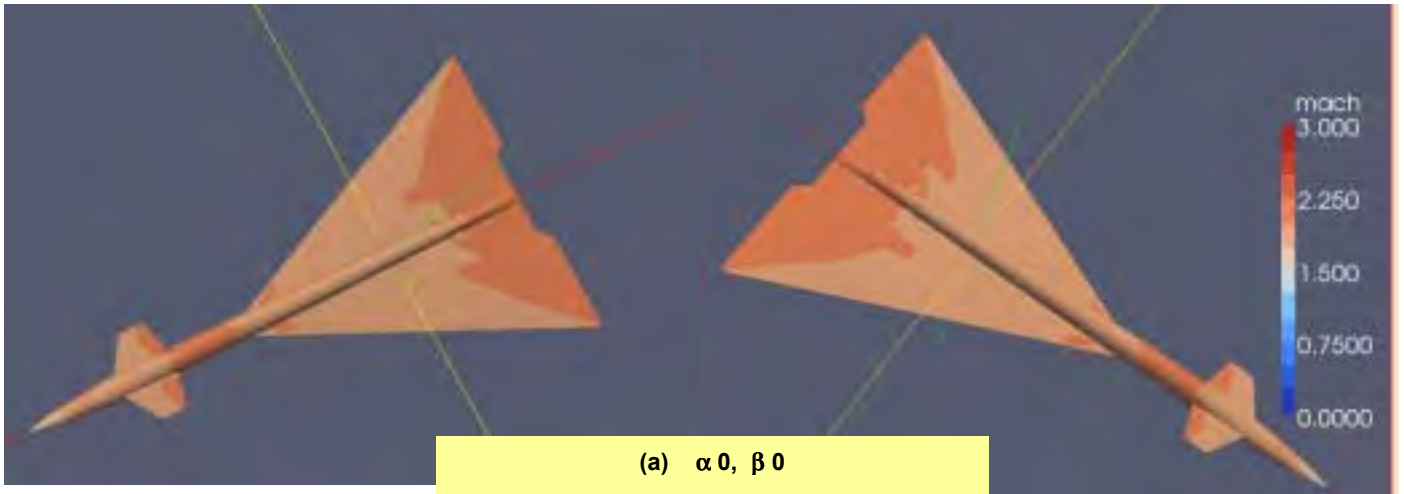

(a) α 0, β 0

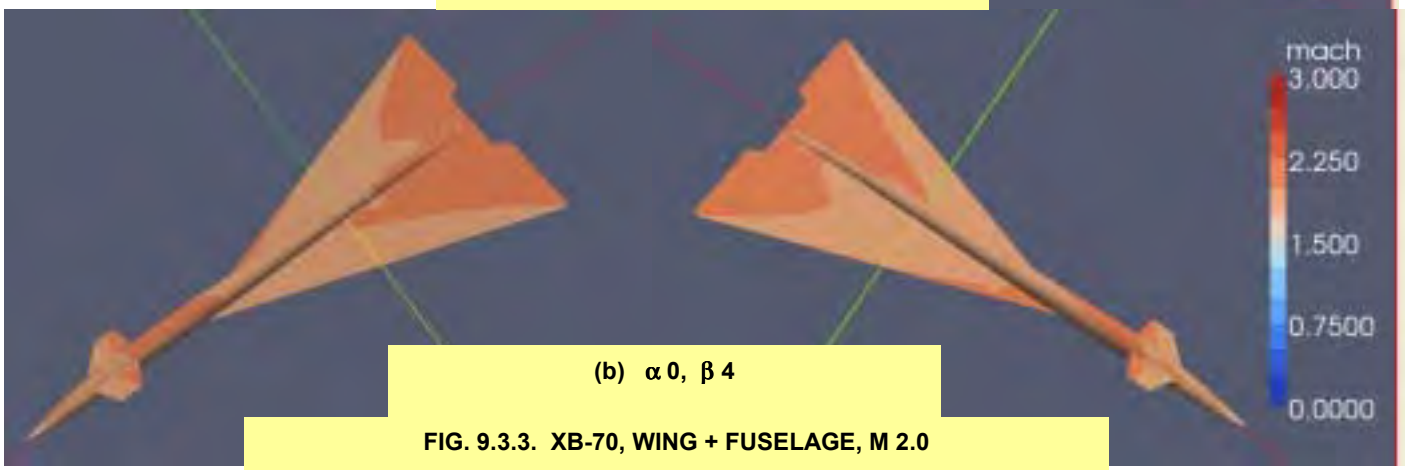

(b) α 0, β 4

FIG. 9.3.3. XB-70, WING + FUSELAGE, M 2.0

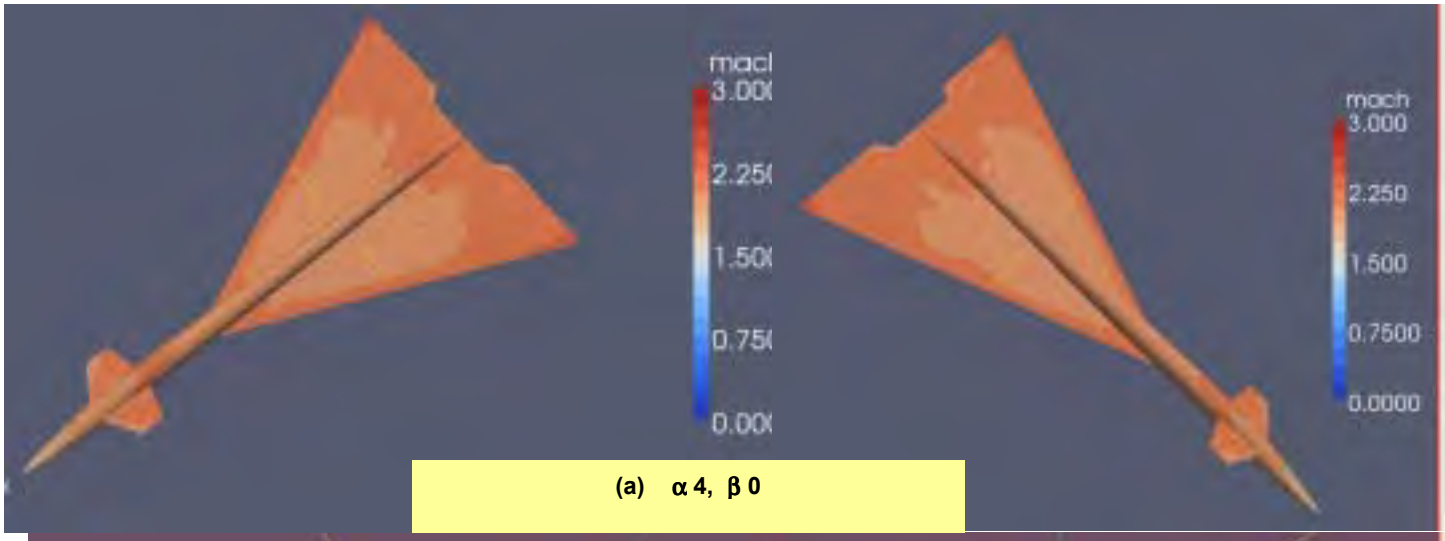

(a) α 4, β 0

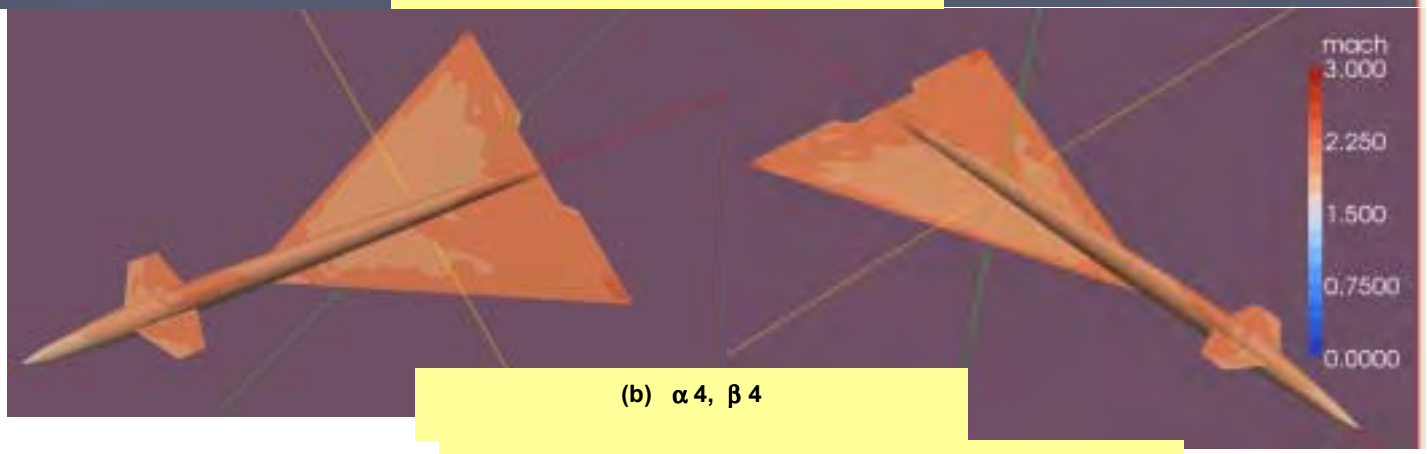

(b) α 4, β 4

FIG. 9.3.4. XB-70, WING + FUSELAGE, M 2.0

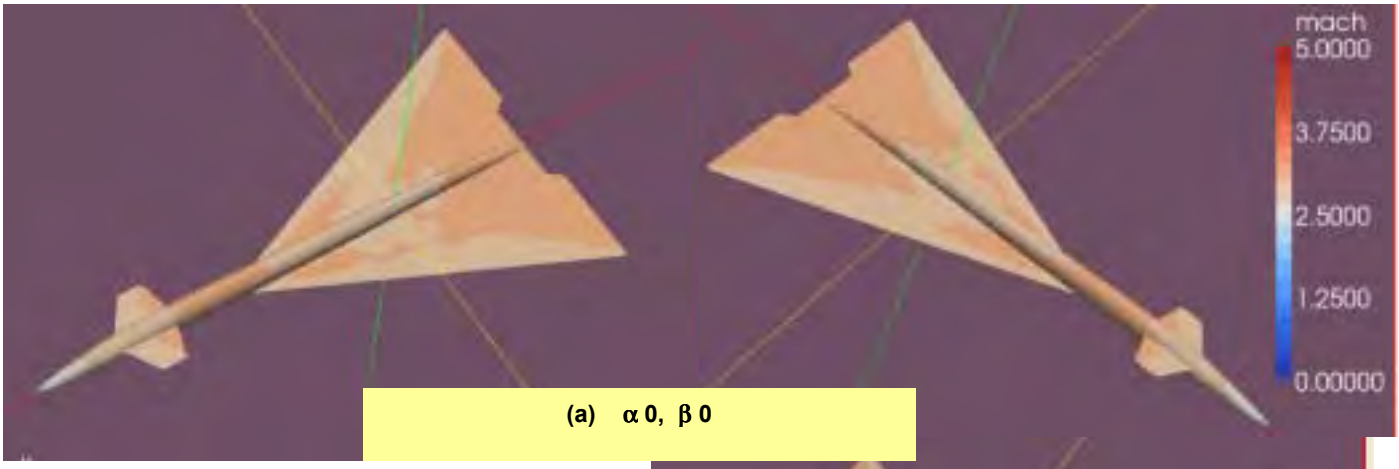

(a) α 0, β 0

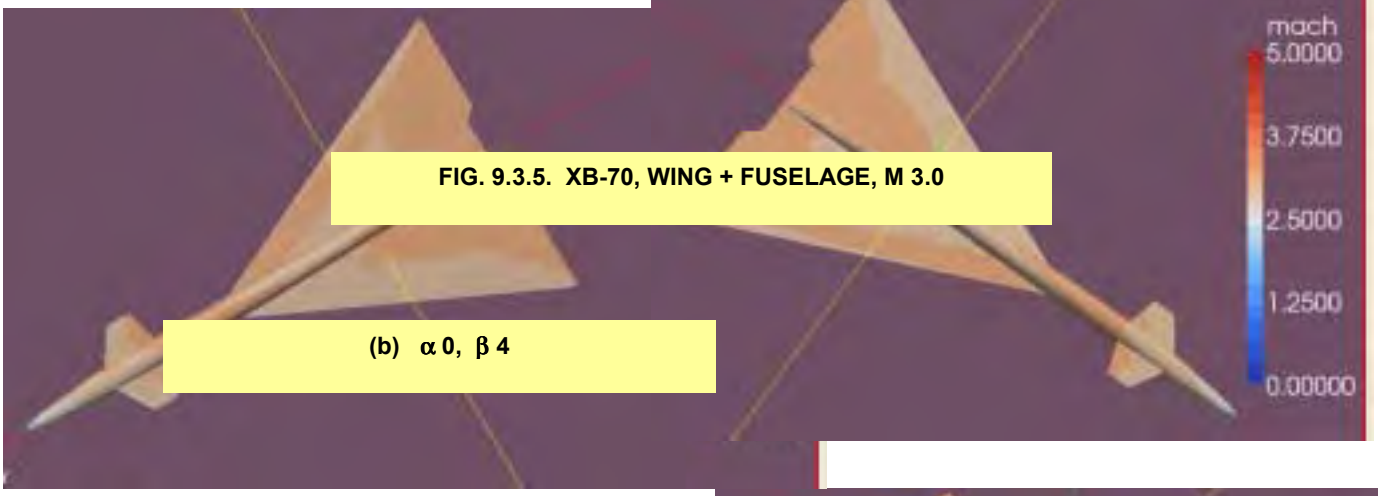

FIG. 9.3.5. XB-70, WING + FUSELAGE, M 3.0

(b) α 0, β 4

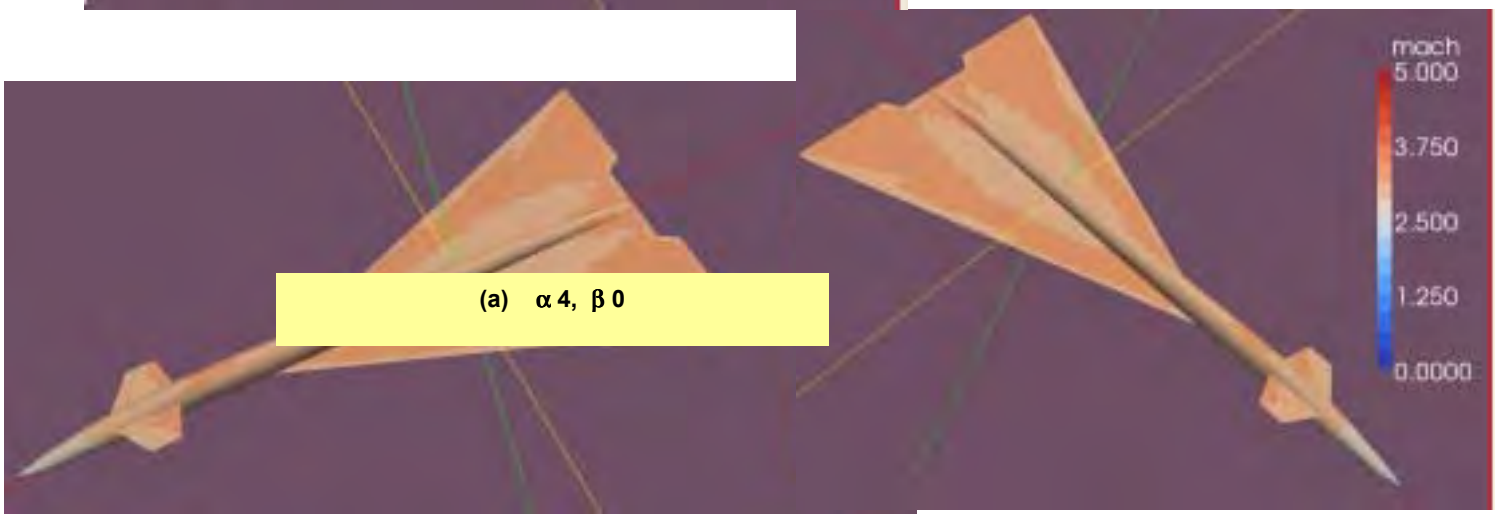

(a) α 4, β 0

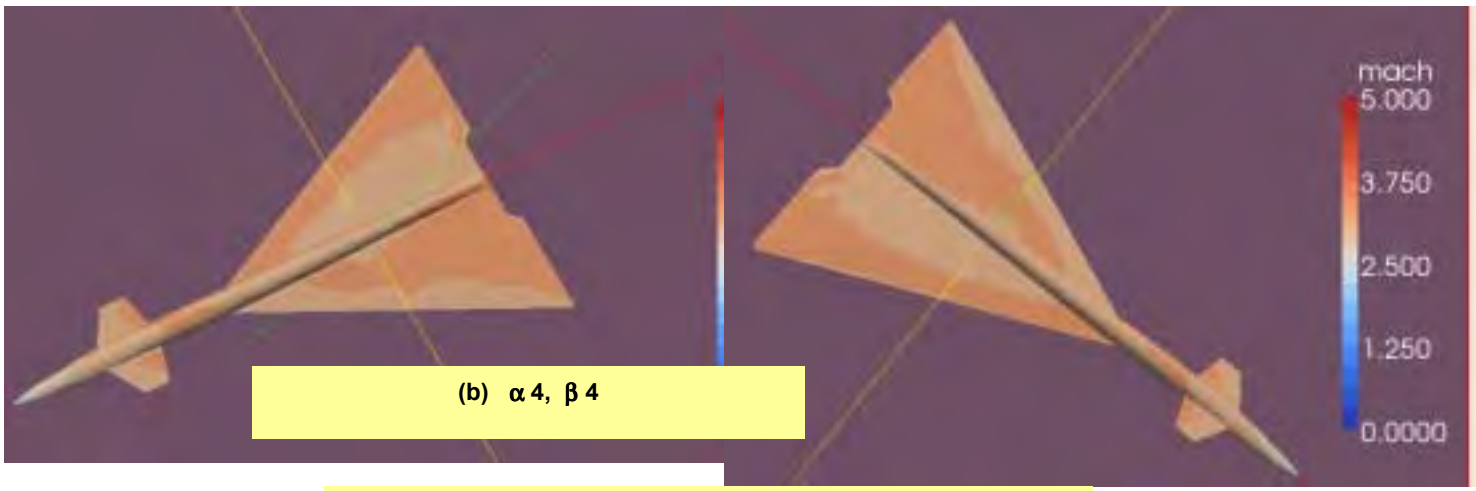

(b) α 4, β 4

FIG. 9.3.6. XB-70, WING + FUSELAGE, M 3.0

Fig. 9.3.7. XB-70, LATERAL DERIVATIVES v M

COMPONENT CONTRIBUTION
Panel Methods and Euler Method

$C_{Y\beta} = dC_Y/d\beta$
$C_{n\beta} = dC_n/d\beta$
$C_{\iota\beta} = dC_\iota/d\beta/C_L$
$C_{m\beta} = dC_m/d\beta/C_L$

\+ Wing/Body/Fins } Euler
O Wing/Body }

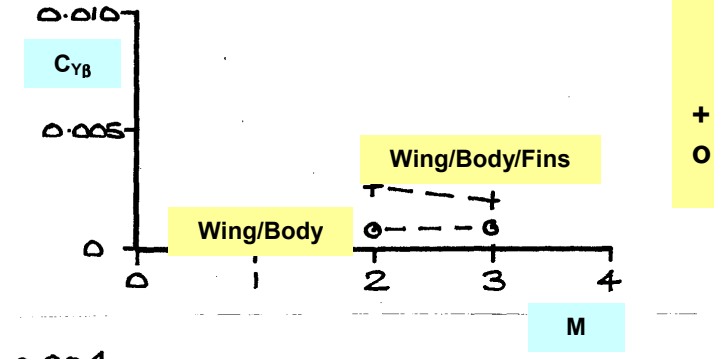

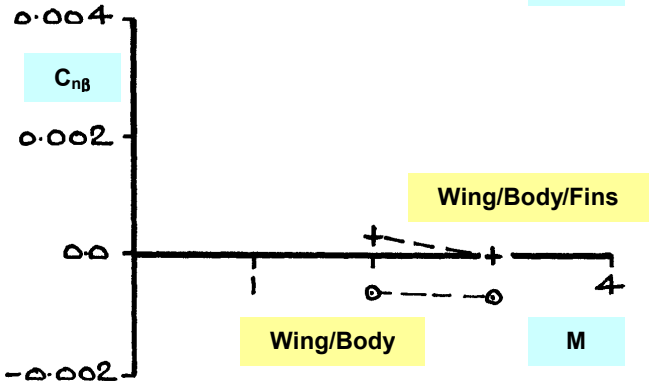

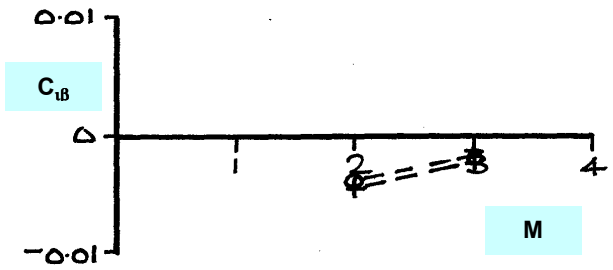

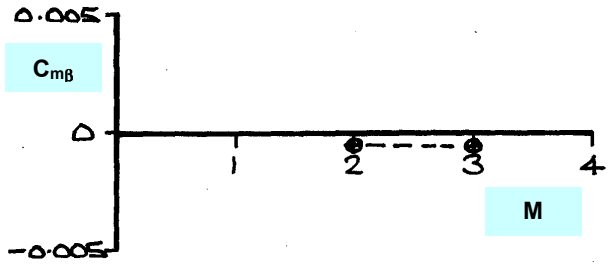

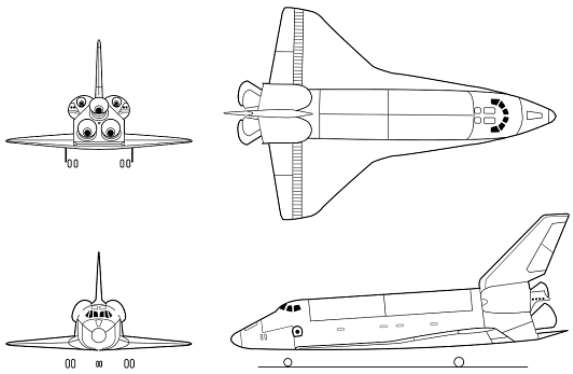

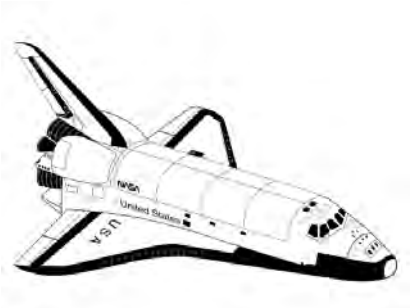

Flight Configuration

Fig. 9.4.1. SPACE SHUTTLE

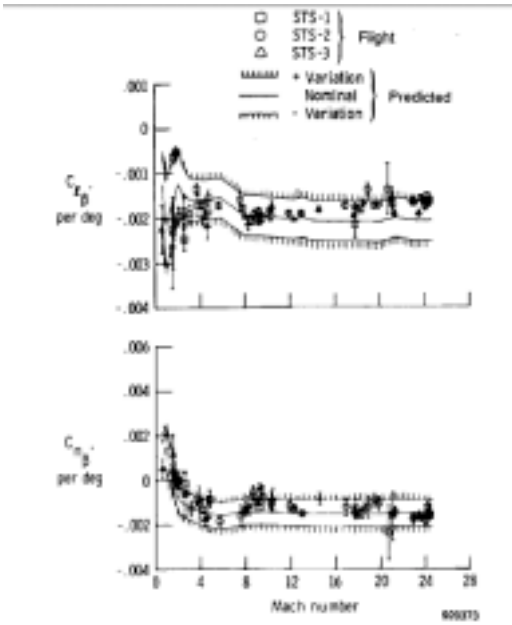

C_l & C_n due to Sideslip
Flight & Predicted, Variation with M

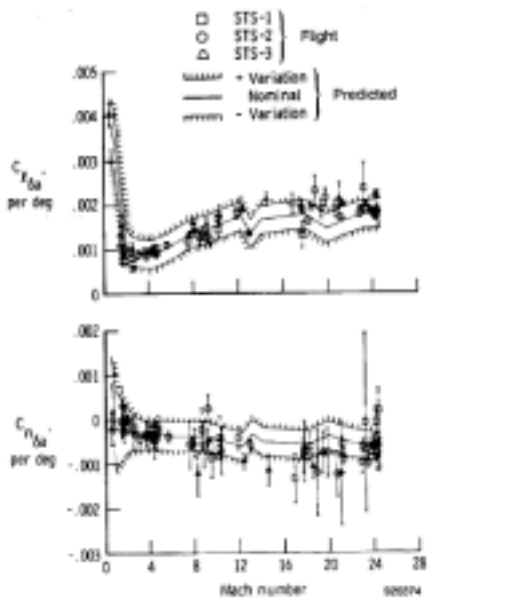

C_l & C_n due to Aileron
Flight & Predicted, Variation with M

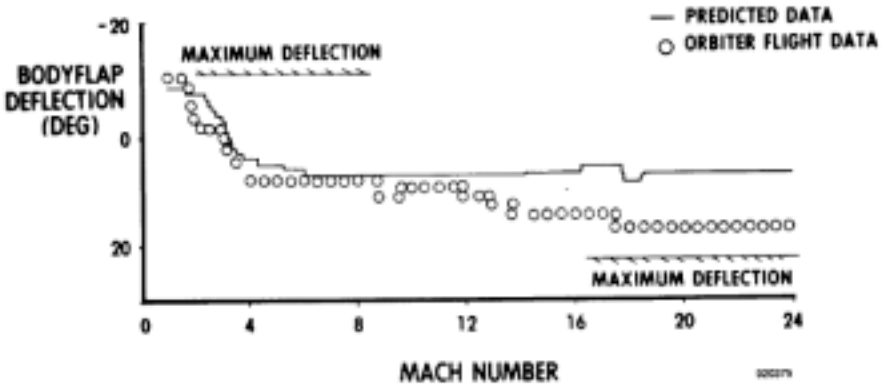

Body Flap Deflection, Flight & Predicted, Variation with M

Fig. 9.4.2. SPACE SHUTTLE, LATERAL & CONTROL POWER DERIVATIVES, VARIATION WITH M

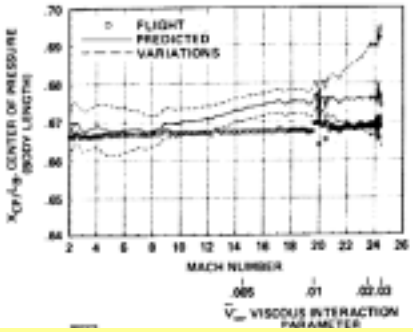

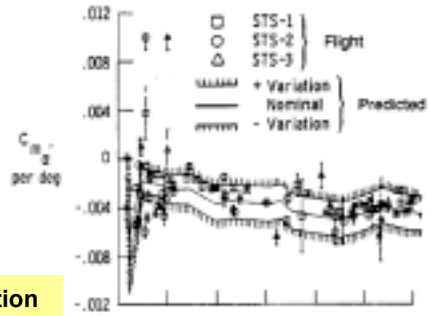

Aerodynamic Centre of Pressure Location Flight & Predicted, Variation with M

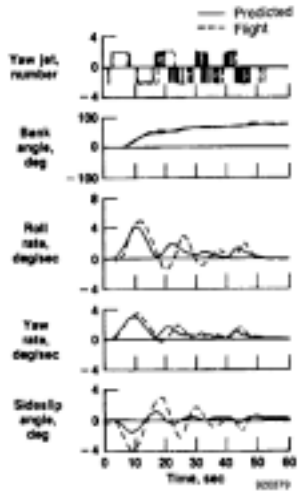

Flight & Predicted Manouvre Data Variation with Time

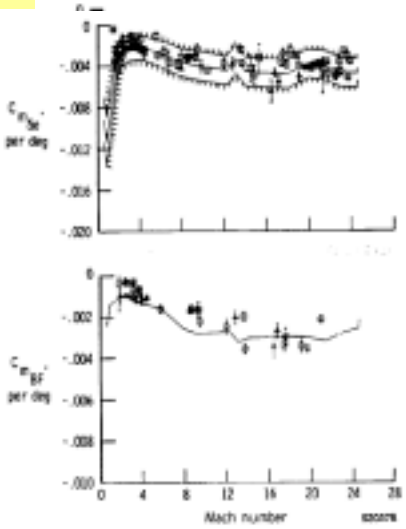

C_m due to α, Elevator & Body Flap Angles Flight & Predicted, Variation with M Manouvre Data

Fig. 9.4.3. SPACE SHUTTLE, CENTRE OF PRESSURE VARIATION, LATERAL & CONTROL POWER DERIVATIVES, VARIATION WITH M

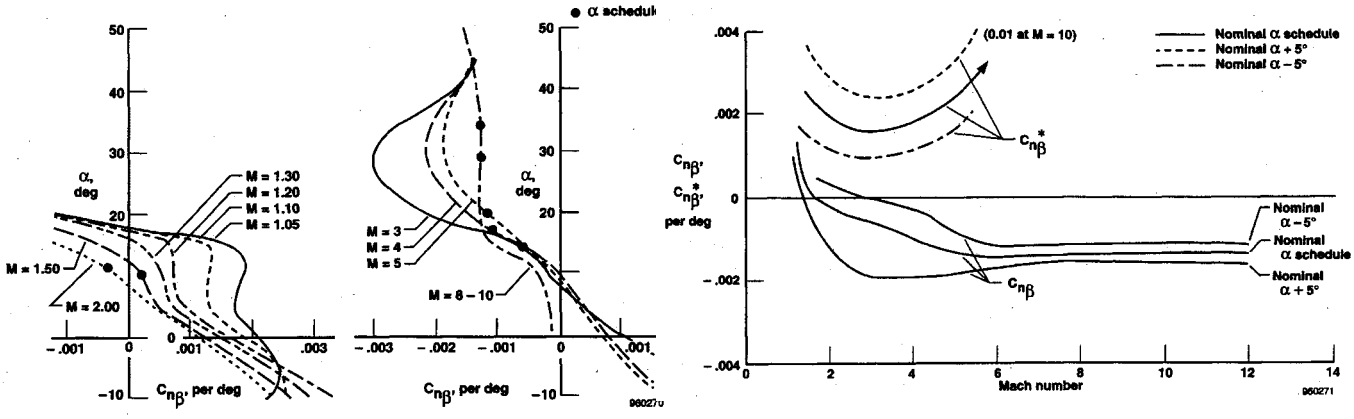

Fig. 9.4.4. SPACE SHUTTLE, STABILITY DERIVATIVES ($C_{n\beta}$) VARIATION WITH α & M

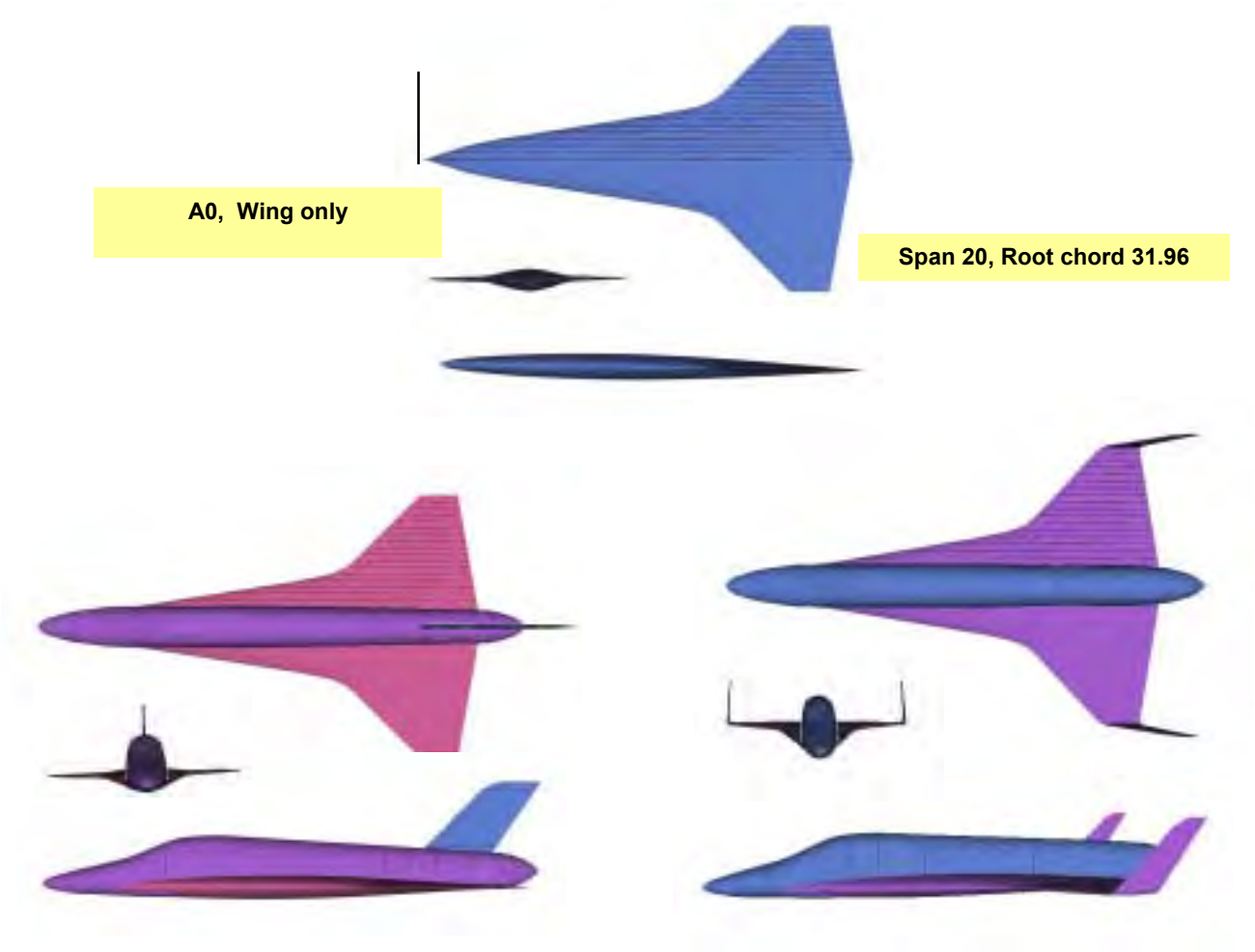

Fig. 9.5.1. A0, A1 and A2 CONFIGURATIONS

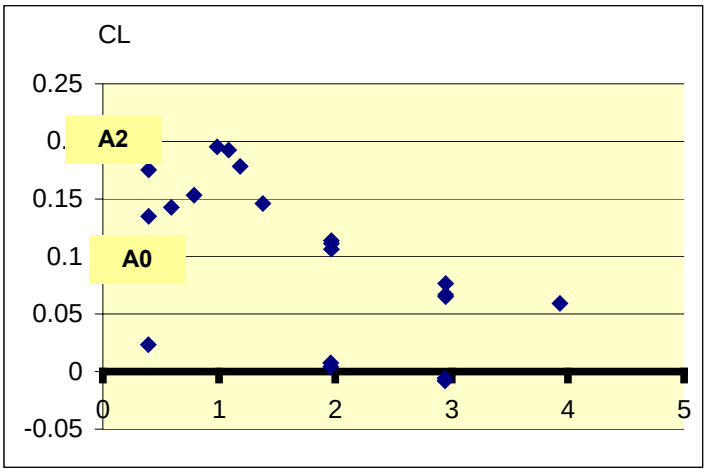

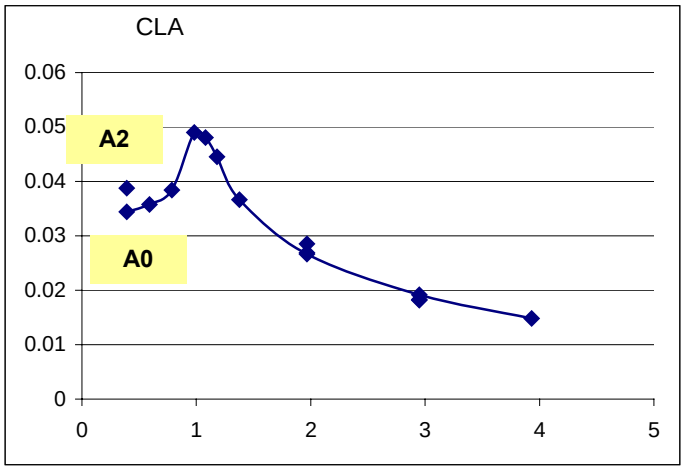

C_L – M, α 4°

Fig. 9.5.2. A0 and A2, LIFT (α 4°) and LIFT CURVE SLOPE VARIATION WITH M

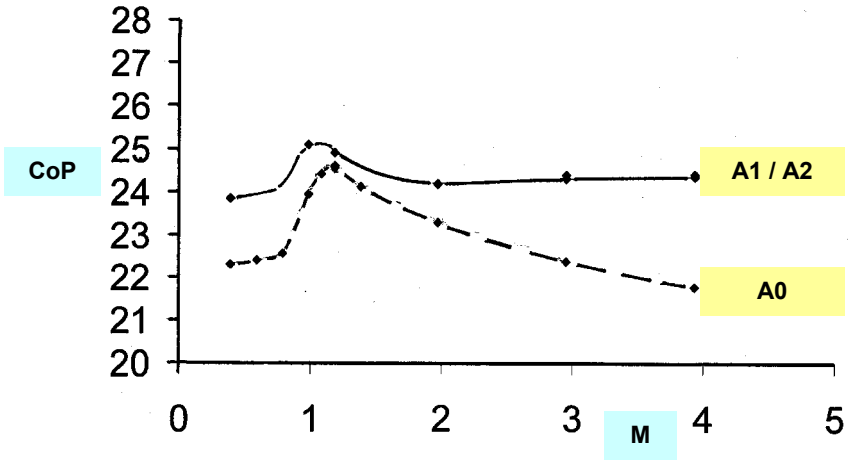

Fig. 9.5.3. A0, A1 and A2, CENTRE OF PRESSURE LOCATION, VARIATION WITH M

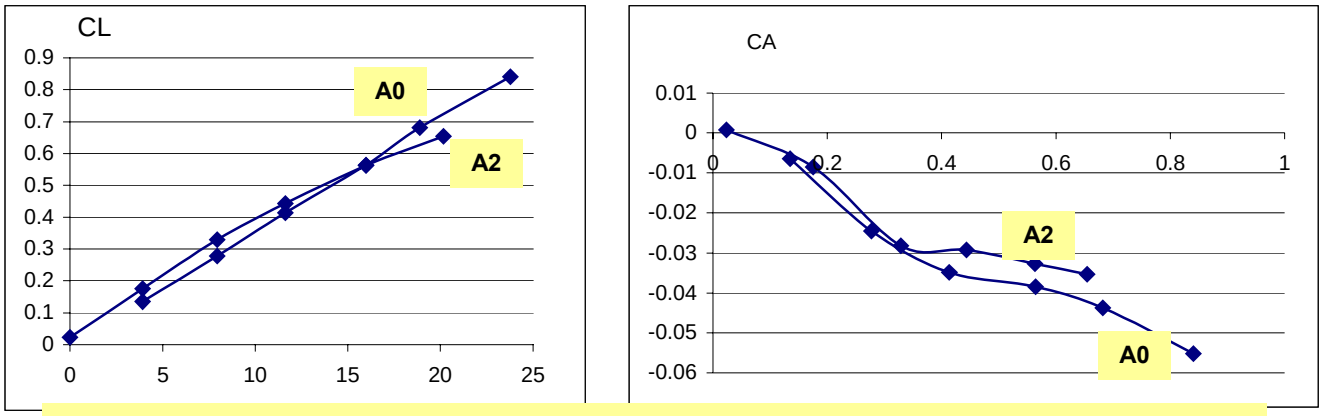

Fig. 9.5.4. A0 and A2, C_L – α & C_A – C_L VARIATIONS, M 0.4 A0 and A2

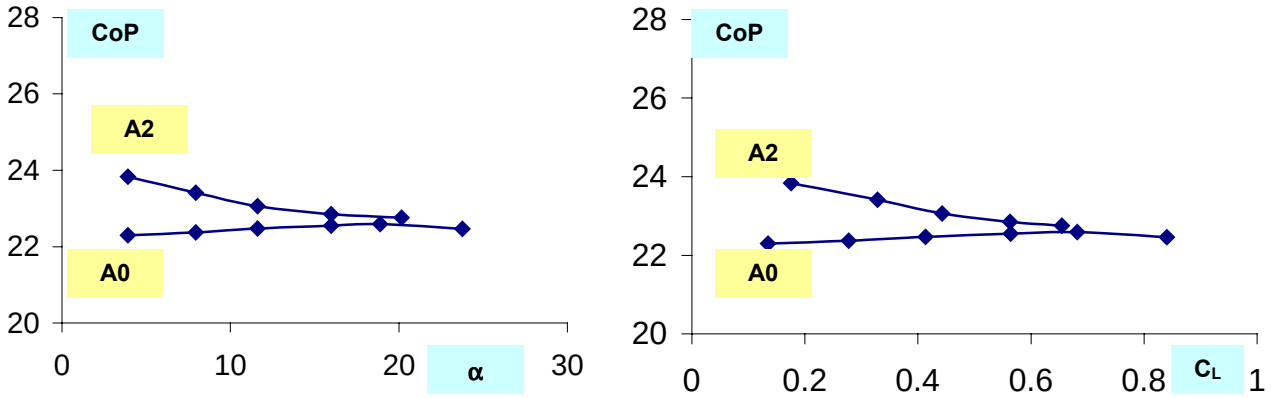

Fig. 9.5.5. A0 and A2, CoP VARIATION WITH α and CL, M 0.4

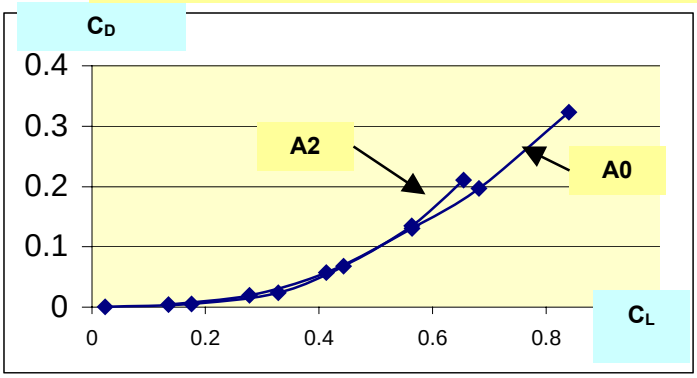

(a) C_D – C_L

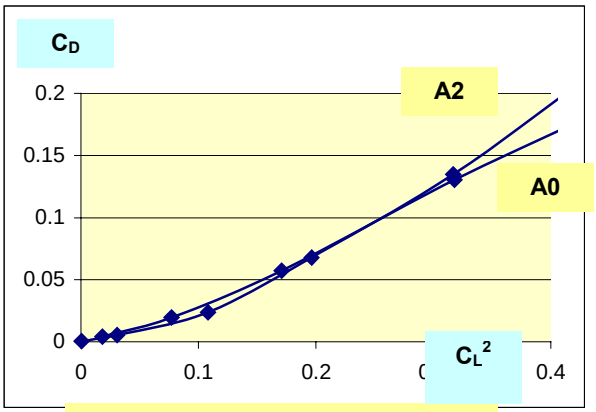

(b) C_D – C_L^2

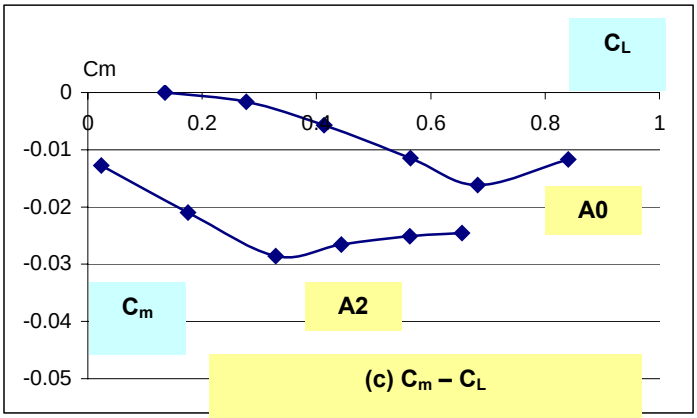

(c) C_m – C_L

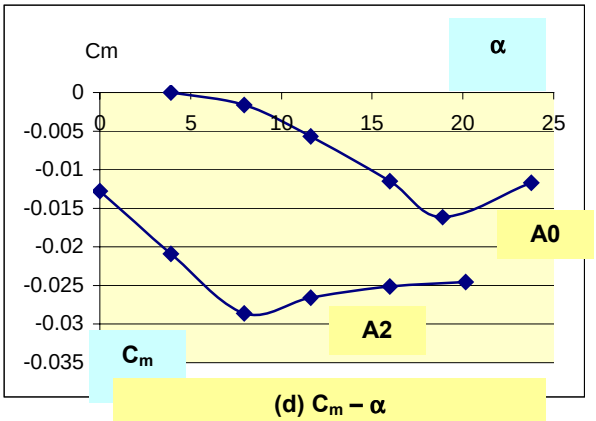

(d) C_m – α

Fig. 9.5.6. A0 and A2, C_D - C_L & C_L^2 , C_m - C_L & α, M 0.4

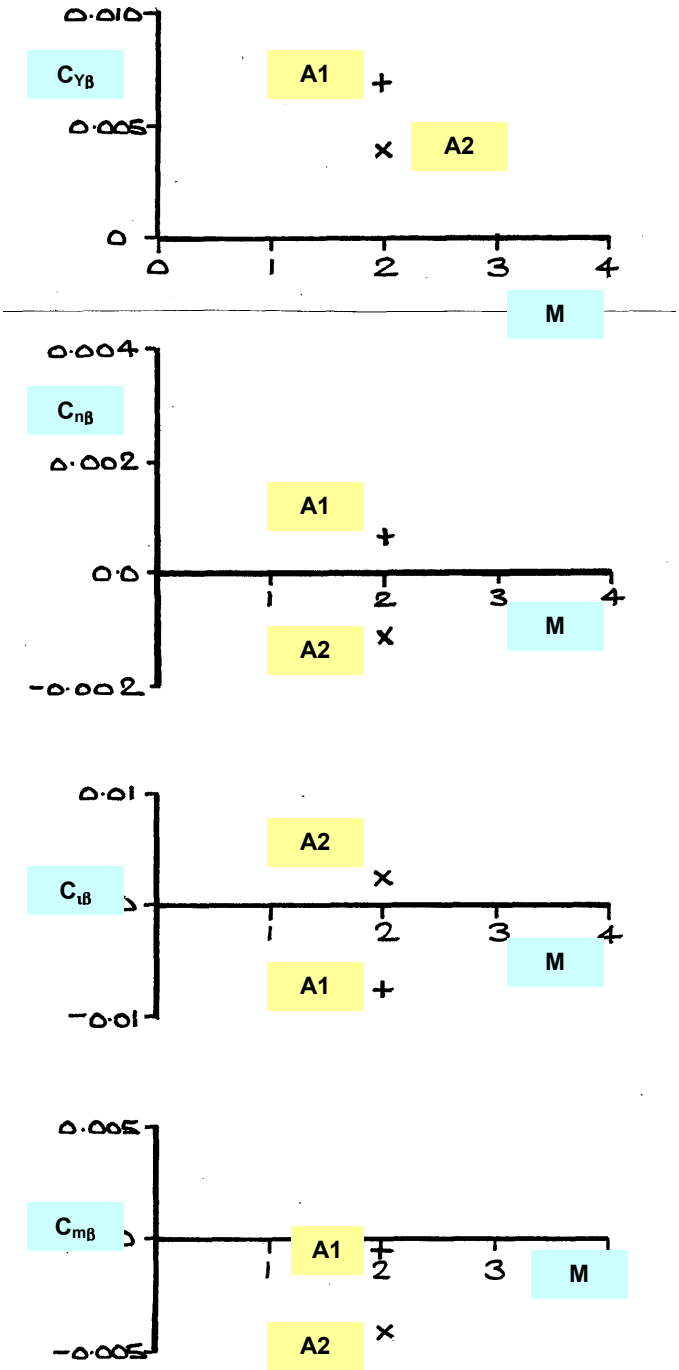

Fig. 9.5.7. LATERAL DERIVATIVES v M

SINGLE & TWIN FIN, A1 / A2
Euler Method

$C_{Y\beta} = dC_Y/d\beta$
$C_{n\beta} = dC_n/d\beta$
$C_{\iota\beta} = dC_\iota/d\beta/C_L$
$C_{m\beta} = dC_m/d\beta/C_L$

\+ A1, Single Fin
X A2, Twin Fin

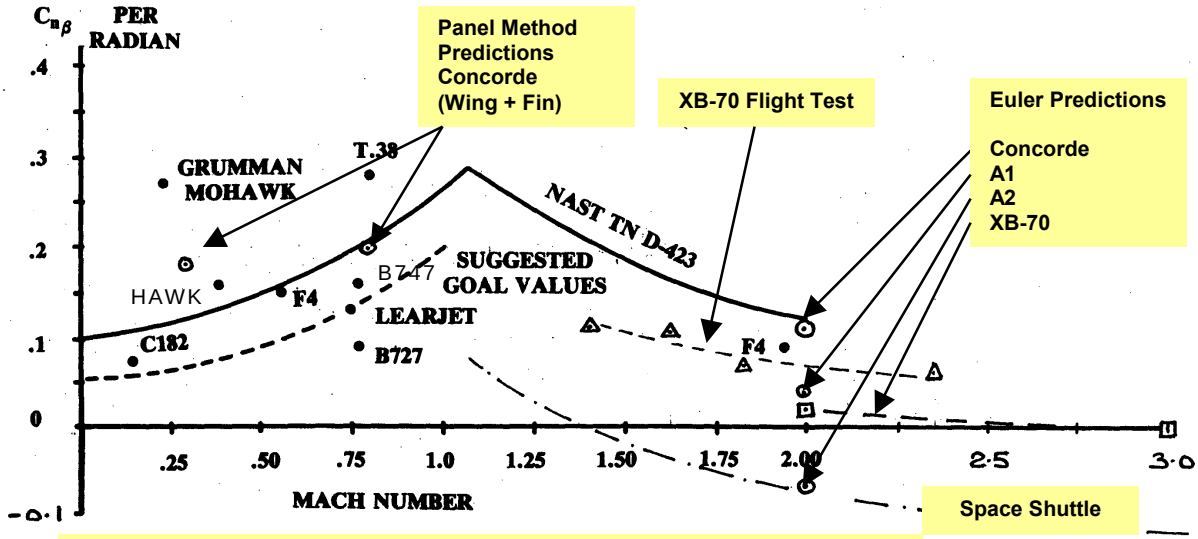

Fig. 9.6.1. LATERAL STABILITY ($C_{n\beta}$) VARIATION WITH M, Ref.14

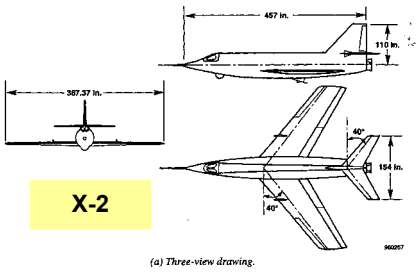

(a) Three-view drawing.

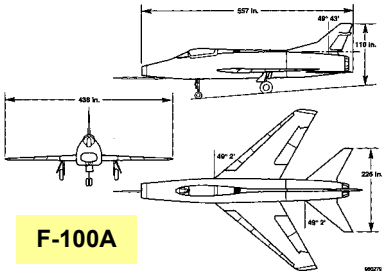

(a) Three-view drawing.

Figure 25. Three-view drawing and photograph of the F-100A (original vertical tail).

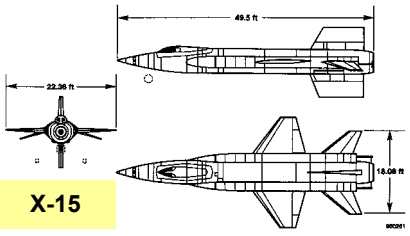

(a) Three-view drawing.

Figure 6. Three-view drawing and photograph of the X-15 research airplane.

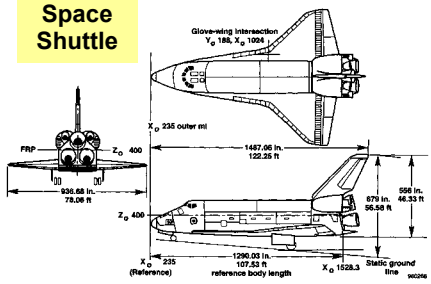

(a) Three view drawing.

Figure 12. Three-view drawing and photograph of the Space Shuttle.

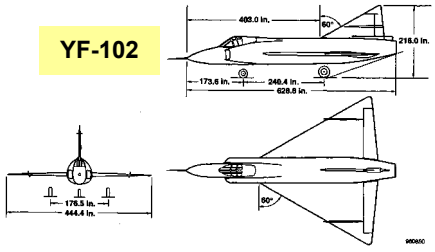

(a) Three-view drawing.

Figure 32. Three view drawing and photograph of the YF-102 airplane.

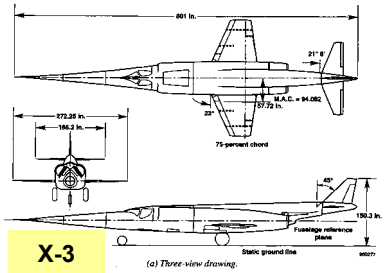

(a) Three-view drawing.

Delta Types

(a) Typical examples, Ref.13

MASS PROPERTIES OF COUPLING PRONE AIRCRAFT

Aircraft	X-15	X-3	Shuttle	YF-102	F-100A	X-2
W	14318	21900	198144	30394	23989	12375
m	445	680	6154	944	745	384
I_x	3600	4100	895000	13200	10976	5043
I_y	85000	61200	6918000	106000	57100	25474
I_z	86500	65100	7199000	114600	64975	29106
I_{xz}	–650	4200	167000	3540	942	782
ε	–0.45	3.95	1.52	2.00	1.00	1.86
$(I_y - I_z)/I_x$	–0.42	–0.95	–0.31	–0.65	–0.72	–0.72
$(I_z - I_x)/I_y$	0.98	1.00	0.91	0.96	0.95	0.94
$(I_x - I_y)/I_z$	–0.94	–0.88	–0.84	–0.81	–0.71	–0.70
I_{xz}/I_x	–0.18	1.02	0.19	0.27	0.086	0.16
I_{xz}/I_y	–0.0076	0.069	0.024	0.033	0.017	0.031
I_{xz}/I_z	–0.0075	0.065	0.023	0.031	0.014	0.027
I_z/I_x	24.0	15.9	8.0	8.7	5.9	5.8

$$\varepsilon = 57.3\frac{I_{xz}}{I_z - I_x}, \text{ deg}$$

(b) Mass Properties, Ref.13

Fig. 10.1.1. AIRCRAFT PRONE TO MULTI-AXIS INERTIAL COUPLING

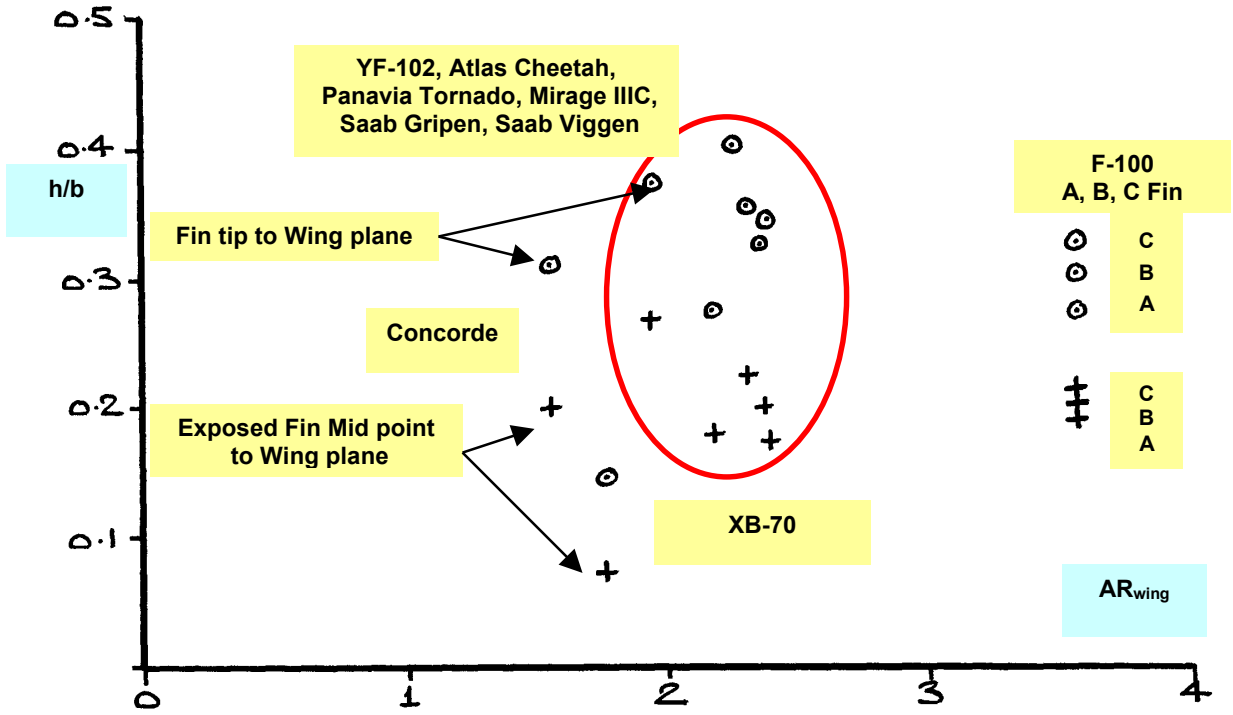

Fig. 10.2.1. FIN SIZING RELATIONSHIPS, DELTA TYPE AIRCRAFT

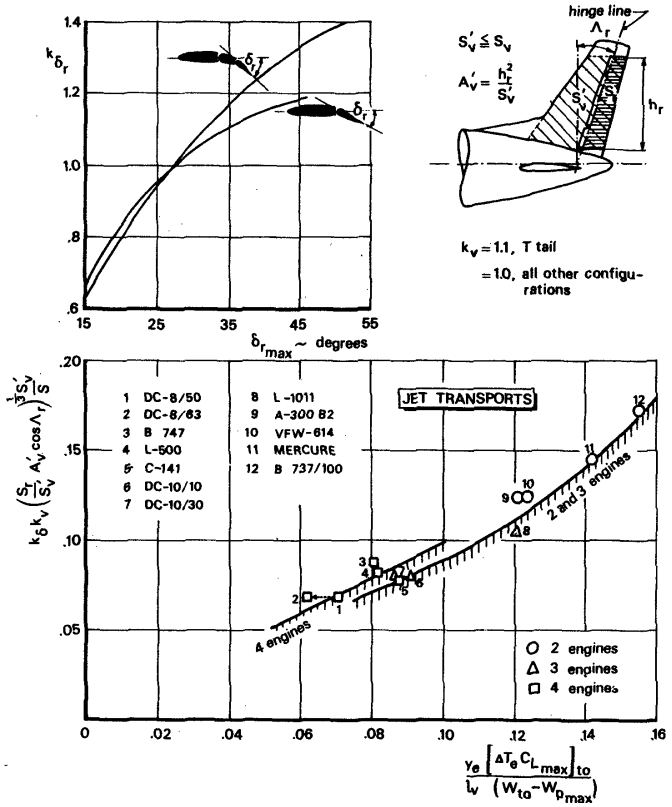

Fig. 10.2.2. FIN-RUDDER EFFECTIVENESS v ENGINE-OUT INDUCED YAW, SUBSONIC JET TRANSPORT AIRCRAFT

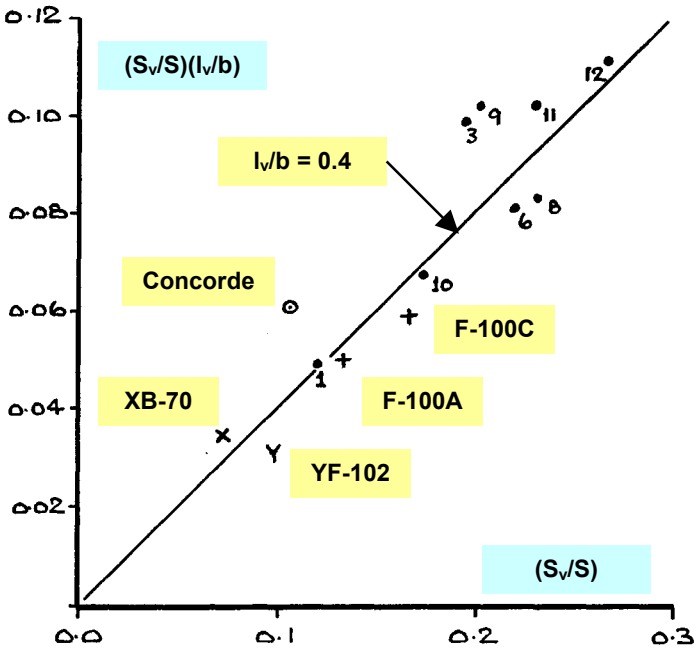

Fig. 10.2.3. VERTICAL TAIL VOLUME COEFFICIENT v FIN AREA COEFFICIENT SUBSONIC JET TRANSPORT AIRCRAFT, F-100, YF-102, CONCORDE and XB-70

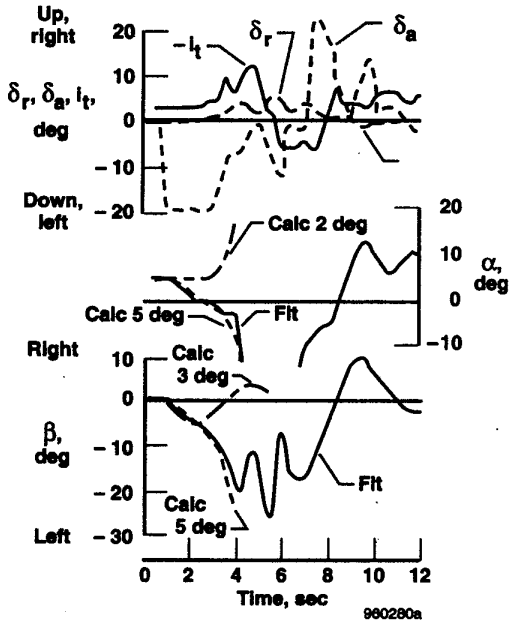

(a) Stability and control parameters during coupled motions.

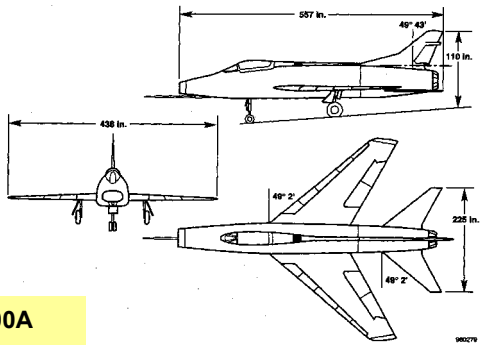

F-100A

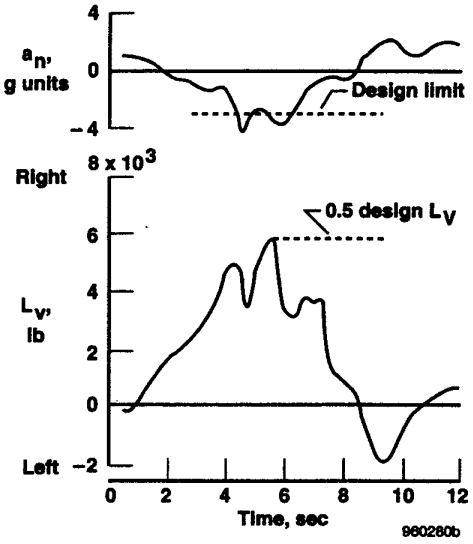

(b) Load and acceleration parameters during coupled motions.

Fig.10.3.1. F-100, TIME HISTORY, ABRUPT AILERON ROLL, Mach 0.7, 32,000 ft.

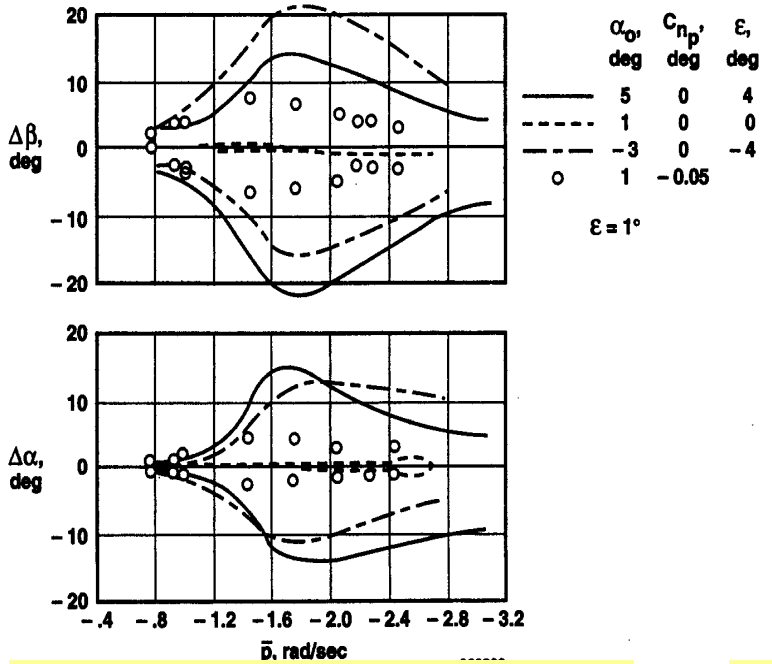

Fig.10.3.2. F-100, EFFECT of ε (Initial α) on Δα & Δβ ARISING as ROLL RATE VARIES

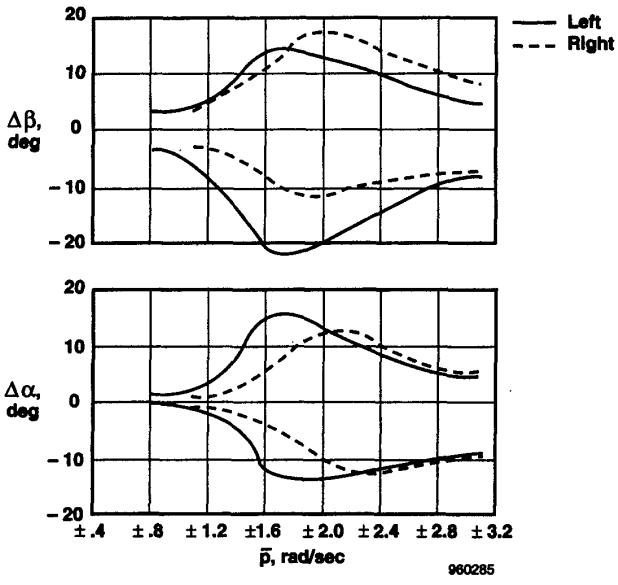

Fig.10.3.3. F-100A, EFFECT of ENGINE GYROSCOPICS on Δα & Δβ , LEFT & RIGHT ROLLS

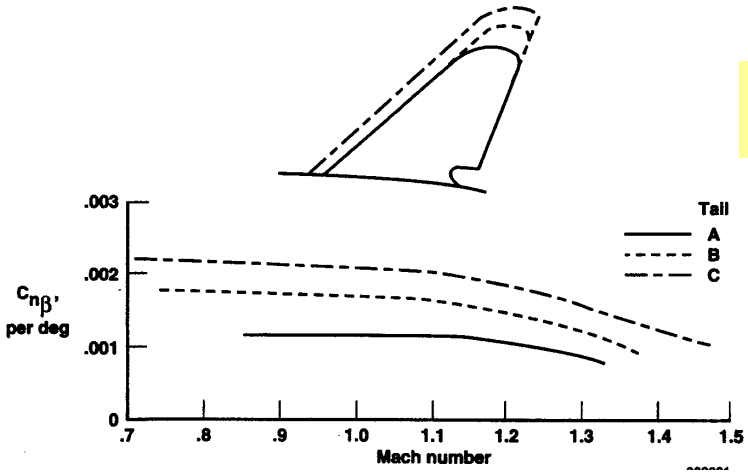

Fig.10.3.4. F-100, EFFECT of TAIL SIZE on FLIGHT DERIVED DIRECTIONAL STABILITY vs Mach No.

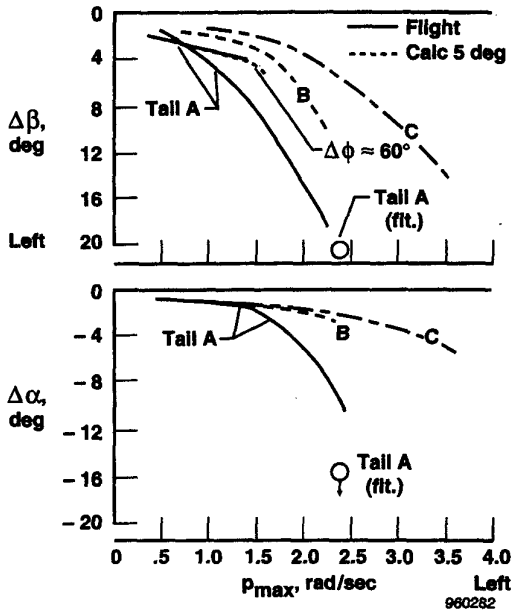

Fig.10.3.5. F-100, EFFECT of TAIL SIZE on LEFT AILERON ROLLS, Mach 0.7, 31,000 ft.

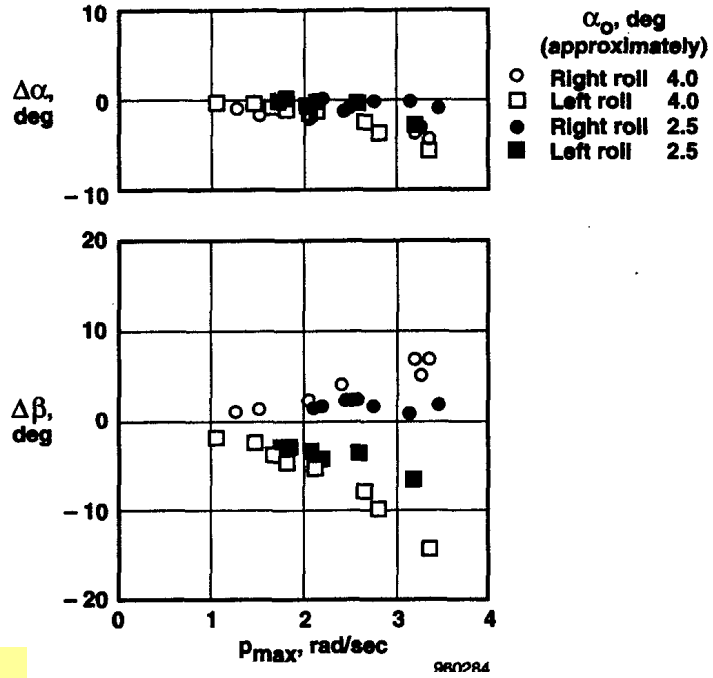

Fig.10.3.6. F-100 (Tail C), EFFECT of α at ROLL ENTRY on $\Delta\alpha$ & $\Delta\beta$ ARISING

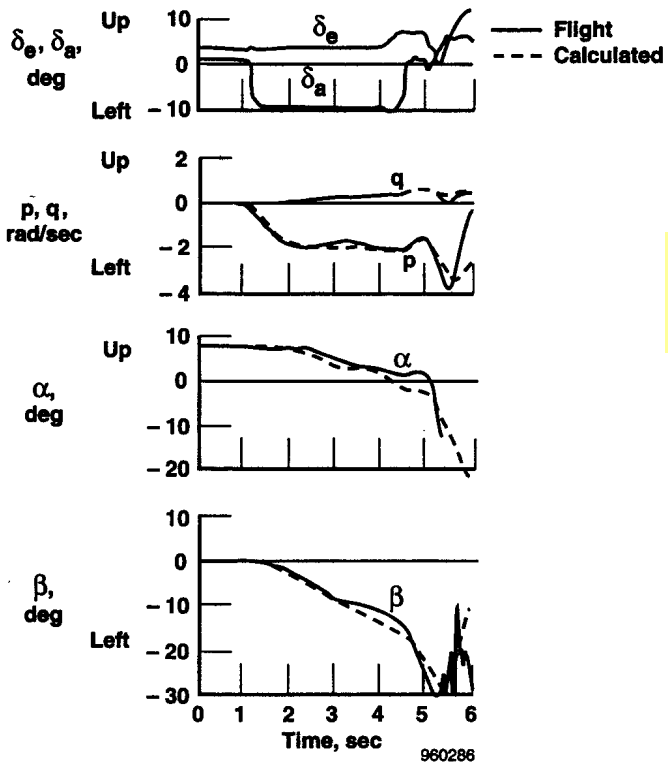

Fig.10.4.1. YF-102, COMPARISON BETWEEN FLIGHT & CACULATED ROLL Mach 0.75 at 39,500 ft

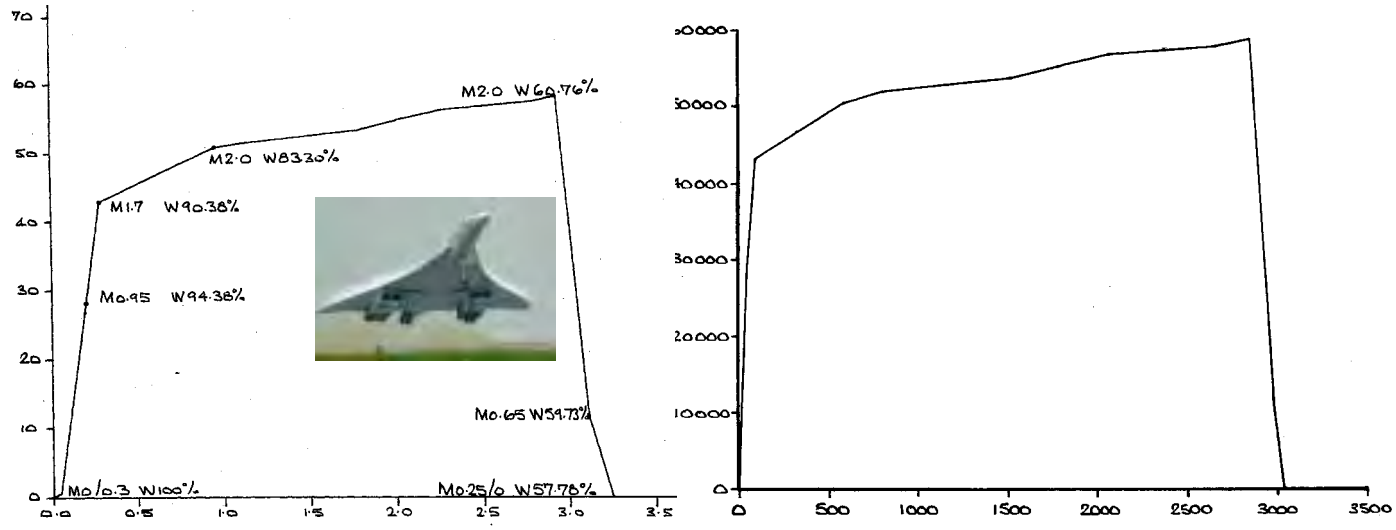

FIG. 11.1.1. CONCORDE, ALTITUDE – TIME & DISTANCE, Mach 2, C_L VARIES

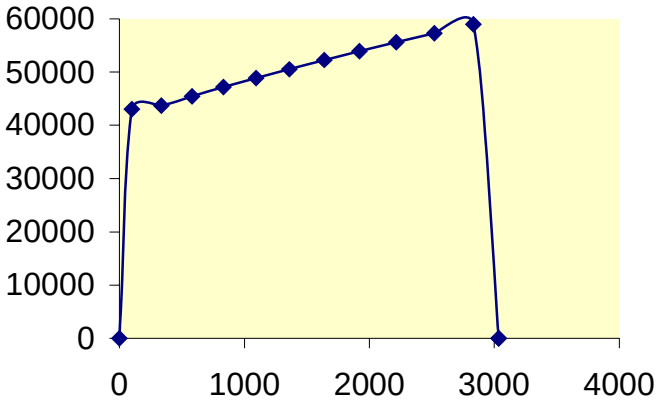

(a) CL at start of cruise = 0.1004, CL at end of cruise 0.147

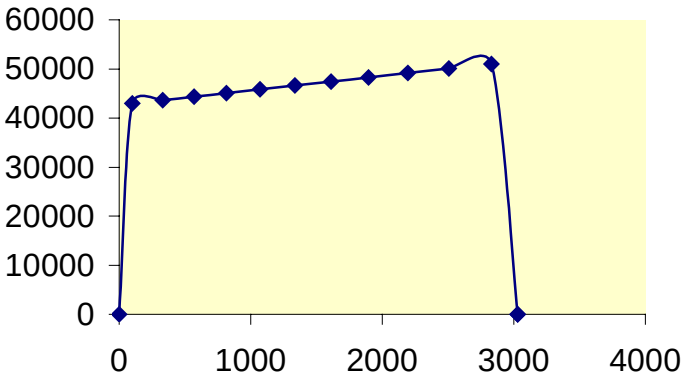

(b) CL at start of cruise = 0.1004, CL at end of cruise 0.1004

FIG. 11.1.2. MATCHING CONCORDE, ALTITUDE – DISTANCE

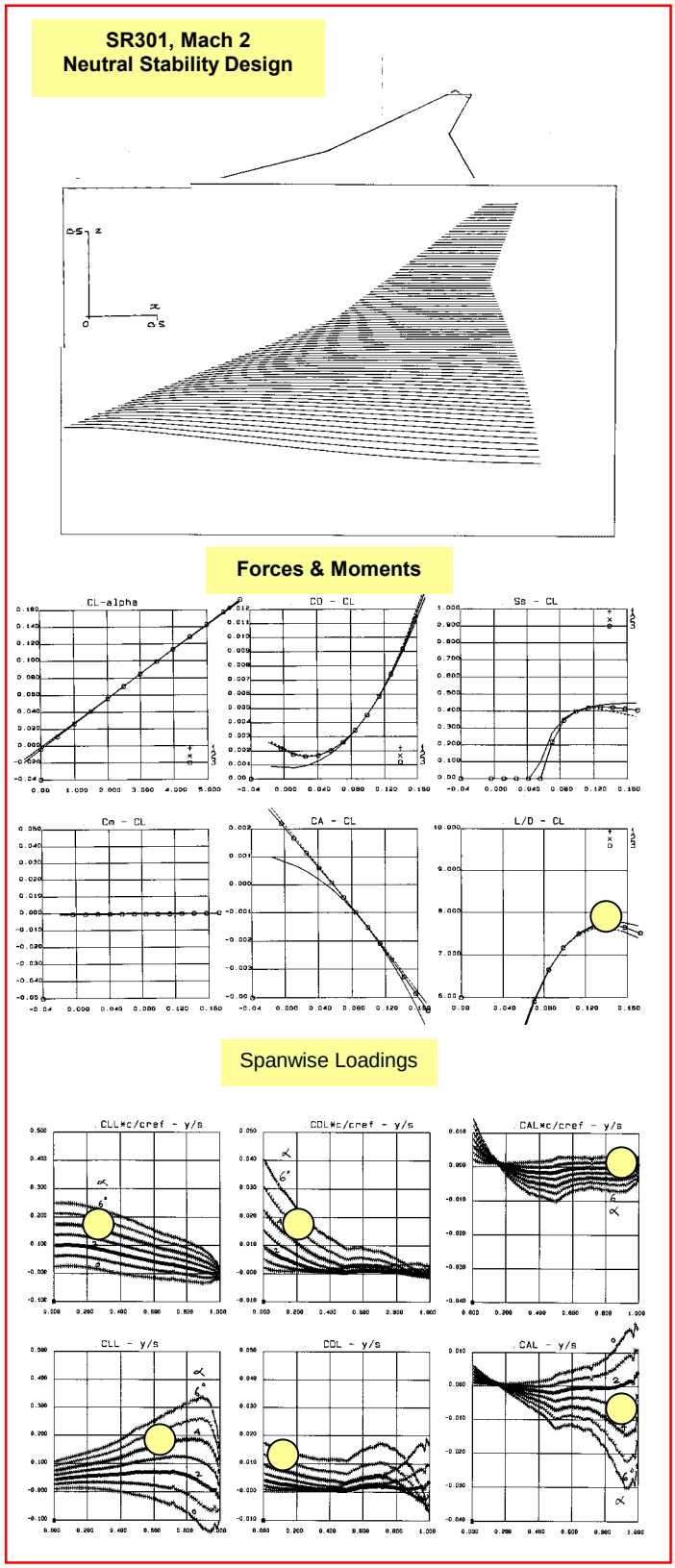

FIG. 11.3.1. SR301, DESIGNED FOR MACH 2 PREDICTED AERODYNAMIC CHARACTERISTICS AT MACH 2

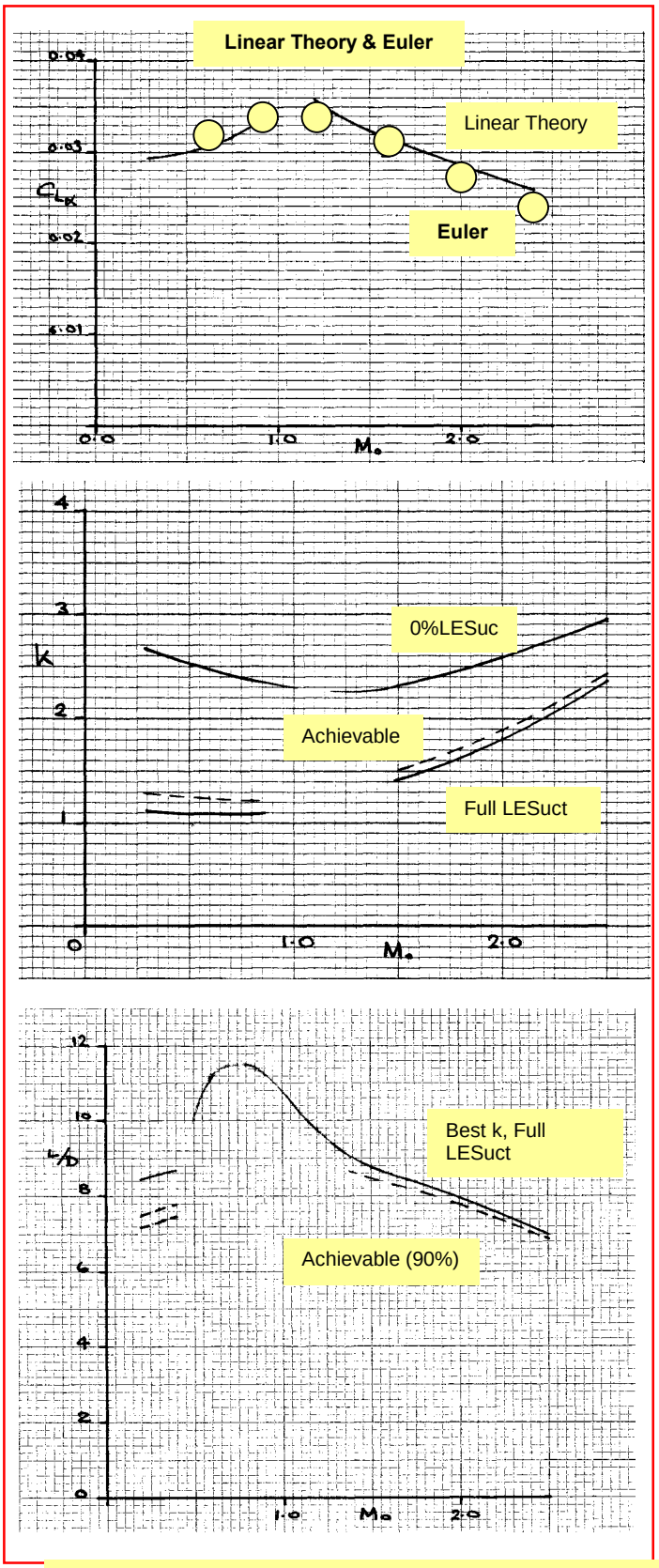

FIG. 11.3.2. SR301, DESIGNED FOR Mach 2 PREDICTED AERODYNAMIC CHARACTERISTICS THROUGH MACH NUMBER RANGE

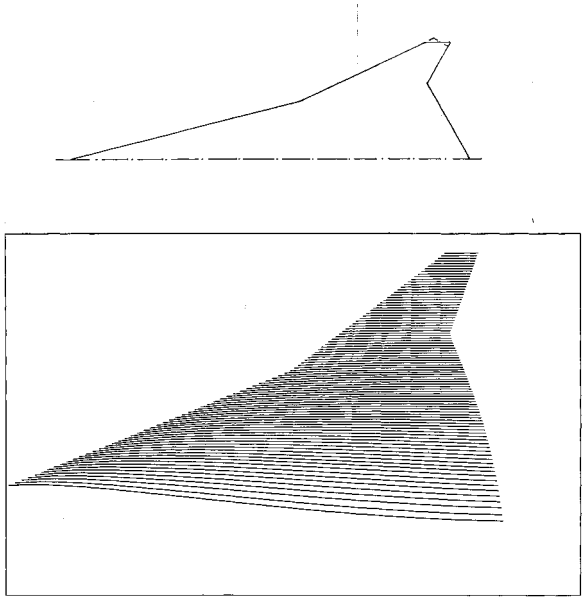

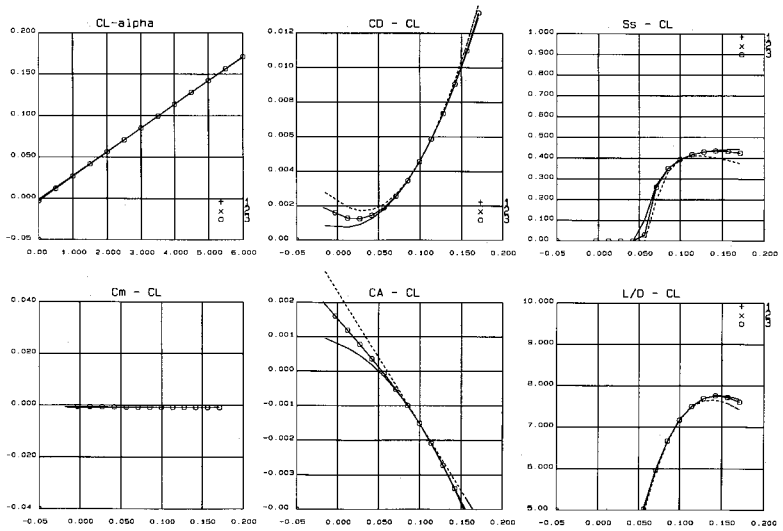

FIG. 11.3.3. SR301, DESIGNED FOR MACH 2, NEUTRALLY STABLE
PREDICTED AERODYNAMIC CHARACTERISTICS AT MACH 2

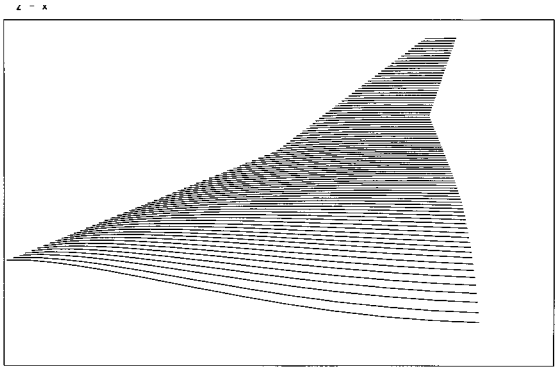

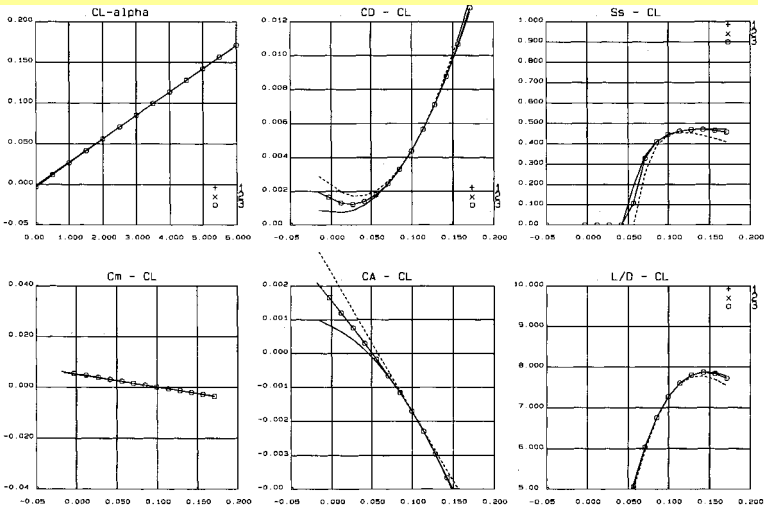

FIG. 11.3.4. SR301, DESIGNED FOR MACH 2, 5%cref STABLE
PREDICTED AERODYNAMIC CHARACTERISTICS AT MACH 2

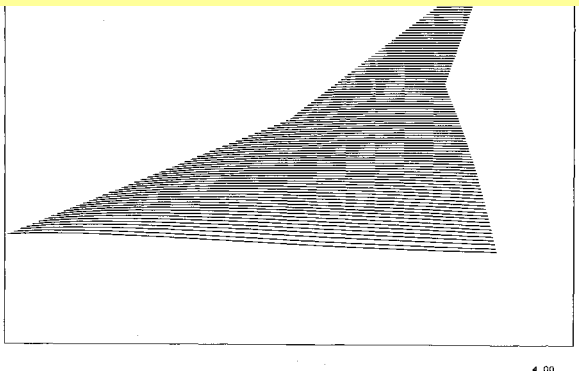

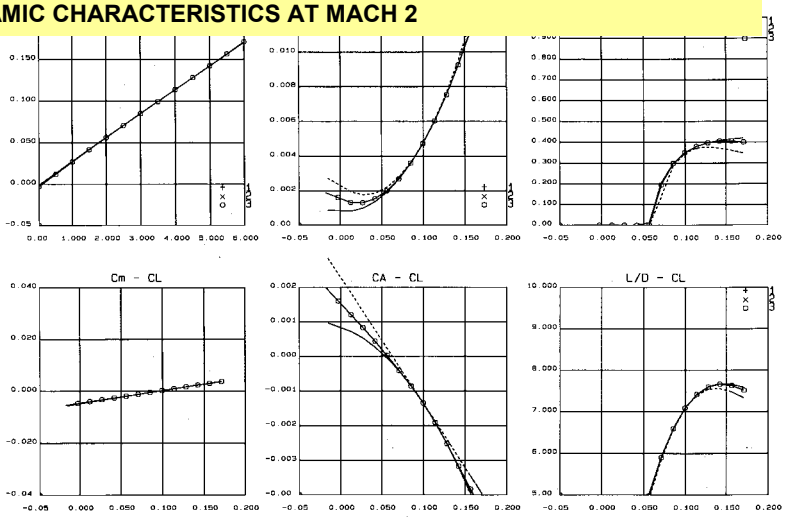

FIG. 11.3.5. SR301, DESIGNED FOR MACH 2, 5%cref UNSTABLE
PREDICTED AERODYNAMIC CHARACTERISTICS AT MACH 2

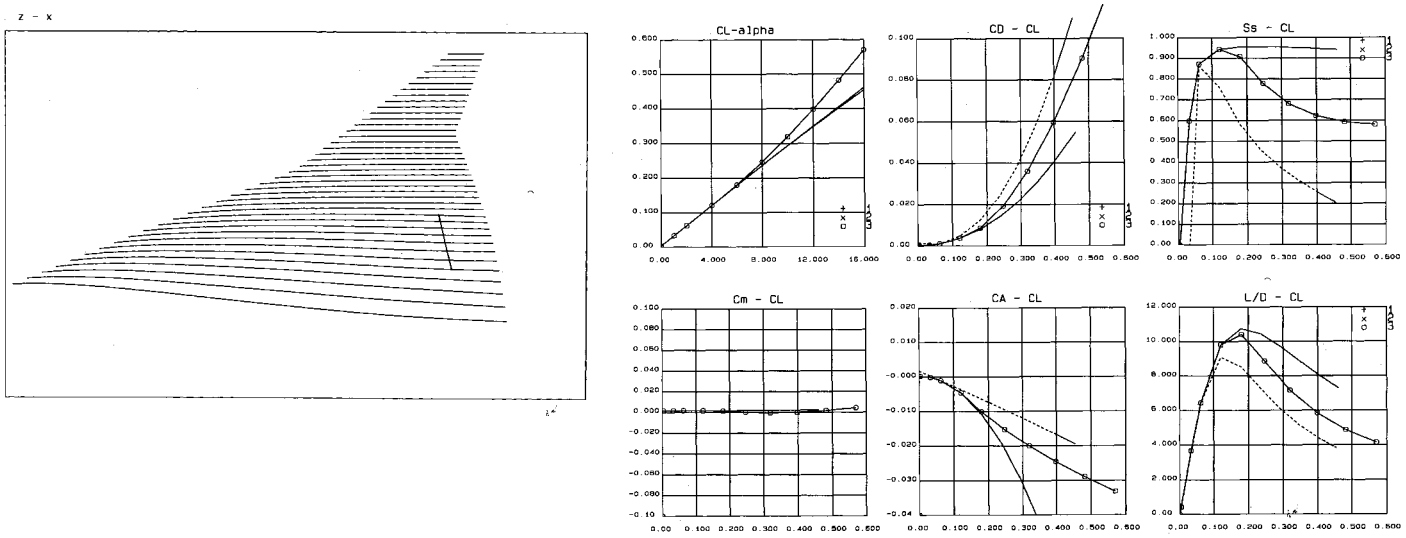

FIG. 11.3.6. SR301, DESIGNED FOR MACH 2, NEUTRALLY STABLE
TEF AREA REDESIGNED FOR MACH 0.3 NEUTRAL STABILITY, AERODYNAMIC CHARACTERISTICS AT M 0.3

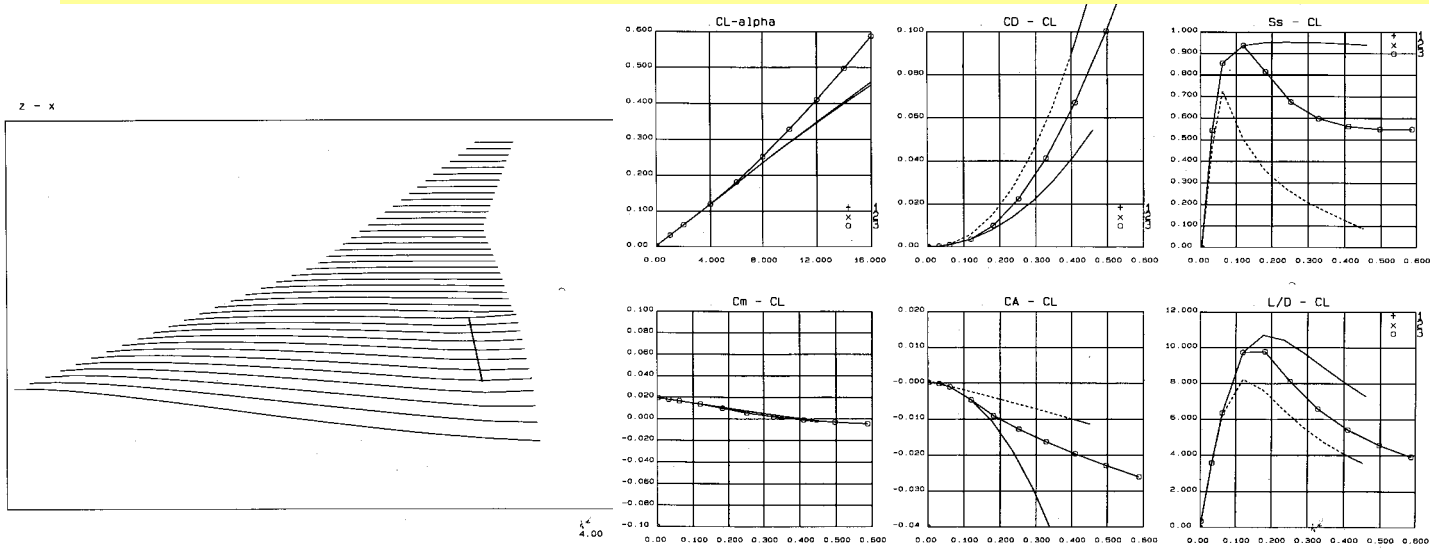

FIG. 11.3.7. SR301, DESIGNED FOR MACH 2, NEUTRALLY STABLE
TEF AREA REDESIGNED FOR MACH 0.3 5%cref STABLE, AERODYNAMIC CHARACTERISTICS AT M 0.3

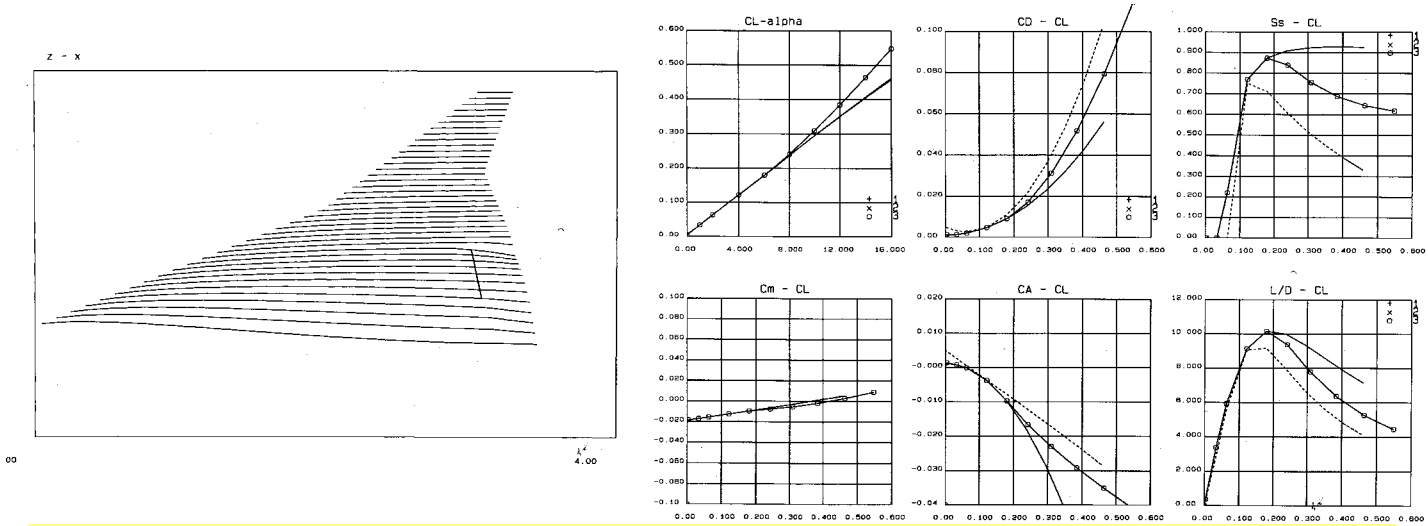

FIG. 11.3.8. SR301, DESIGNED FOR MACH 2, NEUTRALLY STABLE
TEF AREA REDESIGNED FOR MACH 0.3 5%cref UNSTABLE, AERODYNAMIC CHARACTERISTICS AT M 0.3

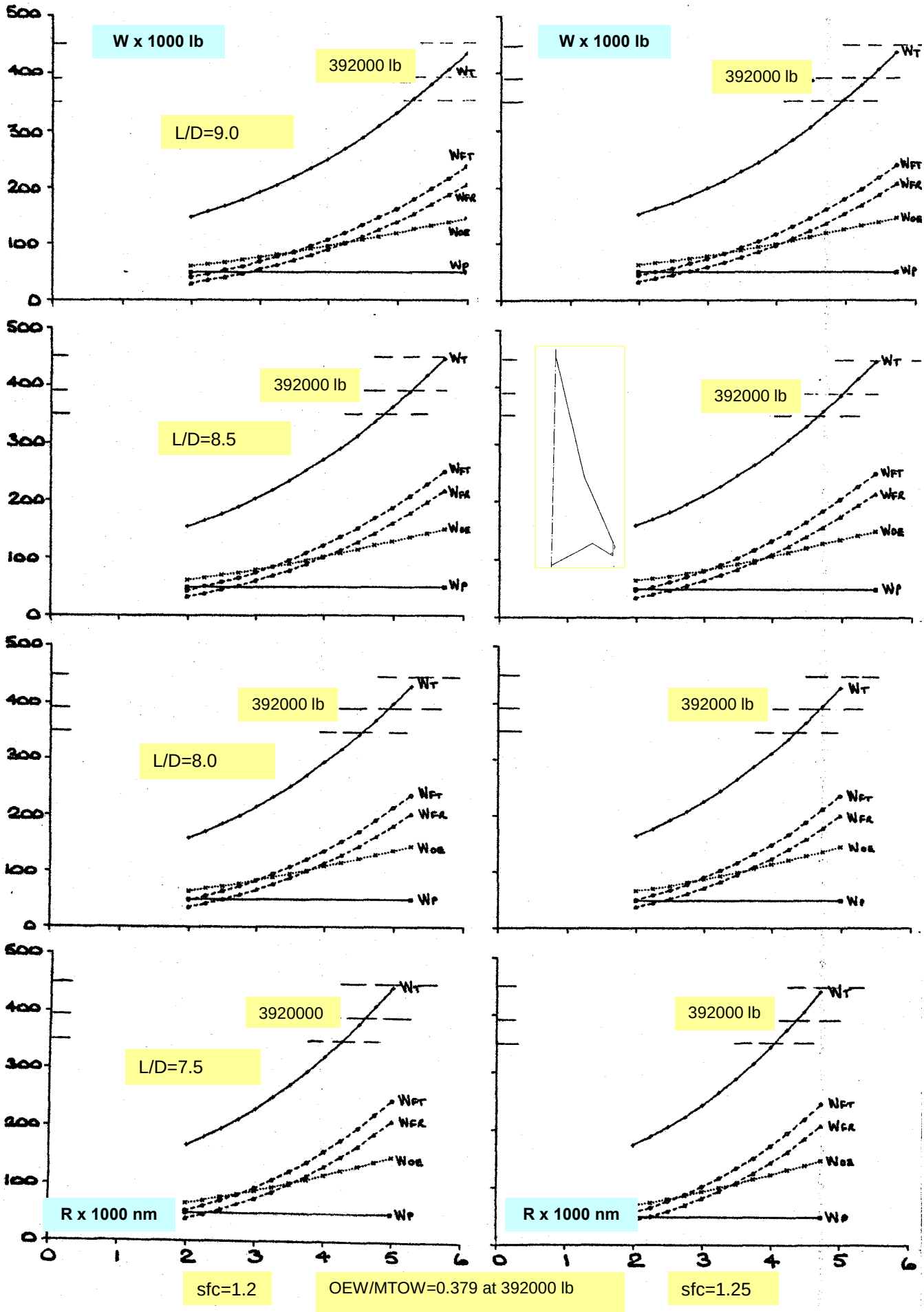

FIG. 11.4.1. SR301, MTOW, OEW, WP, WF (x 1000 lb) – RANGE (x1000 nm) WITH L/D & SFC

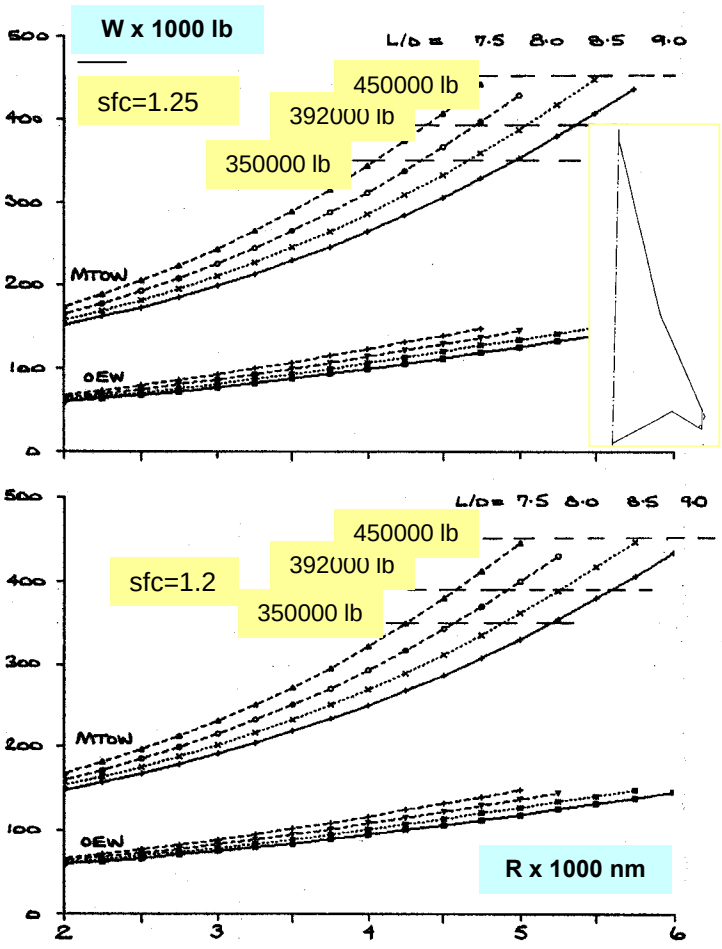

OEW/MTOW=0.379 at 392000 lb

FIG. 11.4.2. SUMMARY SR301, MTOW & OEW (x 1000 lb – RANGE (x 1000 nm) , SFC & L/D VARIATIONS

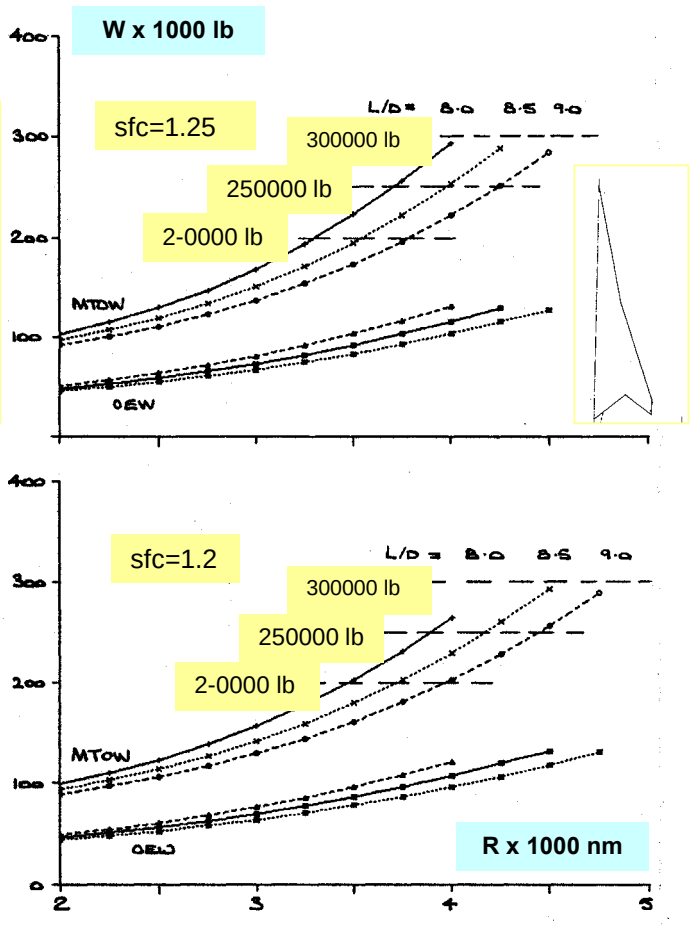

OEW/MTOW=0.461 at 250000 lb

FIG. 11.4.3. SUMMARY SR401, MTOW & OEW (x 1000 lb – RANGE (x 1000 nm) , SFC & L/D VARIATIONS